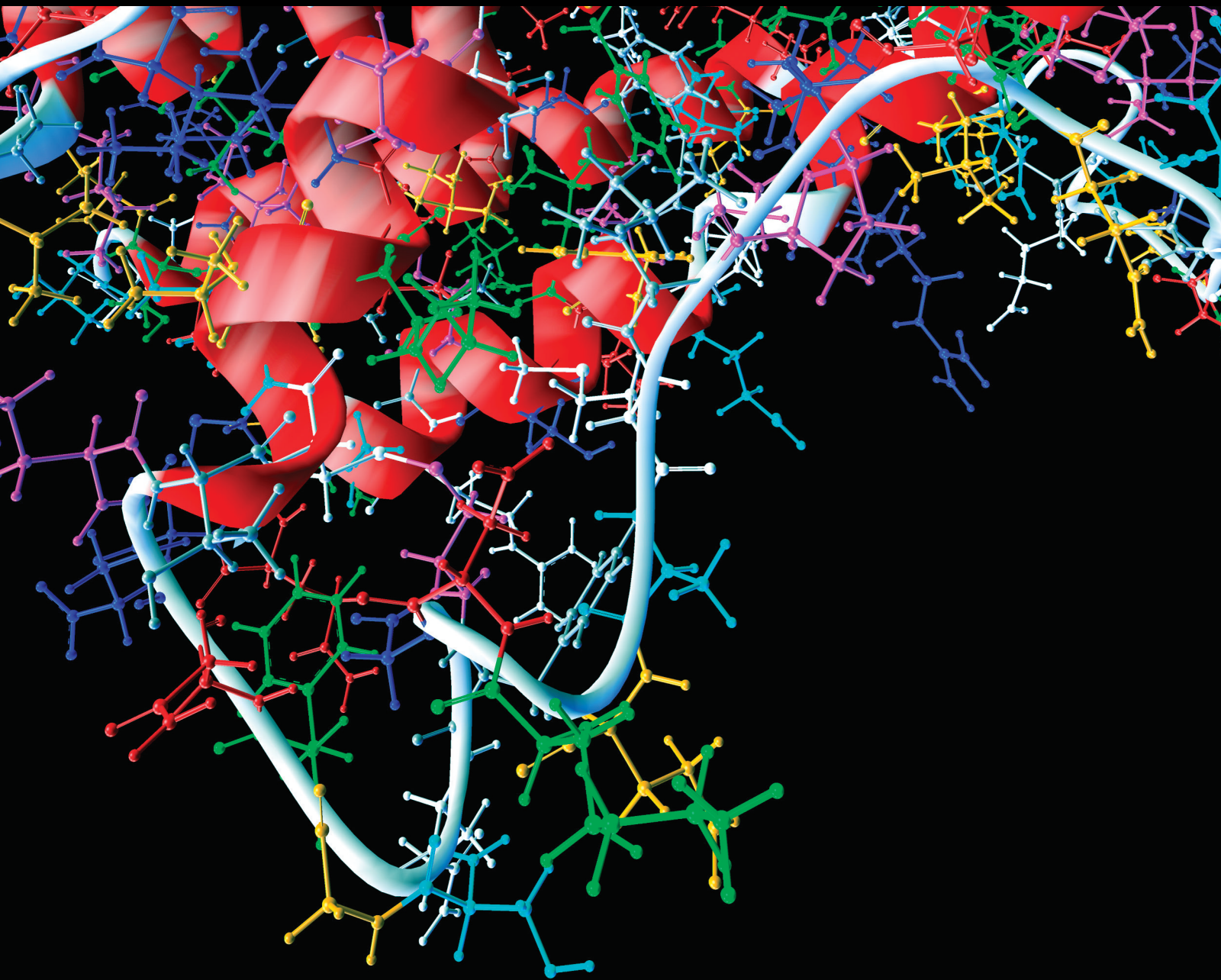# Mathematical Models in Zoonotic Epidemiological Problems

Lead Guest Editor: Asep Kuswandi Supriatna
Guest Editors: Ryusuke Kon and Bapan Ghosh

Mathematical Models in Zoonotic Epidemiological Problems

Mathematical Models in Zoonotic Epidemiological Problems

Lead Guest Editor: Asep Kuswandi Supriatna
Guest Editors: Ryusuke Kon and Bapan Ghosh

Hyuntae Park, Japan
Jovana Paunovic, Serbia
Manuel F. G. Penedo, Spain
Riccardo Pernice, Italy
Kemal Polat, Turkey
Alberto Policriti, Italy
Giuseppe Pontrelli, Italy
Jesús Poza, Spain
Maciej Przybyłek, Poland
Bhanwar Lal Puniya, USA
Mihai V. Putz, Romania
Suresh Rasappan, Oman
Jose Joaquin Rieta, Spain
Fathalla Rihan, United Arab Emirates
Sidheswar Routray, India
Sudipta Roy, India
Jan Rychtar, USA
Mario Sansone, Italy
Murat Sari, Turkey
Shahzad Sarwar, Saudi Arabia
Kamal Shah, Saudi Arabia
Bhisham Sharma, India
Simon A. Sherman, USA
Mingsong Shi, China
Mohammed Shuaib, Malaysia
Prabhishek Singh, India
Neelakandan Subramani, India
Junwei Sun, China
Yung-Shin Sun, Taiwan
Min Tang, China
Hongxun Tao, China
Alireza Tavakkoli, USA
João M. Tavares, Portugal
Jlenia Toppi, Italy
Anna Tsantili-Kakoulidou, Greece
Markos G. Tsipouras, North Macedonia
Po-Hsiang Tsui, Taiwan
Sathishkumar V E, Republic of Korea
Durai Raj Vincent P M, India
Gajendra Kumar Vishwakarma, India
Liangjiang Wang, USA
Ruisheng Wang, USA
Zhouchao Wei, China
Gabriel Wittum, Germany
Xiang Wu, China

KI Yanover, Israel
Xiaojun Yao, China
Kaan Yetilmezsoy, Turkey
Hiro Yoshida, USA
Yuhai Zhao, China

Contents

Research Article

A Mathematical Model for Transmission of Hantavirus among Rodents and Its Effect on the Number of Infected Humans

Asep K. Supriatna [1], **Herlina Napitupulu** [1], **Meksianis Z. Ndii** [2], **Bapan Ghosh** [3], **and Ryusuke Kon** [4]

[1]*Department of Mathematics, Faculty of Mathematics and Natural Sciences, Universitas Padjadjaran, Sumedang 45363, Indonesia*
[2]*Department of Mathematics, Faculty of Mathematics and Natural Sciences, Universitas Nusa Cendana, Kupang 85001, Indonesia*
[3]*Department of Mathematics, Indian Institute of Technology Indore, Khandwa Road, Simrol, Indore 453552, Madhya Pradesh, India*
[4]*Faculty of Engineering, University of Miyazaki, Miyazaki 889-2192, Japan*

Correspondence should be addressed to Asep K. Supriatna; a.k.supriatna@unpad.ac.id

In this paper, we present a mathematical model for the transmission of hantavirus among rodents and its effect on the number of hantavirus-infected human population. We investigate the model and present a standard analysis in mathematical epidemiology, such as determining the equilibria of the system and their stability analysis, together with the relationship to the basic reproduction number. It is found that the endemic equilibrium exists and is locally asymptotically stable when the basic reproduction number is greater than one; otherwise, the disease-free equilibrium is stable. Later on, we also show that by constructing a suitable Lyapunov function, the endemic equilibrium is globally asymptotically stable whenever it exists. Based on the basic reproduction number, we present a critical level of intervention to control the spread of the disease to humans. We found a significant finding from the present model that if the basic reproduction number is greater than one, then it is impossible to completely eliminate hantavirus disease in the system by solely focusing on any intervention for humans, like vaccination and curative action, without paying any attention to interventions for rodent populations. However, we can still decrease the density of infected humans with those interventions. Hence, we suggest that a combination of several interventions is needed to obtain effective control in eliminating the hantavirus. This information is useful for further study in finding an optimal control strategy to reduce or eliminate the transmission of hantavirus to humans.

1. Introduction

Some examples of important zoonoses include zoonotic influenza, salmonellosis, West Nile virus, plague, rabies, brucellosis, dengue, and hantavirus. Rats and mice are among the animals that spread most zoonoses to more than 35 diseases. The diseases are transmitted to humans via direct contact with rodents or extensive contact with rodent excreta-contaminated material [1]. Among the zoonoses spread by rodents is the hantavirus disease which is caused by the Hantaan virus. There are more than one species of rodents that can transmit hantavirus, including rats and mice.

Hantavirus pulmonary syndrome (HPS), or shortly hantavirus disease, is a fatal disease for humans. The virus is spread worldwide and is regarded as an important zoonotic pathogen that may cause severe and adverse effects in humans. It is transmitted to humans via direct contact with rodents or indirectly by rodent excreta (feces, urine, and aerosols). Humans may become infected once they inhale aerosolized droplets of urine or have extensive contact with rodent excreta-contaminated materials [2]. The disease is mainly circulated among rodents of different species and is also able to transmit from rodents to humans. However, there is no evidence of human-to-human transmission [3] or human-to-rodent transmission.

Hantaviruses are a group of viruses consisting of several strains that have been identified as infectious agents that can cause serious illness. Examples of Hantaan viruses are Dobrava, Puumala (PUU), and Seoul (SEOV) subtypes which may cause HFRS and Sin Nombre (SNV), Bayou virus (BAY), Black Canal Creek (BCC), and New York virus (NY) subtypes which may cause HPS [4]. To date, hantavirus infection is still regarded as a global zoonotic challenge, with an estimated more than 20,000 cases of hantavirus disease occurring annually worldwide, especially in Asia [5]. Sin Nombre virus, for example, is a type of hantavirus identified as the infectious agent that caused the deadly outbreak of hantavirus pulmonary syndrome in southwestern North America in 1993. Each hantavirus is harbored by an infected rodent species. Rodents do not lose infection and infect humans who come into contact with them or with their feces [6]. Each hantavirus generally associates with a primary rodent host where substantial coevolutionary adaptation is possible [7, 8].

There are about 30 different hantaviruses worldwide, some of which cause infections in humans [9]. Infection in humans is incidental, usually due to indirect transmission through contact with infectious rodent feces, but can cause hantavirus pulmonary syndrome with a mortality rate of up to 37% [10]. There are two characteristics of hantavirus infection observed in the field. For the first one, it is reported that infections can disappear entirely from rodent populations if environmental conditions are unsuitable, only to reappear when environmental conditions change and become favorable. This is a temporary feature. There are also spatial characteristics in the second one, in which there is evidence of focal infection. This "refugia" of rodent populations can be expanded or reduced [11].

The geographical distribution of hantavirus is mainly in Asia [5], such as in China, the Republic of Korea, and the Far East Region of the Russia Federation. As the most endemic country, more than 1,400,000 clinical cases of HFRS caused by HTNV and Seoul Virus (SEOV), with about 45,000 deaths, were reported in China during the period 1950 to 2001 [12]. This is about 70% to 90% of the total reported worldwide HFRS cases [13]. The remaining cases are reported from 18 countries (Asia), 32 countries (Europe) [13], and 7 countries (America) [14].

Other examples of countries that have already been invaded by hantavirus are Japan, Indonesia, and India (doi:10.1038/nindia.2008.104). Among several known strains of Hantaan viruses, one of them is Puumala (PUU) which may cause hemorrhagic fever with renal syndrome (HFRS) and hantavirus pulmonary syndrome (HPS) in humans [15]. Currently, there are no reported recent HFRS cases in Japan, but there may be some undiagnostic cases since infected brown rats are distributed throughout Japan and grey red-backed voles are massively infected with the PUU virus in Hokkaido [15]. Indonesia is also home to approximately 171 species of rats, and 22 species among them live on Java Island [16]. Wibowo [4] reported that at least 5 species of rats are among the reservoirs of the hantavirus. Recently, Mulyono et al. [17] added 4 more new species of rats which act as the reservoir of the hantavirus.

Sendow et al. [18] and the reference therein pointed out the occurrence of HPS in Indonesia. The first reported cases of HPS in humans were in 2002, and initially, all the patients were suspected of contracting DHF [19]. The prevalence of hantavirus in rodents varies among cities in Indonesia, with the highest being 28.9% in Maumere, the eastern part of Indonesia [4]. This high prevalence of hantavirus in rodents also happens in other parts of the world, indicating the importance of rodents as a source of hantavirus transmission to humans and establishing the disease as a rodent-born disease.

Considering the danger of the disease to humans, some interventions have been proposed to control the spread of the disease to humans. This includes prevention and treatment. Prevention is done mainly by avoiding exposure to materials carrying hantavirus such as rodent's feces, urine, bodily secretions, and tissues. People who have a high risk of this exposure, such as those who are occupationally exposed to rodents, should take extra precautions to avoid this exposure. Some apparatus like gloves, goggles, rubber boots or disposable shoe covers, and coveralls or gowns may be used during their activities [20, 21], and ventilation of the room should be sufficiently good [22]. In general, rodent control to prevent high exposure to hantavirus in any building or house is recommended [23], which includes the use of rodent traps and poisons and the removal of possible nesting sites around the home [22]. Other examples of prevention have been described by Kerins et al. [24] related to pet rats, including euthanasia of the entire colony or testing and culling of infected animals. Intervention in humans to prevent hantavirus infection usually takes the form of vaccination, in which an inactivated hantavirus is injected [25]. While some therapeutics, concerned with the treatment of disease and the action of remedial agents, are given to cure infected humans [26], safe and effective vaccines and immunotherapy as preventives and treatments for hantavirus disease are still being developed [27, 28].

Hantavirus disease now begins to receive much attention from scientists, including mathematicians, in the attempt to understand, to control, and to eliminate it—if possible. In regard to the application of mathematics in the study of disease transmission, there are some authors that have constructed some mathematical models, such as Abramson and Kenkre [11, 29], Sauvage et al. [30], Abramson et al. [29], Allen et al. [31–34], Alvarez et al. [35], Escudero et al. [36], Chu et al. [37], Wesley [38, 39], Abramson [40], Rida et al. [41], Goh et al. [42], Karim et al. (2009), Kaplan et al. [43], Bürger et al. [44], and Yusof et al. [45, 46]. The most influential work in this area is written by Allen et al. whose subsequential works on mathematical modeling of hantavirus transmission have high citations. In this paper, we propose a new model for the transmission of hantavirus among rodents and its effect on the number of hantavirus-infected humans.

2. Formulation of New Model

In this section, we formulate a mathematical model for the transmission of hantavirus by considering the following
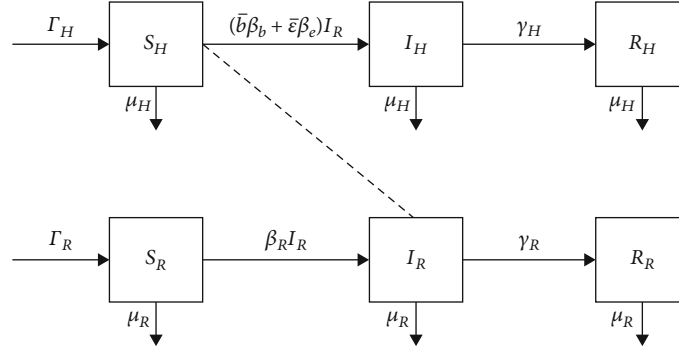
FIGURE 1: A schematic diagram of SIR-SIR transmission of hantavirus between humans and rodents.

assumptions: (i) there is only one species of rodents; (ii) the transmission happens only among rodents and from rodents to humans, and there is no transmission among humans and from humans to rodents since there is no evidence of human-to-human transmission [3]; (iii) transmission from rodents to humans occurs in two different modes, direct and indirect. Direct transmission occurs when there is direct contact between humans and infected rodents that may cause human infection by rodent bites, while indirect transmission can be done through the contact of humans and rodents excreta [2]. (iv) The recruitment to both human and rodent susceptible populations is constant, and (v) there is no vertical transmission [21].

Let us consider a human population, which, due to the circulation of hantavirus, is divided into three compartments, namely, the susceptible (S_H), the infected (I_H), and the recovered (R_H), who are assumed to be immune with $S_H(t) + I_H(t) + R_H(t) = N_H(t)$. For all variables in the model (i.e., $X = S, I, R, N$), the notation $X(t)$ means the number of individuals in X class at time t. The rodent population is also assumed to have similar compartments with S_R denotes the susceptible rodents, I_R denotes the infective rodents, and R_R denotes the recovered rodents with $S_R(t) + I_R(t) + R_R(t) = N_R(t)$. A schematic diagram of disease transmission is shown in Figure 1.

The notations and parameters used in the schematic diagram above are presented in Table 1:

As there are two different routes of infection from rodent to human, i.e., by rodent biting and by contacting the rodent excreta, hence, we have the following equations as the governing hantavirus transmission among rodents and humans:

$$\frac{dS_H(t)}{dt} = \Gamma_H - \bar{b}\beta_b S_H(t) I_R(t) - \bar{\varepsilon}(I_R(t)) S_H(t) \beta_\varepsilon - \mu_H S_H(t),$$ (1)

$$\frac{dI_H(t)}{dt} = \bar{b}\beta_b S_H(t) I_R(t) + \bar{\varepsilon}(I_R(t)) S_H(t) \beta_\varepsilon - (\mu_H + \gamma_H) I_H(t),$$ (2)

$$\frac{dR_H(t)}{dt} = \gamma_H I_H(t) - \mu_H R_H(t),$$ (3)

TABLE 1: Parameters and notations used in the model formulation.

Γ_H; Γ_R	Recruitment rates (human; rodent)
$\bar{b}$	Number of bites/direct contact with rodent
$\bar{\varepsilon}$	Rodent excreta density
β_b; β_ε	Probability of successful contact (bites/direct contact; excreta)
β_H; β_R	Probability of successful contact (human; rodent)
μ_H; μ_R	Death rates (human; rodent)
γ_H; γ_R	Recovery rates (human; rodent)

$$\frac{dS_R(t)}{dt} = \Gamma_R - \beta_R S_R(t) I_R(t) - \mu_R S_R(t),$$ (4)

$$\frac{dI_R(t)}{dt} = \beta_R S_R(t) I_R(t) - (\mu_R + \gamma_R) I_R(t),$$ (5)

$$\frac{dR_R(t)}{dt} = \gamma_R I_R(t) - \mu_R R_R(t).$$ (6)

Let us consider the first case in which the number of rodent excreta is a linear function of the number of infective rodents, i.e., $\bar{\varepsilon}(I_R(t)) = \varepsilon I_R(t)$. Hence, the per capita successful contact rate between a susceptible and the rodent excreta rate, with the successful probability of transmission β_ε, is given by $\varepsilon I_R(t)\beta_\varepsilon$. Furthermore, if we also assume the successful probability of transmissions is the same regardless of its mode of transmission (via biting by the rodent or contact with rodent excreta and aerosol), i.e., $\beta_\varepsilon = \beta_b = \beta_H$, then, we have the total transmission rate from the two different modes given by

$$\begin{aligned} \bar{b}\beta_b S_H(t) I_R(t) &+ \bar{\varepsilon}(I_R(t)) S_H(t) \beta_\varepsilon \\ &= \bar{b}\beta_H S_H(t) I_R(t) + \varepsilon I_R(t) S_H(t) \beta_H \\ &= (\bar{b} + \varepsilon)\beta_H S_H(t) I_R(t) = b\beta_H S_H(t) I_R(t). \end{aligned}$$ (7)

Hence, the complete equations for the SIR-SIR hantavirus transmission in this special case are given by Equations (3)–(6) plus the following equations:

$$\frac{dS_H(t)}{dt} = \Gamma_H - b\beta_H S_H(t)I_R(t) - \mu_H S_R(t), \qquad (8)$$

$$\frac{dI_H(t)}{dt} = b\beta_H S_H(t)I_R(t) - (\mu_H + \gamma_H)I_H(t). \qquad (9)$$

In fact, the last two equations can also be derived in more general ways without assuming $\beta_\varepsilon = \beta_b = \beta_H$. In this case, we let $b\beta'_H = (\bar{b}\beta_b + \varepsilon\beta_\varepsilon)$. In the subsequent section, we analyze the model by showing its steady-state solutions, their stability, and their relation to the basic reproduction number, which is central in mathematical epidemiology studies.

3. Results

In this section, we analyze the system of Equations (3)–(6), (8), and (9) by showing the equilibria and their stability. The relation of the existence of the equilibria and its stability to the basic reproduction number is also presented. Furthermore, we present the sensitivity analysis of the equilibria and the basic reproduction number to the change of parameters to find the most critical parameters affecting the dynamics of the system.

3.1. The Equilibria. An endemic-free or nonendemic equilibrium always exists for any parameters of the model. However, we show that there is a threshold that determines the existence of an endemic equilibrium, say $\mathcal{T}^\varepsilon$, so that the endemic equilibrium exists only if $\mathcal{T}^\varepsilon$ is above a certain value; otherwise, an endemic equilibrium does not exist. We sum up this property in the following theorem.

Theorem 1. *In the SIR-SIR hantavirus model (Equations (3)–(6) and Equations (8) and (9)), the following properties hold:*

(a) *The trivial nonendemic equilibrium of the system always exists, given by $(S_{0H}{}^*, I_{0H}{}^*, R_{0H}{}^*, S_{0R}{}^*, I_{0R}{}^*, R_{0R}{}^*,) = (\Gamma_H/\mu_H, 0, 0, \Gamma_R/\mu_R, 0, 0)$*

(b) *An endemic equilibrium is given by $(S_{eH}{}^*, I_{eH}{}^*, R_{eH}{}^*, S_{eR}{}^*, I_{eR}{}^*, R_{eR}{}^*)$ with $S_{eR}^* = \Gamma_R/\mu_R\mathcal{T}^0$, $I_{eR}^* = \beta_R/\mu_R(\mathcal{T}^0 - 1)$, $R_{eR}^* = \gamma_R\beta_R/\mu_R^2(\mathcal{T}^0 - 1)$, $S_{eH}^* = \beta_R\Gamma_H/b\mu_R\beta_H(\mathcal{T}^0 - 1) + \mu_H\beta_R$, $I_{eH}^* = (\mu_R b\beta_H(\mathcal{T}^0 - 1)/\beta_R(\mu_H + \gamma_H))S_H^*$, and $R_{eH}^* = \gamma_H/\mu_H I_H^*$, and $\mathcal{T}^0 = \beta_R\Gamma_R/\mu_R(\mu_R + \gamma_R)$ is a threshold such that the endemic equilibrium exists only if $\mathcal{T}^0 > 1$; otherwise, the endemic equilibrium does not exist.*

Proof of Theorem 1. By solving Equations (3)–(6) and Equations (8) and (9) simultaneously under steady-state conditions (i.e., when all LHSs of the equations are equal to zero), the system has two equilibria, i.e., $(S_{0H}{}^*, I_{0H}{}^*, R_{0H}{}^*, S_{0R}{}^*, I_{0R}{}^*, R_{0R}{}^*,) = (\Gamma_H/\mu_H, 0, 0, \Gamma_R/\mu_R, 0, 0)$ and $(S_{eH}{}^*, I_{eH}{}^*, R_{eH}{}^*, S_{eR}{}^*, I_{eR}{}^*, R_{eR}{}^*)$ given by

(a) $(S_{0H}{}^*, I_{0H}{}^*, R_{0H}{}^*, S_{0R}{}^*, I_{0R}{}^*, R_{0R}{}^*,) = (\Gamma_H/\mu_H, 0, 0, \Gamma_R/\mu_R, 0, 0)$ which is a nonendemic equilibrium, since all of the infected classes ($I_{0H}{}^*$ and $I_{0R}{}^*$) are zero. Clearly, this trivial one always occurs

(b) $(S_{eH}{}^*, I_{eH}{}^*, R_{eH}{}^*, S_{eR}{}^*, I_{eR}{}^*, R_{eR}{}^*)$ is an endemic equilibrium, with $S_{eH}^* = \beta_R(\mu_R + \gamma_R)\Gamma_H/b\beta_H(-\mu_R(\mu_R + \gamma_R) + \beta_R\Gamma_R) + \beta_R(\mu_R + \gamma_R)\mu_H$, $I_{eH}^* = b\beta_H\Gamma_H(-\mu_R(\mu_R + \gamma_R) + \beta_R\Gamma_R)/(b\beta_H(-\mu_R(\mu_R + \gamma_R) + \beta_R\Gamma_R) + \beta_R(\mu_R + \gamma_R)\mu_H)(\mu_H + \gamma_H)$, $R_{eH}^* = (b\beta_H\Gamma_H(-\mu_R(\mu_R + \gamma_R) + \beta_R\Gamma_R)/(b\beta_H(-\mu_R(\mu_R + \gamma_R) + \beta_R\Gamma_R) + \beta_R(\mu_R + \gamma_R)\mu_H)(\mu_H + \gamma_H))\gamma_H/\mu_H$, $S_{eR}^* = \mu_R + \gamma_R/\beta_R$, $I_{eR}^* = -\mu_R(\mu_R + \gamma_R) - \beta_R\Gamma_R/\beta_R(\mu_R + \gamma_R)$, and $R_{eR}^* = -(\mu_R(\mu_R + \gamma_R) - \beta_R\Gamma_R)\gamma_R/\beta_R(\mu_R + \gamma_R)\mu_R$.

$\square$

To find the condition for the existence of the endemic equilibrium, let us look for a threshold number, so that $S_{eH}{}^* \geq 0$, $I_{eH}{}^* > 0$, $R_{eH}{}^* > 0$, $S_{eR}{}^* \geq 0$, $I_{eR}{}^* > 0$, and $R_{eR}{}^* > 0$. Note that by using some algebraic manipulation, it is easy to show that the components of the equilibrium can be rewritten in the following forms.

(i) First, we focus on $S_{eR}^* = \mu_R + \gamma_R/\beta_R$. This can be written as $S_{eR}^* = \mu_R + \gamma_R/\beta_R = \Gamma_R/\mu_R(\beta_R\Gamma_R/\mu_R(\mu_R + \gamma_R))$. If we define $\mathcal{T}^0 = \beta_R\Gamma_R/\mu_R(\mu_R + \gamma_R)$, then we have $S_{eR}^* = \Gamma_R/\mu_R\mathcal{T}^0$ as required

(ii) Keeping in mind $\mathcal{T}^0 = \beta_R\Gamma_R/\mu_R(\mu_R + \gamma_R)$, then, we have the following- $I_{eR}^* = -\mu_R(\mu_R + \gamma_R) - \beta_R\Gamma_R/\beta_R(\mu_R + \gamma_R) = \beta_R/\mu_R(\mathcal{T}^0 - 1)$

(iii) Similarly, $R_{eR}^* = -(\mu_R(\mu_R + \gamma_R) - \beta_R\Gamma_R)\gamma_R/\beta_R(\mu_R + \gamma_R)\mu_R = \gamma_R\beta_R/\mu_R^2(R_0 - 1)$

(iv) Next, we have $S_{eH}^* = \beta_R(\mu_R + \gamma_R)\Gamma_H/b\beta_H(-\mu_R(\mu_R + \gamma_R) + \beta_R\Gamma_R) + \beta_R(\mu_R + \gamma_R)\mu_H$. Let us look at the inverse which can be manipulated as

$$\begin{aligned}
\frac{1}{S_{eH}^*} &= \frac{b\beta_H(-\mu_R(\mu_R + \gamma_R) + \beta_R\Gamma_R) + \beta_R(\mu_R + \gamma_R)\mu_H}{\beta_R(\mu_R + \gamma_R)\Gamma_H} \\
&= \frac{b\beta_H(-\mu_R(\mu_R + \gamma_R) + \beta_R\Gamma_R)}{\beta_R(\mu_R + \gamma_R)\Gamma_H} + \frac{\beta_R(\mu_R + \gamma_R)\mu_H}{\beta_R(\mu_R + \gamma_R)\Gamma_H} \\
&= \frac{b\mu_R\beta_H}{\beta_R\Gamma_H}\frac{(-\mu_R(\mu_R + \gamma_R) + \beta_R\Gamma_R)}{\mu_R(\mu_R + \gamma_R)} + \frac{\mu_H}{\Gamma_H} \\
&= \frac{b\mu_R\beta_H}{\beta_R\Gamma_H}(R_0 - 1) + \frac{\mu_H}{\Gamma_H} \\
&= \frac{b\mu_R\beta_H(R_0 - 1) + \mu_H\beta_R}{\beta_R\Gamma_H}.
\end{aligned} \qquad (10)$$

Hence, $S_{eH}^* = \beta_R\Gamma_H/b\mu_R\beta_H(\mathcal{T}^0 - 1) + \mu_H\beta_R$ as requested.

(v) Next $I_{eH}^* = b\beta_H\Gamma_H(-\mu_R(\mu_R + \gamma_R) + \beta_R\Gamma_R)/(b\beta_H(-\mu_R(\mu_R + \gamma_R) + \beta_R\Gamma_R) + \beta_R(\mu_R + \gamma_R)\mu_H)(\mu_H + \gamma_H)$

can be rewritten as $I_{eH}^* = b\beta_H \Gamma_H (-\mu_R(\mu_R + \gamma_R) + \beta_R \Gamma_R/\mu_R(\mu_R + \gamma_R))/(\mu_H + \gamma_H)(b\beta_H(-\mu_R(\mu_R + \gamma_R) + \beta_R \Gamma_R) + \beta_R(\mu_R + \gamma_R)\mu_H)/\mu_R(\mu_R + \gamma_R) = b\beta_H \Gamma_H (\mathcal{T}^0 - 1)/(\mu_H + \gamma_H)(b\beta_H(\mathcal{T}^0 - 1) + \beta_R\mu_H/\mu_R)$ as required

(vi) Finally, we have the following algebraic expression

$$R_{eH}^* = \left(\frac{b\beta_H \Gamma_H(-\mu_R(\mu_R + \gamma_R) + \beta_R \Gamma_R)}{(b\beta_H(-\mu_R(\mu_R + \gamma_R) + \beta_R \Gamma_R) + \beta_R(\mu_R + \gamma_R)\mu_H)(\mu_H + \gamma_H)} \right) \frac{\gamma_H}{\mu_H}$$
$$= \frac{\gamma_H}{\mu_H} I_H^*$$

(11)

which completes the proof.

3.2. The Basic Reproduction Number and Stability of the Equilibria. Let us have a look at the form of the threshold $\mathcal{T}^0 = \beta_R \Gamma_R/\mu_R(\mu_R + \gamma_R)$ which can be written as $\mathcal{T}^0 = \beta_R(1/(\gamma_R + \mu_R))\Gamma_R(1/\mu_R)$ and can be read verbally as the multiplication of four rodent epidemiological factors. The multiplication of the four factors mentioned above is (the force of infection from an infectious rodent to a healthy rodent) × (the average length of stay of an infective rodent within the infectious period) × (the life expectancy of a healthy rodent) × (the constant rate of susceptible rodent recruitment). Interestingly, here, human epidemiological factors do not appear in the threshold parameter $\mathcal{T}^0$.

To provide a deeper interpretation of this threshold, let us consider a clinical intervention. In the health context, any intentional action designed to obtain an outcome is called a clinical intervention. If, in the absence of clinical intervention, we have $\mathcal{T}^0 > 1$ (hence, an endemic equilibrium exists), then we could apply a clinical intervention (such as vaccination), so that it is possible to reduce the threshold to be less than 1 by changing $\mathcal{T}^0$ to $\mathcal{T}^\varepsilon$ for a certain choice of $\varepsilon > 0$, resulting in $\mathcal{T}^\varepsilon < 1$ (removing the endemic equilibrium from the system). In the case of hantavirus, intervention other than clinical intervention is also possible such as reducing the rodent recruitment rate, reducing the life expectancy of the rodent, trapping, and culling infective rodents. This is the basic idea behind controlling/eliminating contagious diseases from a mathematical point of view. Finding this kind of threshold is vital in the study of mathematical epidemiology. In modern literature, this threshold is usually called the basic reproduction number (sometimes the basic reproduction/reproductive ratio). It is not easy to find this number for more complex transmissions of a disease. There are some good and rigorous literature studies regarding this concept, such as Diekmann and Heesterbeek [47], Diekmann et al. [48, 49], Van den Driessche and Watmough [50], and Zhao [51], that provide a more systematic way of constructing the basic reproduction number. We prove, by standard theory, that $\mathcal{T}^0$ mentioned above are indeed the basic reproduction number. We begin by defining the basic reproduction number.

The basic reproduction number of an infection is the expected number of cases produced by one case in a population where all the individuals are susceptible to infection.

The authors of [19] (p. 4) defined the basic reproduction number, with the symbol $\mathcal{R}_0$, as the expected number of secondary cases per primary case in a "virgin" population. In the same book, they showed that $\mathcal{R}_0 := \lim_{n \to \infty} \|K^n\|^{1/n}$ ([47], p. 75), where K is the next-generation matrix defined therein. According to the authors, this is a natural definition of the basic reproduction number from which its value can be computed. However, there is another way to compute the basic reproduction number other than from this definition. In fact, there are some methods that are easier to use to obtain the basic reproduction number. As an example, the following method is suggested in Van den Driessche and Watmough [50]. The authors looked at an epidemic multicompartment model $dx_i/dt = f_i(x) = \mathcal{F}_i(x) - \mathcal{V}_i(x)$, $i = 1, \cdots, n$ (as in Equations (3)–(6) and Equations (8) and (9) above). They showed that the function $f_i(x)$ can be decomposed into the rate of appearance of new infections in the ith compartment, $\mathcal{F}_i(x)$, and the rate of transfer of individuals from/into the ith compartment, $\mathcal{V}_i(x)$. Furthermore, they defined F and V to be the Jacobian matrix evaluated at the nonendemic equilibrium and showed that the basic reproduction number can be calculated as the spectral radius $\mathcal{R}_0 = \rho(FV^{-1})$. The following theorem provides the basic reproduction number of the SIR-SIR hantavirus model in Equations (3)–(6) and Equations (8) and (9), which in this case is exactly the same as the threshold $\mathcal{T}^0$ in Theorem 1.

Theorem 2. *The SIR-SIR hantavirus model (Equations (3)–(6) and Equations (8) and (9)) has the basic reproduction number $\mathcal{R}_0 = \beta_R \Gamma_R/\mu_R(\mu_R + \gamma_R)$.*

Proof of Theorem 2. Following the method in [50], with reference to Equations (3)–(6) and Equations (8) and (9), we have the rate of appearance of new infection vectors $\mathcal{F}(x)$ and the rate of transfer of individual vectors $\mathcal{V}(x)$:

$$\mathcal{F} = \begin{pmatrix} 0 \\ b\beta_H S_H I_R \\ 0 \\ 0 \\ \beta_R S_R I_R \\ 0 \end{pmatrix}, \quad (12)$$

$$\mathcal{V} = \begin{pmatrix} -\Gamma_H + b\beta_H S_H I_R + \mu_H S_R \\ (\mu_H + \gamma_H)I_H \\ -\gamma_H I_H + \mu_H R_H \\ -\Gamma_R + \beta_R S_R I_R + \mu_R S_R \\ (\mu_R + \gamma_R)I_R \\ -\gamma_R I_R + \mu_R R_R \end{pmatrix}. \quad (13)$$

Next, from the two vectors, we obtain two matrices

$$F = \begin{pmatrix} 0 & b\beta_H S_H \\ 0 & \beta_R S_R \end{pmatrix}, \tag{14}$$

$$V = \begin{pmatrix} \mu_H + \gamma_H & 0 \\ 0 & \mu_R + \gamma_R \end{pmatrix}. \tag{15}$$

Consequently,

$$V^{-1} = \begin{pmatrix} \dfrac{1}{\mu_H + \gamma_H} & 0 \\ 0 & \dfrac{1}{\mu_R + \gamma_R} \end{pmatrix}, \tag{16}$$

$$FV^{-1} = \begin{pmatrix} 0 & \dfrac{b\beta_H S_H}{\mu_R + \gamma_R} \\ 0 & \dfrac{\beta_R S_R}{\mu_R + \gamma_R} \end{pmatrix}, \tag{17}$$

which gives rise to the effective reproduction number $\mathcal{R}_0 = \rho(FV^{-1}) = \beta_R S_R/\mu_R + \gamma_R$ where $S_R = \Gamma_R/\mu_R$. Hence, $\mathcal{R}_0 = \rho(FV^{-1}) = \beta_R \Gamma_R/\mu_R(\mu_R + \gamma_R)$ which completes the proof. □

Theorem 3. *The SIR-SIR model in Equations (3)–(6) and Equations (8) and (9) always has a trivial equilibrium, while the nontrivial equilibrium exists only if the basic reproduction number is greater than 1, i.e., $\mathcal{R}_0 = \beta_R \Gamma_R/\mu_R(\mu_R + \gamma_R) > 1$.*

Proof of Theorem 3. It is obvious as a consequence of Theorems 1 and 2. □

Theorem 4. *The nonendemic equilibrium $(S_{0H}{}^*, I_{0H}{}^*, R_{0H}{}^*, S_{0R}{}^*, I_{0R}{}^*, R_{0R}{}^*)$ of Equations (3)–(6) and Equations (8) and (9) is locally asymptotically stable whenever $\mathcal{R}_0 = \beta_R \Gamma_R/\mu_R(\mu_R + \gamma_R) < 1$ and unstable otherwise.*

Proof of Theorem 4. It is easy to show that the eigenvalues of the Jacobian matrix at the disease-free are $\lambda_1 = -\mu_R$, $\lambda_2 = -\mu_H$, $\lambda_3 = -(\mu_H + \gamma_H)$, and $\beta_R \Gamma_R - \mu_R(\mu_R + \gamma_R)/\mu_R$. The last eigenvalues is certainly negative if $\mathcal{R}_0 = \beta_R \Gamma_R/\mu_R(\mu_R + \gamma_R) < 1$. □

Theorem 5. *If the endemic equilibrium $(S_{eH}{}^*, I_{eH}{}^*, R_{eH}{}^*, S_{eR}{}^*, I_{eR}{}^*, R_{eR}{}^*)$ of Equations (3)–(6) and Equations (8) and (9) exists (i.e., whenever $\mathcal{R}_0 = \beta_R \Gamma_R/\mu_R(\mu_R + \gamma_R) > 1$), then it is locally asymptotically stable.*

Proof of Theorem 5. As before, it can be shown the eigenvalues of the Jacobian matrix at the disease-free are $\lambda_1 = -\mu_R$, $\lambda_2 = -\mu_H$, $\lambda_3 = -(\mu_H + \gamma_H)$, and $\lambda_4 = -b\beta b_H(\beta_R \Gamma_R - \gamma_R \mu_R - \mu_R^2) + \beta_R \mu_H(\mu_R + \gamma_R)/\beta_R(\mu_R + \gamma_R) = -b\beta b_H(\beta_R \Gamma_R/\mu_R(\mu_R + \gamma_R) - 1) + \beta_R \mu_H(\mu_R + \gamma_R)/\beta_R(\mu_R + \gamma_R)$ which is clearly negative if $\mathcal{R}_0 = \beta_R \Gamma_R/\mu_R(\mu_R + \gamma_R) > 1$. □

Further, we can also show that the endemic equilibrium, if exists, is globally asymptotically stable as follows.

Theorem 6. *If the endemic equilibrium $(S_{eH}{}^*, I_{eH}{}^*, R_{eH}{}^*, S_{eR}{}^*, I_{eR}{}^*, R_{eR}{}^*)$ of Equations (3)–(6) and Equations (8) and (9) exists (i.e., whenever $\mathcal{R}_0 = \beta_R \Gamma_R/\mu_R(\mu_R + \gamma_R) > 1$), then it is globally asymptotically stable.*

Proof of Theorem 6. The system of the last three equations is the famous SIR model. So, by using a standard Lyapunov function for the SIR model, we can show that the endemic equilibrium point of Equations (3)–(6) and Equations (8) and (9) is globally attractive in Ω defined by

$$\Omega = \left\{ (S_H, I_H, R_H, S_R, I_R, R_R) \in \mathbb{R}_+^6 : S_R > 0, I_R > 0 \right\}. \tag{18}$$

Note that the following equations are satisfied at the endemic equilibrium:
$\Gamma_R = \beta_R S_{eR}^* I_{eR}^* + \mu_R S_{eR}^*$ and $\mu_R + \gamma_R = \beta_R S_{eR}^*$. Define the function $V : \Omega \longrightarrow \mathbb{R}$ by $V(S_H, I_H, R_H, S_R, I_R, R_R) = S_R - \log S_R + I_R - \log I_R$. The derivative of V along the trajectories of (3)–(6), (8), and (9) is given by

$$\begin{aligned}
\frac{dV}{dt} &= \left(1 - \frac{S_{eR}^*}{S_R}\right)\frac{dS_R}{dt} + \left(1 - \frac{I_{eR}^*}{I_R}\right)\frac{dI_R}{dt} \\
&= \left(1 - \frac{S_{eR}^*}{S_R}\right)(\beta_R S_{eR}^* I_{eR}^* + \mu_R S_{eR}^* - \beta_R S_R I_R - \mu_R S_R) \\
&\quad + \left(1 - \frac{I_{eR}^*}{I_R}\right)(\beta_R S_R I_R - \beta_R S_{eR}^* I_R) \\
&= -\mu_R \frac{(S_R - S_{eR}^*)^2}{S_R} + \beta_R S_{eR}^* I_{eR}^* \left(1 - \frac{S_{eR}^*}{S_R}\right)\left(1 - \frac{S_R I_R}{S_{eR}^* I_{eR}^*}\right) \\
&\quad + \beta_R S_{eR}^* I_{eR}^* \left(1 - \frac{I_{eR}^*}{I_R}\right)\left(\frac{S_R I_R}{S_{eR}^* I_{eR}^*} - \frac{I_R}{I_{eR}^*}\right) \\
&= -\mu_R \frac{(S_R - S_{eR}^*)^2}{S_R} + \beta_R S_{eR}^* I_{eR}^* \left(2 - \frac{S_{eR}^*}{S_R} - \frac{S_R}{S_{eR}^*}\right).
\end{aligned} \tag{19}$$

To proceed with the last expression, $2 - S_{eR}^*/S_R - S_R/S_{eR}^*$, let us consider the following arithmetic-geometric mean (AGM) relation $x + y/2 \geq \sqrt{xy}$, where the equality holds if and only if $x = y$. Using this AGM relation $x = S_{eR}^*/S_R$ and $y = S_R/S_{eR}^*$ we obtain the expression $S_{eR}^*/S_R + S_R/S_{eR}^*/2 \geq 1$ or equivalently $2 - S_{eR}^*/S_R + S_R/S_{eR}^* \leq 0$, where the equality holds if and only if $S_{eR}^* = S_R$. Thus, we can conclude that $dV/dt = 0$ if and only if $S_{eR}^* = S_R$ otherwise $dV/dt < 0$. By LaSalle's invariant principle, the ω-limit set of any trajectory starting in Ω is contained in the maximal invariant set of Ω. It is straightforward to show that the maximal invariant set of Ω is the singleton consists of the endemic equilibrium point. Since every forward orbit in Ω is bounded, we can conclude that the endemic equilibrium is globally attractive in Ω. □

3.3. The Critical Level of Intervention. When an intervention is carried out to control the spread of the disease, the basic

TABLE 2: Critical intervention level found by setting the effective reproduction number to be less than one.

Intervention to rodent population	Objective	Critical intervention level
Culling/poisoning/trapping	Increase rodent death rate from μ_R to a higher mortality $\mu'_R = c\mu_R$	$$c^* = (\gamma_R/2\mu_R)\left(\sqrt{(4\beta_R\Gamma_R/\gamma_R^2)+1}-1\right)$$ $$= (\gamma_R/2\mu_R)\left(\sqrt{(\mu_R(\mu_R+\gamma_R)/\gamma_R^2)4\mathscr{R}_0+1}-1\right)$$
Curing	Increases rodent recovery rate from γ_R to a higher recovery $\gamma'_R = c\gamma_R$	$c^* = \beta_R\Gamma_R - \mu_R^2/\gamma_R\mu_R = \mathscr{R}_0(\gamma_R + \mu_R/\gamma_R) - (\mu_R^2/\gamma_R\mu_R)$
Isolation/transmission inhibitor	Reduces successful contact rate among rodents from or infection probability of rodent contact from β_R to a lower contact rate $\beta'_R = (1-c)\beta_R$, with $0 < c < 1$.	$c^* = 1 - 1/\mathscr{R}_0$
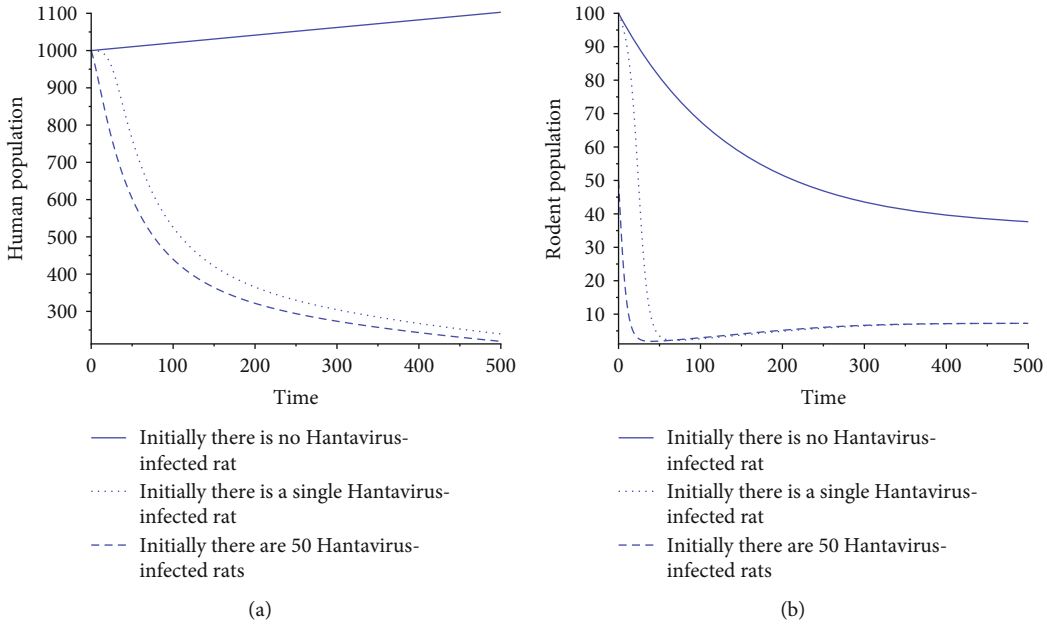
FIGURE 2: The growth of susceptible humans and rodents in the absence of hantavirus (solid lines) and in the presence of hantavirus (dashes and dots).

reproduction number $\mathscr{R}_0 = \beta_R\Gamma_R/\mu_R(\mu_R + \gamma_R)$ in Theorem 2 will change to the effective reproduction number $\mathscr{R}_0^e$ with the exact formula depending on the intervention being used. For example, if we are able to control so that only a portion of rodents could interact, say by a constant c, or decrease the probability successful contact from β_R to $\beta'_R = (1-c)\beta_R$, then the basic reproduction number will reduce to $\mathscr{R}_0^e = (1-c)\beta_R\Gamma_R/\mu_R(\mu_R + \gamma_R)$. To stop the spread of the disease, we need $\mathscr{R}_0^e < 1$ which is equivalent to $c > 1 - 1/\mathscr{R}_0$. We call $c^* = 1 - 1/\mathscr{R}_0$ as the critical intervention level that will be able to change the stability of the endemic equilibrium to an unstable equilibrium whenever $\mathscr{R}_0 > 1$.

In the case above, the critical intervention level has a simple form as a function of the basic reproduction number. Other forms are also possible, for example, when we take rodent culling as the intervention then basically it increases the natural mortality μ_R to a higher mortality μ'_R so that the effective reproduction number becomes $\mathscr{R}_0^e = \beta_R\Gamma_R/\mu'_R(\mu'_R + \gamma_R) = \beta_R\Gamma_R/c\mu_R(c\mu_R + \gamma_R) < 1$. In this case, the critical intervention level c^* is obtained by solving $c\mu_R(c\mu_R + \gamma_R)/\beta_R\Gamma_R > 1$, and given by the following, $c^* = (-1/2\gamma_R + 1/2\sqrt{4\beta_R\Gamma_R + \gamma_R^2})/\mu_R = \gamma_R/2\mu_R(\sqrt{4\beta_R\Gamma_R/\gamma_R^2 + 1} - 1)$ which is positive.

We summarize the formulas for the critical intervention level in the following Table 2.

The critical level of intervention in Table 2 is derived using the effective reproduction number by equalizing it to one and solving for c as described in Section 3.3. Hence, it can only be used to undertake an intervention in the rodent population since the reproduction number does not contain parameters for the human population. The critical level of

(a)

(b)

(c)

(d)
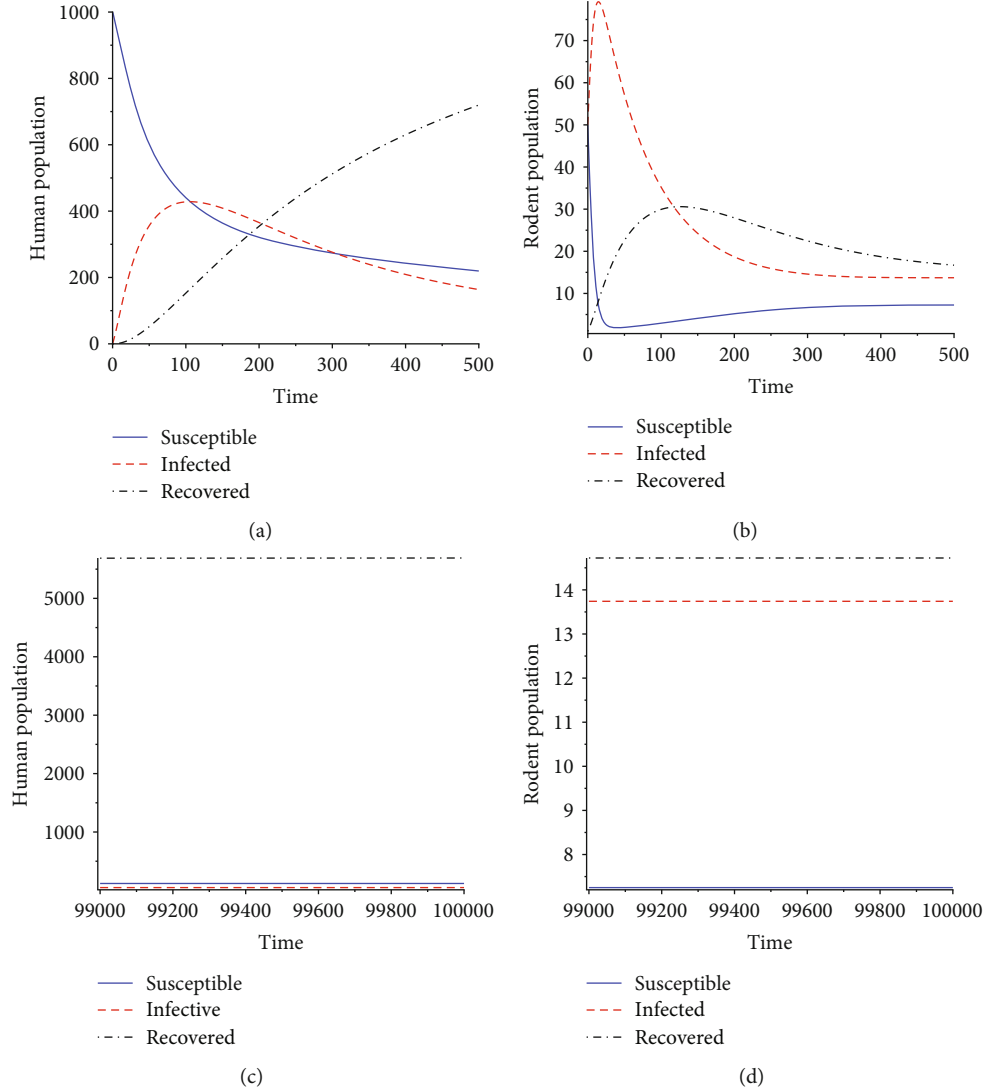
Figure 3: Transient solution of the system with $\mathscr{R}_0 = 4.926108374$ for (a) human subpopulations and (b) rodent subpopulations. The lower figures show the near equilibrium for (c) human subpopulations and (d) rodent subpopulations.

intervention above is aimed at eliminating the hantavirus so that the endemic state I_{eR}^* is zero and hence I_{eH}^* also vanishes. In fact, by observing the endemic state $I_{eH}^* = b\beta_H \Gamma_H(-\mu_R(\mu_R + \gamma_R) + \beta_R\Gamma_R)/(b\beta_H(-\mu_R(\mu_R + \gamma_R) + \beta_R\Gamma_R) + \beta_R (\mu_R + \gamma_R)\mu_H)(\mu_H + \gamma_H)$, we can only decrease this endemic state but will not make it vanish without the intervention of the rodent population. This can be seen as, whenever $\mathscr{R}_0 > 1$, $I_{eH}^* \leq 0$ only if $(-\mu_R(\mu_R + \gamma_R) + \beta_R\Gamma_R) \leq 1$ which is equivalent to either we make $\mathscr{R}_0 \leq 1$ by doing an intervention to the rodent population or making one of b, β_H, Γ_H parameters zero. The following section gives some numerical examples to illustrate the results presented above.

4. Numerical Examples

In this section, we present numerical examples to show the behavior of the SIR-SIR hantavirus model with and without the presence of clinical/nonclinical intervention (trapping/culling/poisoning the rodents, educating people to increase

awareness regarding the danger of hantavirus so they avoid contact with rodents and their excreta, etc.). We use the following parameter values in the simulations:

$$b = 0.1,$$

$$\beta_H = 0.0015,$$

$$\Gamma_H = 0.25,$$

$$\gamma_H = \frac{1}{200},$$

$$\mu_H = \frac{1}{65*365}, \tag{20}$$

$$\beta_R = 0.002,$$

$$\Gamma_R = 0.25,$$

$$\gamma_R = 0.0075,$$

$$\mu_R = 0.007.$$
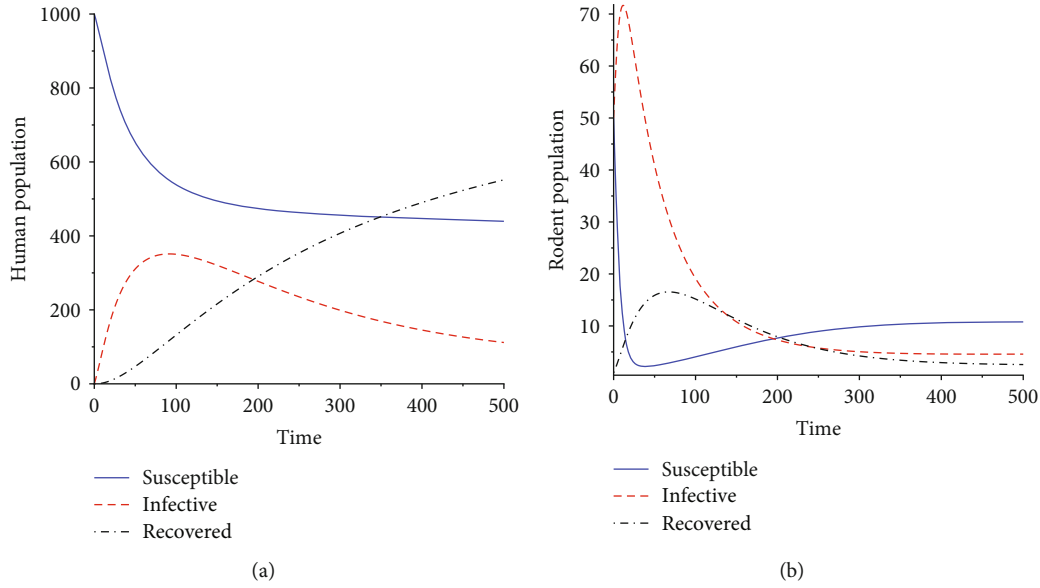
FIGURE 4: Transient solution of the system with the presence of culling to the rodent so that the death rate of the rodents increases up to twice the existing death rate, resulting in an effective reproduction number as low as $\mathscr{R}_0^e = 1.66$. However, this level of culling rate is not sufficient to eliminate the hantavirus.
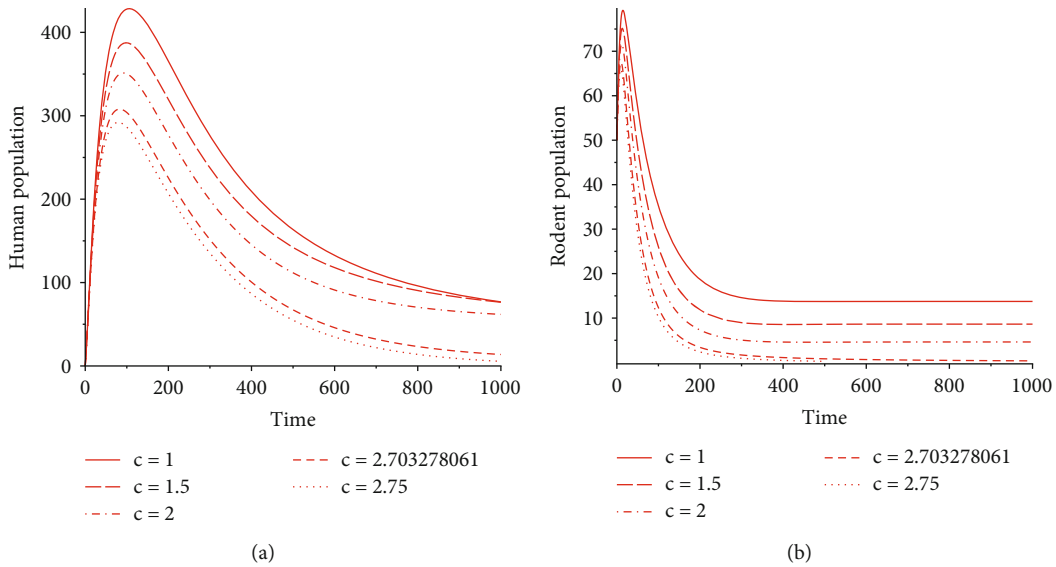
FIGURE 5: The effect of different culling levels of c to the number of infected human and infected rodent subpopulations. The critical culling level is $c = 2.703278061$, meaning that culling with a level lower than that level will not be effective in eliminating the hantavirus.

For comparison, we initially consider that there are 1,000 human individuals and 100 rodents in an environment. If it is assumed that there are no hantavirus-infected rats, both populations grow independently towards their respective equilibrium, as illustrated in Figure 2. In the absence of hantavirus, the growth of healthy human and rodent populations is depicted in the solid lines in Figures 2(a) and 2(b), respectively. Now, in the presence of hantavirus, if it is assumed that there is 1 infected rodent entering the system, the growth of the healthy or susceptible populations is shown in dash-dot lines in Figures 2(a) and 2(b), respectively. Compared to the case of the absence of hantavirus

infection, both subpopulations are lower due to the infection of hantavirus and change their status to infected population. The dashed lines in the figures show the growth for different bigger infected rodent initial values (50 individuals). In the long term, in the presence of hantavirus, all subpopulations will converge to the equilibrium state as predicted by the stability theorem of the endemic state.

For the purpose of comparison, the following examples will assume a high basic reproduction number (chosen by the appropriate parameters above), and the hantavirus is heavily circulated among rodents, as indicated by the high initial value of infected rodents $S_R(0) = 50$, $I_R(0) = 50$, and
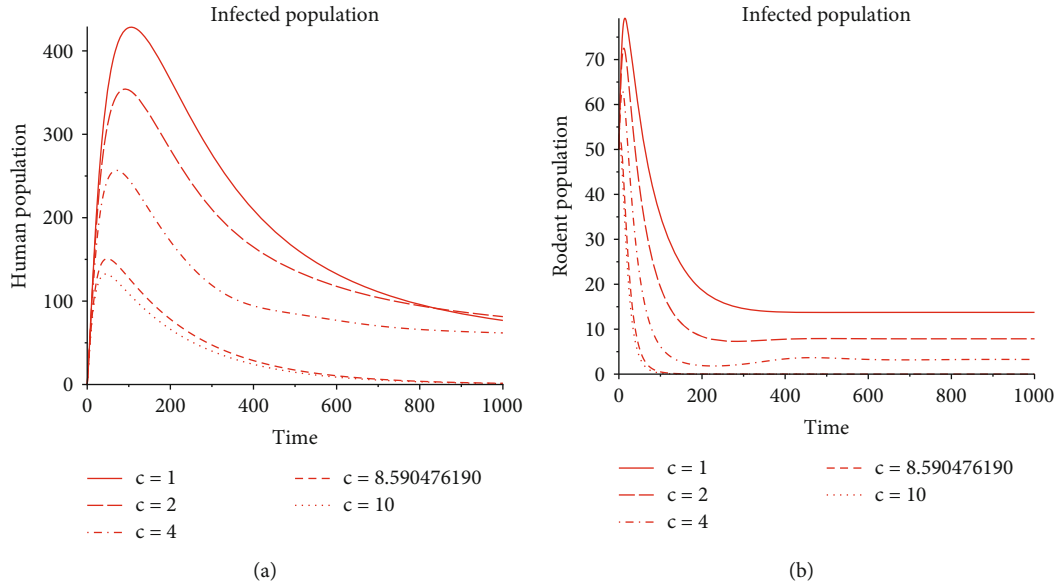
FIGURE 6: The effect of different curing levels of c to the number of infected human and infected rodent subpopulations. The critical curing level is $c = 8.590476190$, meaning that curing with a level lower than that level will not be effective in eliminating the hantavirus.
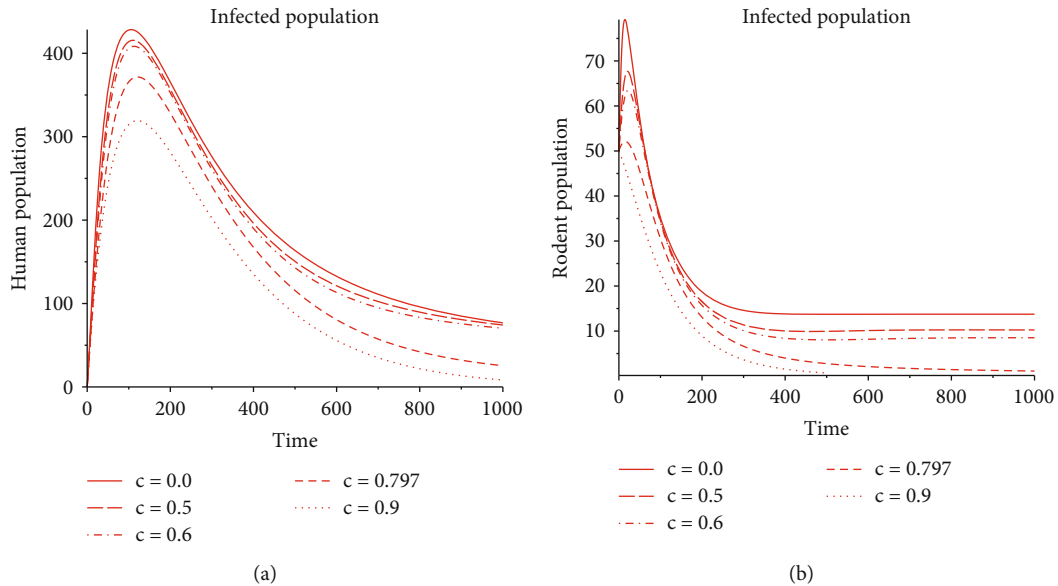
FIGURE 7: The effect of different isolation levels of c to the number of infected human and infected rodent subpopulations. This intervention can also be interpreted as vaccination. The critical isolation level is $c = 0.797$.

$R_R(0) = 1$. These initial values are chosen arbitrarily, just for illustration. The growth of all subpopulations is shown in Figure 3.

Figure 3 shows the transient solution of the system for human subpopulations (Figure 3(a)) and rodent subpopulations (Figure 3(b)). The lower figures show a near-equilibrium solution for human subpopulations (Figure 3(c)) and rodent subpopulations (Figure 3(d)). The resulting basic reproduction number for the chosen parameters indicates that the disease will become endemic eventually. To control the transmission of the hantavirus, we assume that culling is done to increase the death rate of the rodent up to twice the current

death rate. The resulting solution of the system is shown in Figure 4 with the effective reproduction number $\mathscr{R}_0^e = 1.66$. This culling is not effective in eliminating the hantavirus, both in rodent and human population. This level of culling is not sufficient to drive the hantavirus to extinction. In fact, by referring to Table 2 regarding the critical intervention level, to increase the rodent death rate from μ_R to a higher mortality $\mu'_R = c\mu_R$, we need to set $c > 2.703278061$ which makes the effective reproduction number less than one. Figure 5 shows the resulting solution of the system when culling as the intervention on the rodent population is undertaken at various levels of c. Figure 6 shows the resulting solution of the system

(a)

(b)
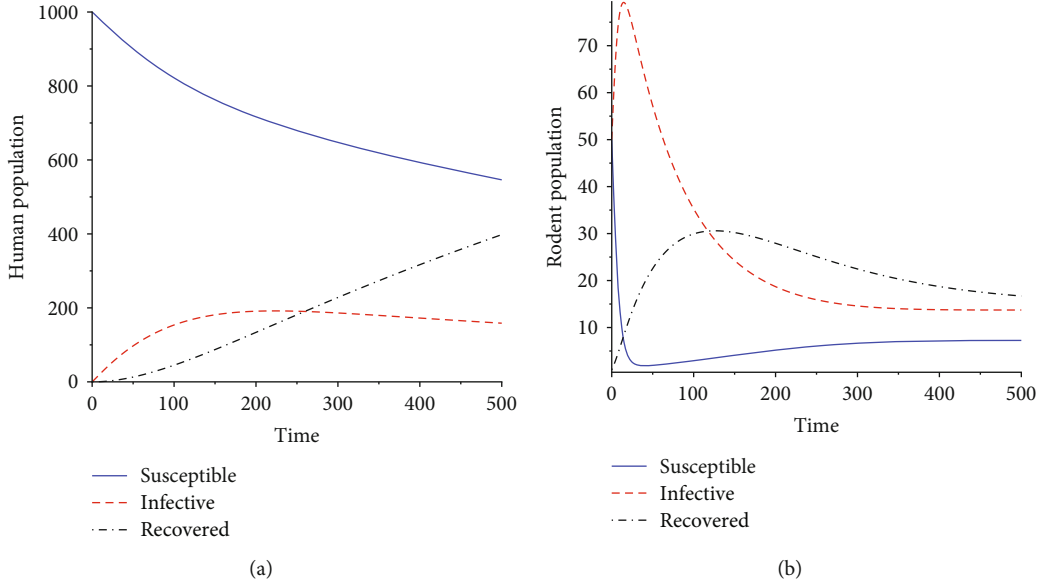
FIGURE 8: An example of the effect of saturated incidence on the number of infected human and infected rodent subpopulations. In this example, we use the functional form $\beta_H S_H(t)(I_R(t)/1 + \alpha I_R(t))$ with $\alpha = 0.05$ instead of $\beta_H S_H(t) I_R(t)$.

for the same parameters as in Figures 4 and 5, when curing as the intervention to the rodent population is undertaken for various levels of c, with the critical curing level is $c = 8.590476190$. This kind of intervention is not common, but it is feasible in terms of application technique since it is analogous to poisoning but with a different objective, i.e., to increase the recovery rate of the infected rodents. Figure 7 shows the resulting solution of the system when isolation to make contact among rodents is applied for various levels of c, with a critical isolation level of $c = 0.767$. This intervention can be viewed mathematically as similar to vaccination; hence, the critical isolation level is analogous to herd immunity to some extent. In reality, this intervention is also uncommon and difficult to implement since we have to vaccinate at least 76.7% of the rodent population unless vaccination can be implemented orally in the form of food bait for the rodents.

The results above are derived by assuming a mass action incidence rate and ignoring the presence of time delays. The results may be different if we do a fine-tuning to the model with the inclusion of more detailed and relevant factors. As an example, we show that if a saturated incidence rate as in Zhang et al. [52] is used in the present model, the solutions in Figure 3 change to those in Figure 8. Other information that also needs to be uncovered is the effect of the uncertainty of the parameters. In the following section, we present one way to analyze the effect of parameter uncertainty on the number of infected human population. We would like to derive the sensitivity indices to see which parameters are most influential on the results of the model (in this case, the number of infected human population).

4.1. Sensitivity Analysis. As most of the parameters have strong uncertainty, we perform a global sensitivity analysis to identify the most influential parameters of the model. It is measured against the increasing number of infected individuals. There are a lot of sensitivity analysis methods, such
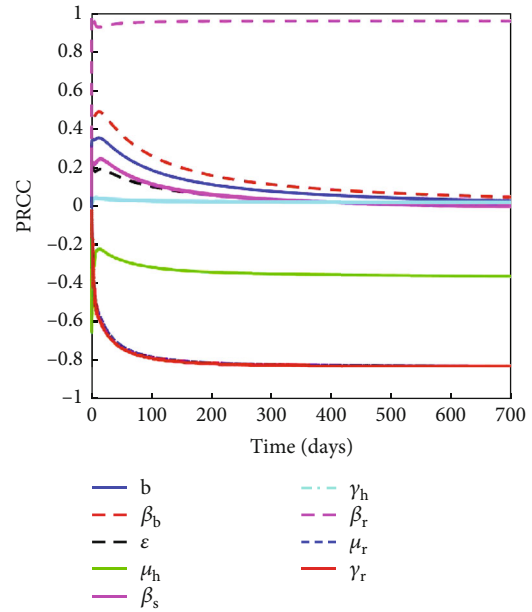
FIGURE 9: The PRCC plot shows the probability of successful contact between rodents β_r is the most influential parameter and has a positive relationship. Meanwhile, the parameters μ_r and γ_r have a negative relationship, which indicates that an increase in these parameter values results in a decrease in the number of hantavirus infections.

as Chitnis et al. [53], Marino et al. [54], and the references therein. Here, we use Latin hypercube sampling (LHS) in combination with the partial rank correlation coefficient (PRCC) [54] since it is among the most popular, reliable, and efficient sensitivity analyses to provide global sensitivity indexes. By following the method of Marino et al. [54], we simulate 2,000 samples, and the result is given in Figure 9. The range of the parameters used is given in Table 3.

TABLE 3: Parameters and the range of parameter values used in sensitivity analysis.

Parameters	Minimum	Expected	Maximum
b	0	1	2
β_b	0	0.1	1
ϵ	0	0.1	1
μ_h	$1/(80 \times 365)$	$1/(65 \times 365)$	$1/(50 \times 365)$
β_ε	0	0.02	1
γ_h	0.05	0.082	0.1
β_r	0	0.02	1
μ_r	0	0.02	0.5
γ_r	0	0.02	0.5

Note that there is a slight difference to notation in the schematic diagram (Figure 1). This difference is clarified by recalling $\bar{\varepsilon}(I_R(t)) = \varepsilon I_R(t)$ and $b \beta_H' = (\bar{b}\beta_b + \varepsilon\beta_\varepsilon)$ as indicated in the text.

Figure 9 shows that the probability of successful contact between rodents β_r is the most influential parameter and has a positive relationship. This is realistic as the rodent is the source of infections, and hence, when humans and rodents interact and they successfully transmit viruses, the number of hantavirus cases increases. On the other hand, the parameters μ_r and γ_r have a negative relationship, which indicates that an increase in these parameter values results in a decrease in the number of hantavirus infections. An increase in the death rate of rodents aids in minimizing the number of hantavirus cases.

The figure shows that the greatest effect of intervention to control the spread of hantavirus is by reducing the contact rate between rodents β_r and by increasing the death rate and recovery rate parameters μ_r and γ_r. In reality, interventions to control the contact rate between rodents are difficult to implement, but increasing the death rate can be done much easier by nonclinical interventions, such as trapping, culling, and poisoning. Theoretically, increasing rodent recovery can also be implemented by using "drug food," although uncommon.

5. Conclusion

We have constructed a simple mathematical model for the transmission of hantavirus among rodents. Apart from the simpleness of the model, we arrive at the following useful insight. The analysis of the model shows that if the basic reproduction number is greater than one, then it is impossible to completely eliminate hantavirus disease in the system by solely focusing on any intervention to humans, like vaccination and curative action, without paying any attention to interventions to the rodent population unless there is no contact at all between human and rodent or between human and rodents' excreta or the successful probability contact rate is zero. However, we can still decrease the density of infected humans with those interventions. Hence, we suggest that a combination of several interventions is needed to obtain effective control in eliminating the hantavirus. Fur-

ther, to determine the most significant parameters that can be used as control variables to reduce or eliminate hantavirus transmission, we use the Latin hypercube sampling in combination with partial rank correlation coefficient sensitivity analysis and found that the contact rate between rodents, the death rate, and the recovery rate of rodent's parameters are among the most significant parameters in determining both the numbers of infected rodents and infected humans. This justifies our first finding that solely focusing on intervention to humans may not succeed in completely eliminating hantavirus infection in the system. Moreover, this information is useful for further study in finding an optimal control strategy to reduce or eliminate the transmission of hantavirus to humans.

Data Availability

The data supporting the results of our study can be found in the article itself.

Conflicts of Interest

The authors declare that there are no conflicts of interest regarding the publication of this paper.

Acknowledgments

References

[1] Florida Health, "Rodents," 2021, https://www.floridahealth.gov/environmental-health/rodents/index.html.

[2] T. M. Fink, "Rodents, human remains, and north American hantaviruses: risk factors and prevention measures for forensic science personnel–a review," *Journal of Forensic Sciences*, vol. 41, no. 6, pp. 1052–1056, 1996.

[3] J. Toledo, M. M. Haby, L. Reveiz, L. Sosa Leon, R. Angerami, and S. Aldighieri, "Evidence for human-to-human transmission of hantavirus: a systematic review," *The Journal of Infectious Diseases*, vol. 13, pp. 1362–1371, 2021.

[4] Wibowo, "Epidemiologi hantavirus di Indonesia," Buletin Penelitian Kesehatan, 2010.

[5] H. Jiang, X. Zheng, L. Wang, H. Du, P. Wang, and X. Bai, "Hantavirus infection: a global zoonotic challenge," *Virologica Sinica*, vol. 32, no. 1, pp. 32–43, 2017.

[6] M. F. Abdul Karim, A. I. Md Ismail, and H. B. Ching, "Cellular automata modelling of hantarvirus infection," *Chaos, Solitons & Fractals*, vol. 41, no. 5, pp. 2847–2853, 2009.

[7] M. C. Monroe, S. P. Morzunov, A. M. Johnson et al., "Genetic diversity and distribution of Peromyscus-borne hantaviruses in North America," *Emerging Infectious Diseases*, vol. 5, no. 1, pp. 75–86, 1999.

[8] A. Plyusnin and S. P. Morzunov, "Virus evolution and genetic diversity of hantaviruses and their rodent hosts," *Current Topics in Microbiology and Immunology*, vol. 256, pp. 47–75, 2001.

[9] J. N. Mills, T. L. Yates, T. G. Ksiazek, C. J. Peters, and J. E. Childs, "Long-term studies of hantavirus reservoir populations in the southwestern United States: rationale, potential and methods," *Emerging Infectious Diseases*, vol. 5, no. 1, pp. 95–101, 1999.

[10] CDC, "Hantavirus pulmonary syndrome—United States: updated recommendations for risk reduction," *Morbidity and Mortality Weekly Report*, vol. 51, no. RR09, pp. 1–12, 2002.

[11] G. Abramson and V. M. Kenkre, "Spatiotemporal patterns in the hantavirus infection," *Physical Review E*, vol. 66, no. 1, 2002.

[12] Z. Bi, P. B. Formenty, and C. E. Roth, "Hantavirus infection: a review and global update," *The Journal of Infection in Developing Countries*, vol. 2, no. 1, pp. 3–23, 2008.

[13] Y. Z. Zhang, D. L. Xiao, Y. Wang et al., "The epidemic characteristics and preventive measures of hemorrhagic fever with renal syndrome in China," *Chinese Journal of Epidemiology*, vol. 25, pp. 466–469, 2004.

[14] WHO, "Hantavirus in the americas guidelines for diagnosis, treatment, prevention, and control," PAHO Technical paper no 47, Pan American Sanitary Bureau, Regional Office of the World Health Organization, 1999.

[15] J. Arikawa, K. Yoshimatsu, and H. Kariwa, "Epidemiology and epizootiology of hantavirus infection in Japan," *Japanese Journal of Infectious Diseases*, vol. 54, no. 3, pp. 95–102, 2001.

[16] A. Suyanto, *Field Guide: Rodent in Java (Panduan Lapangan: Rodent di Jawa)*, Pusat Penelitian Biologi LIPI, Bogor, 2006.

[17] A. Mulyono, F. D. Ristiyanto Handayani, L. Susanti, and J. Raharjo, "New record of hantavirus reservoir from Central Java Province, Indonesia," Balai Besar Penelitian dan Pengembangan Vektor dan Reservoir Penyakit (B2P2VRP) Salatiga, 2017.

[18] I. Sendow, N. L. P. I. Dharmayanti, M. Saepullah, and R. M. A. Adjid, "Hantavirus Infection: Anticipation of Zoonotic Disease in Indonesia," *Indonesian Bulletin of Animal and Veterinary Sciences*, vol. 26, no. 1, pp. 017–026, 2016.

[19] Wibawa, "Hantavirus," 2002, https://dinkes.kulonprogokab.go.id/detil/682/hantavirus.

[20] CFSH, "Hantavirus disease," 2018, https://www.cfsph.iastate.edu/Factsheets/pdfs/hantavirus.pdf.

[21] C. B. Jonsson, L. T. Figueiredo, and O. Vapalahti, "A global perspective on hantavirus ecology, epidemiology, and disease," *Clinical Microbiology Reviews*, vol. 23, no. 2, pp. 412–441, 2010.

[22] D. H. Krüger, R. Ulrich, and Å. Lundkvist, "Hantavirus infections and their prevention," *Microbes and Infection*, vol. 3, no. 13, pp. 1129–1144, 2001.

[23] ECDC, "Prevention measures and communication strategies for hantavirus infection in Europe," in *European Centre for Disease Prevention and Control*, ECDC, Stockholm, 2014.

[24] J. L. Kerins, S. E. Koske, J. Kazmierczak et al., "Outbreak of Seoul virus among rats and rat owners — United States and Canada, 2017," *Morbidity and Mortality Weekly Report*, vol. 67, no. 4, pp. 131–134, 2018.

[25] H. W. Cho and C. R. Howard, "Antibody responses in humans to an inactivated hantavirus vaccine (Hantavax)," *Vaccine*, vol. 17, no. 20-21, pp. 2569–2575, 1999.

[26] R. Liu, H. Ma, J. Shu et al., "Vaccines and therapeutics against hantaviruses," *Frontiers in Microbiology*, vol. 10, p. 2989, 2020.

[27] K. Dheerasekara, S. Sumathipala, and R. Muthugala, "Hantavirus infections–treatment and prevention," *Current Treatment Options in Infectious Diseases*, vol. 12, no. 4, pp. 410–421, 2020.

[28] F. Saavedra, F. E. Díaz, A. Retamal-Díaz, C. Covián, P. A. González, and A. M. Kalergis, "Immune response during hantavirus diseases: implications for immunotherapies and vaccine design," *Immunology*, vol. 163, no. 3, pp. 262–277, 2021.

[29] G. Abramson, V. M. Kenkre, T. L. Yates, and R. R. Parmenter, "Traveling waves of infection in the hantavirus epidemics," *Bulletin of Mathematical Biology*, vol. 65, no. 3, pp. 519–534, 2003.

[30] F. Sauvage, M. Langlais, N. G. Yoccoz, and D. Pontier, "Modelling hantavirus in fluctuating populations of bank voles: the role of indirect transmission on virus persistence," *Journal of Animal Ecology*, vol. 72, pp. 1–13, 2003.

[31] L. J. S. Allen, E. J. Allen, and C. B. Jonsson, "The impact of environmental variation on hantavirus infection in rodents," in *Mathematical Studies on Human Disease Dynamics: Emerging Paradigms and Challenges 1–15, Contemporer Mathematics, Volume 410*, pp. 1–15, American Mathematical Society, Providence, RI, 2006.

[32] L. J. S. Allen, R. K. McCormack, and C. B. Jonsson, "Mathematical models for hantavirus infection in rodents," *Bulletin of Mathematical Biology*, vol. 68, no. 3, pp. 511–524, 2006.

[33] L. J. S. Allen, M. Langlais, and C. J. Phillips, "The dynamics of two viral infections in a single host population with applications to hantavirus," *Mathematical Biosciences*, vol. 186, no. 2, pp. 191–217, 2003.

[34] L. J. S. Allen, C. L. Wesley, R. D. Owen et al., "A habitat-based model for the spread of hantavirus between reservoir and spillover species," *Journal of Theoretical Biology*, vol. 260, no. 4, pp. 510–522, 2009.

[35] F. L. Alvarez and R. Salinas, "Construction of hazard maps of hantavirus contagion using remote sensing, logistic regression and artificial neural networks: case Araucanía Region, Chile," 2016, http://arxiv.org/abs/1610.01493v1.

[36] C. Escudero, J. Buceta, F. de la Rubia, and K. Lindenberg, "Effects of internal fluctuations on the spreading of hantavirus," *Physical Review E*, vol. 70, no. 6, article 061907, 2004.

[37] Y. K. Chu, R. Owen, D. Goodin, L. Allen, and C. Jonsson, "Co-circulation of two different hantaviruses in a hectare sized mark-recapture sites in interior Atlantic forest in Paraguay 2009," *American Journal of Tropical Medicine and Hygiene*, vol. 77, no. 5, pp. 265-266, 2007.

[38] C. L. Wesley, "Discrete-time and continuous-time models with applications to the spread of hantavirus in wild rodents and human populations, [Ph.D. thesis]," Texas Tech University, Lubbock, Texas, USA, 2008.

[39] C. L. Wesley, L. J. S. Allen, and M. Langlais, "Models for the spread and persistence of hantavirus infection in rodents with direct and indirect transmission," *Mathematical Biosciences and Engineering*, vol. 7, no. 1, pp. 195–211, 2010.

[40] G. Abramson, "Mathematical modeling of hantavirus: from the mean field to the individual level," in *Progress in Mathematical Biology Research*, J. T. Kelly, Ed., pp. 1–27, Nova Science Publishers Inc., New York, NY, USA, 2008.

[41] S. Z. Rida, A. S. Abdel Rady, A. A. Arafa, and M. Khalil, "The effect of the environmental parameter on the hantavirus infection through a fractional-order SI model," *International Journal of Basic and Applied Sciences*, vol. 1, pp. 88–99, 2012.

[42] S. M. Goh, A. I. M. Ismail, M. S. M. Noorani, and I. Hashim, "Dynamics of the hantavirus infection through variational

iteration method," *Nonlinear Analysis: Real World Applications*, vol. 10, pp. 2171–2176, 2009.

[43] M. Kaplan, C. A. Manore, and K. H. Bagamian, "Agent-based hantavirus transmission model incorporating host behavior and viral shedding heterogeneities derived from field transmission experiments," *Letters in Biomathematics*, vol. 3, no. 1, pp. 209–228, 2016.

[44] R. Bürger, G. Chowell, E. Gavilán, P. Mulet, and L. M. Villada, "Numerical solution of a spatio-temporal gender-structured model for hantavirus infection in rodents," *Mathematical Biosciences and Engineering*, vol. 15, no. 1, pp. 95–123, 2017.

[45] F. M. Yusof, A. I. M. Ismail, and N. M. Ali, "Modeling population harvesting of rodents for the control of hantavirus infection," *Sains Malays*, 2010.

[46] M. F. Yusof, F. A. Abdullah, and M. A. I. Ismail, "Modeling and optimal control on the spread of hantavirus infection," *Mathematics*, vol. 7, no. 12, p. 1192, 2019.

[47] O. Diekmann and J. A. P. Heesterbeek, *Mathematical Epidemiology of Infectious Diseases: Model Building, Analysis and Interpretation*, Wiley, New York, NY, USA, 1st edition, 2000.

[48] O. Diekmann, J. A. P. Heesterbeek, and J. A. J. Metz, "On the definition and the computation of the basic reproduction ratio R_0 in models for infectious diseases in heterogeneous populations," *Journal of Mathematical Biology*, vol. 28, no. 4, pp. 365–382, 1990.

[49] O. Diekmann, J. A. P. Heesterbeek, and M. G. Roberts, "The construction of next-generation matrices for compartmental epidemic models," *J. R. Soc. Interface*, vol. 7, no. 47, pp. 873–885, 2010.

[50] P. Van den Driessche and J. Watmough, "Reproduction numbers and sub-threshold endemic equilibria for compartmental models of disease transmission," *Mathematical Biosciences*, vol. 180, pp. 29–48, 2002.

[51] X. Q. Zhao, "The theory of basic reproduction ratios," in *Dynamical Systems in Population Biology*, Springer Nature Switzerland AG, Cham, Switzerland, 2003.

[52] J. Zhang, J. Jia, and X. Song, "Analysis of an SEIR epidemic model with saturated incidence and saturated treatment function," *The Scientific World Journal*, vol. 2014, Article ID 910421, 11 pages, 2014.

[53] N. Chitnis, J. M. Hyman, and J. M. Cushing, "Determining important parameters in the spread of malaria through the sensitivity analysis of a mathematical model," *Bulletin of Mathematical Biology*, vol. 70, no. 5, pp. 1272–1296, 2008, Epub 2008 Feb 22.

[54] S. Marino, I. B. Hogue, C. J. Ray, and D. E. Kirschner, "A methodology for performing global uncertainty and sensitivity analysis in systems biology," *Journal of Theoretical Biology*, vol. 254, no. 1, pp. 178–196, 2008.

Hindawi

Research Article

Dynamical Analysis on a Malaria Model with Relapse Preventive Treatment and Saturated Fumigation

Dipo Aldila [ID]

Department of Mathematics, Universitas Indonesia, Depok 16424, Indonesia

Correspondence should be addressed to Dipo Aldila; aldiladipo@sci.ui.ac.id

Malaria has produced health issues in many parts of the world. One of the reason is due to the recurrence phenomenon, which can happen years after the main infection has appeared in the human body. Furthermore, the fumigation intervention, which has become a major worry in several regions of the world, has yielded unsatisfactory results, as seen by the high number of cases reported each year in several African countries. We present a novel mathematical model that integrates tafenoquine treatments to prevent relapse in the human population and saturation fumigation to control mosquito populations in this study. The endemic threshold, also known as the basic reproduction number, is calculated analytically, as is the existence and local stability of the equilibrium points. Through careful investigation, we discovered that the malaria-free equilibrium is locally asymptotically stable if the basic reproduction number is less than one and unstable if it is greater than one. According to the sensitivity analysis, the utilization of tafenoquine treatment is inversely proportional to the basic reproduction number. Although our model never exhibits a backward bifurcation at the basic reproduction number equal to one, we have demonstrated that it is possible; when the basic reproduction number is greater than one, two stable malaria-endemic equilibrium can exist. As a result, when the basic reproduction number is more than one, the final state will be determined by the initial condition of the population. As a result, enormous temporal fumigation can shift the stability of our malaria model from a big endemic size to a smaller endemic size, which is more advantageous in terms of the malaria prevention strategy. Despite the fact that this is not a case study, the numerical results presented in this article are intended to support any theoretical analysis of current malaria eradication tactics in the field.

1. Introduction

Malaria is a vector-borne disease caused by the bite of a female mosquito that has been infected with Plasmodium. Of more than 100 species, only five Plasmodium species cause malaria, namely, Plasmodium vivax, Plasmodium malaria, Plasmodium falciparum, Plasmodium knowlesi, and Plasmodium ovale [1]. When this Plasmodium has entered the human bloodstream, it will attack several vital organs in the human body, especially the liver and red blood cells [2]. People who have been infected with malaria will show a variety of symptoms, including chills, fever, and headache, which can even result in death in most cases in the pediatric population.

Until now, there have been many interventions launched by governments in various countries in the world to tackle the spread of malaria. These interventions include the use of vaccines, treatment, use of insecticide-treated bed nets (ITN), and vector control with fumigation and larvicides [3]. Among these mentioned interventions, vector control with fumigation is considered as the most promising and easiest policy to implement [1]. However, several problems in its implementation arise, such as the tendency of mosquitoes to become resistant to fumigants when the intervention is not well controlled [4] or the problem of limited implementation costs. In some cases in the field, the high fumigation intensity needs to be reduced when infected people are too high. This is due to the difficulty of implementation in the field when intervention costs must also be allocated to treatment for infected individuals in the hospitals.

Vaccines for malaria have become one of the main concerns of governments in many parts of the world and the

World Health Organization [5]. In 2021, the R21/Matrix-M vaccine has been investigated to be the second malaria vaccine, and it is stated that it has reached the minimum efficacy limit required by WHO, which is a minimum efficacy of 75% [6]. This type of vaccine has an efficacy level of 77% to reduce the chance of successful infection in humans due to an infected female Anopheles mosquito bite. In addition to vaccination, treatment interventions are also needed to prevent the severity or incidence of relapse in malaria patients. Until now, it was stated that *primaquine* was the primary drug used to avoid relapse in individuals infected with malaria. However, because this drug has to be taken on a regular basis (every 14 days), it has resulted in many treatments not being successful [7]. Therefore, MMV and GlaxoSmithKline (GSK) collaborated to develop a new malaria drug known as *tafenoquine*, which is a single dose treatment for preventing relapse in malaria-infected individuals [8].

The complexity of malaria has attracted the attention of many researchers to take part in efforts to understand the mechanism of spread and the best intervention for malaria. This is due to the complexity of its infection mechanism, such as recurrence phenomena (relapse, reinfection, and recrudescence), to the problem of the most appropriate intervention. Among these researches, mathematical modeling would play an essential role. Many authors have introduced mathematical models to understand how malaria spreads among human and mosquito populations. The first mathematical model for malaria was introduced by Ross in the early 19th century [9], where he introduced the mechanism of malaria transmission involving mosquito and human populations in his model. Ross' research was then continued by Macdonald [10] where he introduced the concept of basic reproduction number in his model. Since then, many mathematical models have been introduced by researchers to understand various important factors in the spread of malaria. Authors in [11] proposed a malaria model considering immunological memory which boost protection of reinfection phenomenon. Two host types in malaria transmission are discussed by author in [12]. Furthermore, a two-age class model for malaria transmission is discussed in [13]. A periodic biting rate of malaria mosquitoes is modelled by author in [14]. They used Floquet theory to analyze the stability of their model. Recently, author in [15] proposed a malaria model with optimal control on saturated treatment rate. Another new strategy of transmission blocking drugs for malaria is modelled by Wu and Hu in [16]. They found that increasing the transmission blocking drugs is a more pronounced effect compared to treatment intervention. Another important factors have been discussed through mathematical models such as vector-bias effect [15, 17], relapse [18, 19], reinfection [20, 21], fumigation [15, 22], temperature and seasonality [23–25], impact of Wolbachia [26], and coinfection [27]. However, the best that we know, there is no mathematical model considering the impact of potential new treatment (tafenoquine) into their model.

In this paper, we introduce and investigate a new mathematical model on malaria transmission. In this model, we divide the human population into five epidemiological classes based on their health status while the mosquito population into two epidemiological classes. Several vital factors were introduced into our model: the effect of a potential new treatment for malaria to prevent relapse; vector-bias phenomena where mosquitoes are more attracted to bite the infected individuals; and fumigation intervention which depends on the number of infected individuals at time t. We perform our mathematical analysis to show the existence of a forward bifurcation and forward hysteresis phenomena on our model, which allows the possibility of existence of three different endemic equilibrium, where two of them is locally stable. Based on this phenomenon, we show from a numerical simulation that a massive fumigation intervention in a limited time window can change the dynamic direction of the system from a large endemic equilibrium to a smaller endemic point. We also show a sensitivity analysis to determine the most influential parameter to our model.

This paper is organized as follows. We formulate our model in Section 2. The stability of the malaria-free equilibrium point and the form of the respected basic reproduction number are shown in Section 3. In Section 4, we analyze the existence of the malaria-endemic equilibrium point. In addition, we show the possible forward hysteresis from our model in this section. Some numerical experiments on the proposed model are shown in Section 5. Finally, some relevant conclusions are given in the last section.

2. Mathematical Model Formulation

The proposed dynamic model for malaria transmission in this article is inspired by our previous work in [15], by taking into account two important factors. The first factor involved in our new model is the involvement of a malaria relapse prevention drug intervention (for example, tafenoquine [28]). The second factor involves fumigation intervention which is not a monotonous function. We assume that when the number of humans infected with malaria is approaching the outbreak, the intervention given can be quite large. However, when the number of infected people continues to grow, efforts for fumigation will be reduced because of the difficulty of intervention during the outbreak.

This model divides the human population based on their health status and whether they received any malaria treatment or not. Hence, let human population be divided into five epidemiological classes: susceptible (S), latent (E), infected (I), exposed treated (T), and recovered (R). On the other hand, we classify mosquito population only into two classes: susceptible (U) and infected (W). The latent individual is an individual who has already been exposed to malaria and has Plasmodium in their lever. If an individual in E gets treated with tafenoquine to prevent relapse, then they will be classified into the class of T. Only infected individual (I) can transmit the Plasmodium into the susceptible mosquito. Based on this assumption, we have the total human population which is given by

$$N_h = S + E + T + I + R, \tag{1}$$

and the total mosquito population is given by

$$N_v = U + W. \tag{2}$$

The malaria model is governed by the following system of ordinary differential equations:

$$
\begin{aligned}
\frac{dS}{dt} &= \Lambda_h - \Pi_h(N, W) - \mu_h S + \xi R, \\[4pt]
\frac{dE}{dt} &= \Pi_h(N, W) - (u_1 + \eta + \mu_h)E, \\[4pt]
\frac{dT}{dt} &= u_1 E - ((1 - p)\delta + p\kappa + \mu_h)T, \\[4pt]
\frac{dI}{dt} &= (1 - p)\delta T + \eta E - (\gamma + \mu_h)I, \\[4pt]
\frac{dR}{dt} &= p\kappa T + \gamma I - (\mu_h + \xi)R, \\[4pt]
\frac{dU}{dt} &= \Lambda_v - \Pi_v(N, U) - (\mu_v + \Psi(I, u_2))U, \\[4pt]
\frac{dW}{dt} &= \Pi_v(N, U) - (\mu_v + \Psi(I, u_2))W,
\end{aligned}
\tag{3}
$$

where $\Pi_h(N, W)$ and $\Pi_v(N, U)$ are the infection rate in human and mosquito population, respectively, while $\Psi(I, u_2)$ presents the fumigation effectiveness factors.

The per capita of birth on humans and mosquitoes is denoted by Λ_h and Λ_v, respectively. The natural death rate of humans and mosquitoes is given by μ_h and μ_v, respectively. Furthermore, parameters u_1 and u_2 present medical treatment intervention with tafenoquine and vector control with fumigation, respectively. Let p be the proportion of exposed individuals who get tafenoquine and succeeded in avoiding relapse after κ^{-1} duration of treatment. On the other hand, we assume that the $1 - p$ proportion of individuals in T failed in treatment. Hence, we have $(1 - p)\delta T$ as the transition from T to I due to treatment failure, where δ^{-1} is the incubation period of Plasmodium with the effect of tafenoquine. We denote that the recovery rate from malaria is γ, while ξ^{-1} is the duration of temporal immunity.

We construct the force of infection in human ($\Pi_h(N, W)$) as follows. Let b be the average bite per mosquito per day. In our model, we take into account the preference of mosquito to be more attracted to bite infected human, rather than noninfected human. This phenomenon is commonly known as "vector-bias" phenomenon [29]. Based on this "vector-biased" assumption, the probability of a mosquito encountering a susceptible human is given by $S/(S + E + T + \alpha I + R)$, where $\alpha > 1$ is the vector-bias parameter. Hence, total bite of all mosquito per day is given by $bW(S/(S + E + T + \alpha I + R))$. Assuming v_h as the probability that the bite of infected mosquito succeeded in infecting susceptible human, then $bv_h W(S/(S + E + T + \alpha I + R))$ present the total of susceptible human who get infected by malaria per time. Since b and v_h are constant parameters with a dimension

of bite/day and 1/(bite × mosquito), respectively, we assume $\beta_h := bv_h$. Therefore, we have that

$$\Pi_h(N, W) = \beta_h W \frac{S}{S + E + T + \alpha I + R}. \tag{4}$$

Using a similar approach, let v_v be the probability of successful infection in mosquitoes; the force of infection on mosquitoes is given by

$$\Pi_v(N, U) = \beta_v U \frac{\alpha I}{S + E + T + \alpha I + R}, \tag{5}$$

where $\beta_v := bv_v$ with a dimension of bite/day and 1/(bite × human) for b and v_v, respectively.

Now, we construct our fumigation term $\Psi(I, u_2)$. We assume that the fumigation intervention depends on the number of infected individuals. Indicators of the endemic of malaria in the field can not be seen from the number of infected mosquitoes, but it can be identified by the high number of infected individuals which is reported in the media. When the number of infected individuals increases, then the intensity of fumigation will increase. However, when the number of infected individuals increases more significantly, then the effectiveness of fumigation will decrease since the policymaker may concentrate more on the number of infected individuals in the hospital, which makes them overwhelmed to control vector population in the field. Hence, we assume that $\Psi(I, u_2)$ should have the following properties:

(i) When the number of the infected individual is zero, then the fumigation intervention is zero. Hence, we have $\Psi(0, u_2) = 0$

(ii) The fumigation intervention increases at the beginning when the number of infected individual start to increase but will decrease when the number of infected individual is sufficiently large. Hence, we have that $((\partial \Psi(I, u_2))/\partial I) > 0$ for $I \in (0, I^{\text{critical}})$ and $((\partial \Psi(I, u_2))/\partial I) \leq 0$ for $I \in [I^{\text{critical}}, \infty)$. Note that I^{critical} denote the critical number of I when the policymaker is already overwhelmed to conduct an effective fumigation intervention in the field

Based on the above assumption, we model our fumigation intervention as

$$\Psi(I, u_2) = u_2 \frac{I}{a + I^2}, \tag{6}$$

where $a > 0$ is the saturated coefficient.

According to the mentioned assumptions on the infection and fumigation functions, system (3) now is read as

$$\frac{dS}{dt} = \Lambda_h - \beta_h W \frac{S}{S + E + T + \alpha I + R} - \mu_h S + \xi R,$$

$$\frac{dE}{dt} = \beta_h W \frac{S}{S + E + T + \alpha I + R} - (u_1 + \eta + \mu_h)E,$$

$$\frac{dT}{dt} = u_1 E - ((1-p)\delta + p\kappa + \mu_h)T,$$

$$\frac{dI}{dt} = (1-p)\delta T + \eta E - (\gamma + \mu_h)I,$$

$$\frac{dR}{dt} = p\kappa T + \gamma I - (\mu_h + \xi)R,$$

$$\frac{dU}{dt} = \Lambda_v - \beta_v U \frac{\alpha I}{S + E + T + \alpha I + R} - \left(\mu_v + u_2 \frac{I}{a + I^2}\right)U,$$

$$\frac{dW}{dt} = \beta_v U \frac{\alpha I}{S + E + T + \alpha I + R} - \left(\mu_v + u_2 \frac{I}{a + I^2}\right)W,$$

$$(7)$$

with a nonnegative initial conditions given at time $t = 0$. Figure 1 depicts the flow chart of our malaria transmission model. Biological interpretation and the unity of all parameters in system (7) are given in Table 1.

Let system (7) have an initial condition in the following set:

$$\mathcal{D} = \left\{ (S, E, T, I, R, U, W) \in \mathbb{R}_+^7 | S, U > 0, E, T, I, R, W \geq 0 \right\}.$$

$$(8)$$

To describe the feasible solution of system (7) and its biological interpretation, we have the following theorem.

Theorem 1. *For initial values in (8), malaria model in system (7) has a unique solution and remains in $\mathcal{D}$ for all time $t \geq 0$.*

Proof. Please see Appendix A for the proof. □

3. Malaria-Free Equilibrium and the Basic Reproduction Number

The first equilibrium point of our model is the malaria-free equilibrium point. This equilibrium present a situation where all nonsusceptible population do not exist in the equilibrium condition. For this reason, let $E = 0$, $T = 0$, $I = 0$, $R = 0$, and $W = 0$, and then, malaria-free equilibrium (MFE) is obtained by the following subsystem:

$$\frac{dS}{dt} = \Lambda_h - \mu_h S,$$

$$\frac{dU}{dt} = \Lambda_v - \mu_v U.$$

$$(9)$$
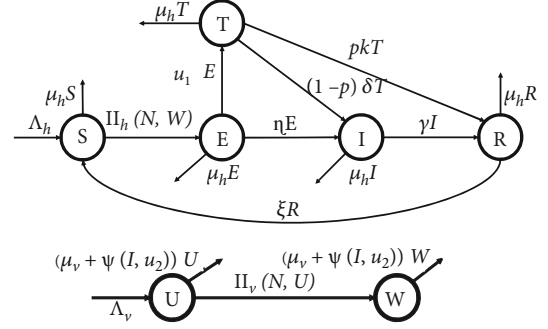
Figure 1: Transmission diagram of malaria model in (7).

Taking the right hand side of the above system, it follows that the malaria-free equilibrium of system (7) is given by

$$MFE = (S^*, E^*, T^*, I^*, R^*, U^*, W^*) = \left(\frac{\Lambda_h}{\mu_h}, 0, 0, 0, 0, \frac{\Lambda_v}{\mu_v}, 0\right).$$

$$(10)$$

To conduct further analysis on the qualitative behaviour of our model, it is important to determine the related basic reproduction number of our proposed model. In many epidemiological models, basic reproduction number holds an important role in determining that the diseases die out or exist in the population [34–38]. Basic reproduction number is defined as the expected number of secondary cases caused by one primary case during infection period in a completely susceptible population [39, 40]. The basic reproduction number is calculated using the next-generation matrix approach [41]. From system (7), we have that the infected compartments consist of E, T, I, and W. The Jacobian matrix of subsystem of infected compartment on system (7) evaluated in MFE can be written as $\mathcal{F} + \mathcal{V}$, where

$$\mathcal{F} = \begin{bmatrix} 0 & 0 & 0 & \beta_h \\ 0 & 0 & 0 & 0 \\ 0 & 0 & 0 & 0 \\ 0 & 0 & \frac{\beta_v \Lambda_v \alpha \mu_h}{\mu_v \Lambda_h} & 0 \end{bmatrix},$$

$$\mathcal{V} = \begin{bmatrix} -u_1 - \eta - \mu_h & 0 & 0 & 0 \\ u_1 & -(1-p)\delta - \kappa p - \mu_h & 0 & 0 \\ \eta & (1-p)\delta & -\gamma - \mu_h & 0 \\ 0 & 0 & 0 & -\mu_v \end{bmatrix},$$

$$(11)$$

TABLE 1: Biological interpretation of parameters in system (7).

Par	Description	Dimension	Value	Ref.
Λ_h	Number of newborn in human per day	Human/Day	$1000/65 \times 365$	[15]
Λ_v	Number of newborn in mosquitoes per day	Mosquitoes/Day	$1000/21$	[15]
β_h	Infection rate of mosquito to human	1/Mosquito × day	0.022	[30, 31]
β_v	Infection rate of human to mosquito	1/Human × day	0.24	[30, 31]
α	Vector-bias coefficient	—	4	[32]
u_1	Rate of treatment with tafenoquine	1/Day	[0,1]	Assumed
u_2	Vector control with fumigation	1/Day	[0,1]	Assumed
μ_h	Natural death rate of human	1/Day	$1/65 \times 365$	[15]
μ_v	Natural death rate of mosquito	1/Day	$1/21$	[30]
η	Natural incubation rate	1/day	0.0833	[18]
p	Proportion of treated individual who succeeds in treatment	—	0.8	Assumed
δ	Incubation rate due to use of tafenoquine	1/Day	0.016	Assumed
κ	Recovery rate tafenoquine treatment	1/Day	0.0166	Assumed
γ	Recovery rate	1/Day	0.0035	[30]
a	Saturation coefficient of fumigation	Human	10	Assumed
ξ	Waning rate of temporal immunity	1/Day	0.005	[33]

where $\mathscr{F}$ and $\mathscr{V}$ present the transmission and transition terms. Using formula in [41], we have the next-generation matrix (NGM) of system (7) which is given by

$$NGM = -E^T \mathscr{F} \mathscr{V}^{-1} E = \begin{bmatrix} 0 & \dfrac{\beta_h}{\mu_v} \\ \dfrac{\alpha \Lambda_v \beta_v \mu_h (\delta \eta p + \delta p u_1 - \eta \kappa p - \delta \eta - \delta u_1 - \eta \mu_h)}{\mu_v \Lambda_h (u_1 + \eta + \mu_h)(\delta p - \kappa p - \delta - \mu_h)(\gamma + \mu_h)} & 0 \end{bmatrix}, \tag{12}$$

where E^T is the transpose of E, with

$$E = \begin{bmatrix} 1 & 0 \\ 0 & 0 \\ 0 & 0 \\ 0 & 1 \end{bmatrix}. \tag{13}$$

Note that each column of $\mathscr{F}$ can be spanned by each column of E. Hence, the basic reproduction number of system (7) is given by

$$\mathscr{R}_0 = \sqrt{\frac{\beta_v \Lambda_v \alpha \mu_h (\delta(\eta + u_1)(1-p) + \eta(\mu_h + p\kappa))\beta_h}{\Lambda_h \mu_v^2 (\delta(1-p) + \mu_h + p\kappa)(u_1 + \eta + \mu_h)(\gamma + \mu_h)}}. \tag{14}$$

More example on the method of next-generation matrix method to determine the basic reproduction number in various epidemiological models can be seen in [42–44]. The above expression can be rewritten as a multiplication between four important component on malaria transmission on system (7) as follows.

$$\mathscr{R}_0 = \sqrt{\mathscr{C}_1 \times \mathscr{C}_2 \times \mathscr{C}_3 \times \mathscr{C}_4}, \tag{15}$$

where $\mathscr{C}_1 = \beta_h/(u_1 + \eta + \mu_h)$ present the number of new latent infected human per infection period of E, $\mathscr{C}_2 = \alpha \beta_v/\mu_v$ present the number of new infected mosquitoes per infection period of W, $\mathscr{C}_3 = N_v/N_h$ present the ratio of mosquitoes and human, and $\mathscr{C}_4 = \eta + u_1(1/(1 + ((p\kappa + \mu_h)/((1-p)\delta))))$ present the impact of tafenoquine intervention.

According to Theorem 2 in [45], we have the following theorem regarding the local stability criteria of the malaria-free equilibrium of system (7).

Theorem 2. *The malaria-free equilibrium of system (7) is locally asymptotically stable if $\mathscr{R}_0 < 1$ and unstable if $\mathscr{R}_0 > 1$.*

3.1. Sensitivity Analysis on the Basic Reproduction Number. In many mathematical epidemiology models, understanding the impact of key parameters in determining the size of the basic reproduction number is essential to find the best optimal strategy. Therefore, we study the normalized sensitivity analysis of the basic reproduction number using the following formula [30]:

$$\Gamma_p^{\mathscr{R}_0} = \frac{\partial \mathscr{R}_0}{\partial p} \times \frac{p}{\mathscr{R}_0}, \tag{16}$$

Table 2: Normalized sensitivity indices of $\mathcal{R}_0$ with respect to β_h, β_v, α, u_1, u_2, η, δ, p, κ, γ, ξ, and a.

Par (ρ)	$\Gamma_\rho^{\mathcal{R}_0}$	Par (ρ)	$\Gamma_\rho^{\mathcal{R}_0}$	Par (ρ)	$\Gamma_\rho^{\mathcal{R}_0}$
β_h	0.5	β_v	0.5	α	0.5
u_1	-0.191	u_2	0	η	0.191
δ	0.129	p	−0.6477	κ	-0.120
γ	-0.494	ξ	0	a	0

where ρ is any key parameter in malaria model in system (7). In our paper, we are only interested in the following parameters: β_h, β_v, α, u_1, u_2, η, δ, p, κ, γ, ξ, and a. Furthermore, we do not show the partial derivative of these parameters since it has a long expressions. Using parameter values as in Table 1, $u_1 = 0.2$, $u_2 = 0$, and $p = 0.8$; the normalized sensitivity of $\mathcal{R}_0$ is given in Table 2 and visualized in Figure 2.

The normalized indices in Table 2 are a nondimensional value, which present the percentage change of $\mathcal{R}_0$ for each increase value of parameter ρ for 1%. For an example, since $\Gamma_p^{\mathcal{R}_0} = -0.6477$, then increasing probability of individuals in T to succeed in treatment for 10% will reduce $\mathcal{R}_0$ for 6.477%. On the other hand, since $\Gamma_{\beta_h}^{\mathcal{R}_0} = 0.5$, then increasing β_h for 10% will increase $\mathcal{R}_0$ for 5%. From Figure 2, we can see that β_h, β_v, α, η, and δ are proportional to $\mathcal{R}_0$. Increasing these mentioned values will increase $\mathcal{R}_0$. On the other hand, parameters p, γ, u_1, and κ are inversely proportional to $\mathcal{R}_0$. Therefore, increasing the value of p, γ, u_1, and κ will reduce $\mathcal{R}_0$. In addition, we can see that fumigation (u_2), rate of loss of immunity (ξ), and saturated parameter (a) do not affect $\mathcal{R}_0$. Figure 2 shows the most to the less influential parameter to $\mathcal{R}_0$ in descending order, from left to the right.

Figure 3 shows the level set of $\mathcal{R}_0$ with respect to u_1, α, and p. From Figure 3(a), we can see that increasing the value of p reduces $\mathcal{R}_0$. It means that more people succeed due to treatment with tafenoquine; then, the possibility to achieve malaria-free equilibrium is bigger. Same interpretation to the rate of treatment u_1. We can see that more intense intervention of tafenoquine will reduce $\mathcal{R}_0$. In addition, we can see clearly that better quality of tafenoquine will reduce the burden of intervention in providing tafenoquine treatment to achieve malaria-free conditions. The effect of vector-bias on the success of tafenoquine intervention to reduce $\mathcal{R}_0$ can be seen in Figure 3(b). We can see that more bias the mosquito to be more preferring infected human will increase the $\mathcal{R}_0$, which makes the intervention of tafenoquine should be given more intense to reduce the value of $\mathcal{R}_0$.

4. The Malaria-Endemic Equilibrium

4.1. Existence of Malaria-Endemic Equilibrium.
The malaria-endemic equilibrium of system (7) is given by

$$MEE = \left(S^\dagger, E^\dagger, T^\dagger, I^\dagger, R^\dagger, U^\dagger, W^\dagger\right), \quad (17)$$

where

$$S^\dagger = \frac{\Lambda_h}{\mu_h} - E^\dagger - I^\dagger - T^\dagger - R^\dagger,$$

$$E^\dagger = \frac{I^\dagger(\delta(\mu_h + \gamma)(1-p) + (\gamma + \mu_h)(\mu_h + p\kappa))}{\delta(u_1 + \eta)(1-p) + \eta(\mu_h + p\kappa)},$$

$$T^\dagger = \frac{I^\dagger u_1(\gamma + \mu_h)}{\delta(u_1 + \eta)(1-p) + \eta(\mu_h + p\kappa)},$$

$$R^\dagger = \frac{(\delta(\gamma + \mu_h)(1-p) + \gamma\kappa p(\eta + \mu_h) + \mu_h(\eta\gamma + p\kappa u_1))}{(\delta(u_1 + \eta)(1-p) + \eta(\mu_h + p\kappa))(\xi + \mu_h)},$$

$$U^\dagger = \frac{\Lambda_v\left(S^\dagger + E^\dagger + \alpha I^\dagger + T^\dagger + R^\dagger\right)\left(a + \left(I^\dagger\right)^2\right)}{\Sigma_{i=0}^3 c_i},$$

$$W^\dagger = \frac{\Lambda_v\left(a + \left(I^\dagger\right)^2\right)}{(u_2 I^\dagger) + \mu_v\left(a + \left(I^\dagger\right)^2\right)} - U^\dagger,$$

$$(18)$$

with $c_0 = \alpha\mu_v(S^\dagger + E^\dagger + T^\dagger + R^\dagger)$, $c_1 = a\alpha(\beta_v + \mu_v) + u_2(S^\dagger + E^\dagger + T^\dagger + R^\dagger)$, $c_2 = \alpha u_2 + \mu_v(S^\dagger + E^\dagger + T^\dagger + R^\dagger)$, and $c_3 = \alpha(\beta_v + \mu_v)$. Note that $I^\dagger$ is taken from the positive root of the following polynomial:

$$G(\Omega, I) = \sum_{j=1}^6 k_j I^j = 0, \quad (19)$$

where Ω is the set of parameter in system (7), and

$$k_6 = -\mu_h^2\mu_v(\xi + \mu_h)(\delta(1-p) + \mu_h + p\kappa)(\alpha - 1)(u_1 + \eta + \mu_h)$$
$$\cdot (\alpha\beta_v + \mu_v(\alpha - 1))(\gamma + \mu_h),$$

$$k_0 = \Lambda_h\mu_v^2(\delta(1-p) + \mu_h + p\kappa)(u_1 + \eta + \mu_h)(\gamma + \mu_h)(\mathcal{R}_0^2 - 1),$$

$$(20)$$

while k_5, k_4, k_3, k_2, and k_1 have a complex form to be written in this article. It can be seen that whenever $I^\dagger > 0$, then $E^\dagger$, $T^\dagger$, $R^\dagger$, and $U^\dagger$ are also positive. On the other hand, $S^\dagger$ is always positive since $N_h \leq (\Lambda_h/\mu_h)$ (see the proof of Theorem 1). On the other hand, since

$$W^\dagger = \frac{\Lambda_v\left(a + \left(I^\dagger\right)^2\right)}{(u_2 I^\dagger) + \mu_v\left(a + \left(I^\dagger\right)^2\right)} - U^\dagger < \frac{\Lambda_v}{\mu_v} - U^\dagger \quad (21)$$
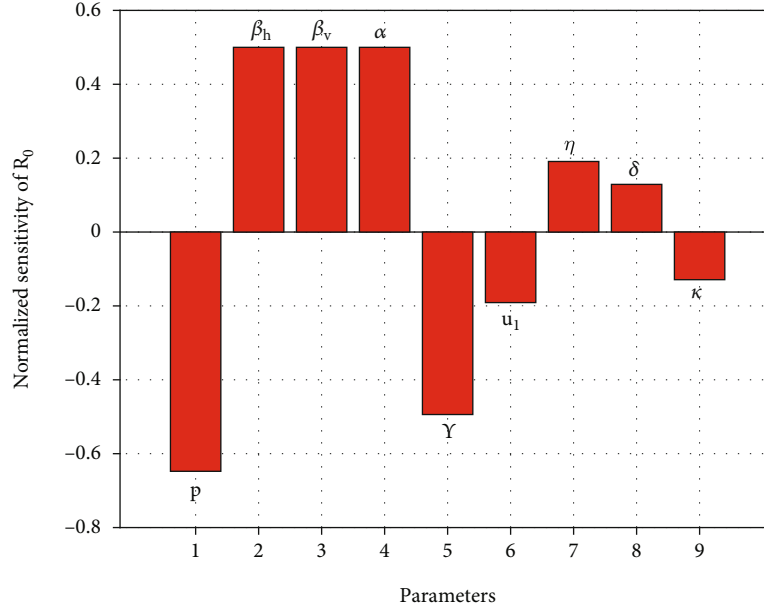
FIGURE 2: Histogram of normalized sensitivity analysis of $\mathcal{R}_0$.

and $N_v \leq (\Lambda_v/\mu_v)$ (see the proof of Theorem 1), then we can guarantee that $W^\dagger$ is also positive.

From the expression of polynomial in (19), k_6 is always negative since $\alpha > 1$, $k_0 > 0 \Leftarrow \mathcal{R}_0 > 1$, while another coefficient is difficult to be determined, whether it was positive or negative. Hence, using the Descartes rules of sign [46], there exists at least one positive root of polynomial (19) whenever $\mathcal{R}_0 > 1$. According to this result and the expression of MEE, we have the following result.

Theorem 3. *System (7) has at least one malaria-endemic equilibrium point if $\mathcal{R}_0 > 1$.*

Since polynomial in (19) is a six-degree polynomial, it is possible that system (7) have more than one malaria-endemic equilibrium point. We use Descartes rules of sign [46] to analyze the maximum possibility of positive root of polynomial in (19). The result is given in Table 3 for the case when $\mathcal{R}_0 > 1$, and Table 4 for the case when $\mathcal{R}_0 < 1$.

From Table 2, we can confirm the result in Theorem 3 that we always have at least one malaria-endemic equilibrium when $\mathcal{R}_0 > 1$. If $\mathcal{R}_0 > 1$, then we always have an odd number possibility of the positive root of polynomial (19), i.e., 1, 3, or 5 positive roots. On the other hand, malaria-endemic equilibrium is possible to vanish only when $\mathcal{R}_0 < 1$. However, we still possible to have 2, 4, or 6 positive roots of polynomial (19) when $\mathcal{R}_0 < 1$.

4.2. Bifurcation Analysis. In this section, we perform the bifurcation analysis of our proposed malaria model in system (7). To do this analysis, we use the well-known Castillo-Song bifurcation theorem [47] (please see [48–51] for more examples on the use of this theorem on

epidemiological models). First, for numerical calculation purposes, let us redefine our proposed system (7) as follows:

$$
\begin{aligned}
f_1 &:= \Lambda_h - \beta_h x_6 \frac{x_1}{x_1 + x_2 + x_3 + \alpha x_4 + x_5} - \mu_h x_1 + \xi x_5, \\
f_2 &:= \beta_h x_6 \frac{x_1}{x_1 + x_2 + x_3 + \alpha x_4 + x_5} - (u_1 + \eta + \mu_h)x_2, \\
f_3 &:= u_1 x_2 - ((1-p)\delta + p\kappa + \mu_h)x_3, \\
f_4 &:= (1-p)\delta x_3 + \eta x_2 - (\gamma + \mu_h)x_4, \\
f_5 &:= p\kappa x_3 + \gamma x_4 - (\mu_h + \xi)x_5, \\
f_6 &:= \Lambda_v - \beta_v x_6 \frac{\alpha x_4}{x_1 + x_2 + x_3 + \alpha x_4 + x_5} - \left(\mu_v + u_2 \frac{x_4}{a + x_4^2}\right)x_6, \\
f_7 &:= \beta_v x_6 \frac{\alpha x_4}{x_1 + x_2 + x_3 + \alpha x_4 + x_5} - \left(\mu_v + u_2 \frac{x_4}{a + x_4^2}\right)x_7,
\end{aligned}
\tag{22}
$$

where x_i for $i = 1, 2, \cdots 7$ present S, E, T, I, R, U, and W, respectively, Next, we determine our bifurcation parameter to replace $\mathcal{R}_0$. By solving $\mathcal{R}_0 = 1$ with respect to β_h, we obtain the bifurcation parameter, namely, $\beta_h = \beta^*$, as follows:

$$
\beta_h = \beta^* = \frac{((p-1)\delta - \kappa p - \mu_h)(\gamma + \mu_h)(u_1 + \eta + \mu_h)\mu_v{}^2 \Lambda_h}{((u_1 + \eta)(p-1)\delta - \eta(\kappa p + \mu_h))\mu_h \beta_v \alpha \Lambda_v}.
\tag{23}
$$

(a) $\mathcal{R}_0(p, u_1)$

(b) $\mathcal{R}_0(\alpha, u_1)$
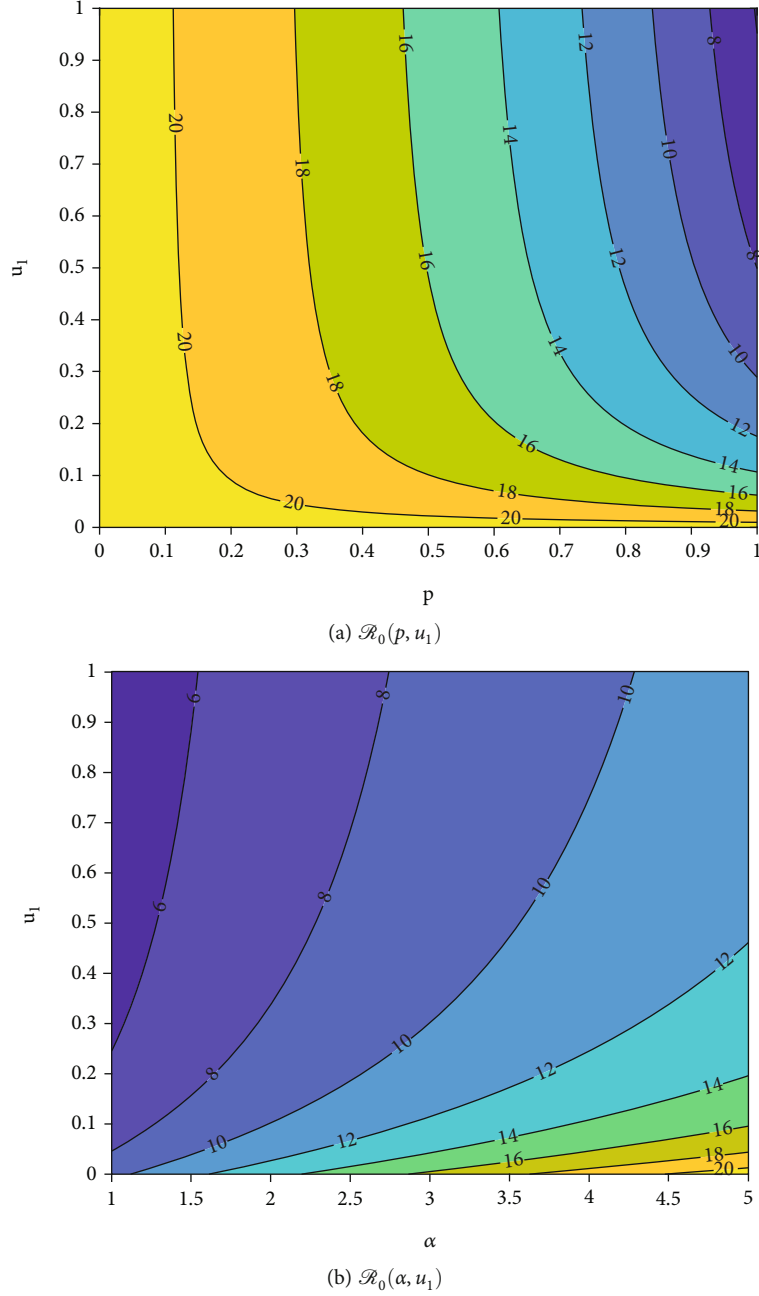
FIGURE 3: Level set of $\mathcal{R}_0$ with respect to p, α, and u_1.

The linearization of MFE of system (22) at $\beta_h = \beta^*$ is given by

$$
J|_{MFE} := \begin{bmatrix} -\mu_h & 0 & 0 & 0 & \xi & 0 & c_{17} \\ 0 & c_{22} & 0 & 0 & 0 & 0 & c_{27} \\ 0 & u_1 & c_{33} & 0 & 0 & 0 & 0 \\ 0 & \eta & (1-p)\delta & -\gamma - \mu_h & 0 & 0 & 0 \\ 0 & 0 & \kappa p & \gamma & -\xi - \mu_h & 0 & 0 \\ 0 & 0 & 0 & c_{64} & 0 & -\mu_v & 0 \\ 0 & 0 & 0 & \dfrac{\beta_v \Lambda_v \alpha \mu_h}{\mu_v \Lambda_h} & 0 & 0 & -\mu_v \end{bmatrix}, \quad (24)
$$

with

$$
c_{17} = -\frac{((p-1)\delta - \kappa p - \mu_h)(\gamma + \mu_h)(u_1 + \eta + \mu_h)\mu_v^{\ 2}\Lambda_h}{((u_1 + \eta)(p-1)\delta - \eta(\kappa p + \mu_h))\mu_h \beta_v \alpha \Lambda_v},
$$

$$
c_{22} = -u_1 - \eta - \mu_h,
$$

$$
c_{27} = \frac{((p-1)\delta - \kappa p - \mu_h)(\gamma + \mu_h)(u_1 + \eta + \mu_h)\mu_v^{\ 2}\Lambda_h}{((u_1 + \eta)(p-1)\delta - \eta(\kappa p + \mu_h))\mu_h \beta_v \alpha \Lambda_v},
$$

$$
c_{33} = -(1-p)\delta - \kappa p - \mu_h,
$$

$$
c_{64} = -\frac{\beta_v \Lambda_v \alpha \mu_h}{\mu_v \Lambda_h} - \frac{u_2 \Lambda_v}{a\mu_v}. \quad (25)
$$

TABLE 3: Possible number of positive roots of polynomial $G(\Omega, I)$, when $\mathcal{R}_0 > 1$.

Case	k_6	k_5	k_4	k_3	k_2	k_1	k_0	Possible positive roots
1	—	+	+	+	+	+	+	1
2	—	+	+	+	+	—	+	1 or 3
3	—	+	+	+	—	+	+	1 or 3
4	—	+	+	+	—	—	+	1 or 3
5	—	+	+	—	+	+	+	1 or 3
6	—	+	+	—	+	—	+	1, 3, or 5
7	—	+	+	—	—	+	+	1 or 3
8	—	+	+	—	—	—	+	1 or 3
9	—	+	—	+	+	+	+	1 or 3
10	—	+	—	+	+	—	+	1, 3, or 5
11	—	+	—	+	—	+	+	1, 3, or 5
12	—	+	—	+	—	—	+	1, 3, or 5
13	—	+	—	—	+	+	+	1 or 3
14	—	+	—	—	+	—	+	1, 3, or 5
15	—	+	—	—	—	+	+	1 or 3
16	—	+	—	—	—	—	+	1 or 3
17	—	—	+	+	+	+	+	1
18	—	—	+	+	+	—	+	1 or 3
19	—	—	+	+	—	+	+	1 or 3
20	—	—	+	+	—	—	+	1 or 3
21	—	—	+	—	+	+	+	1 or 3
22	—	—	+	—	+	—	+	1, 3, or 5
23	—	—	+	—	—	+	+	1 or 3
24	—	—	+	—	—	—	+	1 or 3
25	—	—	—	+	+	+	+	1
26	—	—	—	+	+	—	+	1 or 3
27	—	—	—	+	—	+	+	1 or 3
28	—	—	—	+	—	—	+	1 or 3
29	—	—	—	—	+	+	+	1
30	—	—	—	—	+	—	+	1 or 3
31	—	—	—	—	—	+	+	1
32	—	—	—	—	—	—	+	1

TABLE 4: Possible number of positive roots of polynomial $G(\Omega, I)$, when $\mathcal{R}_0 < 1$.

Case	k_6	k_5	k_4	k_3	k_2	k_1	k_0	Possible positive roots
33	—	+	+	+	+	+	—	0 or 2
34	—	+	+	+	+	—	—	0 or 2
35	—	+	+	+	—	+	—	0, 2, or 4
36	—	+	+	+	—	—	—	0 or 2
37	—	+	+	—	+	+	—	0, 2, or 4
38	—	+	+	—	+	—	—	0, 2, or 4
39	—	+	+	—	—	+	—	0, 2, or 4
40	—	+	+	—	—	—	—	0 or 2
41	—	+	—	+	+	+	—	0, 2, or 4
42	—	+	—	+	+	—	—	0, 2, or 4
43	—	+	—	+	—	+	—	0, 2, 4, or 6
44	—	+	—	+	—	—	—	0, 2, or 4
45	—	+	—	—	+	+	—	0, 2, or 4
46	—	+	—	—	+	—	—	0, 2, or 4
47	—	+	—	—	—	+	—	0, 2, or 4
48	—	+	—	—	—	—	—	0 or 2
49	—	—	+	+	+	+	—	0 or 2
50	—	—	+	+	+	—	—	0 or 2
51	—	—	+	+	—	+	—	0, 2, or 4
52	—	—	+	+	—	—	—	0 or 2
53	—	—	+	—	+	+	—	0, 2, or 4
54	—	—	+	—	+	—	—	0, 2, or 4
55	—	—	+	—	—	+	—	0, 2, or 4
56	—	—	+	—	—	—	—	0 or 2
57	—	—	—	+	+	+	—	0 or 2
58	—	—	—	+	+	—	—	0 or 2
59	—	—	—	+	—	+	—	0, 2, or 4
60	—	—	—	+	—	—	—	0 or 2
61	—	—	—	—	+	+	—	0 or 2
62	—	—	—	—	+	—	—	0 or 2
63	—	—	—	—	—	+	—	0 or 2
64	—	—	—	—	—	—	—	0

The Jacobian matrix J_{MFE} has a simple zero eigenvalue, and the other three eigenvalues are explicitly negative ($-\mu_h$, $-\mu_h$, $-(\mu_h + \xi)$), while the other three is coming from the root of the following polynomial:

$$P(\lambda) = c_3 \lambda^3 + c_2 \lambda^2 + c_1 \lambda + c_0 = 0, \qquad (26)$$

where

$$c_3 = \Lambda_h \mu_v (u_1 + \mu_v + 3\mu_h + \eta + \gamma + p\kappa + \delta(1 - p)),$$

$$c_2 = \delta(1 - p)(\eta + \gamma + u_1 + \mu_v + 2\mu_h)$$
$$\cdot (3\mu_h^2 + \mu_h(2\kappa p + 2\eta + 2\gamma + 3\mu_v + 2u_1) + \cdots + \mu_v$$
$$\cdot (\kappa p + \eta + \gamma + u_1) + \gamma(\kappa p + \eta + u_1) + p\kappa(\eta + u_1)),$$

$$c_1 = [\mu_v^2(3\mu_h^2 + \mu_h(2(1 - p)\delta + 2\kappa p + \eta + \gamma + u_1) + \delta(1 - p)$$
$$\cdot (\eta + \gamma + u_1) + p\kappa(\eta + \gamma + u_1)) + (\eta + u_1 + \mu_h)$$
$$\cdot ((1 - p)\delta + p\kappa + \mu_h)(\gamma + \mu_h)]\Lambda_h + \Lambda_v \alpha \eta \beta^* \beta_v \mu_h,$$

$$c_0 = \Lambda_h \mu_v^2 (\gamma + \mu_h)(u_1 + \eta + \mu_h)((1 - p)\delta + p\kappa + \mu_h)$$
$$+ \beta_h^* \beta_v \mu_h \alpha \Lambda_v (\delta(1 - p)(\eta + u_1) + p\kappa\eta + \eta\mu_h). \qquad (27)$$

Since $(1 - p) > 0$, then c_i for $i = 0, 1, 2, 3$ are positive. Since all the coefficients of $P(\lambda)$ are positive, then all other three eigenvalues of $J|_{MFE}$ are negative. Therefore, we can continue using the center manifold theory to analyze the bifurcation phenomena at $\mathcal{R}_0 = 1$. Next, we use the Castillo-Chavez and Song theorem [47] to analyze the bifurcation phenomena of system (7) at $\mathcal{R}_0 = 1$.

First, we calculate the right and left eigenvector of $J|_{MFE}$ with respect to the zero eigenvalue. The right eigenvector is given by $\mathbf{w} = (w_1, w_2, w_3, w_4, w_5, w_6, w_7)^T$, with

$$
\begin{aligned}
w_1 = \frac{1}{(\gamma + \mu_h)(\xi + \mu_h)u_1} & \left(-\mu_h^3 + ((p-1)\delta - \kappa p - \xi - \eta - \gamma - u_1)\mu_h^2 \right. \\
& + ((\xi + \eta + \gamma + u_1)(p-1)\delta - \kappa(\xi + \eta + \gamma + u_1)p \\
& + (-\xi - \eta - u_1)\gamma - \xi(u_1 + \eta))\mu_h + (p-1)((\xi + \eta + u_1)\gamma \\
& \left. + \xi(u_1 + \eta))\delta - \kappa((\xi + \eta + u_1)\gamma + \eta\xi)p - \gamma\xi u_1\right),
\end{aligned}
$$

$$
w_2 = -\frac{(\delta p - \kappa p - \delta - \mu_h)}{u_1}, w_3 = 1,
$$

$$
w_4 = -\frac{\delta\eta p + \delta p u_1 - \eta\kappa p - \delta\eta - \delta u_1 - \eta\mu_h}{(\gamma + \mu_h)u_1},
$$

$$
w_5 = \frac{(((-\delta + \kappa)p + \delta)u_1 - \eta((\delta - \kappa)p - \delta - \mu_h))\gamma + \kappa p\mu_h u_1}{(\gamma + \mu_h)(\xi + \mu_h)u_1},
$$

$$
w_6 = -\frac{(a\alpha\beta_v\mu_h + u_2\Lambda_h)(-(u_1 + \eta)(p-1)\delta + \eta(\kappa p + \mu_h))w3\,\Lambda_v}{u_1(\gamma + \mu_h)a\Lambda_h\mu_v^2},
$$

$$
w_7 = -\frac{\Lambda_v\alpha\beta_v\mu_h((\eta + u_1)(p-1)\delta - \eta(\kappa p + \mu_h))}{\Lambda_h\mu_v^2(\gamma + \mu_h)u_1}. \tag{28}
$$

On the other hand, the left eigenvector is given by $\mathbf{v} = (v_1, v_2, v_3, v_4, v_5, v_6, v_7)$ where

$$
v_1 = 0,
$$

$$
v_2 = \frac{(\eta + u_1)(p-1)\delta - \eta(\kappa p + \mu_h)}{(\eta + u_1 + \mu_h)\delta(p-1)},
$$

$$
v_3 = 1,
$$

$$
v_4 = \frac{(p-1)\delta - \kappa p - \mu_h}{(p-1)\delta}, \tag{29}
$$

$$
v_5 = 0,
$$

$$
v_6 = 0,
$$

$$
v_7 = \frac{(\gamma + \mu_h)\Lambda_h\mu_v((p-1)\delta - \kappa p - \mu_h)}{\Lambda_v\alpha\beta_v\mu_h\delta(p-1)}.
$$

It is obvious that $v_1 = v_5 = v_6 = 0$. Furthermore, f_3 and f_4 are one degree functions. Thus, we only need to consider the second-order partial derivative of f_2 and f_7. By algebraic computation, we obtain the following second-order partial derivatives which have nonzero values after substituting the MFE.

$$
\frac{\partial^2 f_2}{\partial x_2\partial x_7} = \frac{\partial^2 f_2}{\partial x_7\partial x_2} = -\frac{\beta_h\mu_h}{\Lambda_h}, \frac{\partial^2 f_2}{\partial x_3\partial x_7} = \frac{\partial^2 f_2}{\partial x_7\partial x_3} = -\frac{\beta_h\mu_h}{\Lambda_h},
$$

$$
\frac{\partial^2 f_2}{\partial x_4\partial x_7} = \frac{\partial^2 f_2}{\partial x_7\partial x_4} = -\frac{\beta_h\mu_h\alpha}{\Lambda_h}, \frac{\partial^2 f_2}{\partial x_5\partial x_7} = \frac{\partial^2 f_2}{\partial x_7\partial x_5} = -\frac{\beta_h\mu_h}{\Lambda_h},
$$

$$
\frac{\partial^2 f_7}{\partial x_1\partial x_4} = \frac{\partial^2 f_7}{\partial x_4\partial x_1} = -\frac{\beta_v\Lambda_v\alpha\mu_h^2}{\mu_v\Lambda_h^2}, \frac{\partial^2 f_7}{\partial x_2\partial x_4} = \frac{\partial^2 f_7}{\partial x_4\partial x_2} = -\frac{\beta_v\Lambda_v\alpha\mu_h^2}{\mu_v\Lambda_h^2},
$$

$$
\frac{\partial^2 f_7}{\partial x_3\partial x_4} = \frac{\partial^2 f_7}{\partial x_4\partial x_3} = -\frac{\beta_v\Lambda_v\alpha\mu_h^2}{\mu_v\Lambda_h^2}, \frac{\partial^2 f_7}{\partial x_5\partial x_4} = \frac{\partial^2 f_7}{\partial x_4\partial x_5} = -\frac{\beta_v\Lambda_v\alpha\mu_h^2}{\mu_v\Lambda_h^2},
$$

$$
\frac{\partial^2 f_7}{\partial x_4\partial x_6} = \frac{\partial^2 f_7}{\partial x_6\partial x_4} = \frac{\beta_v\alpha\mu_h}{\Lambda_h}, \frac{\partial^2 f_7}{\partial x_4\partial x_7} = \frac{\partial^2 f_7}{\partial x_7\partial x_4} = -\frac{u_2}{a},
$$

$$
\frac{\partial^2 f_7}{\partial x_4\partial x_4} = -2\frac{\beta_v\Lambda_v\alpha^2\mu_h^2}{\mu_v\Lambda_h^2}. \tag{30}
$$

For the bifurcation indicators, we calculate $\mathscr{A}$ for system (22) which is expressed by

$$
\mathscr{A} = v_2\sum_{i,j=1}^7 w_i\frac{\partial^2 f_2}{\partial x_i\partial x_j} + v_7\sum_{i=1}^7 w_i\frac{\partial^2 f_7}{\partial x_i\partial x_j}. \tag{31}
$$

We can confirm that $\mathscr{A}$ is always negative (please see the expression of $\mathscr{A}$ in Appendix D). Meanwhile, $\mathscr{B}$ is given by

$$
\mathscr{B} = v_2\sum_{i=1}^7 w_i\frac{\partial^2 f_2}{\partial x_i\partial\beta_h} = \frac{((u_1 + \eta)(p-1)\delta - \eta(\kappa p + \mu_h))^2\mu_h\beta_v\alpha\Lambda_v}{(u_1 + \eta + \mu_h)\delta(1-p)\Lambda_h\mu_v^2(\gamma + \mu_h)u_1}. \tag{32}
$$

Since all parameters are positive, and $(1 - p) > 0$, then we have that $\mathscr{B} > 0$. According to Castillo-Chavez and Song theorem [47], since the quantity of $\mathscr{A}$ is negative and $\mathscr{B}$ is positive, then system (22)) indicates a forward bifurcation at $\mathscr{R}_0 = 1$. We state the result in the following theorem.

Theorem 4. *System (7) always exhibits a forward bifurcation at $\mathscr{R}_0 = 1$.*

4.3. Numerical Experiments on Theorem 4. In this section, we show the numerical interpretation of Theorem 4. The first numerical experiment is for the bifurcation diagram of system (7), which is given in Figure 4. We use parameter values as mentioned in Table 1, except that it states differently. With this set of parameter values, we have $\mathscr{R}_0 = 1$ when $\beta_h = 0.0004079$. For the case of $a = 400$, $u_1 = 0.2$, and $u_2 = 0$, the bifurcation diagram is shown in Figure 4(a). It can be seen that the forward bifurcation phenomenon appears, which indicates there always exists a unique endemic equilibrium point when $\mathscr{R}_0 > 1$, and no endemic equilibrium when $\mathscr{R}_0 < 1$. Furthermore, we can see that the malaria-endemic equilibrium is always stable (solid red) when $\mathscr{R}_0 > 1$. The autonomous simulation for various initial conditions is shown in Figure 5. We use Runge-Kutta adaptive step size method in MATLAB to run the autonomous simulation in this article [52] (please see [53] for further detail on the method and its algorithm). It can be seen that when $\mathscr{R}_0 = 0.8 < 1$, then the solution from all different initial conditions tends to the malaria-free equilibrium point (Figure 5). On the other hand, when $\mathscr{R}_0 > 1$, then all trajectories tend to the malaria-endemic equilibrium (Figure 6).

The autonomous simulation of system (7) when forward hysteresis (Figure 4(b)) appears is given in Figures 7 and 8. The numerical results is using the same parameter values as in Figure 4(b). We only conduct two cases for this
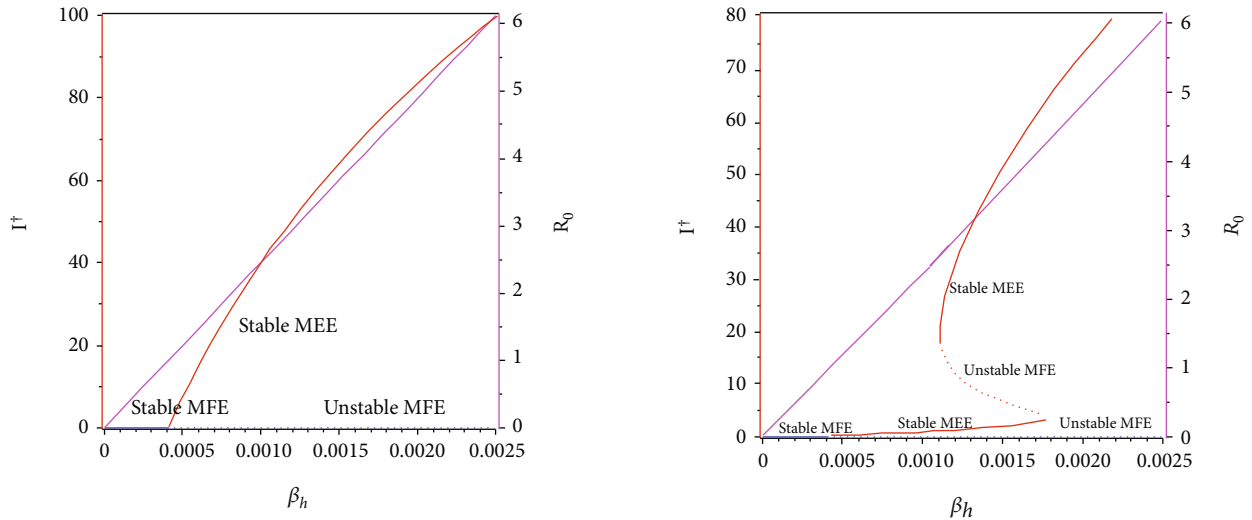
(a) Forward bifurcation phenomena of system (7) when $u_2 = 0$ and $a = 400$

(b) Forward hysteresis phenomena of system (7) when $u_2 = 0.3$ and $a = 10$

FIGURE 4: Type of bifurcation phenomena of system (7). The red figure presents $I^\dagger$ in $MEEE$, the blue curve is I^* in MFE, and the magenta curve presents the basic reproduction number as a function of β_h. The solid and dotted curve present stable and unstable equilibrium point, respectively.

FIGURE 5: Autonomous simulation of Figure 4(a): trajectories of infected compartments for many different initial conditions toward MFE when $\mathcal{R}_0 = 0.98 < 1$. The left figure is simulation for the first 300 days, while the right figure is simulation for days 95000 to 100000.

scenario, namely, when $\mathcal{R}_0 > 1$ but close to one in which only one stable malaria-endemic appears (Figure 7) and when two stable malaria-endemic equilibrium appears (Figure 8) when $\mathcal{R}_0 > 1$, but not too far from 1. In the first case, as shown in Figure 7, we can see that all trajectories from all different initial conditions tend to the same malaria-endemic equilibrium. However, when hysteresis starts to appear, which causes two stable malaria-endemic

equilibrium, the solutions will tend to two different stable malaria-endemic equilibrium points, depending on their initial conditions. We can see that when the initial condition is close enough to the bigger malaria-endemic equilibrium (blue curve), then the solution tends to the bigger size of malaria-endemic equilibrium. The same thing happens when the initial value of infection is small enough, and then, the solution leads to the smallest stable malaria-endemic
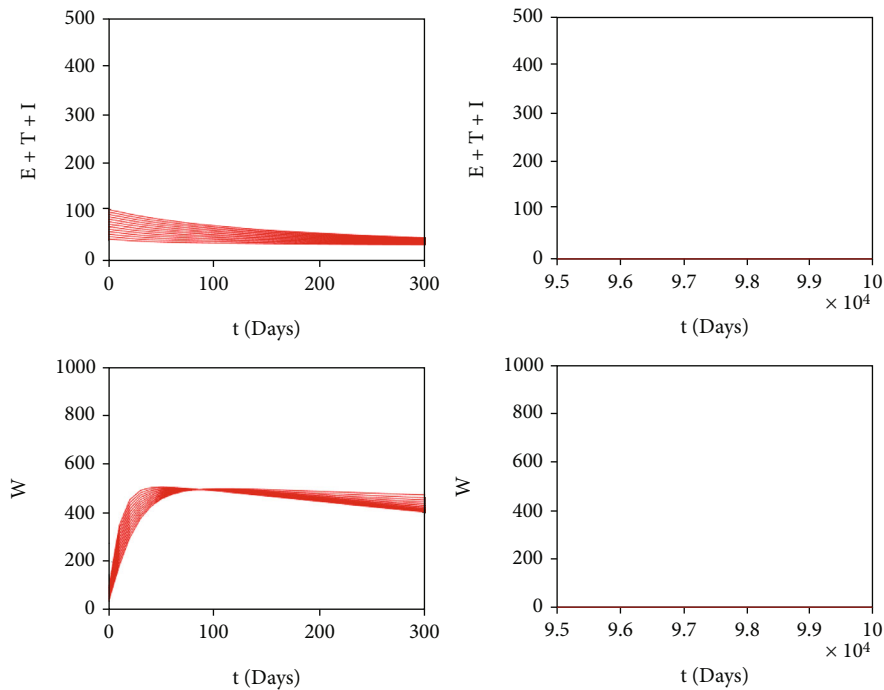
FIGURE 6: Autonomous simulation of Figure 4(a): trajectories of infected compartments for many different initial conditions toward MEE when $\mathscr{R}_0 = 4.902 > 1$. The left figure is simulation for 300 days, while the right figure is simulation for days 95000 to 100000.

FIGURE 7: Autonomous simulation of Figure 4(b): trajectories of infected compartments for many different initial conditions toward single MEE when $\mathscr{R}_0 = 1.225 > 1$. The left figure is simulation for 300 days, while the right figure is simulation for days 95000 to 100000.

equilibrium. These simulation results indicate that fumigation may trigger the existence of multiple stable malaria-endemic equilibrium for some value when $\mathscr{R}_0 > 1$. Figure 9 confirms the statement. It can be seen that an increase in fumigation rate increases the interval when multiple stable malaria-endemic equilibrium appears.

5. Autonomous Simulation

From the previous mathematical analysis, we found that our proposed malaria model always exhibits a forward bifurcation at $\mathscr{R}_0 = 1$. These results indicate that the basic reproduction number becomes the only endemic indicator on
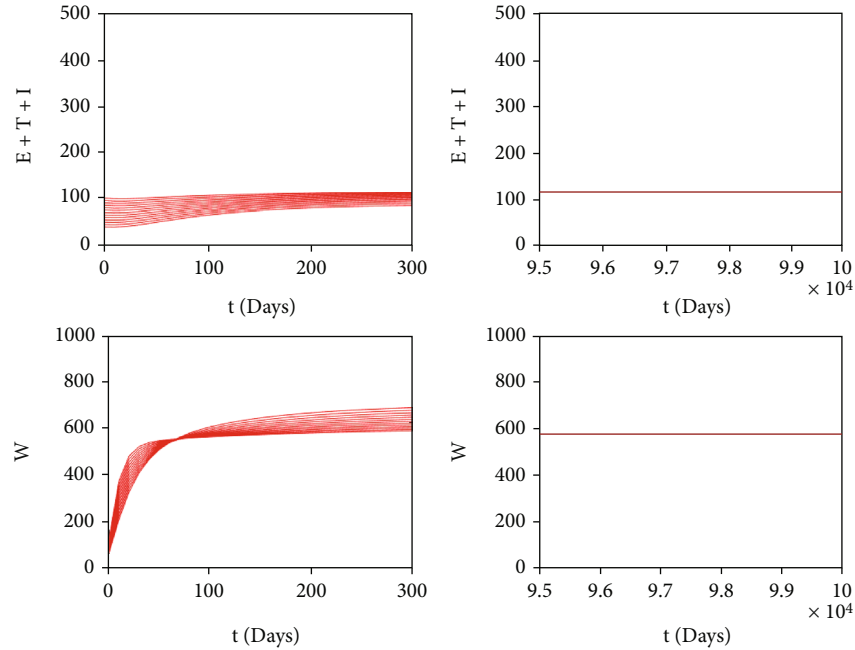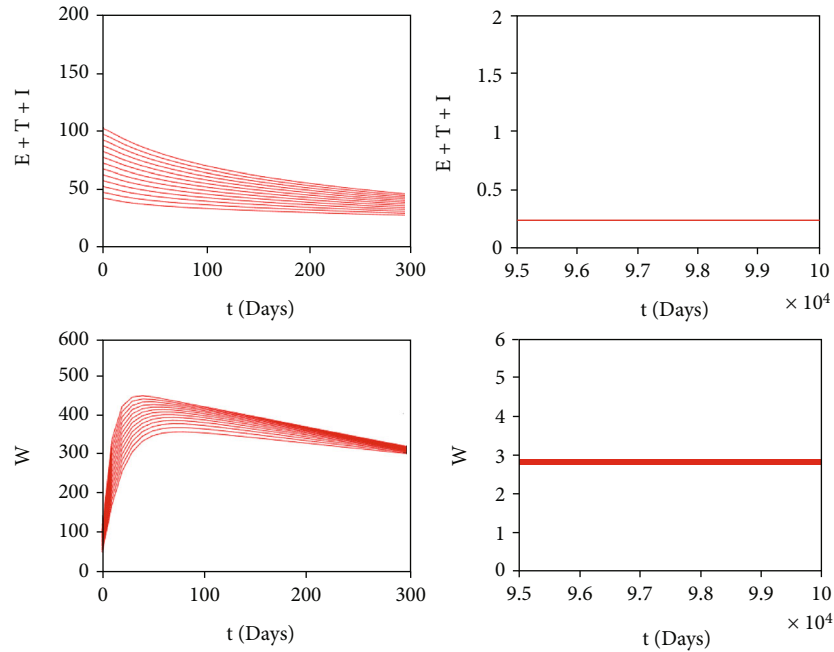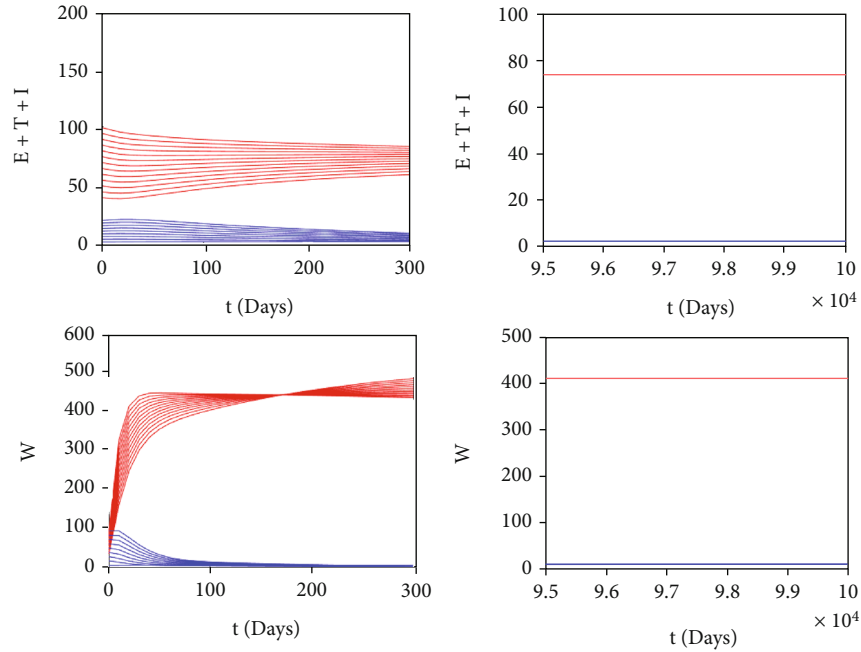
FIGURE 8: Autonomous simulation of Figure 4(b): trajectories of infected compartments for many different initial conditions toward two stable *MEE* when $\mathcal{R}_0 = 3.6769 > 1$, depending on the initial conditions. The left figure is simulation for 300 days, while the right figure is simulation for days 95000 to 100000.
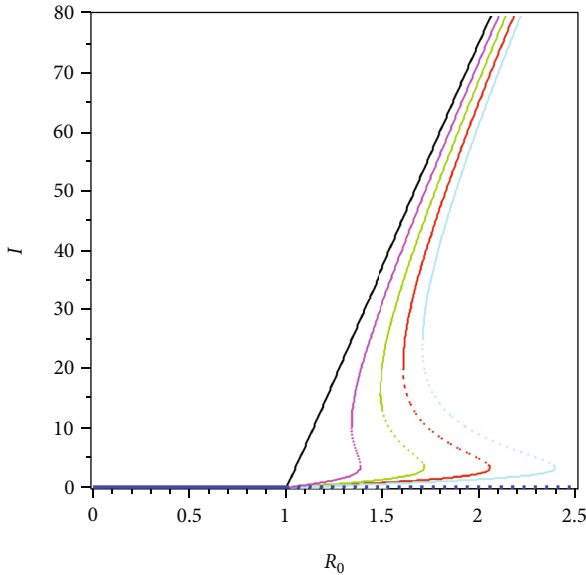
FIGURE 9: The bifurcation diagram of system (7) depends on the value of fumigation rate. We use the same parameter values for each curve, except $u_2 = 0$ (black), $u_2 = 0.1$ (magenta), $u_2 = 0.2$ (green), $u_2 = 0.3$ (red), and $u_2 = 0.4$ (cyan)

our proposed model. However, our model may show a multiple stable endemic equilibrium when $\mathcal{R}_0 > 1$. This phenomenon is called a forward hysteresis [54]. We found that this phenomenon was affected by the intensity of fumigation (u_2) and the level of population awareness (a). Furthermore, our sensitivity analysis indicates how important is the intervention of tafenoquine to prevent the occurrence

of relapse and fumigation to control the number of Anopheles mosquitoes in the environment. To visualize our mentioned results, we perform several numerical simulations on our autonomous simulations for several scenarios.

5.1. Effect of Vector-Bias. In malaria transmission, vector-bias has an important role in determining the endemic condition of the population [29]. The larger the vector-bias values, the more mosquito attracted to hunt infected humans for their meal. Figure 10 depicts the dynamic of the solution of our malaria model in (7) for several values of vector-bias parameter. We use the same parameter values as in Table 2, except $u_1 = 0.1$, $u_2 = 0.05$, $p = 0.8$, and varying α from 1 to 5. With these parameters, $\mathcal{R}_0$ is always larger than 1, which makes the solution of system (7) tends to the malaria-endemic equilibrium. We can see that an increased value of the vector-bias parameter at the malaria-endemic equilibrium situation will increase the total population in infected humans but reduce the size of the infected mosquito population. This means that the more Anopheles mosquitoes attracted to bite infected humans than healthy humans can negatively impact the human population, where the endemic size can increase. Therefore, efforts to control the mosquito population are essential in this situation.

5.2. Effect of Fumigation Saturation Parameter. The first autonomous simulation was conducted to show the impact of the fumigation saturation parameter a. As we mentioned before, a smaller value a indicates a more prepared community to the increasing number of infected individuals. From the expression of $\mathcal{R}_0$ in (15), it can be seen that a does not

(a)

(b)
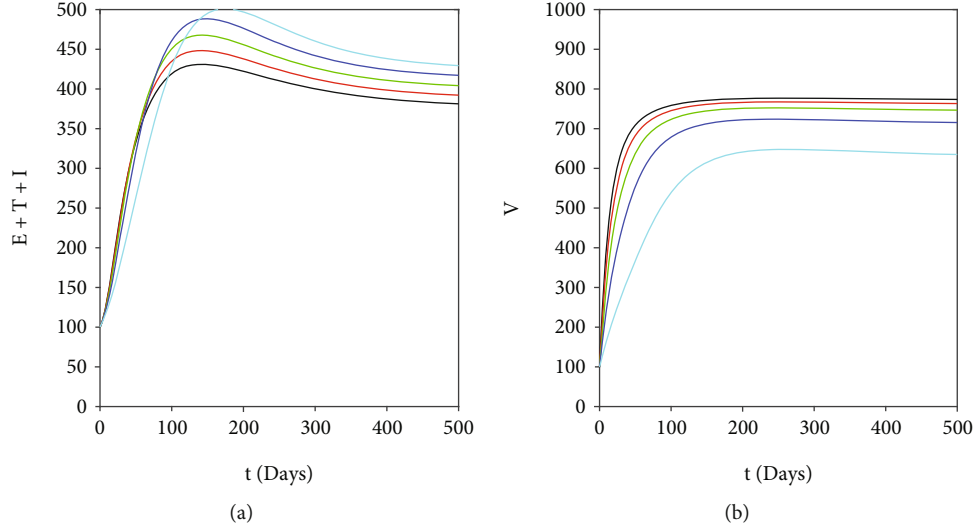
FIGURE 10: Simulations showing the effect of vector-bias parameter (α) on the total of infected human (left) and mosquitoes (right). We use same parameter values as in Table 2, except $u_1 = 0.1$, $u_2 = 0.05$, $p = 0.8$, and α varying: $\alpha = 5$ (black), $\alpha = 4$ (red), $\alpha = 3$ (green), $\alpha = 2$ (blue), and $\alpha = 1$ (cyan).

(a)

(b)
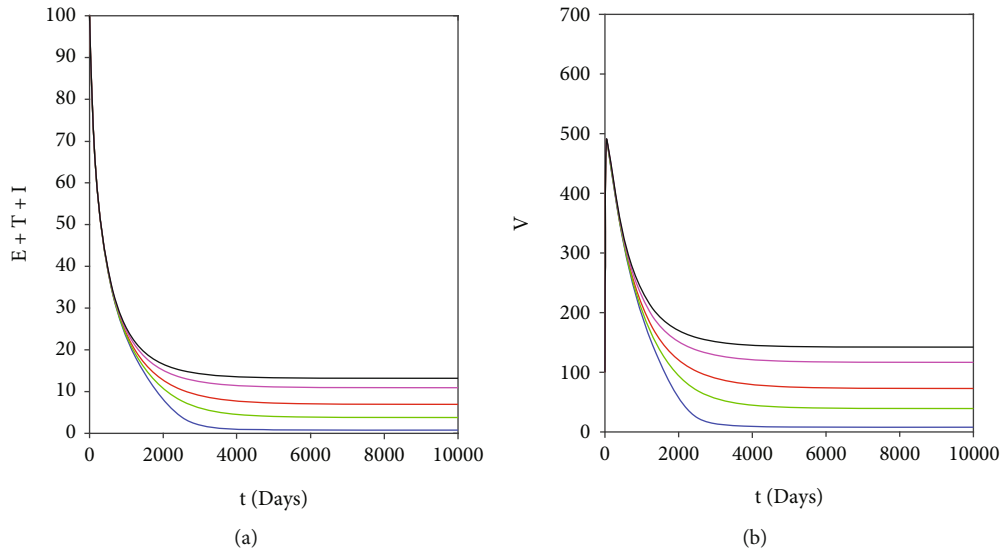
FIGURE 11: Simulations showing the effect of fumigation saturation parameter (a) on the total of infected human (left) and mosquitoes (right). We use same parameter values as in Table 2, except $u_1 = 0.1$, $u_2 = 0.2$, $p = 0.8$, and a varying: $a = 20$ (blue), $a = 50$ (green), $a = 100$ (red), $a = 200$ (cyan), and $a = 300$ (black). With this set of parameter, we have that $\mathcal{R}_0 = 1.23$.

appear in $\mathcal{R}_0$. Hence, we conclude that a does not impact the size of $\mathcal{R}_0$. However, as we have shown in Figure 11, a smaller value of a reduces the size of total infected humans and mosquitoes in the malaria-endemic equilibrium point. Therefore, it can be concluded that although the level of community readiness to carry out fumigation does not affect the final state of population (endemic or not), it is clear that the higher the community readiness (the smaller the value of a), then the smaller the total size of the infected population in malaria-endemic equilibrium.

5.3. Effect of Different Fumigation Strategy. As we have mentioned in sensitivity analysis on $\mathcal{R}_0$, we find that fumigation

does not affect the size of $\mathcal{R}_0$, but it can reduce the size of malaria-endemic equilibrium when fumigation intervention increases, as shown in Figure 12.

Now, we conduct our simulation with three different scenarios, based on the measured fumigation control depending on the implementation time. In the 1st and the 2nd scenarios, we choose u_2 to be changed depending on the time interval, using the following step function:

$$u_2^{1^{\text{st}}\text{scenario}} = \begin{cases} 0.3, & t \le 500, \\ 0.9, & 500 \le t \le 2000, \\ 0.3, & 2000 \le t \le 10000, \end{cases}$$
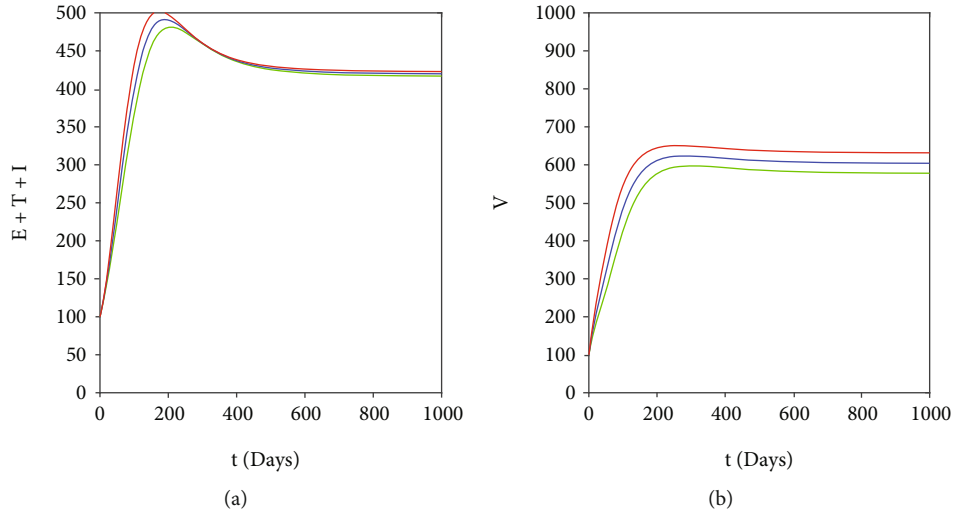
FIGURE 12: Effect of fumigation on the endemic size of total infected human (left) and mosquitoes (right). Three different values of u_2 are given: 0 (red), 0.5 (blue), and 1 (green) do not change the value of $\mathcal{R}_0$, which is always 1.77.
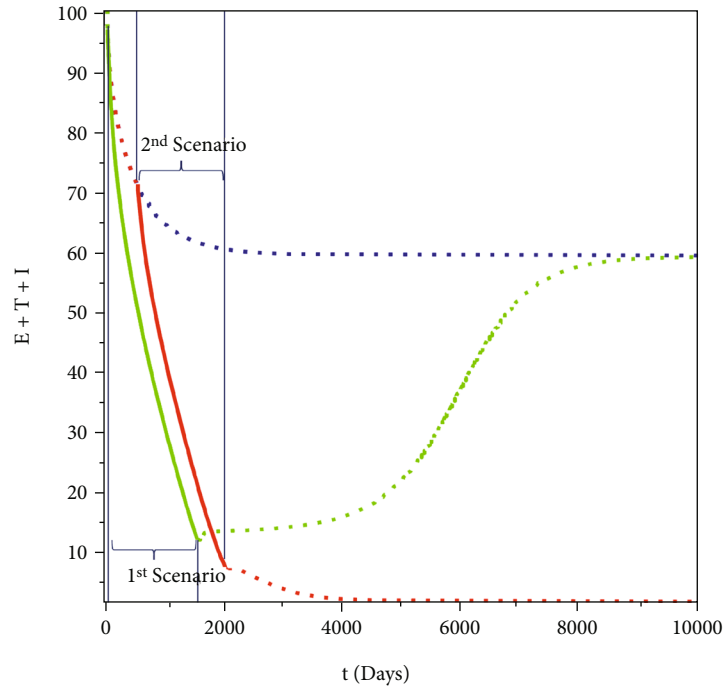
FIGURE 13: Simulations on the total infected human showing the effect of early (green), late (red), and no change (blue) of fumigation intervention.

$$u_2^{2^{\text{nd}}\text{scenario}} = \begin{cases} 0.3, & t \leq 10, \\ 0.9, & 10 \leq t \leq 1510, \\ 0.3, & 1510 \leq t \leq 10000, \end{cases} \quad (33)$$

while the 3$^{\text{rd}}$ scenario when $u_2 = 0.3$ for all time $t \in [0, 10000]$. The result is given in Figure 13. We can see from Figure 13 that when there exist two stable malaria-endemic equilibrium points, then proper fumigation intervention

may change the direction of stability of the system, which in our numerical experiment is from the large endemic size into small endemic size. When the improvement of fumigation is given too early (2$^{\text{nd}}$ scenario), then after the fumigation intervention loosened back into 0.3, then the dynamic of total infected human goes back to the large endemic size. On the other hand, when the intervention is given several times after the first implementation (1$^{\text{st}}$ scenario), then the dynamic of total infected humans is continuously going to the small endemic equilibrium. Based on this, it is necessary

to consider the time for implementing an appropriate increase in fumigation intervention so that the solution dynamics can be directed to a smaller endemic point if the bistability phenomenon appears.

6. Conclusions

Malaria has long been a critical health problem in various parts of the world. Every year, hundreds of millions of people are at risk of becoming infected with malaria, with the majority of cases occurring in Africa. The disease is spread due to the bite of a female Anopheles mosquito and is caused by five different types of Plasmodium. Different types of Plasmodium that infect give different symptoms/serious illness that appears in patients with malaria. Various interventions have been and are being researched, such as vaccination, treatment, vector control with fumigation, and use of insecticide-treated bed net. The high number of cases in various parts of the world until now indicates that our understanding of malaria is still not sufficient to help us optimally control the spread of malaria.

In this research, we introduce a new malaria model that considers two important factors: the use of a new treatment (tafenoquine) to prevent relapse and a saturated fumigation function. The fundamental properties, the existence and stability criteria of the equilibrium points, and how they relate to the basic reproduction number are analyzed in detail. We use Descartes's rule of signs to show a possible number of malaria-endemic equilibrium points when the basic reproduction is less or larger than one. We find that it is possible to have more than one endemic equilibrium when the basic reproduction number is larger than one. Our bifurcation analysis shows how our model consistently exhibits a forward bifurcation at the basic reproduction number equal to one. However, our numerical simulations show forward bifurcation phenomena with hysteresis. This phenomenon results in the emergence of three malaria-endemic equilibrium for a basic reproduction number larger than one.

Our sensitivity analysis shows that tafenoquine has a big potential to control the spread of malaria by preventing the possibility of exposed individuals from relapsing. Furthermore, we also find that although fumigation does not affect the basic reproduction number, it can reduce the number of infected individuals at malaria-endemic equilibrium. Furthermore, a numerical investigation on implementing a high intensity of fumigation in a short time intervention interval may lead to a final switching condition if the forward with hysteresis phenomena appears. We find that when fumigation is implemented in a proper time interval, the direction of endemic equilibrium can be "kicked down" into the smaller size of malaria-endemic equilibrium, which is easier to control with other intervention strategies. We hope that the results of our research in this article can provide another perspective in evaluating the possibility of implementing tafenoquine and fumigation in the field.

Appendix

A. Proof of Theorem 1

We proof our theorem by analyzing the behaviour of each variables on it boundary planes. From malaria model in system (7), we have the dynamics on the boundary of $\mathbb{R}_+^7$ as follows.

$$
\begin{aligned}
\left.\frac{dS}{dt}\right|_{S=0,E\geq 0,T\geq 0,I\geq 0,R\geq 0,U\geq 0,W\geq 0} &= \Lambda_h > 0, \\
\left.\frac{dE}{dt}\right|_{S\geq 0,E=0,T\geq 0,I\geq 0,R\geq 0,U\geq 0,W\geq 0} &= \beta_h W \frac{S}{S+E+T+\alpha I+R} \geq 0, \\
\left.\frac{dT}{dt}\right|_{S\geq 0,E\geq 0,T=0,I\geq 0,R\geq 0,U\geq 0,W\geq 0} &= u_1 E \geq 0, \\
\left.\frac{dI}{dt}\right|_{S\geq 0,E\geq 0,T\geq 0,I=0,R\geq 0,U\geq 0,W\geq 0} &= (1-p)\delta T + \eta E \geq 0, \\
\left.\frac{dR}{dt}\right|_{S\geq 0,E\geq 0,T\geq 0,I\geq 0,R=0,U\geq 0,W\geq 0} &= p\kappa T + \gamma I \geq 0, \\
\left.\frac{dU}{dt}\right|_{S\geq 0,E\geq 0,T\geq 0,I\geq 0,R\geq 0,U=0,W\geq 0} &= \Lambda_v > 0, \\
\left.\frac{dW}{dt}\right|_{S\geq 0,E=0,T\geq 0,I\geq 0,R\geq 0,U\geq 0,W=0} &= \beta_h W \frac{S}{S+E+T+\alpha I+R} \geq 0.
\end{aligned}
\tag{A.1}
$$

It can be seen that all the rates of variables are nonnegative on the boundary of $\mathbb{R}_+^7$. Therefore, if we start in the interior of the nonnegative $\mathscr{D}$, we shall always remain in this region in view that the direction of the vector field is inward on the boundary planes. Thus, the nonnegativity of all solutions of system (7) is guaranteed.

Next, we continue to show the uniqueness solution of system (7) by showing the boundedness of N_h and N_v. Adding the first five equations in system (7) together, we get

$$
\frac{dN_h(t)}{dt} = \Lambda_h - \mu_h(S+E+T+I+R), = \Lambda_h - \mu_h N_h. \tag{A.2}
$$

Solving the above differential equations with respect to $N_h(t)$ and with a positive initial condition $N_h(0) > 0$ gives

$$
N_h(t) = N_h(0) \exp(-\mu_h t) + \frac{\Lambda_h}{\mu_h}. \tag{A.3}
$$

Hence, if we take $t \longrightarrow \infty$, then we have that $N_h(t)$ is eventually bounded by Λ_h/μ_h. To be precise, we have that the biological feasible region of human population of system (7) is

$$
0 \leq S+E+T+I+R \leq \frac{\Lambda_h}{\mu_h}. \tag{A.4}
$$

For mosquito population, by adding the last two equation in system (7), we have

$$
\begin{aligned}
\frac{dN_v(t)}{dt} &= \Lambda_v - \left(\mu_v + u_2 \frac{I}{a + I^2}\right)(U(t) + W(t)), \\
&= \Lambda_v - \left(\mu_v + u_2 \frac{I}{a + I^2}\right)N_v(t), \\
&< \Lambda_v - \mu_v N_v(t).
\end{aligned}
\tag{A.5}
$$

Solving the above expression with respect to $N_v(t)$ and with positive initial condition $N_v(0) > 0$, we get

$$
N_v(t) < N_v(0) \exp(-\mu_v t) + \frac{\Lambda_v}{\mu_v}.
\tag{A.6}
$$

Hence, if we take $t \longrightarrow \infty$, we have that $N_v(t)$ is eventually bounded by Λ_v/μ_v. Hence, the biological feasible region of mosquito population is

$$
0 \leq U + W \leq \frac{\Lambda_v}{\mu_v}.
\tag{A.7}
$$

Hence, the proof is complete.

B. Possible Positive Root of Polynomial (7) when $\mathscr{R}_0 > 1$

For an example, substitute parameter values as in Figure 4(b) and $\beta_h = 0.0015$ to polynomial $G(\Omega, I)$ in (19), we have

$$
\begin{aligned}
G(I) = &-2.3 \times 10^{-17} I^6 - 1.2 \times 10^{-14} I^5 \\
&+ 8.3 \times 10^{-13} I^4 - 4.5 \times 10^{-12} I^3 \\
&+ 3.9 \times 10^{-12} I^2 - 4.3 \times 10^{-11} I + 9.01 \times 10^{-11},
\end{aligned}
\tag{B.1}
$$

which is the case number 22. Solve $G(I) = 0$ with respect to I, and then, we have 3 positive roots of I, i.e., 1.91, 6.23, and 53.6.

C. Possible Positive Root of Polynomial (7) when $\mathscr{R}_0 < 1$

For an example, substituting parameter values as in Figure 4 (a) and $\beta_h = 0.0002$ to polynomial $G(\Omega, I)$ in (19), we have

$$
\begin{aligned}
G(I) = &-2.3 \times 10^{-17} I^6 - 9.3 \times 10^{-15} I^5 - 1.9 \times 10^{-13} I^4 \\
&- 7.4 \times 10^{-12} I^3 - 1.4 \times 10^{-10} I^2 - 1.4 \times 10^{-9} I \\
&- 2.7 \times 10^{-8},
\end{aligned}
\tag{C.1}
$$

which is the case number 64. Solve $G(I) = 0$ with respect to I, and then, we have no positive roots.

D. Expression of $\mathscr{A}$

$$
\mathscr{A} = \mathscr{A}_1 + \mathscr{A}_2,
\tag{D.1}
$$

where

$$
\begin{aligned}
\mathscr{A}_1 = &-m_1 2(\eta\mu_h + \delta(u_1 + \eta)(1 - p) + \eta p\kappa)^2 [\mu_h^3 + (\delta(1 - p) + p\kappa + \eta\alpha + \xi + u_1 + \gamma_1)\mu_h^2 \cdots \\
&+ ((\eta\alpha + \alpha u_1 + \xi + \gamma_1)(1 - p)\delta + p\kappa(\eta\alpha + \xi + \gamma_1 + u_1) + \gamma_1(\xi + \eta + u_1) + \xi(\eta\alpha + u_1))\mu_h \cdots \\
&+ ((\xi + \eta + u_1)\gamma_1 + \xi\alpha(\eta + u_1))(1 - p)\delta + \kappa((\xi + \eta + u_1)\gamma_1 + \xi\eta\alpha)p + \gamma_1\xi u_1,
\end{aligned}
$$

$$
\begin{aligned}
\mathscr{A}_2 = &-\frac{1}{\Lambda_v\alpha\beta_v\mu_h\delta(1 - p)} \left[(\gamma_1 + \mu_h)\Lambda_h\mu_v((1 - p)\delta + p\kappa + \mu_h) \left(\frac{\beta_v\Lambda_v\alpha\mu_h^2}{(\gamma_1 + \mu_h)^2 u_1^2 \Lambda_h^2 (\mu_h + \xi)\mu_v} (2m_2 m_3) \right. \right. \\
&+ \frac{2(\delta(1 - p) + p\kappa + \mu_h)(\delta(\eta + u_1)(1 - p) + \eta(p\kappa + \mu_h))\beta_v\Lambda_v\alpha\mu_h^2}{u_1^2\Lambda_h^2\mu_v(\gamma_1 + \mu_h)} \cdots + \frac{2(\delta(\eta + u_1)(1 - p) + \eta(\kappa p + \mu_h))\beta_v\Lambda_v\alpha\mu_h^2}{(\gamma_1 + \mu_h)u_1 n\mu_v\Lambda_h^2} \cdots \\
&+ \frac{2(\delta(\eta + u_1)(1 - p) + \eta(\kappa p + \mu_h))(\delta\gamma_1(\eta + u_1)(1 - p) + \kappa p\gamma_1(\eta + u_1)\kappa p\mu_h u_1 + \eta\gamma_1\mu_h)\beta_v\Lambda_v\alpha\mu_h^2}{(\gamma_1 + \mu_h)^2 u_1^2(\mu_h + \xi)\mu_v\Lambda_h^2} \cdots \\
&+ \frac{2(\delta(\eta + u_1)(1 - p) + \eta(\kappa p + \mu_h))(\alpha a\beta_v\mu_h + u_2\Lambda_h)((1 - p)(\eta + u_1)\delta + \eta(p\kappa + \mu_h))\Lambda_v\beta_v\alpha\mu_h}{(\gamma_1 + \mu_h)^2 u_1^2 a\Lambda_h^2\mu_v^2} \cdots \\
&\left. \left. + \frac{2(\delta(\eta + u_1)(1 - p) + \eta(\kappa p + \mu_h))\Lambda_v\alpha\beta_v\mu_h u_2(\delta(1 - p)(\eta + u_1) + \eta(p\kappa + \mu_h))}{(\gamma_1 + \mu_h)^2 u_1^2\Lambda_h\mu_v^2 a} \cdots + \frac{2(\delta(\eta + u_1)(1 - p) + \eta(\kappa p + \mu_h))\beta_v\Lambda_v\alpha^2\mu_h^2}{(\gamma_1 + \mu_h)u_1\mu_v\Lambda_h^2} \right) \right],
\end{aligned}
\tag{D.2}
$$

with

$$m_1 = \frac{1}{\delta u_1^2 \Lambda_h^2 \mu_v^2 (1-p)(u_1 + \eta + \mu_h)(\gamma_1 + \mu_h)^2 (\mu_h + \xi)},$$

$$\begin{aligned}
m_2 = &\mu_h^3 + ((1-p)\delta + p\kappa + \xi + \eta + \gamma_1 + u_1)\mu_h^2 \cdots ((\xi + \eta + \gamma_1 + u_1)(1-p)\delta \\
&+ \kappa(\xi + \eta + \gamma_1 + u_1)p + (\xi + \eta + u_1)\gamma + \xi(\eta + u_1))\mu_h \\
&+ \cdots (1-p)((\xi + \eta + u_1)\gamma_1 + \xi(\eta + u_1))\delta \\
&+ \kappa((\xi + \eta + u_1)\gamma_1 + \eta\xi)p + \gamma_1 \xi u_1,
\end{aligned}$$

$$m_3 = (\delta(\eta + u_1)(1-p) + \eta\kappa p + \eta\mu_h). \tag{D.3}$$

Since $\mathscr{A}_1$ and $\mathscr{A}_2$ are negative, then we have $\mathscr{A} < 0$.

Data Availability

No data were used to support this study.

Conflicts of Interest

The author declares that there are no known competing financial interests or personal relationships which have or could be perceived to have influenced the work reported in this article.

Acknowledgments

References

[1] World Health Organization, "Fact sheets: malaria," 2021, https://www.who.int/news-room/fact-sheets/detail/malaria.

[2] World Health Organization, "Severe falciparum malaria," *Transactions of the Royal Society of Tropical Medicine and Hygiene*, vol. 94, supplement 1, pp. 1–90, 2000.

[3] World Health Organization, *World Malaria Report 2018*, World Health Organization, 2018.

[4] World Health Organization, *Test Procedures for Insecticide Resistance Monitoring in Malaria Vector Mosquitoes*, World Health Organization, 2nd edition, 2016.

[5] V. S. Moorthy, R. D. Newman, and J. Okwo-bele, "Malaria vaccine technology roadmap," *The Lancet*, vol. 382, no. 9906, pp. 1700-1701, 2013.

[6] V. S. Moorthy and F. Binka, "R21/matrix-m: a second malaria vaccine?," *The Lancet*, vol. 397, no. 10287, pp. 1782-1783, 2021.

[7] *Medicine for Malaria Venture, Preventing Malaria Relapse with a Single-Dose Treatment*2018, https://www.mmv.org/newsroom/interviews/preventing-malaria-relapse-single-dose-treatment.

[8] J. E. Frampton, "Tafenoquine: first global approval," *Drugs*, vol. 78, no. 14, pp. 1517–1523, 2018.

[9] R. Ross, *The Prevention of Malaria*, John Murray, 1911.

[10] G. Macdonald, "The epidemiology and control of malaria," *The Epidemiology and Control of Malaria*, 1957.

[11] H. Yang, "Malaria transmission model for different levels of acquired immunity and temperature- dependent parameters (vector)," *Revista de Saúde Pública*, vol. 34, no. 3, pp. 223–231, 2000.

[12] A. Ducrot, S. Sirima, B. Somé, and P. Zongo, "A mathematical model for malaria involving differential susceptibility, exposedness and infectivity of human host," *Journal of Biological Dynamics*, vol. 3, no. 6, pp. 574–598, 2009.

[13] F. Forouzannia and A. Gumel, "Mathematical analysis of an age-structured model for malaria transmission dynamics," *Mathematical Biosciences*, vol. 247, pp. 80–94, 2014.

[14] T. Bakery, S. Boureima, and T. Sado, "A mathematical model of malaria transmission in a periodic environment," *Journal of Biological Dynamics*, vol. 12, no. 1, pp. 400–432, 2018.

[15] D. Aldila and M. Angelina, "Optimal control problem and backward bifurcation on malaria transmission with vector bias," *Heliyon*, vol. 7, no. 4, p. e06824, 2021.

[16] H. Wu and Z. Hu, "Malaria transmission model with transmission-blocking drugs and a time delay," *Mathematics Problems in Engineering*, vol. 2021, article 1339086, pp. 1–17, 2021.

[17] Z. Xu, "On the global attractivity of a nonlocal and vector-bias malaria model," *Applied Mathematics Letters*, vol. 121, article 107459, 2021.

[18] J. Li, Y. Zhao, and S. Li, "Fast and slow dynamics of malaria model with relapse," *Mathematical Biosciences*, vol. 246, no. 1, pp. 94–104, 2013.

[19] S. Wang, L. Hu, and L. Nie, "Global dynamics and optimal control of an age-structure malaria transmission model with vaccination and relapse," *Chaos, Solitons & Fractals*, vol. 150, article 111216, 2021.

[20] A. Niger and A. Gumel, "Mathematical analysis of the role of repeated exposure on malaria transmission dynamics," *Differential Equations and Dynamical Systems*, vol. 16, no. 3, pp. 251–287, 2008.

[21] M. Ghosh, S. Olaniyi, and O. S. Obabiyi, "Mathematical analysis of reinfection and relapse in malaria dynamics," *Applied Mathematics and Computation*, vol. 373, p. 125044, 2020.

[22] B. Handari, F. Vitra, R. Ahya, T. S. Nadya, and D. Aldila, "Optimal control in a malaria model: intervention of fumigation and bed nets," *Advances in Difference Equations*, vol. 2019, no. 1, 2019.

[23] F. B. Agusto, "Optimal control and temperature variations of malaria transmission dynamics," *Complexity*, vol. 2020, Article ID 5056432, 32 pages, 2020.

[24] B. Traore, B. Sangare, and S. Traore, "A mathematical model of malaria transmission with structured vector population and seasonality," *Journal of Applied Mathematics*, vol. 2017, Article ID 6754097, 15 pages, 2017.

[25] B. Traore, O. Koutou, and B. Sangare, "A global mathematical model of malaria transmission dynamics with structured mosquito population and temperature variations," *Nonlinear Analysis: Real World Applications*, vol. 53, article 103081, 2020.

[26] S. Andreychuk and L. Yakob, "Mathematical modelling to assess the feasibility of Wolbachia in malaria vector biocontrol," *Journal of Theoretical Biology*, vol. 542, article 111110, 2020.

[27] S. Y. Tchoumi, M. L. Diagne, H. Rwezaura, and J. M. Tchhuenche, "Malaria and covid-19 co-dynamics: a mathematical model and optimal control," *Applied Mathematical Modelling*, vol. 99, pp. 294–327, 2021.

[28] J. D. Maier, S. Siegfried, N. Gultekin et al., "Efficacy and safety of tafenoquine for malaria chemoprophylaxis (1998-2020): a systematic review and meta-analysis," *Travel Medicine and Infectious Disease*, vol. 39, article 101908, 2021.

[29] D. Aldila and H. Seno, "A population dynamics model of mosquito-borne disease transmission, focusing on mosquitoes' biased distribution and mosquito repellent use," *Bulletin of Mathematical Biology*, vol. 81, no. 12, pp. 4977–5008, 2019.

[30] N. Chitnis, J. Hyman, and J. Cushing, "Determining important parameters in the spread of malaria through the sensitivity analysis of a mathematical model," *Bulletin of Mathematical Biology*, vol. 70, no. 5, pp. 1272–1296, 2008.

[31] W. A. Woldegerima, R. Ouifki, and J. Banasiak, "Mathematical analysis of the impact of transmission-blocking drugs on the population dynamics of malaria," *Applied Mathematics and Computation*, vol. 400, article 126005, 2021.

[32] F. Chamchod and N. Britton, "Analysis of a vector-bias model on malaria transmission," *Bulletin of Mathematical Biology*, vol. 73, no. 3, pp. 639–657, 2011.

[33] N. Chitnis, J. Cushing, and J. Hyman, "Bifurcation analysis of a mathematical model for malaria transmission," *SIAM Journal on Applied Mathematics*, vol. 67, no. 1, pp. 24–45, 2006.

[34] M. Naveed, D. Baleanu, A. Raza, M. Ra, A. H. Soori, and M. Mohsin, "Modeling the transmission dynamics of delayed pneumonia-like diseases with a sensitivity of parameters," *Advances in Difference Equations*, vol. 2021, no. 1, 19 pages, 2021.

[35] B. D. Handari, D. Aldila, B. Dewi, H. Rosuliyana, and S. Khosnaw, "Analysis of yellow fever prevention strategy from the perspective of mathematical model and cost-effectiveness analysis," *Mathematical Biosciences and Engineering*, vol. 19, no. 2, pp. 1786–1824, 2022.

[36] D. Aldila, M. Shahzad, S. H. A. Khoshnaw et al., "Optimal control problem arising from COVID-19 transmission model with rapid- test," *Results in Physics*, vol. 37, article 105501, 2022.

[37] M. A. Kuddus and A. Rahman, "Modelling and analysis of human-mosquito malaria transmission dynamics in Bangladesh," *Mathematics and Computers in Simulation*, vol. 193, pp. 123–138, 2022.

[38] S. R. Bandekar and M. Ghosh, "A co-infection model on tb - covid-19 with optimal control and sensitivity analysis," *Mathematics and Computers in Simulation*, vol. 200, pp. 1–31, 2022.

[39] O. Diekmann, J. Heesterbeek, and J. Metz, "On the definition and the computation of the basic reproduction ratio r0 in models for infectious diseases in heterogeneous populations," *Journal of Mathematical Biology*, vol. 28, no. 4, pp. 365–382, 1990.

[40] O. Diekmann and J. Heesterbeek, *Mathematical Epidemiology of Infectious Diseases, Model Building, Analysis and Interpretation*, John Wiley & Son, Chichester, 2020.

[41] O. Diekmann, J. A. P. Heesterbeek, and M. G. Roberts, "The construction of next-generation matrices for compartmental epidemic models," *Journal of the Royal Society Interface*, vol. 7, no. 47, pp. 873–885, 2010.

[42] D. Aldila, "Analyzing the impact of the media campaign and rapid testing for covid-19 as an optimal control problem in East Java, Indonesia," *Chaos, Solitons and Fractals*, vol. 141, article 110364, 2020.

[43] S. Rahmayani, D. Aldila, B. Handari, and Department of Mathematics, Universitas Indonesia, Kampus UI Depok, Depok 16424, Indonesia, "Cost-effectiveness analysis on measles transmission with vaccination and treatment intervention," *AIMS Mathematics*, vol. 6, no. 11, pp. 12491–12527, 2021.

[44] D. Aldila, M. Ndii, and B. Samiadji, "Optimal control on covid-19 eradication program in Indonesia under the effect of community awareness," *Mathematical Biosciences and Engineering*, vol. 17, no. 6, pp. 6355–6389, 2020.

[45] P. van den Driessche and J. Watmough, "Reproduction numbers and sub-threshold endemic equilibria for compartmental models of disease transmission," *Mathematical Biosciences*, vol. 180, no. 1-2, pp. 29–48, 2002.

[46] R. Descartes, *La geometrie (discours de la methode, third part)*, vol. 1637, Ed. of Leyde, 1637.

[47] C. Castillo-Chavez and B. Song, "Dynamical models of tuberculosis and their applications," *Mathematical Biosciences and Engineering*, vol. 1, no. 2, pp. 361–404, 2004.

[48] D. Aldila, S. H. Khoshnaw, E. Safitri et al., "A mathematical study on the spread of covid-19 considering social distancing and rapid assessment: the case of Jakarta, Indonesia," *Chaos, Solitons and Fractals*, vol. 139, article 110042, 2020.

[49] G. Simorangkir, D. Aldila, A. Rizka, H. Tasman, and E. Nugraha, "Mathematical model of tuberculosis considering observed treatment and vaccination interventions," *Journal of Interdisciplinary Mathematics*, vol. 24, no. 6, pp. 1717–1737, 2021.

[50] A. Islamilova, D. Aldila, W. Giyarti, and H. Tasman, "Modelling the spread of atherosclerosis considering relapse and linear treatment," *Journal of Physics: Conference Series*, vol. 1722, no. 1, p. 012039, 2021.

[51] D. Aldila, B. Saslia, W. Gayarti, and H. Tasman, "Backward bifurcation analysis on tuberculosis disease transmission with saturated treatment," *Journal of Physics: Conference Series*, vol. 1821, no. 2021, article 012002, 2021.

[52] MathWorks, 2021, June 2022, https://www.mathworks.com/help/matlab/ref/ode45.html.

[53] L. F. Shampine and M. W. Reichelt, "The matlab ode suite," *SIAM Journal on Scientific Computing*, vol. 18, no. 1, pp. 1–22, 1997.

[54] H. Gulbudak and M. Martcheva, "Forward hysteresis and backward bifurcation caused by culling in an avian influenza model," *Mathematical Biosciences*, vol. 246, no. 1, pp. 202–212, 2013.

Research Article

Analysis and Simulation of Fractional Order Smoking Epidemic Model

Aqeel Ahmad,[1] Muhammad Farman [ID],[2] Abdul Ghafar [ID],[1] Mustafa Inc [ID],[3,4,5] Mohammad Ozair Ahmad,[2] and Ndolane Sene [ID][6]

[1]*Department of Mathematics, Ghazi University, DG Khan, Pakistan*
[2]*Department of Mathematics and Statistics, University of Lahore, Lahore 54590, Pakistan*
[3]*Department of Computer Engineering, Biruni University, Istanbul, Turkey*
[4]*Department of Mathematics, Science Faculty, Firat University, Elazig, Turkey*
[5]*Department of Medical Research, China Medical University, Taichung, Taiwan*
[6]*Laboratoire Lmdan, Departement De Mathematiques De Decision, Facultíe des Sciences Economiques et Gestion, Universite Cheikh Anta Diop De Dakar, BP 5683 Dakar Fann, Senegal*

Correspondence should be addressed to Mustafa Inc; minc@firat.edu.tr and Ndolane Sene; ndolanesene@yahoo.fr

In recent years, there are many new definitions that were proposed related to fractional derivatives, and with the help of these definitions, mathematical models were established to overcome the various real-life problems. The true purpose of the current work is to develop and analyze Atangana-Baleanu (AB) with Mittag-Leffler kernel and Atangana-Toufik method (ATM) of fractional derivative model for the Smoking epidemic. Qualitative analysis has been made to `verify the steady state. Stability analysis has been made using self-mapping and Banach space as well as fractional system is analyzed locally and globally by using first derivative of Lyapunov. Also derive a unique solution for fractional-order model which is a new approach for such type of biological models. A few numerical simulations are done by using the given method of fractional order to explain and support the theoretical results.

1. Introduction

Mathematics was firstly used in biology in the twelfth century when Fibonacci used his popular Fibonacci series to explain a growing population. Daniel Bernoulli used mathematics to describe the effect of small pox. The term biological mathematics was primarily used by Johannes Reinke in 1901. It is aimed at the mathematical image and modeling of biological processes. It is also used to recognize phenomena in the living organism. Bio math has made major progress during the last few decades, and this progress will continue in upcoming decades. Math has played a large role in natural science but now it also will be more useful in biology. We should teach basic concepts of bio math at early stages. The basic steps in mathematical biology are few. The initial step is to explain the biological process and raise a question about the basics. The second step is to build up a mathematical model that represents the underlying biological process. The 3rd step is to apply the method and concepts of math to obtain predictions about the model. The last step is to check whether this prediction answers the raised questions. After this, anyone can further explore the biological question by using mathematical models [1].

Now in the modern world, tobacco smoke is the most inhaled substance. Tobacco is made by mixing its agricultural form with many substances. The smoke is inhaled through the lungs. The most dangerous epidemic in the world is the smoking epidemic. Due to smoking 50% of its users died. Every year, about 60 million people die due to smoking. During the last few decades, there has been a huge boost in deaths. The death rate will rise thrice annually in 2030, almost seventy percent is in developing countries.

According to WHO, 10 million people will die due to smoking. As compared to other diseases, the death ratio is higher than all. The person who uses tobacco dies 14 years earlier than someone who does not smoke [2]. Tobacco smoking is the major reason for cancer and another disease. About 70% of people died due to tobacco-related diseases in developing countries [3]. Three million people died due to smoking yearly.

Nowadays, smoking is the most dangerous habit. The heart attack ratio is 70 percent more than a nonsmoker. There are 900 million men smokers and 200 women smokers in the world. After every 6 seconds, there is a death due to smoking. Smoking is a major cause of lung and heart attack in the world. Due to smoking, the chances of other diseases like heart attack, stroke, especially lung cancer, throat, mouth, esophagus, and pancreas are increased. Tobacco causes many tissue-related diseases. Tobacco smoke is a mixture of several toxic gases. It includes 98 of which are linked with an increased risk of cardiovascular disease, 69 of which are known to be carcinogenic. Daily, a smoker takes 1 or 2 milligrams of nicotine per cigarette. Thus, if a person smokes 5 cigarettes, it takes at least 5-10 milligrams of nicotine. The effect of smoking is not limited to the person who but also adverse effects for other people. It causes 22% of death annually.

The chemical composition of tobacco varies according to the environment. These leaves are mixed with many chemicals. Tobacco smoke contains a large number of different chemicals such as benzopyrene, NNK, aldehydes, carbon monoxide, hydrogen cyanide, phenol, nicotine, and harmala alkoids. The radioactive element polonium 210 is also occurring in tobacco. There are almost 4 thousand noxious substances in smoke which is the main reason for cancer [4, 5]. The chemical composition of smoke depends on puff frequency and other materials. Nicotine is the main issue for disturbing the nervous system, rise in heartbeat, raising blood pressure, and shrinking the small blood vessels which are the main basis of wrinkles. The amount of oxygen decreased in the lungs due to carbon monoxide (CO). The natural lungs cleaner that is minuscule hairs is destroyed by hydrogen cyanide. Lead, nickel arsenic, and cadmium are also present in smoke. Some pesticides like DDT are also found in smoke. The major reason for skin and lung cancer is a toxic chemical that is present in smoke. 10 million deaths will occur in the 20th century and 1 billion in the 21st century due to smoking [6]. Cigarette smoking affects human fertility badly [7].

The generalization of classical calculus is called fractional calculus which is concerned with the operation of integration and differentiation of fractional order. In the 19th century, fractional calculus mathematicians introduced fractional differential equations, fractional dynamics, and fractional geometry. Fractional calculus is used in almost every field of science. It is used to model physical as well as engineering processes. In many cases, standard mathematical models of integer order do not work properly. Due to this reason, fractional calculus made a major contribution to the field of mechanics, chemistry, biology, and image processing. By using fractional calculus, several physical prob-

lems are solved. By using integer-order derivatives, the system shows many problems such as history and nonlocal effects. Primarily, all the studies were dependent on Caputo fractional-order and Reimann Liouville fractional (RLF) derivatives. Nowadays, it has been highlighted that these derivatives have the issue, and the issue is they have a singular kernel. That is the reason so many new definitions were presented in the studies [8–16]. These new definitions were very impactful because they have nonsingular kernels which are according to their needs. Caputo fractional derivatives [17], the Caputo-Fabrizio derivative [11], and AB [18] fractional derivative have differed from each other only because Caputo is defined by a power law, Fabrizio defined by using exponential decay law, and AB defined by ML law. Tateishi et al. describe the role of fractional time operator derivative in a study of anomalous diffusion [12]. With the help of analytical techniques, Bulut et al. deliberate the role of differential equations of arbitrary order [19]. The key concepts of fractional differential equations and their application are explained by Kilbas et al. [20]. Atangana and Koca examined the Keller-Segel model about a fractional derivative having a nonsingular kernel [21]. Fractional logistic maps are newly introduced by Huang et al. [22]. Zaman studied the qualitative response of the dynamics of giving up smoking [23]. The giving up smoking model linked with Caputo fractional derivative is a probe by Singh et al. [24].

Numerous studies identified sociodemographic, environmental, and behavioral risk factors such as age, sex, occupations, indoor air pollutions, smoking, and alcohol consumption [25–27] as being associated with the development of TB in humans. In [28], a simple model for the effect of tobacco smoking in the in-host dynamics of HIV is formulated with the aim of studying how tobacco smoking affects HIV in-host dynamics. Zoonotic tuberculosis (zTB) knowledge, prevention, and control practices via a survey in Bangladesh considering impact of smoking are also in [29].

In this work, we get the approximate solutions of the fractional smoking model by using the Atangana-Toufik method.

2. Basic Concepts of Fractional Operators

Definition 1. For a function $g(t) \in W_2^1(0, 1)$, $b > a$ and $\sigma \in [0, 1]$, the definition of AB derivative in the Caputo sense is given by

$$
{}_0^{ABC}D_t^\sigma g(t) = \frac{\text{AB}(\sigma)}{1 - \sigma} \int_0^t \frac{d}{d\tau} g(\tau) M_\sigma \\
\cdot \left[-\frac{\sigma}{1 - \sigma} (t - \tau)^\sigma \right] d\tau, \quad n - 1 < \sigma < n, \tag{1}
$$

where

$$
\text{AB}(\sigma) = 1 - \sigma + \frac{\sigma}{\Gamma(\sigma)}. \tag{2}
$$

By using ST for (1), we obtain

$$ST\left[{}_0^{ABC}D_t^\sigma g(t)\right](s) = \frac{q(\sigma)}{1-\sigma}\left\{\sigma\Gamma(\sigma+1)M_\sigma\left(-\frac{1}{1-\sigma}V^\sigma\right)\right\}$$
$$\times[ST(g(t)) - g(0)]. \tag{3}$$

Definition 2. The Laplace transform (LT) of the Caputo fractional derivative of a function $g(t)$ of order $\sigma > 0$ is defined as

$$L\left[{}_0^C D_t^\sigma g(t)\right] = s^\sigma g(s) - \sum_{\sigma=0}^{n-1} g^{(\sigma)}(0)s^{\sigma-\nu-1}. \tag{4}$$

Definition 3. The LT of the function $t^{\sigma_1-1}E_{\sigma,\sigma_1}(\pm\mu t^\sigma)$ is defined as

$$L\left[t^{\sigma_1-1}E_{\sigma,\sigma_1}(\pm\mu t^\sigma)\right] = \frac{s^{\sigma-\sigma_1}}{s^\sigma \mp \mu}, \tag{5}$$

where E_{σ,σ_1} is the two-parameter ML function with σ, $\sigma_1 > 0$. Further, the ML function satisfies the following equation [17].

$$E_{\sigma,\sigma_1}(f) = fE_{\sigma,\sigma+\sigma_1}(f) + \frac{1}{\Gamma(\sigma_1)}. \tag{6}$$

Definition 4. Suppose that $g(t)$ is continuous on an open interval (a, b), then the fractal-fractional integral of $g(t)$ of order σ having ML type kernel and given by

$${}^{FFM}J_{0,t}^{\sigma,\sigma_1}(g(t)) = \frac{\sigma\sigma_1}{AB(\sigma)\Gamma(\sigma_1)}\int_0^t s^{\sigma_1-1}g(s)(t-s)^\sigma ds$$
$$+ \frac{\sigma_1(1-\sigma)t^{\sigma_1-1}g(t)}{AB(\sigma)}. \tag{7}$$

3. Model Formulation

We will study the giving up smoking model for overall population at time t. We separate the population into 5 groups, potential smokers $P(t)$, occasional smokers $L(t)$, heavy smokers $S(t)$, temporary quitters $Q(t)$, and smokers who quit permanently $R(t)$ specified by $T(t) = P(t) + L(t) + S(t) + Q(t) + R(t)$. Due to smoking, the chances of other diseases like heart attack, stroke, especially lung cancer, throat, mouth, esophagus, and pancreas are increased [24]. The model is developed as follows

$$\frac{dP}{dt} = a(1-P) - bPS, \tag{8}$$

$$\frac{dL}{dt} = -aL + bPL - cLS, \tag{9}$$

$$\frac{dS}{dt} = -(a+d) + cLS + fQ, \tag{10}$$

$$\frac{dQ}{dt} = -(a+f)Q + d(1-e)S, \tag{11}$$

$$\frac{dR}{dt} = -aR + edS. \tag{12}$$

With the initial conditions

$$P(0) = \delta_1, \tag{13}$$
$$L(0) = \delta_2, \tag{14}$$
$$S(0) = \delta_3, \tag{15}$$
$$Q(0) = \delta_4, \tag{16}$$
$$R(0) = \delta_5. \tag{17}$$

The rate of change between potential smoker and occasional smokers is represented by b, a represents the rate of natural death, the rate of occasional smoker and temporary smokers by c, the rate of change between quitters and smoker is shown by f, the rate of giving up smoking is shown by d, fraction of temporary giving up smoker is represented by $(1-e)$ (at the rate of d), e shows the remaining fraction of smokers who give up smoking forever (at a rate d).

4. Qualitative Analysis

By substituting the values of parameters in given system of differential equations and the rate of change with respect to time is zero, we get

$$a(1-P) - bPS = 0, \tag{18}$$
$$-aL + bPS - cLS = 0, \tag{19}$$
$$-(a+d)S + cLS + fQ = 0, \tag{20}$$
$$-(a+f)Q + d(1-e)S = 0, \tag{21}$$
$$-aR + edS = 0. \tag{22}$$

By simplifying the above equations, we get disease-free equilibrium, denoted by E_0, i.e., $E_0 = (1, 0, 0, 0, 0)$.

Endemic equilibrium is found in terms of one of the infected compartment, denoted by E_1, i.e., $E_1 = (P^*, L^*, S^*, Q^*, R^*)$ where $P^* = a/a + bS^*$, $L^* = ab/(a+bS^*)(a+cS^*)$, $Q^* = d(1-e)S^*/a + f$, $R^* = edS^*/a$.

4.1. Stability Analysis and Reproductive Number. It is important to find the verge conditions to check the status of population, whether the disease persist or dies out. In case of disease free equilibrium point, $R_0 < 1$, which shows

that the disease will die out. In case of endemic equilibrium, $R_0 > 1$. Consider the Jacobian matrix (JM) as

$$
J = \begin{bmatrix}
-a - bS & 0 & -bP & 0 & 0 \\
bS & -a - cS & bP - cL & 0 & 0 \\
0 & cS & -a - d + cL & f & 0 \\
0 & 0 & d(1 - e) & -a - f & 0 \\
0 & 0 & ed & 0 & -a
\end{bmatrix}.
\tag{23}
$$

Since the JM is $J = F - V$ where

We know that $K = FV^{-1}$ and using the relation $|K - \lambda I| = 0$ solving on mathematica for the Eigenvalue λ, which represents the reproductive number R_0, i.e.,

$$
R_0 = \frac{df(1 - e)}{(a + d)(a + f)}.
\tag{24}
$$

Hence, $R_0 = 0.431034 < 1$, according to the given parameter values.

Theorem 5. *The disease free equilibrium E_0 is locally asymptotically stable for $R_0 < 1$, if $\mathrm{Re}\,(\lambda) < 0$, otherwise, unstable.*

Proof. E_0 of the given system is locally asymptotically stable if $\mathrm{Re}\,(\lambda) < 0$ where λ can be evaluated from the relation $|J_0 - \lambda I| = 0$.

By using the relation $|J_0 - \lambda I| = 0$, we get. $\mathrm{Re}\,(\lambda)$ as

$$
\lambda_1 = -a, \lambda_2 = \frac{1}{2}\left[-2a - d - f - \sqrt{d^2 + 2df - 4def + f^2}\right] < 0,
\tag{25}
$$

$$
\lambda_3 = \frac{1}{2}\left[-2a - d - f + \sqrt{d^2 + 2df - 4def + f^2}\right] < 0\lambda_1.
\tag{26}
$$

All the Eigenvalues are negative real parts which represent that the given system is locally asymptotically stable. $\square$

Theorem 6. *When the reproductive number $R_0 > 1$, the endemic equilibrium points E_1 of the PLSQR model is globally asymptotically stable.*

Proof. The Lyapunov function can be written as

$$
\begin{aligned}
&M(P^*, L^*, S^*, Q^*, R^*)\\
&= \left(P - P^* - P^* \log \frac{P^*}{P}\right) + \left(L - L^* - L^* \log \frac{L^*}{L}\right)\\
&\quad + \left(S - S^* - S^* \log \frac{S^*}{S}\right) + \left(Q - Q^* - Q^* \log \frac{Q^*}{Q}\right)\\
&\quad + \left(R - R^* - R^* \log \frac{R^*}{R}\right).
\end{aligned}
\tag{27}
$$

Therefore, applying the derivative respect to t on both sides yields

$$
\begin{aligned}
\frac{dM}{dt} = \dot{M} &= \left(\frac{P - P^*}{P}\right)\dot{P} + \left(\frac{L - L^*}{L}\right)\dot{L} + \left(\frac{S - S^*}{S}\right)\dot{S}\\
&\quad + \left(\frac{Q - Q^*}{Q}\right)\dot{Q} + \left(\frac{R - R^*}{R}\right)\dot{R}.
\end{aligned}
\tag{28}
$$

Now, we can write their values for derivatives as follows

$$
\begin{aligned}
\frac{dM}{dt} = \dot{M} &= \left(\frac{P - P^*}{P}\right)(a(1 - P) - bPS)\\
&\quad + \left(\frac{L - L^*}{L}\right)(-aL + bPS - cLS)\\
&\quad + \left(\frac{S - S^*}{S}\right)(-(a + d)S + cLS + fQ)\\
&\quad + \left(\frac{Q - Q^*}{Q}\right)(-(a + f)Q + d(1 - e)S)\\
&\quad + \left(\frac{R - R^*}{R}\right)(-aR + edS).
\end{aligned}
\tag{29}
$$

Putting $P = P - P^*$, $L = L - L^*$, $S = S - S^*$, $Q = Q - Q^*$, $R = R - R^*$ leads to

$$
\begin{aligned}
\frac{dM}{dt} &= \left(\frac{P - P^*}{P}\right)(a(1 - (P - P^*)) - b(P - P^*)(S - S^*))\\
&\quad + \left(\frac{L - L^*}{L}\right)(-a(L - L^*) + b(P - P^*)(S - S^*)\\
&\quad - c(L - L^*)(S - S^*)) + \left(\frac{S - S^*}{S}\right)(-(a + d)(S - S^*)\\
&\quad + c(L - L^*)(S - S^*) + f(Q - Q^*))\\
&\quad + \left(\frac{Q - Q^*}{Q}\right)(-(a + f)(Q - Q^*) + d(1 - e)(S - S^*))\\
&\quad + \left(\frac{R - R^*}{R}\right)(-a(R - R^*) + ed(S - S^*)).
\end{aligned}
\tag{30}
$$

We can organize the above as follows

$$
\begin{aligned}
\frac{dM}{dt} &= a - \left(\frac{P^*}{P}\right)a - \frac{1}{P}(P - P^*)^2 - \frac{b}{P}(P - P^*)^2(S)\\
&\quad + \frac{b}{P}(P - P^*)^2(S^*) - \frac{a}{L}(L - L^*)^2 + bPS - bP^*S\\
&\quad + bP^*S^* - bPS^* - \left(\frac{L^*}{L}\right)bPS + \left(\frac{L^*}{L}\right)bP^*S\\
&\quad - \left(\frac{L^*}{L}\right)bP^*S^* + \left(\frac{L^*}{L}\right)bPS^* - \frac{C}{L}(L - L^*)^2(S)\\
&\quad + \frac{C}{L}(L - L^*)^2(S^*) - \frac{(a + d)}{S}(S - S^*)^2 + \frac{c}{S}(L)(S - S^*)^2
\end{aligned}
$$

$$- \frac{c}{S}(L^*)(S - S^*)^2 + f(Q) - f(Q^*) - \left(\frac{S^*}{S}\right)fQ$$

$$+ \left(\frac{S^*}{S}\right)fQ^* - \frac{(a+f)}{Q}(Q - Q^*)^2 + d(1-e)(S)$$

$$- d(1-e)(S^*) - d(1-e)(S)\left(\frac{Q^*}{Q}\right)$$

$$+ d(1-e)(S^*)\left(\frac{Q^*}{Q}\right) - \frac{a}{R}(R - R^*)^2 + ed(S) - ed(S^*)$$

$$- ed(S)\left(\frac{R^*}{R}\right) + ed(S^*)\left(\frac{R^*}{R}\right). \tag{31}$$

To avoid the complexity, the above can be written as

$$\frac{dM}{dt} = \Sigma - \Omega, \tag{32}$$

where

$$\Sigma = a + \frac{b}{P}(P - P^*)^2(S^*) + bPS + bP^*S^* + \left(\frac{L^*}{L}\right)bP^*S$$

$$+ \left(\frac{L^*}{L}\right)bPS^* + \frac{C}{L}(L - L^*)^2(S^*) + \frac{c}{S}(L)(S - S^*)^2 + f$$

$$+ \left(\frac{S^*}{S}\right)fQ^* + d(1-e)(S) + d(1-e)(S^*)\left(\frac{Q^*}{Q}\right)$$

$$+ ed(S) + ed(S^*)\left(\frac{R^*}{R}\right), \tag{33}$$

$$\Omega = \left(\frac{P^*}{P}\right)a + \frac{1}{P}(P - P^*)^2 + \frac{b}{P}(P - P^*)^2(S) + \frac{a}{L}(L - L^*)^2$$

$$+ bP^*S + bPS^* + \left(\frac{L^*}{L}\right)bPS + \left(\frac{L^*}{L}\right)bP^*S^*$$

$$+ \frac{C}{L}(L - L^*)^2(S) + \frac{(a+d)}{S}(S - S^*)^2 + \frac{c}{S}(L^*)(S - S^*)^2$$

$$+ fQ^* + \left(\frac{S^*}{S}\right)fQ + \frac{(a+f)}{Q}(Q - Q^*)^2 + d(1-e)(S^*)$$

$$+ d(1-e)(S)\left(\frac{Q^*}{Q}\right) + \frac{a}{R}(R - R^*)^2 + ed(S^*)$$

$$+ ed(S)\left(\frac{R^*}{R}\right). \tag{34}$$

It is concluded that if $\Sigma < \Omega$, this yields, $dM/dt < 0$, however when, $P = P^*, L = L^*, S = S^*, Q = Q^*, R = R^*$

$$0 = \Sigma - \Omega \Rightarrow \frac{dM}{dt} = 0. \tag{35}$$

We can see that the largest compact invariant set for the suggested model in

$$\left\{(P^*, L^*, S^*, Q^*, R^*) \in \Gamma; \frac{dM}{dt} = 0\right\}, \tag{36}$$

is the point $\{E_1\}$ the endemic equilibrium of the considered model. By the help of the Lasalles invariance concept, it follows that E_1 is globally asymptotically stable in Γ if $\Sigma < \Omega$. $\square$

5. Atangana-Baleanu Caputo Sense with Mittag-Leffler Kernel

By applying AB fractional derivative of order σ and $\sigma \in (0, 1]$, into ML kernel, then, the system (8) becomes

$$_0^{ABC}D_t^\sigma P = a(1 - P) - bPS, \tag{37}$$

$$_0^{ABC}D_t^\sigma L = -aL + bPL - cLS, \tag{38}$$

$$_0^{ABC}D_t^\sigma S = -(a + d)S + cLS + fQ, \tag{39}$$

$$_0^{ABC}D_t^\sigma Q = -(a + f)Q + d(1 - e)S, \tag{40}$$

$$_0^{ABC}D_t^\sigma R = -aR + edS. \tag{41}$$

The initial conditions associated with the system (37) are

$$P(0) = \delta_1, \tag{42}$$

$$L(0) = \delta_2, \tag{43}$$

$$S(0) = \delta_3, \tag{44}$$

$$Q(0) = \delta_4, \tag{45}$$

$$R(0) = \delta_5. \tag{46}$$

We will discuss the numerical value of solution of system for different values of ρ. With the help of iterative method and the Padè approximation results are obtained.

We use the values of the parameters $a = 0.04$, $b = 0.23$, $c = 0.3$, $d = 0.2$, $e = 0.4$, and $f = 0.25$. The initial conditions are given by $P(0) = 0.60301$, $L(0) = 0.24000$, $S(0) = 0.10628$, $Q(0) = 0.03260$, and $R(0) = 0.01811$.

Taking ST on both sides of (37), we get

$$\frac{q(\sigma)\sigma\Gamma(\sigma + 1)}{1 - \sigma}N_\sigma\left(-\frac{1}{1 - \sigma}V^\sigma\right)ST\{P(t) - P(0)\}$$

$$= ST[a(1 - P) - bPS], \tag{47}$$

$$\frac{q(\sigma)\sigma\Gamma(\sigma + 1)}{1 - \sigma}N_\sigma\left(-\frac{1}{1 - \sigma}V^\sigma\right)ST\{L(t) - L(0)\}$$

$$= ST[-aL + bPL - cLS], \tag{48}$$

$$\frac{q(\sigma)\sigma\Gamma(\sigma + 1)}{1 - \sigma}N_\sigma\left(-\frac{1}{1 - \sigma}V^\sigma\right)ST\{S(t) - S(0)\}$$

$$= ST[-(a + d)S + cLS + fQ], \tag{49}$$

$$\frac{q(\sigma)\sigma\Gamma(\sigma+1)}{1-\sigma}N_\sigma\left(-\frac{1}{1-\sigma}V^\sigma\right)\mathrm{ST}\{Q(t)-Q(0)\}$$
$$=\mathrm{ST}[-(a+f)Q+d(1-e)S], \tag{50}$$

$$\frac{q(\sigma)\sigma\Gamma(\sigma+1)}{1-\sigma}N_\sigma\left(-\frac{1}{1-\sigma}V^\sigma\right)\mathrm{ST}\{R(t)-R(0)\}$$
$$=\mathrm{ST}[-aR+edS]. \tag{51}$$

Rearranging, we get

$$\mathrm{ST}(P(t))=P(0)+\frac{1-\sigma}{q(\sigma)\sigma\Gamma(\sigma+1)N_\sigma(-(1/1-\sigma)V^\sigma)}$$
$$\cdot\mathrm{ST}[a(1-P)-bPS], \tag{52}$$

$$\mathrm{ST}(L(t))=L(0)+\frac{1-\sigma}{q(\sigma)\sigma\Gamma(\sigma+1)N_\sigma(-(1/1-\sigma)V^\sigma)}$$
$$\cdot\mathrm{ST}[-aL+bPL-cLS], \tag{53}$$

$$\mathrm{ST}(S(t))=S(0)+\frac{1-\sigma}{q(\sigma)\sigma\Gamma(\sigma+1)N_\sigma(-(1/1-\sigma)V^\sigma)}$$
$$\cdot\mathrm{ST}[-(a+d)S+cLS+fQ], \tag{54}$$

$$\mathrm{ST}(Q(t))=Q(0)+\frac{1-\sigma}{q(\sigma)\sigma\Gamma(\sigma+1)N_\sigma(-(1/1-\sigma)V^\sigma)}$$
$$\cdot\mathrm{ST}[-(a+f)Q+d(1-e)S], \tag{55}$$

$$\mathrm{ST}(R(t))=R(0)+\frac{1-\sigma}{q(\sigma)\sigma\Gamma(\sigma+1)N_\sigma(-(1/1-\sigma)V^\sigma)}$$
$$\cdot\mathrm{ST}[-aR+edS]. \tag{56}$$

Now taking inverse ST on both sides of equation (52), we get

$$P(t)=P(0)+\mathrm{ST}^{-1}\left[\frac{1-\sigma}{q(\sigma)\sigma\Gamma(\sigma+1)N_\sigma(-(1/1-\sigma)V^\sigma)}\right.$$
$$\left.\cdot\mathrm{ST}\{a(1-P)-bPS\}\right], \tag{57}$$

$$L(t)=L(0)+\mathrm{ST}^{-1}\left[\frac{1-\sigma}{q(\sigma)\sigma\Gamma(\sigma+1)N_\sigma(-(1/1-\sigma)V^\sigma)}\right.$$
$$\left.\cdot\mathrm{ST}\{-aL+bPL-cLS\}\right], \tag{58}$$

$$S(t)=S(0)+\mathrm{ST}^{-1}\left[\frac{1-\sigma}{q(\sigma)\sigma\Gamma(\sigma+1)N_\sigma(-(1/1-\sigma)V^\sigma)}\right.$$
$$\left.\cdot\mathrm{ST}\{-(a+d)S+cLS+fQ\}\right], \tag{59}$$

$$Q(t)=Q(0)+\mathrm{ST}^{-1}\left[\frac{1-\sigma}{q(\sigma)\sigma\Gamma(\sigma+1)N_\sigma(-(1/1-\sigma)V^\sigma)}\right.$$
$$\left.\cdot\mathrm{ST}\{-(a+f)Q+d(1-e)S\}\right], \tag{60}$$

$$R(t)=R(0)+\mathrm{ST}^{-1}\left[\frac{1-\sigma}{q(\sigma)\sigma\Gamma(\sigma+1)N_\sigma(-(1/1-\sigma)V^\sigma)}\right.$$
$$\left.\cdot\mathrm{ST}\{-aR+edS\}\right]. \tag{61}$$

We next attain the following recursive formula.

$$P_{(n+1)}(t)=P_n(0)+\mathrm{ST}^{-1}\left[\frac{1-\sigma}{q(\sigma)\sigma\Gamma(\sigma+1)N_\sigma(-(1/1-\sigma)V^\sigma)}\right.$$
$$\left.\cdot\mathrm{ST}\{a(1-P_n)-bP_nS_n\}\right], \tag{62}$$

$$L_{(n+1)}(t)=L_n(0)+\mathrm{ST}^{-1}\left[\frac{1-\sigma}{q(\sigma)\sigma\Gamma(\sigma+1)N_\sigma(-(1/1-\sigma)V^\sigma)}\right.$$
$$\left.\cdot\mathrm{ST}\{-aL_n+bP_nL_n-cL_nS_n\}\right], \tag{63}$$

$$S_{n+1}(t)=S_n(0)+\mathrm{ST}^{-1}\left[\frac{1-\sigma}{q(\sigma)\sigma\Gamma(\sigma+1)N_\sigma(-(1/1-\sigma)V^\sigma)}\right.$$
$$\left.\cdot\mathrm{ST}\{-(a+d)S_n+cL_nS_n+fQ_n\}\right], \tag{64}$$

$$Q_{(n+1)}(t)=Q_n(0)+\mathrm{ST}^{-1}\left[\frac{1-\sigma}{q(\sigma)\sigma\Gamma(\sigma+1)N_\sigma(-(1/1-\sigma)V^\sigma)}\right.$$
$$\left.\cdot\mathrm{ST}\{-(a+f)Q_n+d(1-e))S_n\}\right], \tag{65}$$

$$R_{(n+1)}(t)=R_n(0)+\mathrm{ST}^{-1}\left[\frac{1-\sigma}{q(\sigma)\sigma\Gamma(\sigma+1)N_\sigma(-(1/1-\sigma)V^\sigma)}\right.$$
$$\left.\cdot\mathrm{ST}\{-aR_n+edS_n\}\right]. \tag{66}$$

And the solution of (62) is

$$P(t)=\lim_{n\longrightarrow\infty}P_n(t), \tag{67}$$

$$L(t)=\lim_{n\longrightarrow\infty}L_n(t), \tag{68}$$

$$S(t)=\lim_{n\longrightarrow\infty}S_n(t), \tag{69}$$

$$Q(t)=\lim_{n\longrightarrow\infty}Q_n(t), \tag{70}$$

$$R(t) = \lim_{n \longrightarrow \infty} R_n(t). \tag{71}$$

Theorem 7. *Let* $(X, |.|)$ *be a Banach space and* H *a self-map of* X *satisfying*

$$\|H_x - H_r\| \le \theta\|X - H_x\| + \theta\|x - r\|, \tag{72}$$

for all $x, r \in X$, *and* $0 \le \theta < 1$. *Suppose that* H *is Picard* H-*stable. Suppose that system (62), we have*

$$P_{n+1}(t) = P_n(0) + ST^{-1}\left\{\frac{1-\sigma}{q(\sigma)\sigma\Gamma(\sigma+1)N_\sigma(-(1/1-\sigma)V^\sigma)}\right.$$
$$\left. \cdot ST[a(1-P_n) - bP_nS_n]\right\},$$
$$\tag{73}$$

$$L_{n+1}(t) = L_n(0) + ST^{-1}\left\{\frac{1-\sigma}{q(\sigma)\sigma\Gamma(\sigma+1)N_\sigma(-(1/1-\sigma)V^\sigma)}\right.$$
$$\left. \cdot ST[-aL_n + bP_nL_n - cL_nS_n]\right\},$$
$$\tag{74}$$

$$S_{n+!}(t) = S_n(0) + ST^{-!}\left\{\frac{1-\sigma}{q(\sigma)\sigma\Gamma(\sigma+1)N_\sigma(-(1/1-\sigma)V^\sigma)}\right.$$
$$\left. \cdot ST[-(a+d)S_n + cL_nS_n + fQ_n]\right\},$$
$$\tag{75}$$

$$Q_{n+1}(t) = Q_n(0) + ST^{-1}\left\{\frac{1-\sigma}{q(\sigma)\sigma\Gamma(\sigma+1)N_\sigma(-(1/1-\sigma)V^\sigma)}\right.$$
$$\left. \cdot ST[-(a+f)Q_n + d(1-e)S_n]\right\},$$
$$\tag{76}$$

$$R_{n+1}(t) = R_n(0) + ST^{-1}\left\{\frac{1-\sigma}{q(\sigma)\sigma\Gamma(\sigma+1)N_\sigma(-(1/1-\sigma)V^\sigma)}\right.$$
$$\left. \cdot ST[-aR_n + edS_n]\right\},$$
$$\tag{77}$$

where $1-\sigma/q(\sigma)\sigma\Gamma(\sigma+1)N_\sigma(-1/1-\sigma V^\sigma)$ *is the fractional Lagrange multiplier.*

Theorem 8. *Define* K *be a self-map is given by*

$$K\left[P_{(n+1)}(t)\right] = P_n(0) + ST^{-1}$$
$$\cdot \left[\frac{1-\sigma}{q(\sigma)\sigma\Gamma(\sigma+1)N_\sigma(-(1/1-\sigma)V^\sigma)}\right.$$
$$\left. \cdot ST\{a(1-P_n) - bP_nS_n\}\right],$$
$$\tag{78}$$

$$K\left[L_{(n+1)}(t)\right] = L_n(0) + ST^{-1}$$
$$\cdot \left[\frac{1-\sigma}{q(\sigma)\sigma\Gamma(\sigma+1)N_\sigma(-(1/1-\sigma)V^\sigma)}\right.$$
$$\left. \cdot ST\{-aL_n + bP_nL_n - cL_nS_n\}\right],$$
$$\tag{79}$$

$$K[S_{n+1}(t)] = S_n(0) + ST^{-1}\left[\frac{1-\sigma}{q(\sigma)\sigma\Gamma(\sigma+1)N_\sigma(-(1/1-\sigma)V^\sigma)}\right.$$
$$\left. \cdot ST\{-(a+d)S_n + cL_nS_n + fQ_n\}\right],$$
$$\tag{80}$$

$$Q_{(n+1)}(t) = Q_n(0) + ST^{-1}\left[\frac{1-\sigma}{q(\sigma)\sigma\Gamma(\sigma+1)N_\sigma(-(1/1-\sigma)V^\sigma)}\right.$$
$$\left. \cdot ST\{-(a+f)Q_n + d(1-e))S_n\}\right],$$
$$\tag{81}$$

$$R_{(n+1)}(t) = R_n(0) + ST^{-1}\left[\frac{1-\sigma}{q(\sigma)\sigma\Gamma(\sigma+1)N_\sigma(-(1/1-\sigma)V^\sigma)}\right.$$
$$\left. \cdot ST\{-aR_n + edS_n\}\right],$$
$$\tag{82}$$

$$K[S_{n+1}(t)] = S_n(0) + ST^{-1}\left[\frac{1-\sigma}{q(\sigma)\sigma\Gamma(\sigma+1)N_\sigma(-(1/1-\sigma)V^\sigma)}\right.$$
$$\left. \cdot ST\{-(a+d)S_n + cL_nS_n + fQ_n\}\right],$$
$$\tag{83}$$

$$K\left[Q_{(n+1)}(t)\right] = Q_n(0) + ST^{-1}$$
$$\cdot \left[\frac{1-\sigma}{q(\sigma)\sigma\Gamma(\sigma+1)N_\sigma(-(1/1-\sigma)V^\sigma)}\right.$$
$$\left. \cdot ST\{-(a+f)Q_n + d(1-e))S_n\}\right],$$
$$\tag{84}$$

$$K\left[R_{(n+1)}(t)\right] = R_n(0) + ST^{-1}$$
$$\cdot \left[\frac{1-\sigma}{q(\sigma)\sigma\Gamma(\sigma+1)N_\sigma(-(1/1-\sigma)V^\sigma)}\right.$$
$$\left. \cdot ST\{-aR_n + edS_n\}\right].$$
$$\tag{85}$$

Proof. In first step, we will show that K is fixed point

$$\forall(m, n) \in N \times N, \tag{86}$$

$$K(P_n(t)) - K(P_m(t))$$
$$= P_n(t) - P_m(t) + \text{ST}^{-1}\left[\frac{1 - \sigma}{q(\sigma)\sigma\Gamma(\sigma + 1)N_\sigma(-(1/1 - \sigma)V^\sigma)}\right.$$
$$\left. \cdot \text{ST}\{a(1 - P_n) - bP_nS_n\}\right] - \text{ST}^{-1}$$
$$\cdot \left[\frac{1 - \sigma}{q(\sigma)\sigma\Gamma(\sigma + 1)N_\sigma(-(1/1 - \sigma)V^\sigma)}\right.$$
$$\left. \cdot \text{ST}\{a(1 - P_m) - bP_mS_m\}\right],$$

$$(87)$$

$$K(L_n(t)) - K(L_m(t))$$
$$= L_n(t) - L_m(t) + \text{ST}^{-1}\left[\frac{1 - \sigma}{q(\sigma)\sigma\Gamma(\sigma + 1)N_\sigma(-(1/1 - \sigma)V^\sigma)}\right.$$
$$\left. \cdot \text{ST}\{-aL_n + bP_nL_n - cL_nS_n\}\right] - \text{ST}^{-1}$$
$$\cdot \left[\frac{1 - \sigma}{q(\sigma)\sigma\Gamma(\sigma + 1)N_\sigma(-(1/1 - \sigma)V^\sigma)}\text{ST}\right.$$
$$\left. \cdot \{-aL_m + bP_mL_m - cL_mS_m\}\right],$$

$$(88)$$

$$K(S_n(t)) - K(S_m(t))$$
$$= S_n(t) - S_m(t) + \text{ST}^{-1}$$
$$\cdot \left[\frac{1 - \sigma}{q(\sigma)\sigma\Gamma(\sigma + 1)N_\sigma(-(1/1 - \sigma)V^\sigma)}\right.$$
$$\left. \cdot \text{ST}\{-(a + d)S_n + cL_nS_n + fQ_n\}\right] - \text{ST}^{-1}$$
$$\cdot \left[\frac{1 - \sigma}{q(\sigma)\sigma\Gamma(\sigma + 1)N_\sigma(-(1/1 - \sigma)V^\sigma)}\right.$$
$$\left. \cdot \text{ST}\{-(a + d)S_m + cL_mS_m + fQ_m\}\right],$$

$$(89)$$

$$K(Q_n(t)) - K(Q_m(t))$$
$$= Q_n(t) - Q_m(t) + \text{ST}^{-1}$$
$$\cdot \left[\frac{1 - \sigma}{q(\sigma)\sigma\Gamma(\sigma + 1)N_\sigma(-(1/1 - \sigma)V^\sigma)}\right.$$
$$\left. \cdot ST\{-(a + f)Q_n + d(1 - e))S_n\}\right]$$
$$- \text{ST}^{-1}\left[\frac{1 - \sigma}{q(\sigma)\sigma\Gamma(\sigma + 1)N_\sigma(-(1/1 - \sigma)V^\sigma)}\right.$$
$$\left. \cdot ST\{-(a + f)Q_m + d(1 - e))S_m\}\right],$$

$$(90)$$

$$K(R_n(t)) - K(R(t))$$
$$= R_n(t) - R_m(t) + \text{ST}^{-1}\left[\frac{1 - \sigma}{q(\sigma)\sigma\Gamma(\sigma + 1)N_\sigma(-(1/1 - \sigma)V^\sigma)}\right.$$
$$\left. \cdot \text{ST}\{-aR_n + edS_n\}\right] - \text{ST}^{-1}$$
$$\cdot \left[\frac{1 - \sigma}{q(\sigma)\sigma\Gamma(\sigma + 1)N_\sigma(-(1/1 - \sigma)V^\sigma)}\right.$$
$$\left. \cdot \text{ST}\{-aR_m + edS_m\}\right].$$

$$(91)$$

Applying the properties of the norm and also using the triangular inequality, we obtain

$$\|K(P_n(t)) - K(P_m(t))\|$$
$$\leq \|P_n(t) - P_m(t)\|\, \text{ST}^{-1}$$
$$\cdot \left[\frac{1 - \sigma}{q(\sigma)\sigma\Gamma(\sigma + 1)N_\sigma(-(1/1 - \sigma)V^\sigma)}\right.$$
$$\left. \cdot \text{ST}\{\|a(1 - (P_n - P_m))\| + \|-b(P_nS_n - P_mS_m)\|\}\right],$$

$$(92)$$

$$\|K(L_n(t)) - K(L_m(t))\|$$
$$\leq \|L_n(t) - L_m(t)\| + \text{ST}^{-1}$$
$$\cdot \left[\frac{1 - \sigma}{q(\sigma)\sigma\Gamma(\sigma + 1)N_\sigma(-(1/1 - \sigma)V^\sigma)}\right.$$
$$\cdot \text{ST}\{-\|a(L_n - L_m)\| + \|b(P_nL_n - P_mL_m)\|$$
$$\left. + \|-c(L_nS_n - L_mS_m)\|\}\right],$$

$$(93)$$

$$\|K(S_n(t)) - K(S_m(t))\|$$
$$\leq \|S_n(t) - S_m(t)\| + \text{ST}^{-1}$$
$$\cdot \left[\frac{1 - \sigma}{q(\sigma)\sigma\Gamma(\sigma + 1)N_\sigma(-(1/1 - \sigma)V^\sigma)}\right.$$
$$\cdot \text{ST}\{-\|(a + d)(S_n - S_m)\| + \|c(L_nS_n - L_mS_m)\|$$
$$\left. + \|f(Q_n - Q_m)\|\}\right],$$

$$(94)$$

$$\|K(Q_n(t)) - K(Q_m(t))\|$$
$$\leq \|Q_n(t) - Q_m(t)\| + \text{ST}^{-1}$$
$$\cdot \left[\frac{1 - \sigma}{q(\sigma)\sigma\Gamma(\sigma + 1)N_\sigma(-(1/1 - \sigma)V^\sigma)}\right.$$
$$\cdot \text{ST}\{-\|(a + f)(Q_n - Q_m)\| + \|d(1 - e)(S_n - S_m)\|\}\right],$$

$$(95)$$

$$\|K(R_n(t)) - K(R_m(t))\|$$
$$\leq \|R_n(t) - R_m(t)\| + ST^{-1}$$
$$\cdot \left[\frac{1 - \sigma}{q(\sigma)\sigma\Gamma(\sigma + 1)N_\sigma(-(1/1 - \sigma)V^\sigma)} \right] \quad (96)$$
$$\cdot ST\{\|-a(R_n - R_m)\| + \|ed(S_n - S_m)\|\}.$$

K fulfills the conditions associated with Theorem 6, when

$$\theta = (0,0,0,0,0), \theta \begin{cases} \|P_n(t) - P_m(t)\| \times \|-P_n(t) - P_m(t)\| + a\|(1 - (P_n - P_m))\| - b\|(P_nS_n - P_mS_m)\|, \\ \times \|L_n(t) - L_m(t)\| \times \|-L_n(t) - L_m(t)\| - a\|L_n(t) - L_m(t)\| + b\|(P_nL_n - P_mL_m)\| - c\|(L_nS_n - L_mS_m)\|, \\ \times \|S_n(t) - S_m(t)\| \times \|-S_n(t) - S_m(t)\| - (a + d)\|P_n - P_m\| + c\|(L_nS_n - L_mS_m)\| + f\|(Q_n - Q_m)\|, \\ \times \|Q_n(t) - Q_m(t)\| \times \|-Q_n(t) - Q_m(t)\| - (a + f)\|Q_n - Q_m\| + d(1 - e)\|d(1 - e)(S_n - S_m)\|, \\ \times \|R_n(t) - R_m(t)\| \times \|-R_n(t) - R_m(t)\| - a\|R_n - R_m\| + ed\|(S_n - S_m)\|. \end{cases} \quad (97)$$

And we add that K is Picard K-stable. □

Theorem 9. *Prove that system (27) has special solution is unique.*

Proof. Let H be the Hilbert space defined as $H = L^2((p,q) \times (0,T))$ where

$$h : (p,q) \times (0,T) \longrightarrow \mathbb{R}, \iint ghdgdh < \infty. \quad (98)$$

So, the following operators are considered

$$\theta(0,0,0,0,0), \theta = \begin{cases} a(1 - p) - bps, \\ -aL + bPL - cLS, \\ -(a + d)S + cLS + fQ, \\ -(a + f)Q + d(1 - e)S, \\ -aR + edS. \end{cases} \quad (99)$$

We establish the inner product of

$$P((P_{11} - P_{12}, L_{21} - L_{22}, S_{31} - S_{32}, Q_{41} - Q_{42}, R_{51} - R_{52}), (V_1, V_2, V_3, V_4, V_5)). \quad (100)$$

where $(S_{11} - S_{12}, I_{21} - I_{22}, A_{31} - A_{32}, T_{41} - T_{42}, R_{51} - R_{52})$ are the special solutions of the system. By using the inner function and the norm, we have

$$\{a - a(P_{11} - P_{12}) - b(P_{11} - P_{12})(S_{31} - S_{32})\}$$
$$\leq a\|V_1\| + a\|P_{11} - P_{12}\| + b\|P_{11} - P_{12}\| \quad (101)$$
$$\times \|S_{31} - S_{32}\|\|V_1\|,$$

$$\{-a(L_{21} - L_{22}) + b(P_{11} - P_{12})(L_{21} - L_{22})$$
$$- c(L_{21} - L_{22})(S_{31} - S_{32})\}$$
$$\leq a\|L_{21} - L_{22}\|\|V_2\| + b\|P_{11} - P_{12}\|\|L_{21} - L_{22}\|\|V_2\|$$
$$+ c\|L_{21} - L_{22}\|\|S_{31} - S_{32}\|\|V_2\|,$$
$$\quad (102)$$

$$\{-(a + d)(S_{31} - S_{32}) + c(L_{21} - L_{22})(S_{31} - S_{32})$$
$$+ f(Q_{41} - Q_{42})\}$$
$$\leq (a + d)\|S_{31} - S_{32}\|\|V_3\| + c\|L_{21} - L_{22}\|\|S_{31} - S_{32}\|\|V_3\|$$
$$+ f\|Q_{31} - Q_{32}\|\|V_3\|,$$
$$\quad (103)$$

$$\{-(a + f)(Q_{41} - Q_{42}) + d(1 - e)(S_{31} - S_{32})\}$$
$$\leq (a + f)\|Q_{31} - Q_{32}\|\|V_4\| + d(1 - e)\|S_{31} - S_{32}\|\|V_4\|,$$
$$\quad (104)$$

$$\{-a(R_{51} - R_{52}) + ed(S_{31} - S_{32})\}$$
$$\leq a\|R_{31} - R_{32}\|\|V_5\| + ed\|S_{31} - S_{32}\|\|V_5\|.$$
$$\quad (105)$$

Due to large number of $e_1, e_2, e_3, e_4,$ and e_5, both solutions converge to the exact solution. Applying the

topological idea, we have the very small positive five parameters $(\chi_{e_1}, \chi_{e_2}, \chi_{e_3}, \chi_{e_4},$ and $\chi_{e_5})$.

$$\|P - P_{11}\|, \|P - P_{12}\| \leq \frac{\chi_{e_1}}{\varpi}, \tag{106}$$

$$\|L - L_{21}\|, \|L - L_{22}\| \leq \frac{\chi_{e_2}}{\varsigma}, \tag{107}$$

$$\|S - S_{31}\|, \|S - S_{32}\| \leq \frac{\chi_{e_3}}{\upsilon}, \tag{108}$$

$$\|Q - Q_{41}\|, \|Q - Q_{42}\| \leq \frac{\chi_{e_4}}{\kappa}, \tag{109}$$

$$\|R - R_{51}\|, \|R - R_{52}\| \leq \frac{\chi_{e_5}}{\varrho}, \tag{110}$$

$$\varpi = 5(a + a\|P_{11} - P_{12}\| + b\|P_{11} - P_{12}\|\|S_{31} - S_{32}\|)\|V_1\|, \tag{111}$$

$$\begin{aligned}\varsigma = 5(a\|L_{21} - L_{22}\| &+ b\|P_{11} - P_{12}\|\|L_{21} - L_{22}\| \\ &+ c\|L_{21} - L_{22}\|\|S_{31} - S_{32}\|)\|V_2\|,\end{aligned} \tag{112}$$

$$\begin{aligned}\upsilon = 5((a + d)\|S_{31} - S_{32}\| &+ c\|L_{21} - L_{22}\|\|S_{31} - S_{32}\| \\ &+ f\|Q_{31} - Q_{32}\|)\|V_3\|,\end{aligned} \tag{113}$$

$$\kappa = 5((a + f)\|Q_{31} - Q_{32}\| + d(1 - e)\|S_{31} - S_{32}\|)\|V_4\|, \tag{114}$$

$$\varrho = 5(a\|R_{31} - R_{32}\| + ed\|S_{31} - S_{32}\|)\|V_5\|. \tag{115}$$

But, it is obvious that

$$(a + a\|P_{11} - P_{12}\| + b\|P_{11} - P_{12}\|\|S_{31} - S_{32}\|) \neq 0, \tag{116}$$

$$\begin{aligned}(a\|L_{21} - L_{22}\| &+ b\|P_{11} - P_{12}\|\|L_{21} - L_{22}\| \\ &+ c\|L_{21} - L_{22}\|\|S_{31} - S_{32}\|) \neq 0,\end{aligned} \tag{117}$$

$$\begin{aligned}((a + d)\|S_{31} - S_{32}\| &+ c\|L_{21} - L_{22}\|\|S_{31} - S_{32}\| \\ &+ f\|Q_{31} - Q_{32}\|) \neq 0,\end{aligned} \tag{118}$$

$$((a + f)\|Q_{31} - Q_{32}\| + d(1 - e)\|S_{31} - S_{32}\|) \neq 0, \tag{119}$$

$$(a\|R_{31} - R_{32}\| + ed\|S_{31} - S_{32}\|) \neq 0, \tag{120}$$

where $\|V_1\|, \|V_2\|, \|V_3\|, \|V_4\|, \|V_5\| \neq 0$.

Therefore, we have

$$\|P_{11} - P_{12}\| = 0, \tag{121}$$

$$\|L_{21} - L_{22}\| = 0, \tag{122}$$

$$\|S_{31} - S_{32}\| = 0, \tag{123}$$

$$\|Q_{41} - Q_{42}\| = 0, \tag{124}$$

$$\|R_{51} - R_{52}\| = 0. \tag{125}$$

Which yields that

$$P_{11} = P_{12}, \tag{126}$$

$$L_{21} = L_{22}, \tag{127}$$

$$S_{31} = S_{32}, \tag{128}$$

$$Q_{41} = Q_{42}, \tag{129}$$

$$R_{51} = R_{52}. \tag{130}$$

This completes the proof of uniqueness. □

6. New Numerical Scheme

We define the AT proposed scheme for fractional derivative model (37) for the smoking epidemic. For this purpose, we suppose that we obtain the following results for system (37)

$$\begin{aligned}P(t) - P(0) = &\frac{(1 - \sigma)}{\text{ABC}(\sigma)}\{a - aP(t) - bP(t)S(t)\} \\ &+ \frac{\sigma}{\Gamma(\sigma) \times \text{ABC}(\sigma)} \\ &\cdot \int_0^t \{a - aP(\tau) - bP(\tau)S(\tau)\}(t - \tau)^{\sigma-1}d\tau,\end{aligned} \tag{131}$$

$$\begin{aligned}L(t) - L(0) = &\frac{(1 - \sigma)}{\text{ABC}(\sigma)}\{-aL(t) + bP(t)L(t) - cL(t)S(t)\} \\ &+ \frac{\sigma}{\Gamma(\sigma) \times \text{ABC}(\sigma)}\int_0^t \{-aL(\tau) + bP(t)L(\tau) \\ &- cL(\tau)S(\tau)\}(t - \tau)^{\sigma-1}d\tau,\end{aligned} \tag{132}$$

$$\begin{aligned}S(t) - S(0) = &\frac{(1 - \sigma)}{\text{ABC}(\sigma)}\{-(a + d)S(t) + cL(t)S(t) + fQ(t)\} \\ &+ \frac{\sigma}{\Gamma(\sigma) \times \text{ABC}(\sigma)}\int_0^t \{-(a + d)S(\tau) + cL(t)S(\tau) \\ &+ fQ(\tau)\}(t - \tau)^{\sigma-1}d\tau,\end{aligned} \tag{133}$$

$$\begin{aligned}Q(t) - Q(0) = &\frac{(1 - \sigma)}{\text{ABC}(\sigma)}\{-(a + f)Q(t) + d(1 - e)S(t)\} \\ &+ \frac{\sigma}{\Gamma(\sigma) \times \text{ABC}(\sigma)}\int_0^t \{-(a + f)Q(\tau) \\ &+ d(1 - e)S(\tau)\}(t - \tau)^{\sigma-1}d\tau,\end{aligned} \tag{134}$$

$$\begin{aligned}R(t) - R(0) = &\frac{(1 - \sigma)}{\text{ABC}(\sigma)}\{-aR(t) + edS(t)\} \\ &+ \frac{\sigma}{\Gamma(\sigma) \times \text{ABC}(\sigma)} \\ &\cdot \int_0^t \{-aR(\tau) + edS(\tau)\}(t - \tau)^{\sigma-1}d\tau.\end{aligned} \tag{135}$$

At a given point t_{n+1}, $n = 0, 1, 2, 3, \cdots$, the above equation is reformulated as

$$P(t) - P(0) = \frac{(1-\sigma)}{\text{ABC}(\sigma)} \{a - aP(t_n) - bP(t_n)S(t_n)\}$$
$$+ \frac{\sigma}{\Gamma(\sigma) \times \text{ABC}(\sigma)}$$
$$\cdot \int_0^t \{a - aP(\tau) - bP(\tau)S(\tau)\}(t-\tau)^{\sigma-1}d\tau, \tag{136}$$

$$L(t) - L(0) = \frac{(1-\sigma)}{\text{ABC}(\sigma)} \{-aL(t_n) + bP(t_n)L(t_n) - cL(t_n)S(t_n)\}$$
$$+ \frac{\sigma}{\Gamma(\sigma) \times \text{ABC}(\sigma)} \int_0^t \{-aL(\tau) + bP(\tau)L(\tau)$$
$$- cL(\tau)S(\tau)\}(t-\tau)^{\sigma-1}d\tau, \tag{137}$$

$$S(t) - S(0) = \frac{(1-\sigma)}{\text{ABC}(\sigma)} \{-(a+d)S(t_n) + cL(t_n)S(t_n) + fQ(t_n)\}$$
$$+ \frac{\sigma}{\Gamma(\sigma) \times \text{ABC}(\sigma)} \int_0^t \{-(a+d)S(\tau)$$
$$+ cL(\tau)S(\tau) + fQ(\tau)\}(t-\tau)^{\sigma-1}d\tau, \tag{138}$$

$$Q(t) - Q(0) = \frac{(1-\sigma)}{\text{ABC}(\sigma)} \{-(a+f)Q(t_n) + d(1-e)S(t_n)\}$$
$$+ \frac{\sigma}{\Gamma(\sigma) \times \text{ABC}(\sigma)} \int_0^t \{-(a+f)Q(\tau)$$
$$+ d(1-e)S(\tau)\}(t-\tau)^{\sigma-1}d\tau, \tag{139}$$

$$R(t) - R(0) = \frac{(1-\sigma)}{\text{ABC}(\sigma)} \{-aR(t_n) + edS(t_n)\}$$
$$+ \frac{\sigma}{\Gamma(\sigma) \times \text{ABC}(\sigma)} \int_0^t \{-aR(\tau)$$
$$+ edS(\tau)\}(t-\tau)^{\sigma-1}d\tau. \tag{140}$$

Also, we have

$$P(t_{n+1}) - P(0) = \frac{(1-\sigma)}{\text{ABC}(\sigma)} \{a - aP(t_n) - bP(t_n)S(t_n)\}$$
$$+ \frac{\sigma}{\Gamma(\sigma) \times \text{ABC}(\sigma)} \sum_{j=0}^n \int_{t_j}^{t_{j+1}} \{a - aP(\tau)$$
$$- bP(\tau)S(\tau)\}(t_{n+1}-\tau)^{\sigma-1}d\tau, \tag{141}$$

$$L(t_{n+1}) - L(0) = \frac{(1-\sigma)}{\text{ABC}(\sigma)} \{-aL(t_n) + bP(t_n)L(t_n)$$
$$- cL(t_n)S(t_n) - cL(\tau)S(\tau)\}$$
$$+ \frac{\sigma}{\Gamma(\sigma) \times \text{ABC}(\sigma)} \sum_{j=0}^n \int_{t_j}^{t_{j+1}} \{-aL(\tau)$$
$$+ bP(\tau)L(\tau) - cL(\tau)S(\tau)\}(t_{n+1}-\tau)^{\sigma-1}d\tau, \tag{142}$$

$$S(t_{n+1}) - S(0)$$
$$= \frac{(1-\sigma)}{\text{ABC}(\sigma)} \{-(a+d)S(t_n) + cL(t_n)S(t_n) + fQ(t_n)\}$$
$$+ \frac{\sigma}{\Gamma(\sigma) \times \text{ABC}(\sigma)} \sum_{j=0}^n \int_{t_j}^{t_{j+1}} \{-(a+d)S(\tau) + cL(\tau)S(\tau)$$
$$+ fQ(\tau)\}(t_{n+1}-\tau)^{\sigma-1}d\tau, \tag{143}$$

$$Q(t_{n+1}) - Q(0) = \frac{(1-\sigma)}{\text{ABC}(\sigma)} \{-(a+f)Q(t_n) + d(1-e)S(t_n)\}$$
$$+ \frac{\sigma}{\Gamma(\sigma) \times \text{ABC}(\sigma)} \sum_{j=0}^n \int_{t_j}^{t_{j+1}} \{-(a+f)Q(\tau)$$
$$+ d(1-e)S(\tau)\}(t_{n+1}-\tau)^{\sigma-1}d\tau, \tag{144}$$

$$R(t_{n+1}) - R(0) = \frac{(1-\sigma)}{\text{ABC}(\sigma)} \{-aR(t_n) + edS(t_n)\}$$
$$+ \frac{\sigma}{\Gamma(\sigma) \times \text{ABC}(\sigma)}$$
$$\cdot \sum_{j=0}^n \int_{t_j}^{t_{j+1}} \{-aR(\tau) + edS(\tau)\}(t_{n+1}-\tau)^{\sigma-1}d\tau. \tag{145}$$

By using equation (133), we have

$$P_{n+1} = P_0 + \frac{(1-\sigma)}{\text{ABC}(\sigma)} \{a - aP(t_n) - bP(t_n)S(t_n)\} + \frac{\sigma}{\Gamma(\sigma) \times ABC(\sigma)}$$
$$\cdot \sum_{j=0}^n \left(\frac{\{a - aP_j - bP_jS_j\}}{h} \times \int_{t_j}^{t_{j+1}} (\tau - t_{j-1})(t_{n+1}-\tau)^{\sigma-1}d\tau \right.$$
$$\left. - \frac{\{a - aP_{j-1} - bP_{j-1}S_{j-1}\}}{h} \times \int_{t_j}^{t_{j+1}} (\tau - t_j)(t_{n+1}-\tau)^{\sigma-1}d\tau \right), \tag{146}$$

$$L_{n+1} = L_0 + \frac{(1-\sigma)}{\mathrm{ABC}(\sigma)}\{-aL(t_n) + bP(t_n)L(t_n) - cL(t_n)S(t_n)\}$$
$$+ \frac{\sigma}{\Gamma(\sigma)\times\mathrm{ABC}(\sigma)}\sum_{j=0}^{n}\left(\frac{\{-aL_j + bP_jL_j - cL_jS_j\}}{h}\right.$$
$$\times \int_{t_j}^{t_{j+1}}(\tau - t_{j-1})(t_{n+1}-\tau)^{\sigma-1}d\tau$$
$$\left. - \frac{\{-aL_{j-1} + bP_{j-1}L_{j-1} - cL_{j-1}S_{j-1}\}}{h}\times\int_{t_j}^{t_{j+1}}(\tau - t_j)(t_{n+1}-\tau)^{\sigma-1}d\tau\right),$$

(147)

$$S_{n+1} = S_0 + \frac{(1-\sigma)}{\mathrm{ABC}(\sigma)}\{-(a+d)S(t_n) + cL(t_n)S(t_n) + fQ(t_n)\}$$
$$+ \frac{\sigma}{\Gamma(\sigma)\times\mathrm{ABC}(\sigma)}\sum_{j=0}^{n}\left(\frac{\{-(a+d)S_j + cL_jS_j + fQ_j\}}{h}\right.$$
$$\times \int_{t_j}^{t_{j+1}}(\tau - t_{j-1})(t_{n+1}-\tau)^{\sigma-1}d\tau$$
$$\left. - \frac{\{-(a+d)S_{j-1} + cL_{j-1}S_{j-1} + fQ_{j-1}\}}{h}\times\int_{t_j}^{t_{j+1}}(\tau - t_j)(t_{n+1}-\tau)^{\sigma-1}d\tau\right),$$

(148)

$$Q_{n+1} = Q_0 + \frac{(1-\sigma)}{\mathrm{ABC}(\sigma)}\{-(a+f)Q(t_n) + d(1-e)S(t_n)\}$$
$$+ \frac{\sigma}{\Gamma(\sigma)\times\mathrm{ABC}(\sigma)}\sum_{j=0}^{n}\left(\frac{\{-(a+f)Q_j + d(1-e)S_j\}}{h}\right.$$
$$\times \int_{t_j}^{t_{j+1}}(\tau - t_{j-1})(t_{n+1}-\tau)^{\sigma-1}d\tau$$
$$\left. - \frac{\{-(a+f)Q_{j-1} + d(1-e)S_{j-1}\}}{h}\times\int_{t_j}^{t_{j+1}}(\tau - t_j)(t_{n+1}-\tau)^{\sigma-1}d\tau\right),$$

(149)

$$R_{n+1} = R_0 + \frac{(1-\sigma)}{\mathrm{ABC}(\sigma)}\{-aR(t_n) + edS(t_n)\}$$
$$+ \frac{\sigma}{\Gamma(\sigma)\times\mathrm{ABC}(\sigma)}\sum_{j=0}^{n}\left(\frac{\{-aR_j + edS_j\}}{h}\right.$$
$$\times \int_{t_j}^{t_{j+1}}(\tau - t_{j-1})(t_{n+1}-\tau)^{\sigma-1}d\tau$$
$$\left. - \frac{\{-aR_{j-1} + edS_{j-1}\}}{h}\times\int_{t_j}^{t_{j+1}}(\tau - t_j)(t_{n+1}-\tau)^{\sigma-1}d\tau\right).$$

(150)

By using equations (133) and (144), we get

$$P_{n+1} = P_0 + \frac{(1-\sigma)}{\mathrm{ABC}(\sigma)}\{\mathrm{a} - aP(t_n) - bP(t_n)S(t_n)\}$$
$$+ \frac{\sigma}{\mathrm{ABC}(\sigma)}\sum_{j=0}^{n}\left(\frac{h^\sigma\{\mathrm{a} - aP_j - bP_jS_j\}}{\Gamma(\sigma+2)}\times\{p_1p_2 - p_3p_4\}\right.$$
$$\left. - \frac{h^\sigma\{\mathrm{a} - aP_{j-1} - bP_{j-1}S_{j-1}\}}{\Gamma(\sigma+2)}\times\{p_5 - p_3p_6\}\right),$$

(151)

$$L_{n+1} = L_0 + \frac{(1-\sigma)}{\mathrm{ABC}(\sigma)}\{-aL(t_n) + bP(t_n)L(t_n) - cL(t_n)S(t_n)\}$$
$$+ \frac{\sigma}{\mathrm{ABC}(\sigma)}\sum_{j=0}^{n}\left(\frac{h^\sigma\{-aL_j + bP_jL_j - cL_jS_j\}}{\Gamma(\sigma+2)}\times\{p_1p_2 - p_3p_4\}\right.$$
$$\left. - \frac{h^\sigma\{-aL_{j-1} + bP_{j-1}L_{j-1} - cL_{j-1}S_{j-1}\}}{\Gamma(\sigma+2)}\times\{p_5 - p_3p_6\}\right),$$

(152)

$$S_{n+1} = S_0 + \frac{(1-\sigma)}{\mathrm{ABC}(\sigma)}\{-(a+d)S(t_n) + cL(t_n)S(t_n) + fQ(t_n)\}$$
$$+ \frac{\sigma}{\mathrm{ABC}(\sigma)}\sum_{j=0}^{n}\left(\frac{h^\sigma\{-(a+d)S_j + cL_jS_j + fQ_j\}}{\Gamma(\sigma+2)}\times\{p_1p_2 - p_3p_4\}\right.$$
$$\left. - \frac{h^\sigma\{-(a+d)S_{j-1} + cL_{j-1}S_{j-1} + fQ_{j-1}\}}{\Gamma(\sigma+2)}\times\{p_5 - p_3p_6\}\right),$$

(153)

$$Q_{n+1} = Q_0 + \frac{(1-\sigma)}{\mathrm{ABC}(\sigma)}\{-(a+f)Q(t_n) + d(1-e)S(t_n)\}$$
$$+ \frac{\sigma}{\mathrm{ABC}(\sigma)}\sum_{j=0}^{n}\left(\frac{h^\sigma\{-(a+f)Q_j + d(1-e)S_j\}}{\Gamma(\sigma+2)}\times\{p_1p_2 - p_3p_4\}\right.$$
$$\left. - \frac{h^\sigma\{-(a+f)Q_{j-1} + d(1-e)S_{j-1}\}}{\Gamma(\sigma+2)}\times\{p_5 - p_3p_6\}\right),$$

(154)

$$R_{n+1} = R_0 + \frac{(1-\sigma)}{\mathrm{ABC}(\sigma)}\{-aR(t_n) + edS(t_n)\}$$
$$+ \frac{\sigma}{\mathrm{ABC}(\sigma)}\sum_{j=0}^{n}\left(\frac{h^\sigma\{-aR_j + edS_j\}}{\Gamma(\sigma+2)}\times\{p_1p_2 - p_3p_4\}\right.$$
$$\left. - \frac{h^\sigma\{-aR_{j-1} + edS_{j-1}\}}{\Gamma(\sigma+2)}\times\{p_5 - p_3p_6\}\right).$$

(155)

Proposed Method
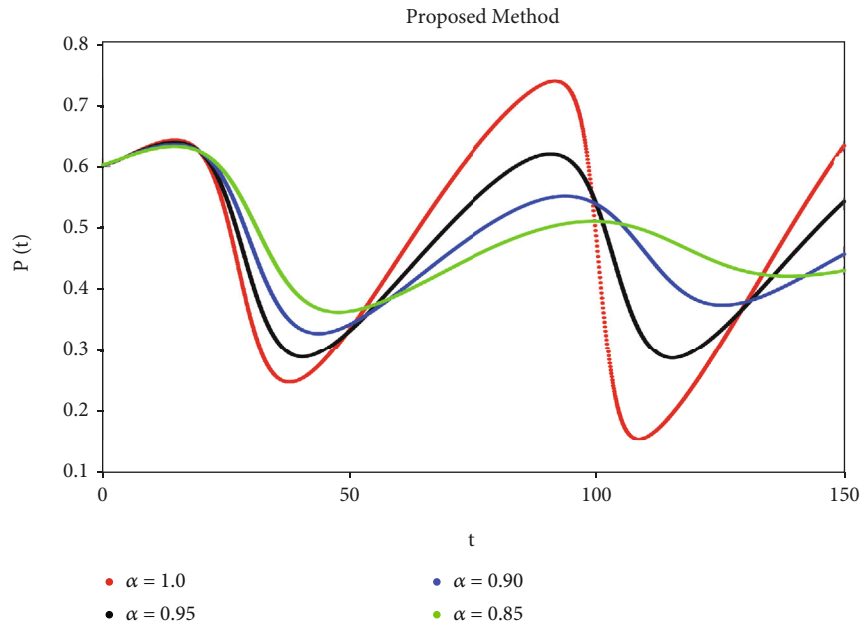
FIGURE 1: Simulation of $P(t)$ with ABC fractional-order scheme.

Proposed Method
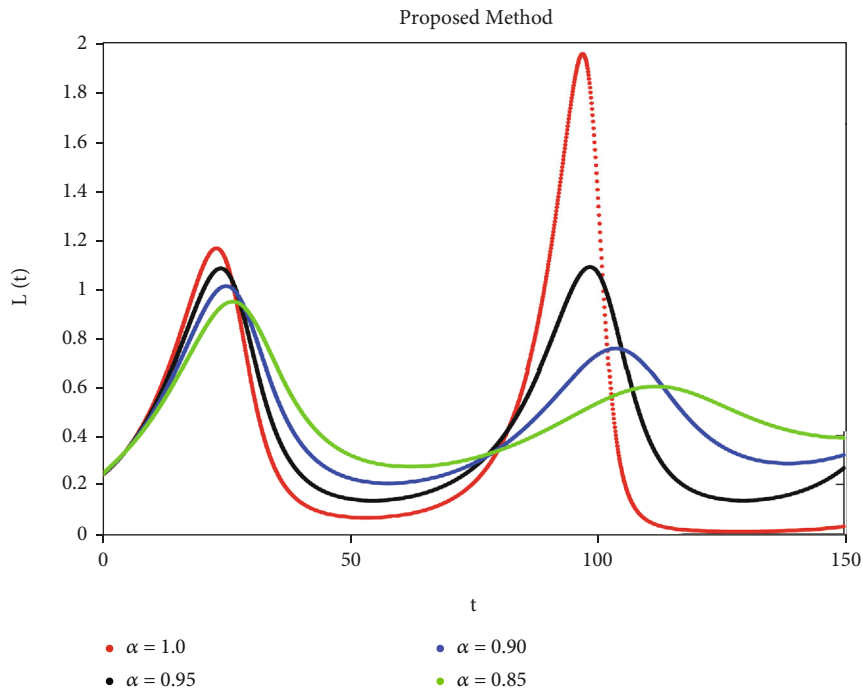
FIGURE 2: Simulation of $L(t)$ with ABC fractional-order scheme.

where

$$p_1 = (m + 1 - j)^\sigma, \tag{156}$$

$$p_2 = (m - j + 2 + \sigma), \tag{157}$$

$$p_3 = (m - j)^\sigma, \tag{158}$$

$$p_4 = (m - j + 2 + 2\sigma), \tag{159}$$

$$p_5 = (m + 1 - j)^{\sigma+1}, \tag{160}$$

$$p_6 = (m - j + 1 + \sigma). \tag{161}$$

7. Numerical Results and Discussion

A mathematical study of the nonlinear epidemic model of smoking has been presented. For checking of parameters effects on smoking dynamical model, relatively some numerical simulations according to the value of the parameters are
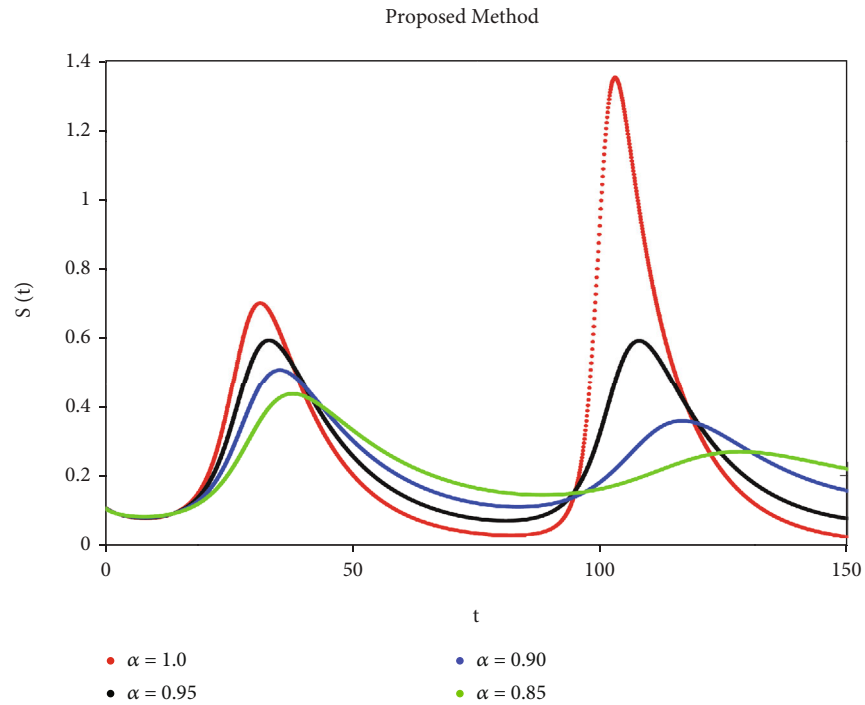
FIGURE 3: Simulation of S(t) with ABC fractional-order scheme.
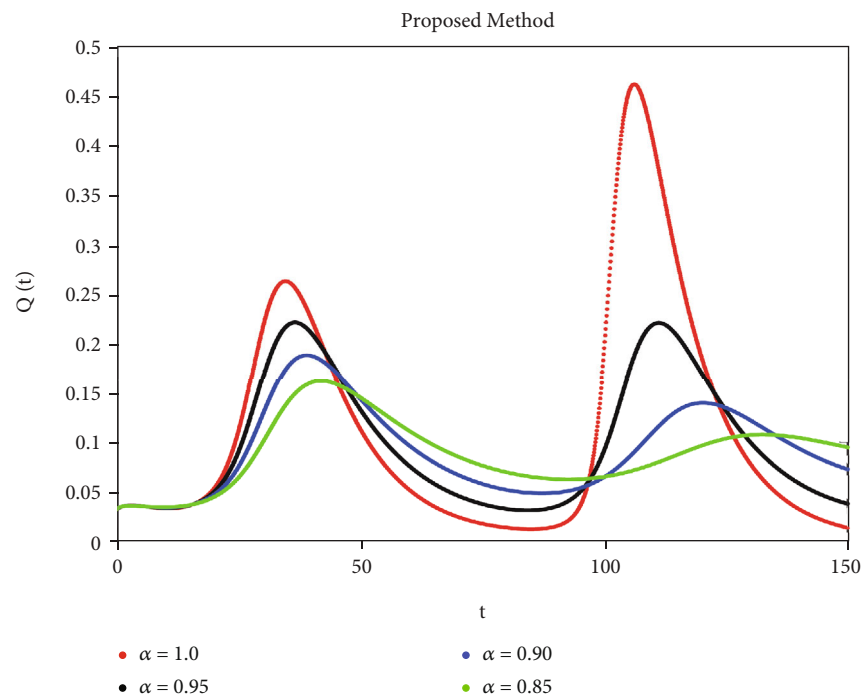
FIGURE 4: Simulation of $Q(t)$ with ABC fractional-order scheme.

accomplished to confirm the effect of the fractional derivative on the different compartments. We got mathematical consequences of the model for different fractional values with the help of the ATM. If we note the impacts of variables on the dynamics of the model of fractional order, the end-time value of the given parameter can be observed in various numerical ways. We can observe that the results of fractional value are more accurate as compared to classical derivatives. Desired results can be achieved to analyze the epidemic that occurs due to smoking. The graphs of the approximate
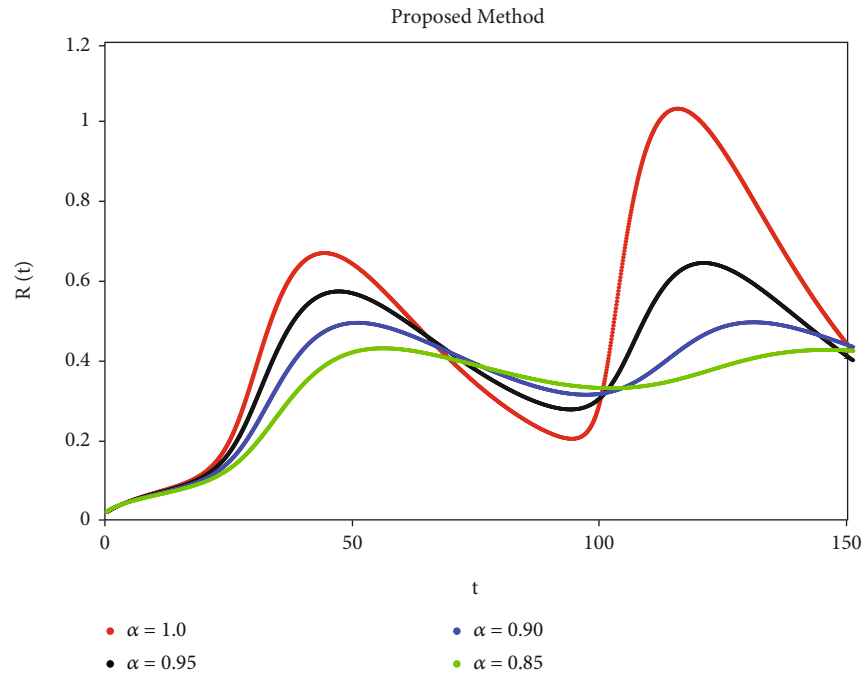
FIGURE 5: Simulation of $R(t)$ with ABC fractional-order scheme.

solutions are given in Figures 1–5 against different fractional-order α. $P(t)$ and $R(t)$ start decreasing by decreasing the fractional values while $L(t)$, $S(t)$, and $Q(t)$ start increasing by decreasing fractional values which can be easily observed in Figures 1–5. When the fractional values decrease then the behavior approaches steady-state in all figures, which shows that the solution will be more effective by decreasing the fractional values.

8. Conclusion

The advanced numerical scheme of fractional differential equation has been investigated in this article for smoking model by using ATM. With the help of fixed point theory uniqueness and stability of the smoking, the model has been examined. System is analyzed qualitatively to verify the steady state position of the dynamic. Proposed system is analyzed locally; also, global stability has been made using first derivative of Lyapunov. The arbitrary derivative of fractional order has been taken in ATM with no singular kernel. Effective results are obtained for the proposed model. Also discussed some theoretical results and proved the efficiency of the proposed techniques. Numerical simulations are carried out to check the actual behavior of the dynamic using the advanced ATM. These results will be helpful to understand further analysis and to control different outbreak caused by smoking.

Data Availability

No data were used to support this study.

Conflicts of Interest

The authors state that there is no conflict of interest.

Authors' Contributions

All authors contributed equally and significantly to writing this article. All authors read and approved the final manuscript.

References

[1] C. S. Chou and A. Friedman, "Introduction," in *Introduction to Mathematical Biology. Springer Undergraduate Texts in Mathematics and Technology*, Springer, Cham, 2016.

[2] Centers for Disease Control and Prevention (CDC), "Annual smoking –attributable mortality, years of potential life lost, and economic cost-united state 1995-1999," *MMWR. Morbidity and Mortality Weekly Report*, vol. 51, no. 14, pp. 300–303, 2002.

[3] A. Jemal, M. M. Center, C. Desantis, and E. M. Ward, "Global patterns of cancer incidence and mortality rates and trends," *Cancer Epidemiology, Biomarkers & Prevention*, vol. 19, pp. 1893–1907, 2010.

[4] D. Hoffmann, I. Hoffmann, and K. El-Bayoumy, "The less harmful cigarette: a controversial issue. A tribute to Ernst L Wynder," *Chemical Research in Toxicology*, vol. 14, pp. 767–790, 2001.

[5] A. Charlton, "Medicinal use of tobacco in history," *Journal of the Royal Society of Medicine*, vol. 97, pp. 292–296, 2004.

[6] P. Garodia, H. Ichikawa, N. Malani, G. Sethi, and B. B. Aggarwal, "From ancient medicine to modern medicine: ayurvedic concepts of health and their role in inflammation and cancer," *Journal of the Society for Integrative Oncology*, vol. 5, no. 1, pp. 25–27, 2007.

[7] J. Handelsman, J. Conway, M. Boylan, and R. Turtle, "Testicular function in potential sperm donors: normal ranges and the effects of smoking and varicocele," *International Journal of Andrology*, vol. 7, no. 5, pp. 369–382, 1984.

[8] A. Atangana and B. S. T. Alkahtani, "Analysis of the Keller–Segel model with a fractional derivative without singular kernel," *Entropy*, vol. 17, no. 12, pp. 4439–4453, 2015.

[9] A. Alsaedi, J. J. Nieto, and V. Venktesh, "Fractional electrical circuits," *Mechanical Engineering*, vol. 7, no. 12, 2015.

[10] M. Caputo and M. Fabrizio, "A new definition of fractional derivative without singular kernel," *Progress in Fractional Differentiation and Applications (PFDA)*, vol. 1, no. 2, pp. 1–13, 2015.

[11] J. Losada and J. J. Nieto, "Properties of a new fractional derivative without singular kernel," *Progress in Fractional Differentiation and Applications (PFDA)*, vol. 1, no. 2, pp. 87–92, 2015.

[12] A. A. Tateishi, H. V. Ribeiro, and E. K. Lenzi, "The role of fractional time-derivative operators on anomalous diffusion," *Frontiers of Physics*, vol. 5, p. 52, 2017.

[13] D. Kumar, J. Singh, M. al Qurashi, and D. Baleanu, "Analysis of logistic equation pertaining to a new fractional derivative with non-singular kernel," *Advances in Mechanical Engineering*, vol. 9, no. 2, 2017.

[14] K. M. Owolabi and A. Atangana, "Analysis and application of new fractional Adams–Bashforth scheme with Caputo–Fabrizio derivative," *Chaos, Solitons and Fractals*, vol. 105, pp. 111–119, 2017.

[15] D. Kumar, F. Tchier, J. Singh, and D. Baleanu, "An efficient computational technique for fractal vehicular traffic flow," *Entropy*, vol. 20, p. 259, 2018.

[16] J. Singh, D. Kumar, and D. Baleanu, "New aspects of fractional Biswas–Milovic model with Mittag–Leffler law," *Mathematical Modelling of Natural Phenomena*, vol. 14, no. 3, p. 303, 2019.

[17] K. Diethelm, *The Analysis of Fractional Differential Equations: An Application-Oriented Exposition Using Differential Operators of Caputo Type*, Springer, Berlin, 2010.

[18] A. Atangana, "Blind in a commutative world: simple illustrations with functions and chaotic attractors," *Chaos, Solitons and Fractals*, vol. 114, pp. 347–363, 2018.

[19] H. Bulut, H. M. Baskonus, and F. B. M. Belgecam, "The analytic solutions of some fractional ordinary differential equation by Sumudu transform method," *Abstr. Appl. Anal.*, vol. 2013, article 203875, 6 pages, 2013.

[20] A. A. Kilbas, H. M. Srivastava, and J. J. Trujillo, *Theory and Applications of Fractional Differential Equations*, Elsevier, Amsterdam, 2006.

[21] A. Atangana and I. Koca, "Chaos in a simple nonlinear system with Atangana-Baleanu derivatives with fractional order," *Chaos, Solitons and Fractals*, vol. 89, pp. 447–454, 2016.

[22] L. L. Huang, D. Baleanue, and S. D. Wu Zeng, "A new application of the fractional logistic map," *Romanian Journal of Physics*, vol. 61, pp. 1172–1179, 2016.

[23] G. Zaman, "Qualitative behavior of giving up smoking model," *Bulletin of the Malaysian Mathematical Sciences Society*, vol. 34, pp. 403–415, 2011.

[24] J. Singh, D. Kumar, M. A. Qurashi, and D. Baleanu, "A new fractional model for giving up smoking dynamics," *Advances in Difference Equations*, vol. 2017, no. 1, Article ID 88, 2017.

[25] A. E. Nava, "Risk factors associated with recent transmission of tuberculosis: systematic review and meta-analysis," *The International Journal of Tuberculosis and Lung Disease*, vol. 13, pp. 17–26, 2009.

[26] A. K. Pokhrel, M. N. Bates, S. C. Verma, H. S. Joshi, C. T. Sreeramareddy, and K. R. Smith, "Tuberculosis and indoor biomass and kerosene use in Nepal: a case–control study," *Environmental Health Perspectives*, vol. 118, pp. 558–564, 2010.

[27] P. Narasimhan, J. Wood, C. R. MacIntyre, and D. Mathai, "Risk factors for tuberculosis," *Pulmonary Medicine*, vol. 2013, Article ID 828939, 11 pages, 2013.

[28] J. I. Irunde, L. S. Luboobi, and Y. Nkansah-Gyekye, "Modeling the effect of tobacco smoking on the in-host dynamics of hiv/aids," *Journal of Mathematical and Computational Science*, vol. 6, no. 3, p. 406, 2016.

[29] S. S. Islam, T. B. Rumi, S. L. Kabir et al., "Zoonotic tuberculosis knowledge and practices among cattle handlers in selected districts of Bangladesh," *PLoS Neglected Tropical Diseases*, vol. 15, no. 4, article e0009394, 2021.

Research Article

Exploring the Effects of Prescribed Fire on Tick Spread and Propagation in a Spatial Setting

Alexander Fulk ⬤,[1] Weizhang Huang ⬤,[2] and Folashade Agusto ⬤[1]

[1]*Department of Ecology and Evolutionary Biology, University of Kansas, Lawrence KS, USA*
[2]*Department of Mathematics, University of Kansas, Lawrence KS, USA*

Correspondence should be addressed to Folashade Agusto; fbagusto@gmail.com

Lyme disease is one of the most prominent tick-borne diseases in the United States, and prevalence of the disease has been steadily increasing over the past several decades due to a number of factors, including climate change. Methods for control of the disease have been considered, one of which is prescribed burning. In this paper, the effects of prescribed burns on the abundance of ticks present in a spatial domain are assessed. A spatial stage-structured tick-host model with an impulsive differential equation system is developed to simulate the effect that controlled burning has on tick populations. Subsequently, a global sensitivity analysis is performed to evaluate the effect of various model parameters on the prevalence of infectious nymphs. Results indicate that while ticks can recover relatively quickly following a burn, yearly, high-intensity prescribed burns can reduce the prevalence of ticks in and around the area that is burned. The use of prescribed burns in preventing the establishment of ticks into new areas is also explored, and it is observed that frequent burning can slow establishment considerably.

1. Introduction

Since its discovery in the United States in the 1970s, Lyme disease has become one of the most prevalent tick-borne diseases therein [1] while the prevalence of tick-borne diseases in general has been increasing around the world [2]. Lyme disease is one of the most debilitating tick-borne diseases if left untreated [3]. It spreads via a diseased tick which carries and transmits the bacterium, *Borrelia burgdorferi*. Several *Ixodes* tick species can transmit the bacterium that causes Lyme disease, including *I. pacificus*, *I. ricinus*, *I. persulcatus*, and *I. scapularis*. *Ixodes scapularis*, also known as the black-legged tick, is one of the primary vectors for Lyme disease. These ticks can both carry and transmit *B. burgdorferi* and keep Lyme disease endemic in many parts of the world when combined with their hosts [2, 4, 5]. *B. burgdorferi* spreads mostly via ticks and their hosts, which is significant because ticks are generalists, meaning that they feed on many hosts, basically whichever hosts are available in a given environment. This fact may have also conditioned the bacterium to evolve to

be a generalist pathogen as well, which only adds to the difficulty of reduction or eradication of Lyme disease [6].

There are about 30,000 cases of Lyme disease reported each year in the United States, and this number has risen steadily for over two decades. The actual prevalence of the disease is estimated to be about 450,000 cases per year [7]. Various factors influence the surveillance of this particular disease. One such factor is the variability in both symptoms reported and severity of those symptoms. The short-term effects of infection vary widely and are generally not very severe. They include rash or lymph nodes, fever, chills, fatigue, joint and muscle pain, and erythema (EM) or bull's-eye rash. Lyme disease is almost never fatal; however, the long-term effects of infection can be very detrimental as they include severe headaches and neck stiffness, an increase in EM rashes, joint swelling (particularly in large joints like the knee and elbow), facial palsy, and dizziness, as well as other neurological effects. Due to these wide-ranging symptoms, this disease is also difficult to diagnose and not enough research has been done to develop an effective vaccine for the disease, although two are currently being

tested and refined [3]. There is also well-founded fear that the geographic range of the disease is expanding, and in addition to that increased public health threat, new tick-borne pathogens could emerge from mutations of the disease [2, 7–10]. Though this disease is almost never fatal, the excess strain on public healthcare systems as well as the potential of mutation of the disease into a more virulent strain means that reduction of cases is of paramount importance.

There are many possible methods of control available for Lyme disease such as education on best practices when entering an area where ticks are known to inhabit, culling of deer, the primary host for adult females, and the use of pesticides [11]. Each of these methods has its own benefits and drawbacks, but one method in particular that has seen rising popularity among researchers in recent decades is prescribed fire [12–17]. This method can significantly reduce the number of ticks in an area, and it can also destroy forest litter that ticks typically dwell in, making reestablishment more difficult. It is relatively cost-effective and easy to implement and, in some cases, essential to the environment [18].

Several studies have been conducted to determine the effect of fire on ticks. Some of these studies determined the effect of fire by the removal or counting of ticks on captured hosts [17, 19–22]. Other studies focused more on the effects of burning on ticks in different environments [12, 13, 16, 23–25]. There were studies that analyzed the effects of seasonal burning on tick populations [14, 15, 26]. Overall, these studies were conducted to elucidate both the short- and long-term effects of prescribed burns on tick populations.

The majority of these studies showed that in the time immediately following a prescribed burn there is a considerable reduction in the number of ticks at the burn site [12, 13, 16, 23–25]. However, some studies have found contradictory evidence on this short-term effect, but those studies largely did not reflect the reality of prescribed burning [13–15, 17, 19, 20, 22, 27]. Those studies focused on small plots of land and in some cases used previously unburned sites, which is the opposite of what is typically seen with prescribed burning. Studies on the long-term effects of prescribed burning are few and far between. More recent studies have shown that frequent prescribed burns can effectively reduce the prevalence of ticks and even the prevalence of certain tick-borne diseases [12, 23].

Regardless of whether or not prescribed burns reduce the prevalence of disease in ticks, the benefits of greatly reduced tick populations should not be understated. With a reduction of the prevalence of ticks in an area, there is also a reduction in encounter rates with humans and thus a reduction in the number of humans infected with Lyme disease. This indicates that regions struggling with Lyme disease that are also well suited for prescribed burns may have a simple, effective method for reducing the annual number of cases of human Lyme disease due to the fact that prescribed burns lead to a short-term reduction in the prevalence of ticks in an area.

In this study, we develop a mathematical model that incorporates the effect of prescribed burning in a spatially explicit manner in order to investigate both short-term and long-term effects of burning on tick populations in different scenarios. Our goal is to study the effect of persistent prescribed burns on the prevalence of ticks over time. A preprint of this study is available on medRxiv [28].

The paper is outlined as follows. The mathematical model is formulated in Section 2. In Section 2.2, the finite element method used for the numerical exploration is described, and then, a global sensitivity analysis of the model parameters is carried out to identify the parameters with the most impact on the number of infectious nymphs. In Section 3, the effects of prescribed burning and diffusion are examined in different scenarios that may arise in various environments in the real world. The results are discussed in Section 4, and the conclusions are drawn from the results of the numerical simulations and directions for future research are discussed in Section 5.

2. Materials and Methods

2.1. Model Formulation. The model used in this study is adapted from Guo and Agusto [29] which investigates the effect of fire intensity (low and high intensities) and duration of the burn on tick population and disease prevalence. We extend their model by adding spatial dependencies on the model variables. The variables included in this model are given as follows: eggs $S_E = S_E(x, y, t)$, susceptible larvae $S_L = S_L(x, y, t)$, infectious larvae $I_L = I_L(x, y, t)$, susceptible nymphs $S_N = S_N(x, y, t)$, infectious nymphs $I_N = I_N(x, y, t)$, susceptible adults $S_A = S_A(x, y, t)$, infectious adults $I_A = I_A(x, y, t)$, susceptible mice $S_M = S_M(x, y, t)$, and infectious mice $I_M = I_M(x, y, t)$. These variables are defined over the two-dimensional rectangle, $\Omega = (a, b) \times (c, d)$. Moreover, we add diffusion into this model in order to evaluate the effect of movement of populations on the viability of prescribed fire.

To model the dynamics of tick eggs, we assume that both susceptible and infectious adult female ticks contribute to egg laying at a rate π_T, which is limited by the carrying capacity, K [30, 31]. Maturation of eggs into larvae occurs at the rate σ_T, while mortality or inviability is given by the rate μ_E. There is no diffusion component for eggs since female often lay eggs in and under leaf litter after dropping off of the hosts following successful feeding. There is some evidence for transovarial transmission of the family of the bacterium that causes Lyme disease among ticks [32]; however, it seems that *B. burgdorferi* is not able to be transmitted [33]; thus, we do not incorporate an infected egg compartment into the model. Thus, the equation governing how the susceptible egg population changes across time and space reads as

$$\frac{\partial S_E}{\partial t} = \underbrace{\pi_T \left(1 - \frac{S_E}{K}\right)(S_A + I_A)}_{\text{Egg laying rate}} - \underbrace{\sigma_T S_E}_{\text{Maturation}} - \underbrace{\mu_E S_E}_{\text{Death}}. \quad (1)$$

Next, we describe the dynamics of the susceptible and infectious larvae. We assume that the motion of ticks is due to their attachment to hosts they feed on [2, 34]. The rate of diffusion for juvenile ticks is denoted by D_M. Since diffusion only occurs when ticks are attached to hosts, the diffusion rate

for juvenile ticks is the same as the diffusion rate of mice. To model the movement of the larvae in space, we use the Laplacian operator Δ to denote the sum of the second partial derivatives with respect to each spatial variable, that is,

$$\Delta S_L = \frac{\partial^2 S_L}{\partial x^2} + \frac{\partial^2 S_L}{\partial y^2}. \tag{2}$$

We assume that any significant movement of ticks is due to their attachment to hosts, which is assumed to be Brownian motion, and it has been shown that the Laplacian operator approximates Brownian motion. This is a common simplification of the dispersal of organisms [35]. The susceptible larvae become infected after feeding on an infectious mouse at the rate λ_{LM}, the force of infection which we define as

$$\lambda_{LM} = \frac{\beta_{LM} I_M}{S_M + I_M}, \tag{3}$$

where the parameter β_{LM} is the probability that a larval tick is infected when feeding on an infectious mouse. Both susceptible and infectious larvae mature into nymphs at the rate τ_T and die naturally at the rate μ_L. Hence, the equations governing susceptible and infectious larval tick populations are given by

$$\frac{\partial S_L}{\partial t} = \sigma_T S_E + \underbrace{D_M \Delta S_L}_{\text{Random Diffusive Motion}} - \underbrace{\lambda_{LM} S_L}_{\text{Infection}} - \underbrace{\tau_T S_L}_{\text{Maturation}} - \underbrace{\mu_L S_L}_{\text{Death}},$$
$$\frac{\partial I_L}{\partial t} = \overbrace{D_M \Delta I_L} + \overbrace{\lambda_{LM} I_L} - \overbrace{\tau_T I_L} - \overbrace{\mu_L I_L}. \tag{4}$$

The dynamics and equations of the other tick populations follow a similar form to the larvae, and we only substitute γ_T for the maturation rate of nymphs to adults and μ_N and μ_A for the natural death rates of nymphs and adults, respectively, so we will not describe them in detail. Note that adult female ticks preferentially seek out deer for their final blood meal, which plays an important role in their dispersal and is the reason why adult ticks have a significantly higher rate of diffusion compared to juvenile ticks [2, 34]. We denote the diffusion rate for adult ticks as D_A. Note that the force of infection for nymph and adult ticks is given by λ_{NM} and λ_{AM}, respectively, and they are formulated similarly to the force of infection for larval ticks given above. Thus, the equations of the nymphs and adult ticks are given as

$$\frac{\partial S_N}{\partial t} = \tau_T S_L + D_M \Delta S_N - \lambda_{NM} S_N - (\gamma_T + \mu_N) S_N,$$
$$\frac{\partial I_N}{\partial t} = \tau_T I_L + D_M \Delta I_N + \lambda_{NM} S_N - (\gamma_T + \mu_N) I_N,$$
$$\frac{\partial S_A}{\partial t} = \gamma_T S_N + D_A \Delta S_A - \lambda_{AM} S_A - \mu_A S_A,$$
$$\frac{\partial I_A}{\partial t} = \gamma_T I_N + D_A \Delta I_A + \lambda_{AM} S_A - \mu_A I_A. \tag{5}$$

For simplicity, we assume that $\beta_{LM} = \beta_{NM} = \beta_{AM} = \beta_T$,

and subsequently, $\lambda_{LM} = \lambda_{NM} = \lambda_{AM} = \lambda_T$. Next, we describe the dynamics and equations of the susceptible and infectious mouse populations. We assume the mouse populations increase at a constant rate π_M due to birth and move across the domain at the rate D_M. The susceptible mice become infected if fed on by infectious ticks at the rate λ_M which is expressed as

$$\lambda_M = \frac{(\beta_{ML} I_L + \beta_{MN} I_N + \beta_{MA} I_A)}{S_M + I_M}. \tag{6}$$

We also assume that $\beta_{ML} = \beta_{MN} = \beta_{MA} = \beta_M$. The parameter β_M denotes the probability that a mouse is infected when being fed on by an infectious tick. Notice that we consider all tick life stages (except for eggs) when calculating the force of infection since ticks at every life stage have a tendency to feed on mice, especially if other hosts are scarce [2, 34, 36]. The mouse populations diminish due to natural death at the rate μ_M. From this, the population dynamics for mice are described by

$$\frac{\partial S_M}{\partial t} = \underbrace{\pi_M}_{\text{Birth}} + \underbrace{D_M \Delta S_M}_{\text{Random Diffusive Motion}} - \underbrace{\lambda_M S_M}_{\text{Infection}} - \underbrace{\mu_M S_M}_{\text{Death}},$$
$$\frac{\partial I_M}{\partial t} = \overbrace{D_M \Delta I_M} + \overbrace{\lambda_M S_M} - \overbrace{\mu_M I_M}. \tag{7}$$

To summarize, we have the following partial differential equation (PDE) model: for $t \neq nT$, $n = 1, 2, \cdots$,

$$\begin{cases} \frac{\partial S_E}{\partial t} = \pi_T \left(1 - \frac{S_E}{K}\right)(S_A + I_A) - (\sigma_T + \mu_E) S_E, \\[1mm] \frac{\partial S_L}{\partial t} = D_M \Delta S_L + \sigma_T S_E - \lambda_T S_L - (\tau_T + \mu_L) S_L, \\[1mm] \frac{\partial I_L}{\partial t} = D_M \Delta I_L + \lambda_T S_L - (\tau_T + \mu_L) I_L, \\[1mm] \frac{\partial S_N}{\partial t} = D_M \Delta S_N + \tau_T S_L - \lambda_T S_N - (\gamma_T + \mu_N) S_N, \\[1mm] \frac{\partial I_N}{\partial t} = D_M \Delta I_N + \tau_T I_L + \lambda_T S_N - (\gamma_T + \mu_N) I_N, \\[1mm] \frac{\partial S_A}{\partial t} = D_A \Delta S_A + \gamma_T S_N - \lambda_T S_A - \mu_A S_A, \\[1mm] \frac{\partial I_A}{\partial t} = D_A \Delta I_A + \gamma_T I_N + \lambda_T S_A - \mu_A I_A, \\[1mm] \frac{\partial S_M}{\partial t} = D_M \Delta S_M + \pi_M - \lambda_M S_M - \mu_M S_M, \\[1mm] \frac{\partial I_M}{\partial t} = D_M \Delta I_M + \lambda_M S_M - \mu_M I_M. \end{cases} \tag{8}$$

To implement prescribed fire, we assume that a certain proportion (ν_E, ν_L, ν_N, ν_A, and ν_M) of the tick and mouse populations is reduced following a burn in a patch of the domain Ω once every T period of time. Thus, tick and mouse populations following a burn at time instant $t = nT$

$(n = 1, 2, \cdots)$ are given as

$$\begin{cases} S_E(nT^+) & = (1 - \nu_E)S_E(nT^-), \\ S_L(nT^+) & = (1 - \nu_L)S_L(nT^-), \\ I_L(nT^+) & = (1 - \nu_L)I_L(nT^-), \\ S_N(nT^+) & = (1 - \nu_N)S_N(nT^-), \\ I_N(nT^+) & = (1 - \nu_N)S_N(nT^-), \\ S_A(nT^+) & = (1 - \nu_A)S_A(nT^-), \\ I_A(nT^+) & = (1 - \nu_A)I_A(nT^-), \\ S_M(nT^+) & = (1 - \nu_M)S_M(nT^-), \\ I_M(nT^+) & = (1 - \nu_M)I_M(nT^-). \end{cases} \quad (9)$$

The proportion (ν_E, ν_L, ν_N, ν_A, and ν_M) is chosen to be between zero and one; zero indicated no reduction and one indicating total loss of the tick and mouse population in the burned patch. The PDE system (8) is subject to homogeneous Neumann boundary conditions, viz.,

$$\frac{\partial S_E}{\partial \hat{n}}, \frac{\partial S_L}{\partial \hat{n}}, \frac{\partial I_L}{\partial \hat{n}}, \frac{\partial S_N}{\partial \hat{n}}, \frac{\partial I_N}{\partial \hat{n}}, \frac{\partial S_A}{\partial \hat{n}}, \frac{\partial I_A}{\partial \hat{n}}, \frac{\partial S_M}{\partial \hat{n}}, \frac{\partial I_M}{\partial \hat{n}} = 0, \quad (10)$$

which means that no ticks are transported in or out of the domain Ω. The PDE system, the above boundary conditions, and proper initial conditions form a well-posed boundary-initial value problem.

A flow diagram for the above model is shown in Figure 1, and variable and parameter descriptions along with the values for the parameters and references are listed in Table 1.

2.2. Numerical Simulations. Our goal is to study the effects of prescribed burning in a more realistic setting compared to the ODE model presented in Guo and Agusto [29]. In the absence of diffusion, our results are the same as the results of the ODE system in [29]. Moreover, several of the results from [29] hold in a spatial setting such as the conclusions that high-intensity burns are more effective than low-intensity burns and that yearly burning is most effective at reducing tick populations.

First, we detail the numerical method used to solve our system of PDEs in Section 2.2.2. We simulate the impulsive model (8) and (9) using parameter values given in Table 1 and the proportion of ticks and mice reduced due to prescribed fire estimated in Section 2.2.1. However, there is little data available on the average movement of ticks. Clow et al. [39] provided an estimation of the northward range front expansion rate, but did not provide much insight into westward expansion or establishment. Adult females preferentially seek out deer for their final blood meal, which plays an important role in their dispersal and is the reason why adult ticks have a significantly higher rate of diffusion compared to juvenile ticks. In this work, we assume a rate of diffusion of 2 km/year for juvenile ticks and 4 km/year for adult ticks.

2.2.1. Estimating the Proportion of Ticks Reduced due to Prescribed Fire. There is very limited data available on the survival rate of ticks following a prescribed burn, so we use what little data is available and make several assumptions in order to determine the proportions (ν_E, ν_L, ν_N, ν_A, and ν_M). The data used to calculate the proportions for high- and low-intensity fires are taken from [25, 38], respectively; see Table 1. The sites for [38] were located in Hancock County, Illinois, and consisted of several overstory trees including white oak and post oak trees. The burns performed during the study were low intensity since the height of the flames was largely not higher than 1 m. 54 *I. scapularis* ticks were collected over the study period, and for our calculations, we assume that these were the ticks remaining following a low-intensity burn. 40 larvae, 12 nymphs, and 2 adults were collected. We divide the number of ticks in each life stage by the total number of ticks and subtract that proportion from one to get our estimate for the proportion of ticks reduced following a low-intensity burn (i.e., $\nu_L = 1 - 40/54 = 0.2593$). No mice or eggs were collected for this study; thus, we assume that those two populations are reduced at the same rate as a high-intensity fire, so our results for low-intensity fires likely overestimate their effectiveness.

The sites used in the high-intensity fires were located in Mendocino County, California, and consisted of chaparral habitat, which is not ideal habitat for ticks, so our estimates may be higher than the true values. To calculate the proportions for high-intensity fires from the data in [25], we assume that equal numbers of ticks and mice are in each site preburn and that any differences in the number of ticks are due to the burn performed. Then, we subtract the number of ticks present in the treatment sites from the number of ticks present in the control sites and divide it by the total number of ticks in the control sites. Lastly, we subtract these values from one to give the proportion of ticks reduced following a high-intensity burn, i.e., $\nu_L = 1 - (159 - 118)/184 = 0.7421$.

2.2.2. Numerical Method. The system of PDEs (8) and (10) is solved using MMPDElab [40], a package written in Matlab for adaptive mesh movement and finite element computation in 1D, 2D, and 3D. The package uses the linear finite element method to discretize PDE systems in space and an implicit Runge-Kutta (fifth-order Radau IIA) method in time with variable time stepping. The linear finite element method gives second-order convergence in space [41], while the implicit Runge-Kutta method ensures a strong stability in the computation [42]. The mesh adaptivity function of the package is not used in the current work. We use a triangular mesh constructed as follows: the domain Ω is first partitioned into small rectangles of same length in each of the x and y directions. Each small rectangle is subsequently partitioned into four triangles to obtain the final triangular mesh. In our computation, we use 49×49 small rectangles and thus a total of 9604 triangular elements in the mesh.

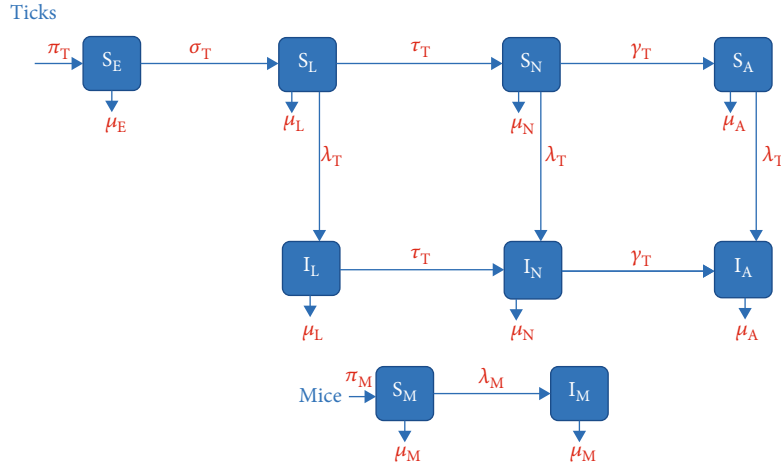*2.2.3. Global Sensitivity Analysis.* We now perform a global sensitivity analysis (GSA) to explore which model

FIGURE 1: The flow diagram for model (8).

TABLE 1: Description of the variables and parameters for model (8).

Parameter	Meaning	Value	Reference
π_M	Birthrate of mice	0.02	[30]
μ_M	Death rate of mice	0.01	[30]
β_M	Probability of infection in mice	0.9	[37]
K	Carrying capacity for ticks	5000	[31]
π_T	Birthrate of ticks	456.36	[30]
μ_E	Death rate of eggs	0.0025	[30]
μ_L	Death rate of larvae	0.015	[30]
μ_n	Death rate of nymphs	0.015	[30]
μ_A	Death rate of adults	0.015	[30]
β_T	Probability of infection in ticks	0.9	[37]
α	Attack rate of ticks on mice	0.002	Assumed
σ_T	Rate at which eggs develop into larvae	0.00677	[30]
τ_T	Rate at which larvae develop into nymphs	0.00618	[30]
γ_T	Rate at which nymphs develop into adults	0.00491	[30]
v_E	Proportion of eggs reduced following a high- or low-intensity burn	1	[25]
v_L	Proportion of larvae reduced following a high- or low-intensity burn	0.7421, 0.2593	[25, 38]
v_N	Proportion of nymphs reduced following a high- or low-intensity burn	1, 0.7778	[25, 38]
v_A	Proportion of adults reduced following a high- or low-intensity burn	0.5454, 0.9629	[25, 38]
v_M	Proportion of mice reduced following a high- or low-intensity burn	0.4728	[25]
D_M	Diffusion coefficient for mice	2, 0.5	Assumed
D_A	Diffusion coefficient for adults	4, 1	Assumed

parameters have the greatest effect on model outcomes. The results of this analysis also inform several parameter values to be used in the subsequent scenarios. Latin Hypercube Sampling (LHS) is used to create representative distributions of each of the model parameters, we generate 1000 samples for each parameter [43] to create the LHS matrix, and we subsequently calculate partial rank correlation coefficients (PRCC) for each of the parameters [43]. Since there is little data available on the actual distributions of our parameters, we assume a uniform distribution for each centered on the baseline values given in Table 1 with minimums and maximums for each parameter being minus and plus 20% of the baseline, respectively.

The outcome measure here is the total number of infectious nymphs in one dimension for expediency, and we perform this analysis using high-intensity burns and using low-intensity burns. We perform the analysis for a case with homogenous initial conditions as well as a case with heterogeneous initial conditions. The results are largely the same aside from slightly more significant PRCC values for diffusion of mice and adults; thus, we only include the heterogeneous results here.

We also want to investigate the impact of the number of burns and the time between burns on the model outcome, so we sample those parameter values from two Poisson distributions that exclude zero. The number of burns is pulled from a Poisson distribution centered on 10 since we run the first scenario for 10 years. The time between burns is pulled from a Poisson distribution centered on 1 since a period of 1 year between burns is used for Scenario 3.1. After creating the initial distributions, any zeros in either sample are changed to ones to avoid issues with implementing the burns. These samples are combined with our LHS matrix, and we subsequently calculate partial rank correlation coefficients (PRCC) for each of the parameters [43]. The results are given in Figure 2 for low and high intensity, respectively. We also record in Figure 3 the total number of infectious nymphs present at the end of each simulation performed from the parameter space created from the LHS method.

From the result of the sensitivity analysis in Figure 2, we see that the significant parameters for low- and high-intensity burns are time between burns, number of burns, carrying capacity (K), nymph development rate (γ_T), tick transmission probability (β_T), larva development rate (τ_T), and tick birth rate (π_T). Diffusion of adults is significant in the high-intensity analysis, but not in the low-intensity analysis.

Upon a closer look at Figure 2, we observe that the transmission probability is high with high-intensity burns which will favor more infections. However, the high-intensity environment is hostile since vital parameters like tick developmental rates and the carrying capacity have a relatively low impact on the number of infectious nymphs, unlike the low-intensity burn domain which has high sensitivity indices for these parameters.

Looking at the time between burns and number of burns closely, we see that regardless of whether we are performing low- or high-intensity burns, the timing between burns remains crucial, indicated by a PRCC value near one in both cases. This means that even if there is a case where low-intensity burning is the only type possible for any reason, whether that be due to lack of fuel or proximity to homes or businesses, there is a significant negative effect on the total number of infectious nymphs present in that habitat as time between burns decreases. This is reflected in the results by the large positive PRCC value for time between burns. This positive value indicates a positively correlated relationship between this parameter and the model outcome, so when the value of this parameter increases, so does the number of infectious nymphs and vice versa.

We also observe that the number of burns being performed over time plays an important role, but less so than

timing between burns. The number of burns plays a slightly larger role in the high-intensity case since many more nymphs are killed off with each burn compared to the low-intensity case (see Figure 3). The negative PRCC value for this parameter indicates that it has a negatively correlated relationship with the model outcome, so when this parameter increases, the number of infectious nymphs tends to decrease.

Considering tick and host diffusion across the domain, we observe that diffusion of the ticks and hosts does not have significant effects on the model outcome. It may be that we have not tested a wide enough range for these parameters to see their effect.

All these observations help inform some model parameters for the scenarios presented in the following sections, namely, the use of high-intensity burns and a reasonable time between burns of one year, unless otherwise stated. All other parameters are kept at their baseline values for these scenarios unless otherwise stated.

Now, using the parameters created from the LHS, we see in Figure 3 as with the results from [29] that in a spatial setting high-intensity burns are more effective than low-intensity burns at reducing tick populations. Furthermore, we see that the minimum of the boxplot for low-intensity burns is more than the maximum from the high-intensity burns.

3. Results

In this section, we examine the effect of prescribed burns and diffusion in different scenarios that may arise in various environments in the real world.

3.1. Scenario 1: Prescribed Fire in a Homogeneous Domain. The effects of consistent burning and diffusion are addressed in this scenario where ticks are distributed evenly across the domain Ω of size $30 \, \text{km} \times 30 \, \text{km}$ and a prescribed burn occurs in a $10 \, \text{km} \times 10 \, \text{km}$ block in the middle of the domain every twelve months for ten years. This equates to roughly 2500 acres of burned area, which is a large prescribed fire typical in larger uniform environments such as oak woodlands or grasslands [44]. We assume an initial condition of 500 infectious nymphs at every point in the domain, meaning that Lyme disease is already endemic in this area. Figure 4 shows the simulation results for this scenario.

From these results, one can see an immediate reduction in the number of ticks at $t = 1$ following the burn in Figure 4(a); unfortunately, this is followed by ticks diffusing into the burned area and a slow recovery of the burned patch in terms of the number of ticks. At $t = 3$ (Figure 4(b)), we can see just how effective burning is at reducing the number of ticks in the burn site and the effects of diffusion begin to become clear. Ticks begin to diffuse into the burned environment during the year following a burn and increase the recovery rate of ticks in that area while simultaneously decreasing the number of ticks in the area surrounding the burn. The recovery rate of ticks is still low enough that the number of ticks remains lower in the consistently burned area even after long periods of time (see Figure 4(c)). By
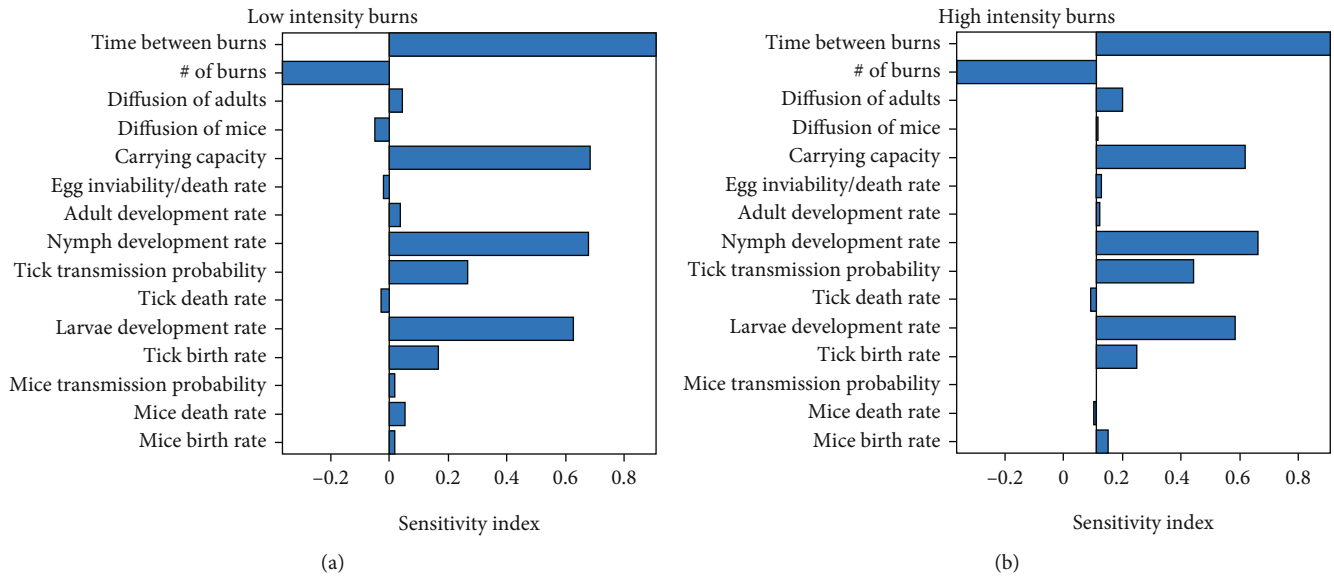
(a)

(b)

FIGURE 2: The partial rank correlation coefficients for the parameters for (a) low-intensity burns and (b) high-intensity burns. Values significantly greater or less than zero indicate parameters that have the greatest impact on model outcome (number of infectious nymphs).
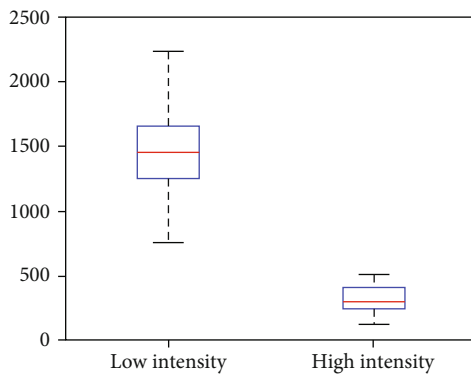

FIGURE 3: Distribution of the total number of infectious nymphs using the parameters created from the LHS. This graph displays the distribution of those totals via a boxplot. The median is shown as the red bar within the box. The upper and lower quartiles are the upper and lower portions of the box, respectively. Finally, the maximum and minimums for low and high intensity are displayed at the ends of the upper and lower dashed lines, respectively.

the end of the ninth year, just before a burn in the tenth year, we can see in Figure 4(d) that the number of ticks in and around the burn site has been reduced significantly compared to the areas near the edge of the domain that were unaffected by both the burns and the diffusion of ticks into the burned area.

To further explore the effectiveness of prescribed burns in a homogeneous domain, we examine the effect of a different number of burns and time between burns over a period of 10 years.

3.1.1. Effects of a Different Number of Burns and Time between Burns. In Figure 5(a), we examine the effect of the number of burns. In other words, we perform a set number of yearly burns and let the simulation run for a total of 10 years to determine whether or not the number of burns has a significant impact on the number of infectious nymphs present in the burned area at the end of the simulation. For example, the case with 4 burns means that 4 yearly burns are performed starting at $t = 1$ and no burns are performed for the rest of the years. The results indicate that consistent prescribed burning is an effective control method for tick populations. In addition, we see that there is nearly a linear relationship between the number of burns performed and the percentage of ticks that remain at the end of the scenario, so the more burns that are able to be performed, the better.

Next, in Figure 5(b), we look to the time between burns to explore the effectiveness of burns at different times since yearly burning might not be possible in every environment. Note that the burning pattern in this situation is different from that considered in Figure 5(b). For example, with the number of the years between burns being 4, the burn is performed every four years with the first burn occurring at $t = 4$ and the total number of burns is 2. We observe that the best case is a yearly burn, this of course agrees with our earlier result from the sensitivity analysis. Moreover, we see that burning at any interval is very effective at reducing the number of ticks in an area where they are endemic. Even a single burn every five years led to a 30% reduction in the number of ticks compared to the unburned case.

3.1.2. Effects of Different Burn Patch Sizes. Finally, we explore the effect of changing the patch size of the burn being performed. To better compare the relative effectiveness of each size of the burn patch, we divide the number of infectious nymphs remaining in the burned area at the end of a simulation by the number of infectious nymphs present in a patch of the same size in a simulation that ran for ten years, but had no burning occurring. This measure allows us to compare the effectiveness of burning with larger and smaller
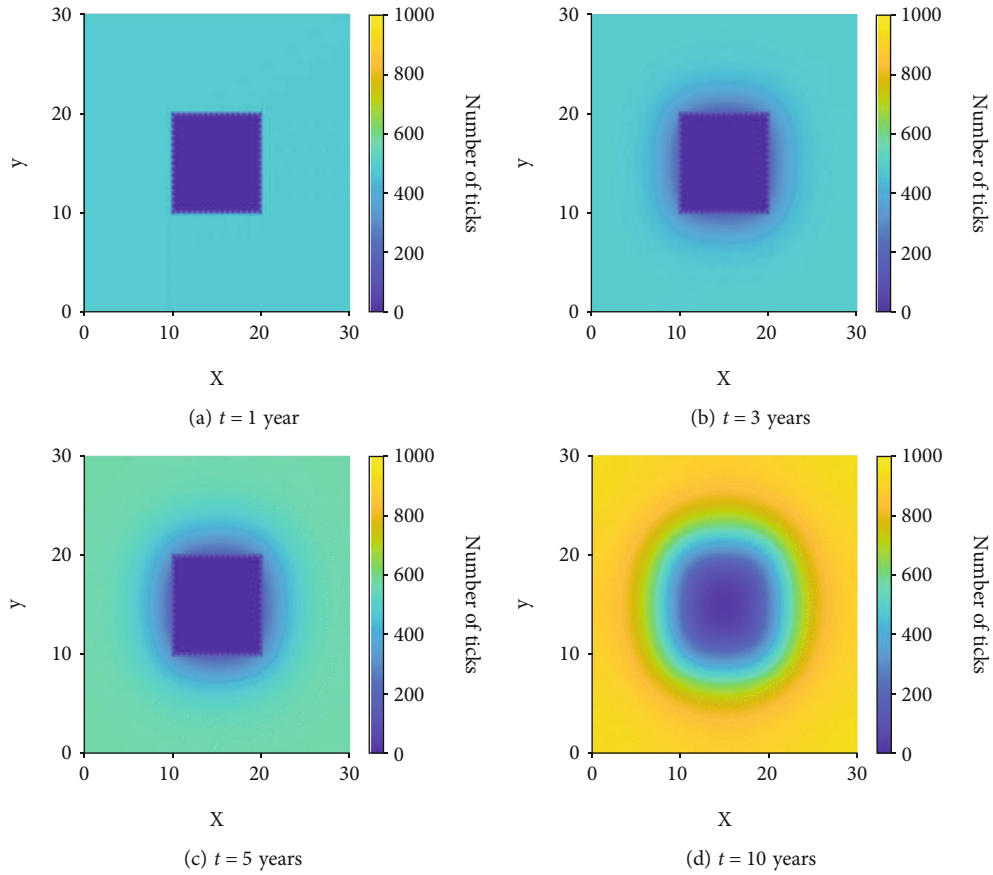
(a) $t = 1$ year

(b) $t = 3$ years

(c) $t = 5$ years

(d) $t = 10$ years

FIGURE 4: The distribution of infectious nymphs in a homogeneous domain at various times.
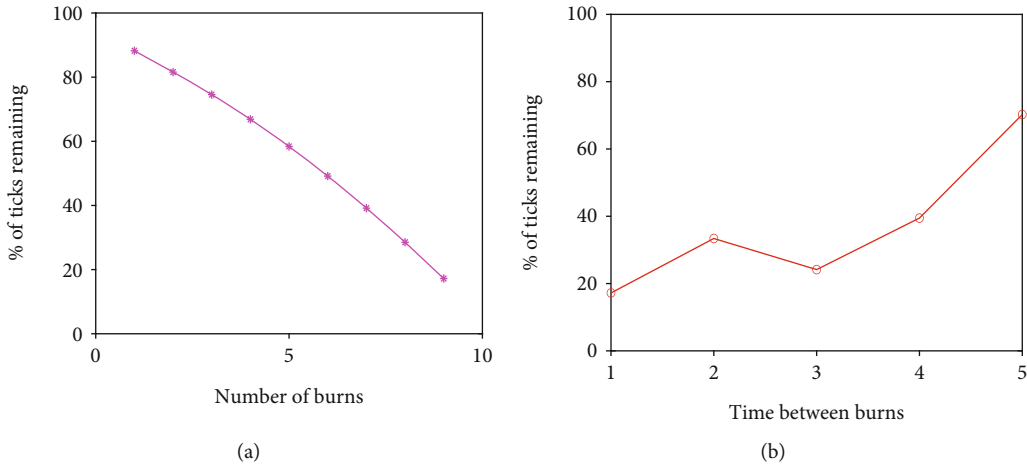

(a)

(b)

FIGURE 5: Simulation of model (8) for different numbers of burns and time between burns. (a) The number of burns performed yearly starting at $t = 1$ vs. the percentage of ticks that remain after a 10-year simulation. (b) The number of the years between burns vs. the percentage of ticks that remain after a 10-year simulation.

patches. We see in Figure 6 that the bigger the patch, the more effective burning is at reducing the number of infectious nymphs.

Thus, patch size plays a very important role in determining the effectiveness of a burn. One may argue that this is due to the simple fact that we are killing off more ticks as burn size increases, but notice that the percentage remaining decreases nonlinearly as the patch size increases. This can be attributed, in part, to the effect of diffusion. Since nymphs diffuse at a rate of 2 km/yr, we expect that a burn patch whose length is less than that rate will be significantly less effective than one that is greater than that rate and this is reflected in our results based on the large increase in effectiveness, which is signified by a large decrease in the
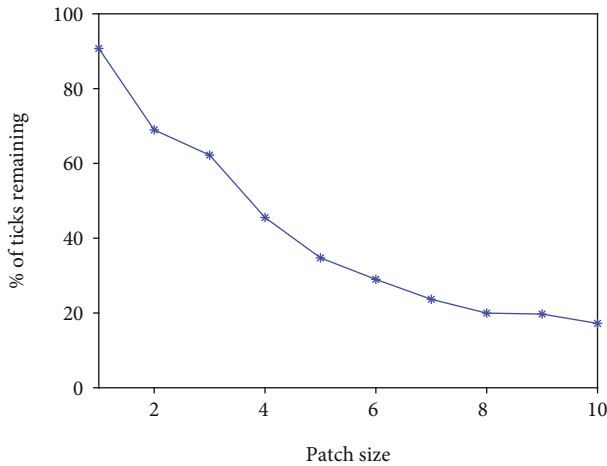
FIGURE 6: Scenario 1: the percentage of the number of infectious nymphs remaining in the burned area after 10 years of yearly, high-intensity burns is plotted against the patch size.

percentage of ticks remaining, when moving from a patch size of $1\,km \times 1\,km$ to a patch size of $2\,km \times 2\,km$. We see a similar reduction when moving from a patch size of $3\,km \times 3\,km$ to $4\,km \times 4\,km$. This is due to the effect of adult tick diffusion, which occurs at a rate of $4\,km/yr$. There are diminishing returns as patch size increases, but if the goal of a burn is reducing the prevalence of ticks, then the larger the patch, the better. The relationship seen here highlights the need for additional studies on the aggregate movement of ticks in the Midwest as this data can inform burning management strategies.

In the next section, we further explore the effectiveness of prescribed burns in a heterogeneous domain that captures different environments that ticks can be found.

3.2. Scenario 2: Prescribed Fire in a Heterogeneous Domain. In order to explore how burning in different environments might affect tick populations, Scenario 2 has a nonuniform domain with $x > 15\,km$ being a wooded environment for ticks, which typically leads to better survival rates and easier traversal. This is interpreted as the ticks having a higher rate of diffusion compared to $x < 15\,km$, which is considered grassland with burns occurring in $10\,km \times 10\,km$ blocks on opposite corners of the domain. Grassland is a less suitable environment for ticks because it generally has higher temperature and lower humidity relative to a wooded environment, which also tends to have significant leaf litter so ticks have plenty of space to hide when temperature increases or humidity drops. Ticks in the wooded environment have a rate of diffusion 4 times greater than those in the grassland environment. The relatively low rates of diffusion in both environments mean that there is no significant effect of the ticks in the wooded environment on the area that is burned in the grassland environment and vice versa.

Figure 7(a) shows the results of Scenario 2. By the time of the first burn at $t = 1$ (Figure 7(c)), we can see that the results are very similar for the two environments. However, by $t = 5$ (Figure 6), there is a clear difference between them. Since the rate of diffusion is higher for $x > 15\,km$, the num-

ber of ticks surrounding the area that has been burned is lower compared to the area around the burn for $x < 15\,km$. At the end of the final year, the effects of burning in a wooded environment indicate that it is more effective in reducing the number of ticks when considering the total area in and around the area that is being burned. To verify this, we calculated the number of ticks in each area that is burned as well as the number of ticks present in the regions $x < 15$, $15 < y < 30\,km$ and $x > 15, y < 15\,km$ (i.e., the upper left and lower right quadrants, respectively). Interestingly, the number of ticks present in the grassland burned area was less than that in the woodland burned area; however, the number of ticks present in the upper left quadrant was greater than the number of ticks present in the lower right quadrant. This is compelling evidence that burning in an environment that is better suited to ticks is significantly more effective at reducing the number of ticks both in and around the area that is burned. As time goes on and burning continues, this negative effect on ticks becomes more and more noticeable. On the other hand, if the goal of the burn is strictly to reduce the number of ticks in the area that is burned, then burning in the grassland area would lead to a better outcome. This scenario indicates that careful consideration should be taken when planning prescribed burns as the goal of the burning will inform the best areas for that burning to occur.

3.3. Scenario 3: Prescribed Fire at the Invasion Front. In this final scenario, we explore the effect that prescribed burns have on the invasion of ticks into a new area. Suppose that ticks are discovered in high numbers in the region $x, y < 5\,km$ and burns are performed for $x, y < 10\,km$ in an attempt to halt the spread of ticks into the rest of the domain. Note that susceptible hosts are assumed to be present throughout the domain; otherwise, establishment would not be possible. These final scenarios (Figures 8 and 9) contain one example without burns and three different examples with burning in order to explore the applicability of fire in reducing the number of ticks invading into a new area. For the latter three variations, we only show the results at the end of the simulation (that is, at $t = 20$).

In this last section, we further explore the effectiveness of prescribed burns at the invasion front where ticks are establishing in a new environment.

3.3.1. Invasion Front without Prescribed Fire. Figures 8(a)–8(d) show what occurs after 20 years of uninhibited spread. A traveling wave is formed and begins to propagate across the domain. This situation is likely occurring in many places across the Midwest and further North as ticks continue to spread across the continent.

When left unchecked, it is clear why tick numbers have been increasing over the past several decades. The lack of fire management in many areas combined with the effects of climate change and an abundance of hosts has made many areas of the United States prime environments for ticks, and once they are established, they can spread rapidly. Next, we analyze the results of the three different burning examples mentioned previously.
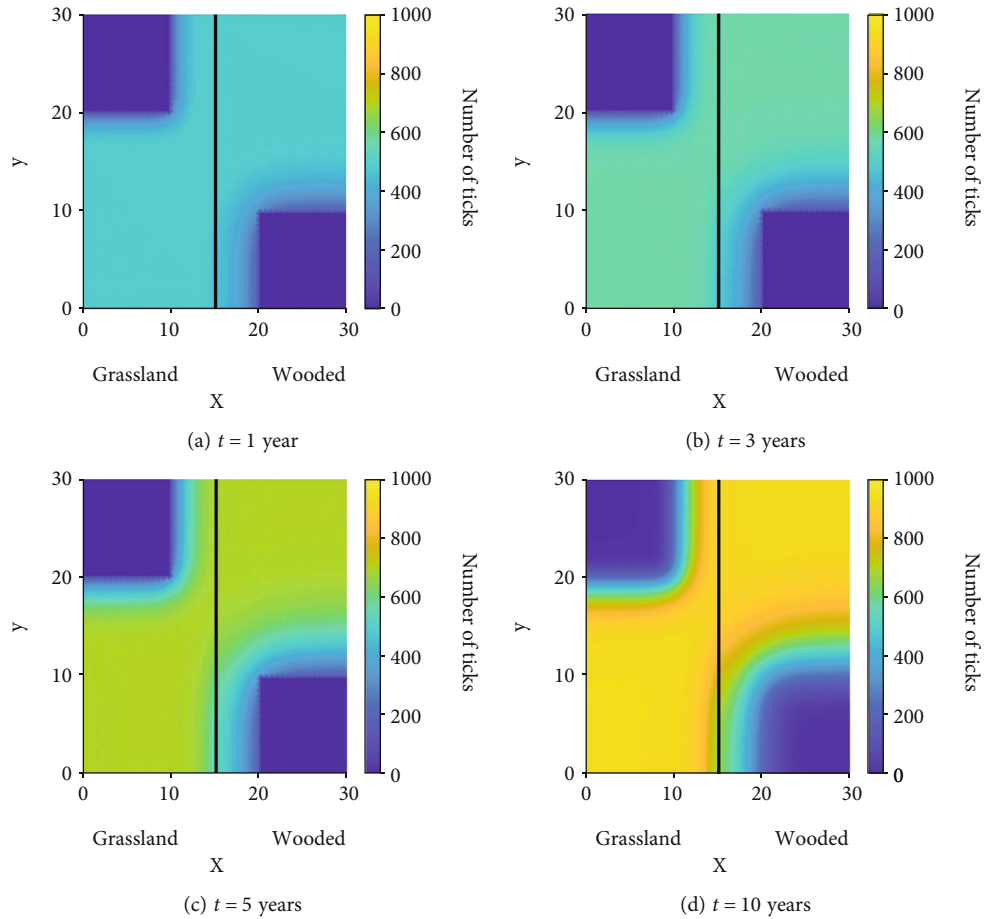
Figure 7: The distribution of infectious nymphs in a heterogeneous domain at various times.

3.3.2. Invasion Front with Prescribed Fire. The first burning regime is one in which prescribed burns are implemented every 5 years after ticks are discovered in the corner of the domain. Figure 9(b) displays the results of the simulation after 20 years. We see that burning every 5 years has a significant impact on the number of ticks remaining at $t = 20$ years. Compared to the example without burning, there is a 23% decrease in the number of ticks remaining. However, we can also see that burning every 5 years has had almost no effect on the spread of ticks into the region. The edge of the wave is in virtually the same position as the case without burning.

The second burning example, which is depicted in Figure 9(c), is a case where the high prevalence of ticks in the corner of the domain is not noticed until the tenth year of the simulation and a yearly burning regiment is performed for a decade. In this case, it is clear that even after a decade of burning, burning alone is not entirely effective at preventing the spread of ticks. There has been a significant reduction in the percentage of ticks, with 32% of ticks being killed off compared to the unburned case.

The final case is depicted in Figure 9(d). This is a case where the invading ticks are detected early in the first year and a yearly burning regiment is planned and executed for one decade. Again, we let this example run until

$t = 20$ years to evaluate the effectiveness of the approach compared to the previous examples. By $t = 20$, we can see that despite a decade of high-intensity burning, some of the ticks have survived and made their way to a majority of the rest of the domain. This indicates that if ticks are noticed early enough, burns may be able to limit the number of ticks that are able to spread into a new area, though establishment may be inevitable. Pairing prescribed burns with other forms of tick population management would likely slow and possibly prevent spread and establishment. Comparing this with the unburned example, we have a 42% reduction in the number of ticks at the end of the simulation. From this, we can conclude that burning as early as possible is crucial to the effectiveness of prescribed burns on the invasion of ticks. The results of this final scenario paint a difficult picture. Many areas in the Midwestern United States are experiencing or expect to experience increasing numbers of ticks as the effects of climate change worsen. If prescribed burning is to be used as an effective control method, then the time for action is now as waiting any amount of time gives these organisms the chance that they need to establish themselves firmly enough that prescribed fire can only be used as a mitigation strategy rather than as part of a strategy for eradication.
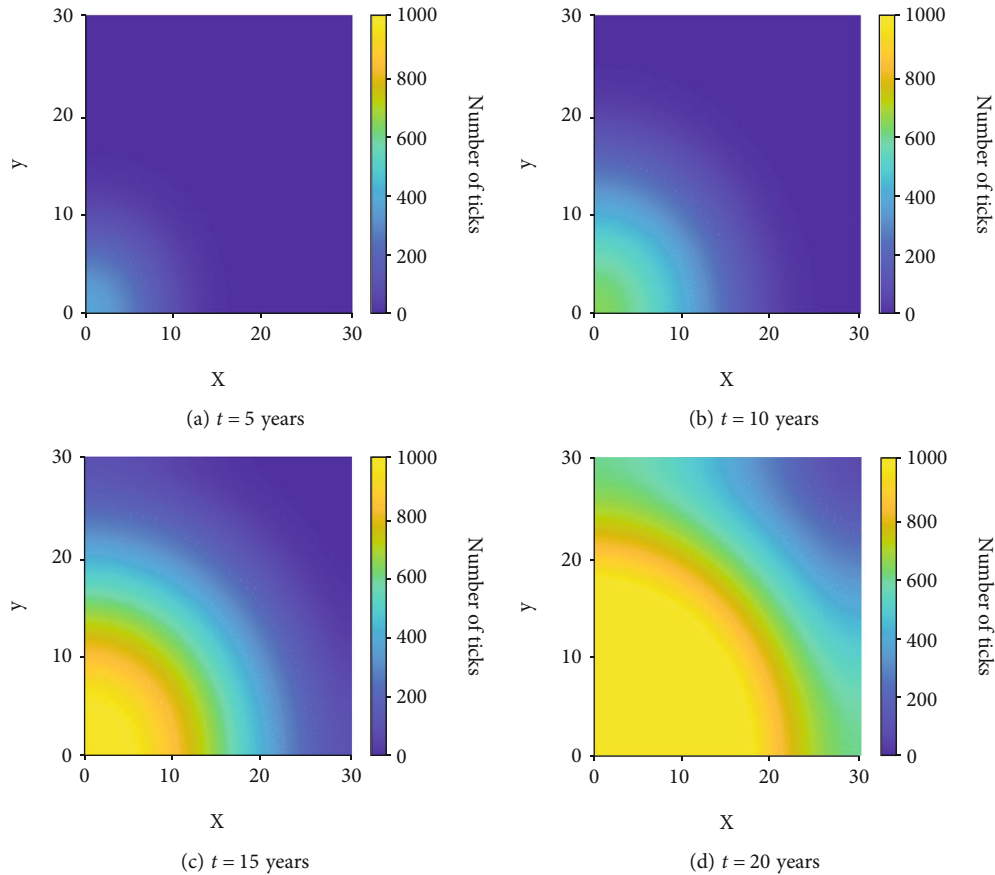
(a) $t = 5$ years

(b) $t = 10$ years

(c) $t = 15$ years

(d) $t = 20$ years

FIGURE 8: The distribution of infectious nymphs for Scenario 3 without prescribed fire at various times.

4. Discussion

As stated previously, one of the primary papers in this study is Guo and Agusto [29]. This work on the effects of prescribed fire on tick populations provided crucial information that guided several of the numerical simulations considered, namely, those in Scenario 1. Since one of the main conclusions of the paper is that high-intensity fires are significantly more effective than low-intensity fires, we do not need to explore the two variations too deeply to come to a similar conclusion. Thus, we performed an extension of the sensitivity analysis given there and further analyzed the effects of those results in Scenario 1. Based on the results from Figures 2 and 3, combined with the results from [29], we conclude that further testing of the effects of low-intensity burning, while interesting, has little practical importance since low-intensity fires are unable to reduce the number of ticks in an area at a similar rate as high-intensity fires, so high-intensity fires should be used whenever possible. Our results have several implications for the future of prescribed fire as a method of control for tick populations. In particular, Scenario 1 highlights the waning effectiveness of burning as patch size decreases, which may explain conflicting results observed by several studies conducted on the topic thus far [13–15, 17, 19, 20, 22, 27]. As stated above, many of these studies focused on small plots of land and were sometimes performed on previously unburned sites.

Burning on small plots can have little to no effect depending on the recovery rate of ticks which is governed by several factors including the average movement of hosts in the region as well as the environment in which the burn is being performed. As the average rate of movement of hosts in and around the area that is being burned increases, an example of this being the transition time between winter and spring when both small and large mammalian hosts become more active, a larger and larger area is required for a prescribed burn to significantly reduce the number of ticks in that area. Burning previously unburned plots of land has increasing effectiveness as subsequent burns are performed, and if patch size is large enough and intensity is high enough, there can be a significant reduction in the number of ticks in the burned area. Since the site was previously unburned, however, recovery of ticks can occur relatively quickly since a single burn does little to reduce the number of ticks around the area being burned; thus, multiple burns should be performed over longer periods of time to consistently reduce the number of ticks in and around the area being burned.

Based on our results, we theorize that the effectiveness of prescribed burning is dependent on the average movement of hosts in and around the area being burned. The study sites used in [12, 23] combined with our results from Scenario 2 paint an interesting picture. The plots used in [12, 23] mostly consisted of pine and mixed-pine forested environments, and Georgia and Florida have large deer populations
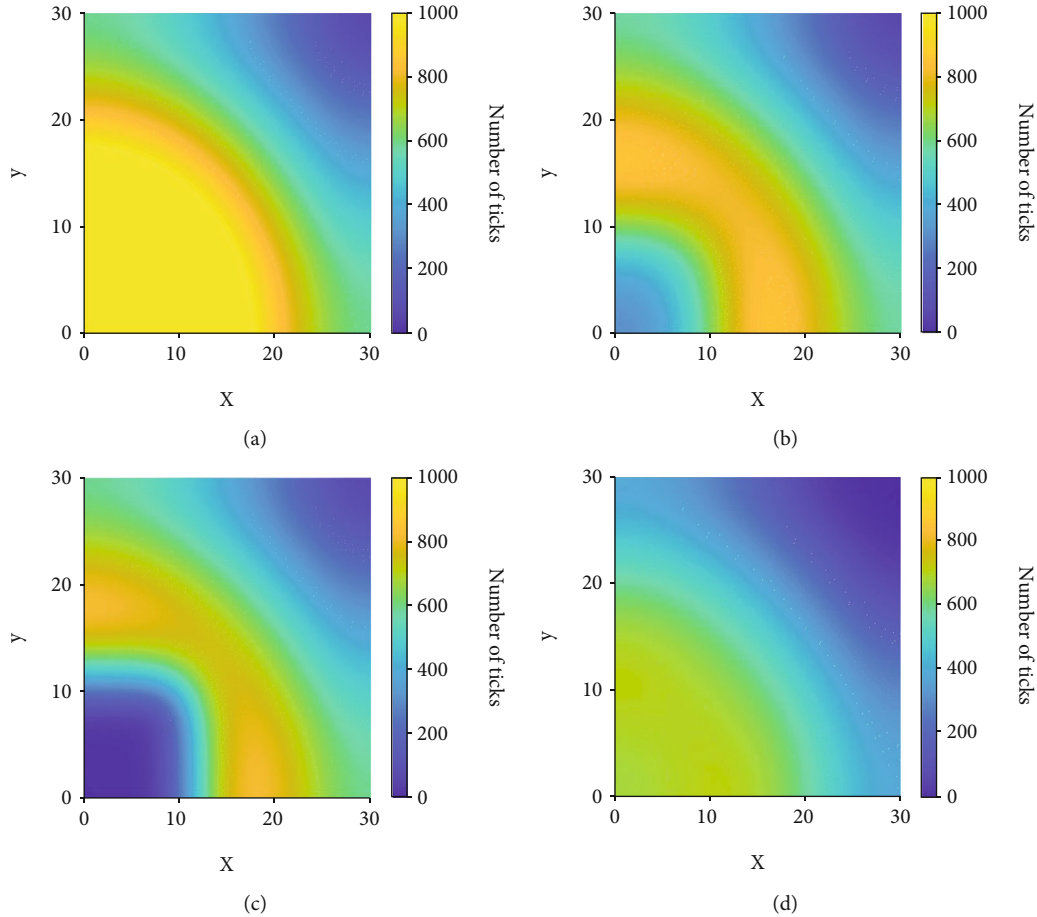
FIGURE 9: The distributions of infectious nymphs at $t = 20$ years for Scenario 3 with different burning patterns. (a) No burns. (b) Burning implemented every 5 years. (c) 10 years of no burning followed by yearly burning for the remaining decade. (d) Yearly burning implemented for the first 10 years and no burns later.

and few white-footed mice. The lack of this extremely viable host should further inhibit recovery of ticks following a burn and that seems to hold true based on the observed results. Since there was also a reduction in the prevalence of certain diseases in the population [23] may indicate that a combination of hosts is required for effective tick and disease reestablishment or that host composition is extremely important when determining the effectiveness of a prescribed burn. Thus, several factors need to be considered when deciding on the best control methods for ticks in an area, including the type of tick hosts present in and around the area and their prevalence, the local environment, and the type of burn (low vs. high) that is able to be performed regularly.

When we look at all of this information alongside the results presented in Scenario 3, there is major concern for several areas in the United States. Those states located in the Great Plains seem to be particularly vulnerable to invasion of ticks. This is due to the various factors mentioned in the previous paragraph. Since the area is largely covered by grassland and farmland and these environments are either not suited for consistent burning or more quickly provide renewed cover for ticks via fast-growing grasses, prescribed burning as a means of tick population management in these areas may not be as feasible or effective. This is espe-

cially true considering the limited effect of burning on tick establishment in our simulations.

5. Conclusions

In this study, we extended the model provided in Guo and Agusto [29] in order to explore how the effects of prescribed burning impact tick population dynamics in a spatial setting. The results of this study indicate that prescribed fire is an extremely useful tool for tick population management, but a limited tool for prevention of tick establishment. The relationship between burn patch size and percentage of ticks remaining in the burned area was explored, and this relationship coupled with other results presented here provides the insight that the effectiveness of prescribed burns can vary widely depending on biological factors related to the aggregate movement of ticks and their hosts. When the patch being burned is less than the rate of diffusion of ticks, we see a less significant effect of burning compared to larger patch sizes which yield a much lower proportion of ticks remaining after a decade of regimented burning. The results from Scenario 2 support the idea that the location of burns is crucial depending on the goal of the burning. This is due to the fact that burning in areas where ticks cannot easily

spread due to increased rates of desiccation or lack of hosts, such as grasslands which tend to be hotter and drier than forested environments, is only effective at reducing the number of ticks in the area that is burned, while burning in a more advantageous environment leads to a greater overall reduction in the number of ticks over time both in and around the area that is burned. Since the location of burns plays a crucial role in determining the effectiveness of prescribed fire, not all areas that ticks inhabit will be suitable for this method of control. In those cases, other methods of control mentioned in the introduction may be more effective over time. Lastly, Scenario 3 indicates that so long as hosts are available in an area where ticks are not yet present, ticks will spread and prescribed fire may need to be used in conjunction with other control methods for eradication to have a chance of success. It is our hope that this paper informs those that perform controlled burns in the future on how and where those burns should be executed for the purpose of tick population management.

There are several future directions that are being considered. First and foremost, incorporation of seasonality into the model that was used is crucial to ensure that our results hold when considering a more realistic situation regarding tick population dynamics. It is likely that if a burn is performed during periods of extremely low tick activity, then it would be considerably less effective; thus, timing of burns must be explored once this additional layer of complexity is added to the current model. A more subtle question in this vein is regarding the effectiveness of prescribed burns during peak activity of the different life stages of ticks. Is it more effective to perform a burn when tick nymphs are more active, or when larvae are most active, or adults? This is a very interesting question and one that has no clear answer since each life stage handles environmental changes differently. A more realistic incorporation of prescribed fire would also be beneficial in finding out the level of detail needed to best model the effects of prescribed fire. For example, [12] indicates that prescribed burning changes the microclimate in forested habitats, making it hotter and drier over time. These changes are important to consider since slight changes in temperature and humidity can be devastating to the survival rate of ticks. The changes would likely be incorporated via a microclimate function that contains all of the relevant information for calculating temperature and humidity over time and space including how these are affected by prescribed burning. Lastly, the role that location of burning may play on the effectiveness of a burn has not been explored in the current study. This is likely a key consideration particularly in the case where ticks are invading into a new area and would be worth exploring further. All these issues will be addressed in future publications.

Data Availability

All data used in this study came from published, cited sources and are included in the text. Code used in this study can be found at github: \url {https://github.com/alxjfulk/LDPF/tree/main}. MMPDElab is available at \url {http://github.com/weizhanghuang/MMPDElab}.

Conflicts of Interest

The authors declare that there are no conflicts of interest.

Acknowledgments

References

[1] R. Rosenberg, N. Lindsey, M. Fischer et al., "Vital signs: trends in reported vectorborne disease cases-United States and territories, 2004–2016," *Morbidity and Mortality Weekly Report (MMWR)*, vol. 67, no. 17, pp. 496–501, 2018.

[2] B. L. Stone, Y. Tourand, and C. A. Brissette, "Brave new worlds: the expanding universe of Lyme disease," *Vector-Borne and Zoonotic Diseases*, vol. 17, no. 9, pp. 619–629, 2017.

[3] CDC, *Signs and Symptoms of Untreated Lyme Disease*https://www.cdc.gov/lyme/signs_symptoms/index.html.

[4] H. B. Vuong, C. D. Canham, D. M. Fonseca et al., "Occurrence and transmission efficiencies of _Borrelia burgdorferi ospC_ types in avian and mammalian wildlife," *Infection, Genetics and Evolution*, vol. 27, pp. 594–600, 2014.

[5] T. Hotaling, *Prevalence of Tick-Borne Pathogens in Small Mammals and White-Tailed Deer in Southeast Nebraska*, the University of Nebraska, 2015.

[6] A. Mysterud, V. M. Stigum, H. Linlkken, A. Herland, and H. Viljugrein, "How general are generalist parasites? The small mammal part of the Lyme disease transmission cycle in two ecosystems in Northern Europe," *Oecologia*, vol. 190, no. 1, pp. 115–126, 2019.

[7] K. J. Kugeler, A. M. Schwartz, M. J. Delorey, P. S. Mead, and A. F. Hinckley, "Estimating the frequency of Lyme disease diagnoses, United States, 2010–2018," *Emerging Infectious Diseases*, vol. 27, no. 2, pp. 616–619, 2021.

[8] N. K. Madhav, J. S. Brownstein, J. I. Tsao, and D. Fish, "A dispersal model for the range expansion of blacklegged tick (Acari: Ixodidae)," *Journal of Medical Entomology*, vol. 41, no. 5, pp. 842–852, 2004.

[9] R. S. Ostfeld and J. L. Brunner, "Climate change andIxodestick-borne diseases of humans," *Philosophical Transactions of the Royal Society B: Biological Sciences*, vol. 370, no. 1665, 2015.

[10] X. Wu, V. R. Duvvuri, Y. Lou, N. H. Ogden, Y. Pelcat, and J. Wu, "Developing a temperature-driven map of the basic reproductive number of the emerging tick vector of Lyme disease _Ixodes scapularis_ in Canada," *Journal of Theoretical Biology*, vol. 319, pp. 50–61, 2013.

[11] C. Beard, "Lyme disease prevention and control – the way forward," *Canada Communicable Disease Report*, vol. 40, no. 5, pp. 91–94, 2014.

[12] E. R. Gleim, L. M. Conner, R. D. Berghaus, M. L. Levin, G. E. Zemtsova, and M. J. Yabsley, "The phenology of ticks and the effects of long-term prescribed burning on tick population dynamics in southwestern Georgia and northwestern Florida," *PLoS One*, vol. 9, no. 11, article e112174, 2014.

[13] A. L. Hoch, P. J. Semtner, R. W. Barker, and J. A. Hair, "Preliminary observations on controlled burning for lone star tick (Acarina: Ixodidae) control in Woodlots1," *Journal of Medical Entomology*, vol. 9, no. 5, pp. 446–451, 1972.

[14] M. L. Drew, W. M. Samuel, G. M. Lukiwski, and J. N. Willman, "An evaluation of burning for control of winter ticks, Dermacentor albipictus, in Central Alberta," *Journal of Wildlife Diseases*, vol. 21, no. 3, pp. 313–315, 1985.

[15] W. R. Davidson, D. A. Siefken, and L. H. Creekmore, "Influence of annual and biennial prescribed burning during March on the abundance of Amblyomma americanum (Acari: Ixodidae) in Central Georgia," *Journal of Medical Entomology*, vol. 31, no. 1, pp. 72–81, 1994.

[16] D. Willis, R. Carter, C. Murdock, and B. Blair, "Relationship between habitat type, fire frequency, andAmblyomma americanumpopulations in East-Central Alabama," *Journal of Vector Ecology*, vol. 37, no. 2, pp. 373–381, 2012.

[17] J. K. Bailey and T. G. Whitham, "Interactions among fire, aspen, and elk affect insect diversity: reversal of a community response," *Ecology*, vol. 83, no. 6, pp. 1701–1712, 2002.

[18] L. K. Kirkman, R. J. Mitchell, R. C. Helton, and M. B. Drew, "Productivity and species richness across an environmental gradient in a fire-dependent ecosystem," *American Journal of Botany*, vol. 88, no. 11, pp. 2119–2128, 2001.

[19] H. A. Jacobson and G. A. Hurst, "Prevalence of parasitism by Amblyomma americanum on wild Turkey poults as influenced by prescribed burning," *Journal of Wildlife Diseases*, vol. 15, no. 1, pp. 43–47, 1979.

[20] J. Cully Jr., "Lone star tick abundance, fire, and bison grazing in Tallgrass prairie," *Journal of Range Management*, vol. 52, no. 2, pp. 139–144, 1999.

[21] V. Polito, K. Baum, M. Payton, S. Little, S. Fuhlendorf, and M. Reichard, "Tick abundance and levels of infestation on cattle in response to patch burning," *Rangeland Ecology & Management*, vol. 66, no. 5, pp. 545–552, 2013.

[22] H. Frater, *Impact of Prescribed Burning for Oak Regeneration on Forest Vegetation, White-Footed Mouse Populations, and Lyme Disease*, MS Thesis, Iowa State University, 2011.

[23] E. R. Gleim, G. E. Zemtsova, R. D. Berghaus, M. L. Levin, M. Conner, and M. J. Yabsley, "Frequent prescribed fires can reduce risk of tick-borne diseases," *Scientific Reports*, vol. 9, no. 1, p. 9974, 2019.

[24] K. C. Stafford III, J. S. Ward, and L. A. Magnarelli, "Impact of controlled burns on the abundance of Ixodes scapularis (Acari: Ixodidae)," *Journal of Medical Entomology*, vol. 35, no. 4, pp. 510–513, 1998.

[25] K. A. Padgett, L. E. Casher, S. L. Stephens, and R. S. Lane, "Effect of prescribed fire for tick control in California chaparral," *Journal of Medical Entomology*, vol. 46, no. 5, pp. 1138–1145, 2009.

[26] J. E. Cilek and M. A. Olson, "Seasonal distribution and abundance of ticks (Acari: Ixodidae) in northwestern Florida," *Journal of Medical Entomology*, vol. 37, no. 3, pp. 439–444, 2000.

[27] T. N. Mather, D. C. Duffy, and S. R. Campbell, "An unexpected result from burning vegetation to reduce Lyme disease transmission risks," *Journal of Medical Entomology*, vol. 30, no. 3, pp. 642–645, 1993.

[28] A. Fulk, W. Huang, and F. B. Agusto, *Exploring the Effects of Prescribed Fire on Ticks Spread and Propagation in a Spatial Setting*, 2022, https://www.medrxiv.org/content/10.1101/2022.01.12.22268825v1.

[29] E. Guo and F. B. Agusto, *Baptism of Fire: Modeling the Effects of Prescribed Fire on Tick-Borne Disease*, 2021.

[30] Y. Lou, L. Liu, and D. Gao, "Modeling co-infection of Ixodes tick-borne pathogens," *Mathematical Biosciences and Engineering (MBE)*, vol. 14, no. 5/6, pp. 1301–1316, 2017.

[31] R. Llera and E. Ward, *Ticks in Dogs*VCA animal hospitalhttps://vcahospitals.com/know-your-pet/ticks-in-dogs.

[32] D. Hauck, D. Jordan, A. Springer et al., "Transovarial transmission of borrelia spp., rickettsia spp. and anaplasma phagocytophilum in ixodes ricinus under field conditions extrapolated from DNA detection in questing larvae," *BMC Parasites Vectors*, vol. 13, no. 1, 2020.

[33] L. Rollend, D. Fish, and J. E. Childs, "Transovarial transmission of _Borrelia_ spirochetes by _Ixodes scapularis: a summary of the literature and recent observations," *Ticks and Tick-borne Diseases*, vol. 4, no. 1-2, pp. 46–51, 2013.

[34] T. Caraco, S. Glavanakov, G. Chen, J. E. Flaherty, T. K. Ohsumi, and B. K. Szymanski, "Stage-structured infection transmission and a spatial epidemic: a model for Lyme disease," *The American Naturalist*, vol. 160, no. 3, pp. 348–359, 2002.

[35] E. E. Holmes, M. A. Lewis, J. E. Banks, and R. R. Veit, "Partial differential equations in ecology: spatial interactions and population dynamics," *America*, vol. 75, no. 1, pp. 17–29, 1994.

[36] *Blacklegged Tick or Deer Tick*Cooperative Extension: Tick Lab, University of Mainehttps://extension.umaine.edu/ticks/maine-ticks/deer-tick-or-black-legged-tick/.

[37] T. Levi, A. M. Kilpatrick, M. Mangel, and C. C. Wilmers, "Deer, predators, and the emergence of Lyme disease," *Proceedings of the National Academy of Sciences of the United States of America*, vol. 109, no. 27, pp. 10942–10947, 2012.

[38] M. E. Gilliam, W. T. Rechkemmer, K. W. McCravy, and S. E. Jenkins, "The influence of prescribed fire, habitat, and weather on amblyomma americanum (ixodida: Ixodidae) in West-Central Illinois, USA," *Insects*, vol. 9, no. 2, p. 36, 2018.

[39] K. M. Clow, P. A. Leighton, N. H. Ogden et al., "Northward range expansion of ixodes scapularis evident over a short timescale in Ontario, Canada," *PLoS One*, vol. 12, no. 12, article e0189393, 2017.

[40] W. Huang, "An introduction to MMPDElab," 2019, arXiv:1904.05535.

[41] C. Johnson, *Numerical Solution of Partial Differential Equations by the Finite Element Method*, Cambridge University Press, 1987.

[42] E. Hairer and G. Wanner, *Solving Ordinary Differential Equations II: Stiff and Differential-Algebraic Problems*, Springer, 2010.

[43] S. Marino, I. B. Hogue, C. J. Ray, and D. E. Kirschner, "A methodology for performing global uncertainty and sensitivity analysis in systems biology," *Journal of Theoretical Biology*, vol. 254, no. 1, pp. 178–196, 2008.

[44] J. Kane, *Prescribed Fire Definition, History, & Benefits*Britannicahhttps://www.britannica.com/science/prescribed-fire.

Research Article

Global Stability Analysis and Parameter Estimation for a Diphtheria Model: A Case Study of an Epidemic in Rohingya Refugee Camp in Bangladesh

Zahurul Islam [iD],[1] **Shohel Ahmed** [iD],[1] **M. M. Rahman** [iD],[1] **M. F. Karim** [iD],[2] and **M. R. Amin** [iD][2]

[1]*Department of Mathematics, Bangladesh University of Engineering and Technology, Dhaka 1000, Bangladesh*
[2]*Department of Mathematical and Physical Sciences, East West University, Dhaka, Bangladesh*

Correspondence should be addressed to M. M. Rahman; mmustafizurrahman@math.buet.ac.bd

In this article, we have developed a deterministic Susceptible-Latent-Infectious-Recovered (SLIR) model for diphtheria outbreaks. Here, we have studied a case of the diphtheria outbreak in the Rohingya refugee camp in Bangladesh to trace the disease dynamics and find out the peak value of the infection. Both analytical and numerical investigations have been performed on the model to find several remarkable behaviors like the positive and bounded solution, basic reproductive ratio, and equilibria such as disease extinction equilibrium and disease persistence equilibrium which are characterized depending on the basic reproductive ratio and global stability of the model using Lyapunov function for both equilibria. Parameter estimation has been performed to determine the values of the parameter from the daily case data using numerical technique and determined the value of the basic reproductive number for the outbreak as $\mathcal{R}_0 = 5.86$.

1. Introduction

Diphtheria is a rapidly spreading disease which is generated by *Corynebacterium diphtheriae*. Diphtheria transmits in the populations, usually through respiratory droplets, like coughing or sneezing [1, 2]. When the bacteria release the poison or toxin into the body, then the actual disease appears. Fever and throat bruises are the initial symptoms of diphtheria. Besides, a thick grey layer induces the "croup," which can block the airway and cause a barking cough. Anyone can be infected by diphtheria, but 5-7-aged children who did not receive the appropriate vaccine are usually infected [3–6]. During 1990-1995, above cases 140,000 and 4000 mortalities have been recorded worldwide through the Regional Office of World Health Organization (WHO) for Europe [7–9]. Nowadays, diphtheria is a rare outbreak in the developed world. However, in 2017, several diphtheria outbreaks occurred in Yemen and refugee camps in Bangladesh [10, 11]. In the Rohingya refugee camp in Cox's Bazar, Bangladesh, a massive-scale diphtheria pestilence was reported. Until December

26, 2017, there were an aggregate number of 2,526 cases and 27 mortalities [12]. There are diphtheria antitoxins in diphtheria treatments to stop poisons from the bacteria and antitoxins to kill the bacteria. The best way to repel diphtheria is through vaccinations [3, 4, 13]. The three shots of the diphtheria-tetanus-pertussis (DTP) vaccine were applied in massive levels to children to control the diphtheria outbreak. To break the transmission chains of the diphtheria outbreak in the Rohingya refugee camp in Bangladesh, emergency vaccination has been applied to children since December 12, 2017, and at the end of 2017, above 90% overall coverage [12].

Many researchers have studied epidemic or pandemic disease using mathematical techniques such as Wu and Zhao [14] who have mathematically analyzed an age-structured epidemic model of HIV/AIDS with HAART and spatial diffusion. In a discrete-time SIVS model with saturation incidence rate, Parsamanesh and Erfanian [15] investigated the stability and bifurcations. To examine the impact of an environmental toxin on the spread of infectious illnesses in the population, Saha and Samanta [16] used a toxin-dependent

dynamical model. In a discrete time epidemic model including vaccination and vital dynamics, Parsamanesh et al. [17] investigated the stability and bifurcations. Kabir et al. [18] have analyzed the effect of border enforcement measures and socioeconomic cost in export-importation epidemic dynamics using game theory. In a random environment, Samanta and Bera [19] looked at a dynamical model of Chlamydia illness with changing total population size, bilinear incidence rate, and pulse vaccination approach. Parsamanesh and Erfanian [20] looked at the global dynamics of a model with a standard incidence rate and immunization approach. Shahrear et al. [21] have predicted and mathematically analyzed the COVID-19 outbreak in Bangladeshi scenario, and Maugeri et al. [22] have analyzed the transmission of the COVID-19 pandemic in Saudi Arabia and Indonesia. By eliciting behavioural reactions in the community, Saha et al. [23] explored an epidemic model of the COVID-19 outbreak. Liu and Zhang [24] have analyzed global stability for a tuberculosis model. Gao and Huang [25] have investigated a tuberculosis model with optimal control.

Some of the researchers have also analyzed the diphtheria epidemic, such as Vitek and Wharton [26] who have studied the potential of the reemergence of diphtheria and other vaccine-preventable infections. Zakikhany and Efstratiou [27] analyzed the current problems and new challenges of diphtheria in Europe. Torrea et al. [28] have studied the diphtheria outbreak with the SIRM model. Ilahi and Widiana [29] have developed an SEIR model for the diphtheria outbreak and analyze vaccination's effectiveness against the outbreak. Matsuyama et al. [30] have analyzed the sensitivity and ambiguity based on the basic reproductive ratio $\mathscr{R}_0$ of the diphtheria epidemic in the Rohingya refugee camp in Bangladesh.

Due to the vulnerability of diphtheria epidemics in a confined area, we propose a controlled Susceptible-Latent-Infectious-Recovered (SLIR) model, which is an extension of the simple Susceptible-Infectious-Recovered (SIR) model by adjoining a compartment (L) that tracks the latent people in the cohort. Analytical analysis of the proposed model is performed to prove the existence, uniqueness, positivity, and bounds of the solution. Equilibria of the system and the basic reproductive ratio are also evaluated, and the global stability of the model is proven depending on the basic reproductive ratio. To illustrate the disease dynamics, parameter values are estimated from the daily case data of the outbreak in the Rohingya refugee camp in Bangladesh and found to be the equilibria of the system.

2. Mathematical Model

In this section, a mathematical model [31] is developed for the expanse of diphtheria into the populations, which is shown diagrammatically in Figure 1. The entire population at time t is indicated by $N(t)$ that is partitioned into four groups: susceptible $(S(t))$, latent (asymptotic) stage $(L(t))$, individual affected by diphtheria in the acutely infected stage $(I(t))$, and recovered individuals affected by diphtheria $(R(t))$; here, we suppose that the recovered people are not fur-
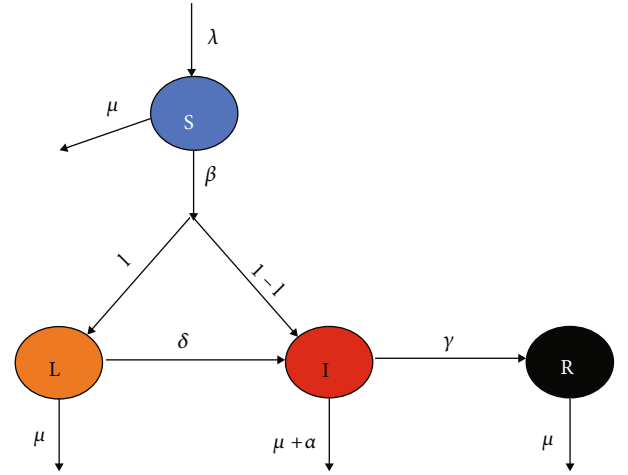

Figure 1: Diagram interaction of each compartment.

ther contagious. Here, λ is a constant that signifies all recruitment that enters the susceptible class, and μ is the natural mortality rate that leaves all classes. The infectious state has an extra mortality rate due to diseases by α, and δ is that rate in which latent infection in people becomes an acute infection. Thus, the people move to state I from state L at a rate of δL. Infectious people are successfully treated with a fixed rate γ, listing to the recovered state. Susceptible people acquire diphtheria infection among active diphtheria at rate βSI, where β signifies the infection transmission coefficient. Moreover, l signifies a fraction of susceptible people that earn diphtheria infection and migrate to the latent diphtheria state(L), at rate$l\beta SI$, and the residual portion,$(1 - l)$, departs to the active diphtheria state(I). Here, the individuals of the latent class are assumed not to transmit infection.

Assembling all the aforenamed suppositions, the model concerning the transmission dynamics of diphtheria is presented by the subsequent system of differential equations:

$$
\begin{cases}
\dfrac{dS(t)}{dt} = \lambda - \beta S(t)I(t) - \mu S(t), \\[2mm]
\dfrac{dL(t)}{dt} = l\beta S(t)I(t) - (\mu + \delta)L(t), \\[2mm]
\dfrac{dI(t)}{dt} = (1 - l)\beta S(t)I(t) + \delta L(t) - (\mu + \gamma + \alpha)I(t), \\[2mm]
\dfrac{dR(t)}{dt} = \gamma I(t) - \mu R(t), \\[2mm]
N(t) = S(t) + L(t) + I(t) + R(t),
\end{cases}
\tag{1}
$$

with following subsidiary conditions:

$$
S(0) = S_0 > 0, \tag{2}
$$

$$
L(0) = L_0 \geq 0, \tag{3}
$$

$$
I(0) = I_0 \geq 0, \tag{4}
$$

TABLE 1: Description and value of the parameters of the diphtheria model.

| Parameter	Description	Value	Source
λ	The recruitment of susceptible class	200 persons day^{-1}	Estimated
μ	Natural mortality rate	0.002 day^{-1}	Estimated
α	Disease induced mortality rate	0.0054 day^{-1}	Estimated
β	Disease transmission rate	0.000097 persons^{-1} day^{-1}	Fitted
l	The fraction of $S(t)$ which moves to $L(t)$	0.95	Estimated
γ	Recovered rate	0.156 day^{-1}	Fitted
δ	The rate which leaves $L(t)$ for $I(t)$	0.143 day^{-1}	Estimated

(a)

(b)

(c)
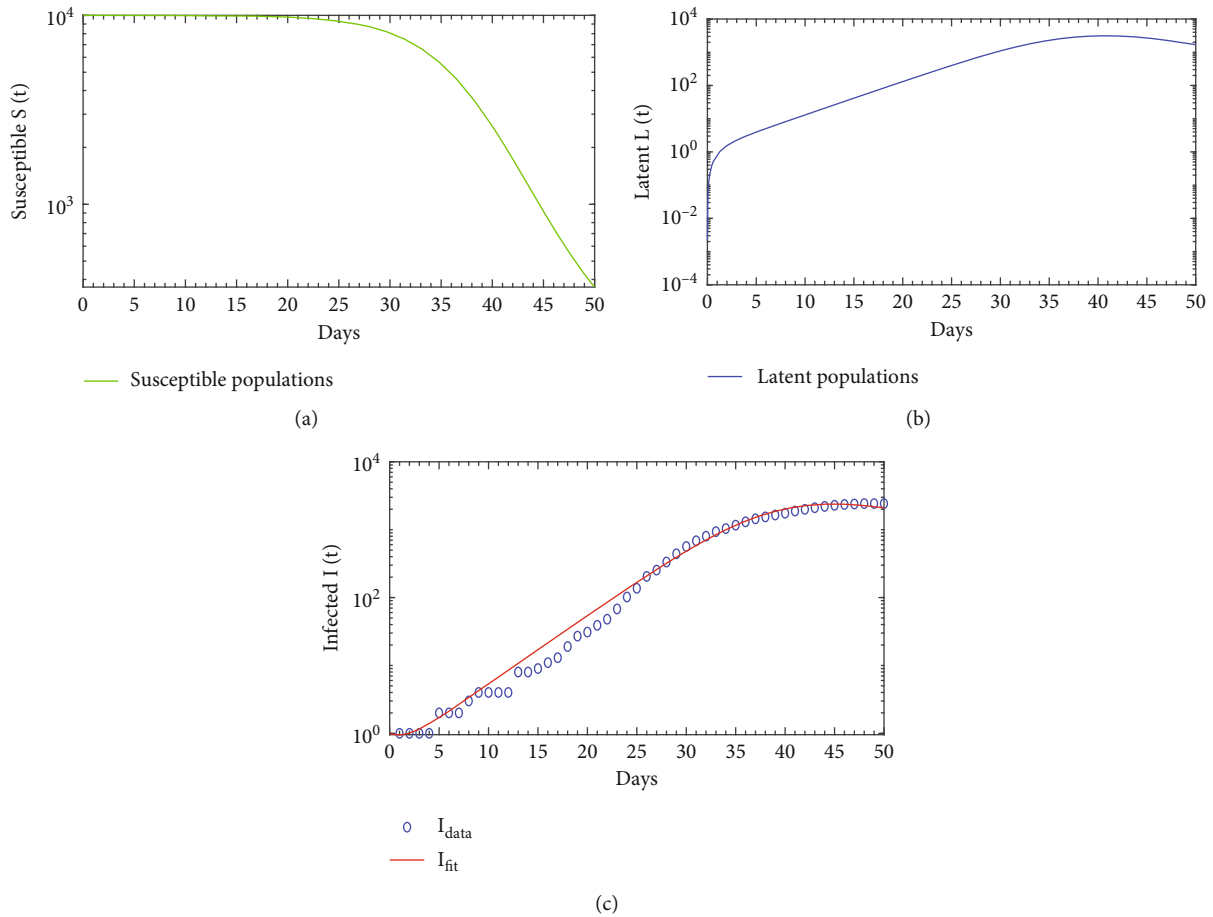
FIGURE 2: The diphtheria model (1) simulation in log scale.

$$R(0) = R_0 \geq 0. \qquad (5)$$

3. Some Basic Characteristic of the Model

To retain the model's biological efficacy, we want to show the existence, positivity, and boundedness of the solutions to the differential equations for all time.

Theorem 1 (existence of unique solution). *Suppose that* S_0, $L_0, I_0, R_0 \in \mathbb{R}$. *Then, there exists continuous differentiable*

functions $\{S, ,L, I, R : [0, t_0) \longrightarrow \mathbb{R}\}$ *for positive time* $(t_0 > 0$ *) such that the 4-tuple* (S, L, I, R) *covers (1) and* $(S, L, I, R)($ $0) = (S_0, L_0, I_0, R_0)$.

Proof of Theorem 1. By Picard-Lindelöf theorem, it is narrated that the initial value problem $\mathbf{y}'(t) = \mathbf{g}(\mathbf{y}(t)), \mathbf{y}(t_0) = \mathbf{y}_0$ has a unique solution $\mathbf{y}(t)$ for locally Lipschitz and continuous function $\mathbf{g}$ in time $t \in [t_0 - \epsilon, t_0 + \epsilon]$, where $\epsilon > 0$. As the system (1) is autonomous, it is enough to prove that the function $\mathbf{g} : \mathbb{R}^4 \longrightarrow \mathbb{R}^4$ is locally Lipschitz in $\mathbf{y}$. Here, $\mathbf{g}$ is
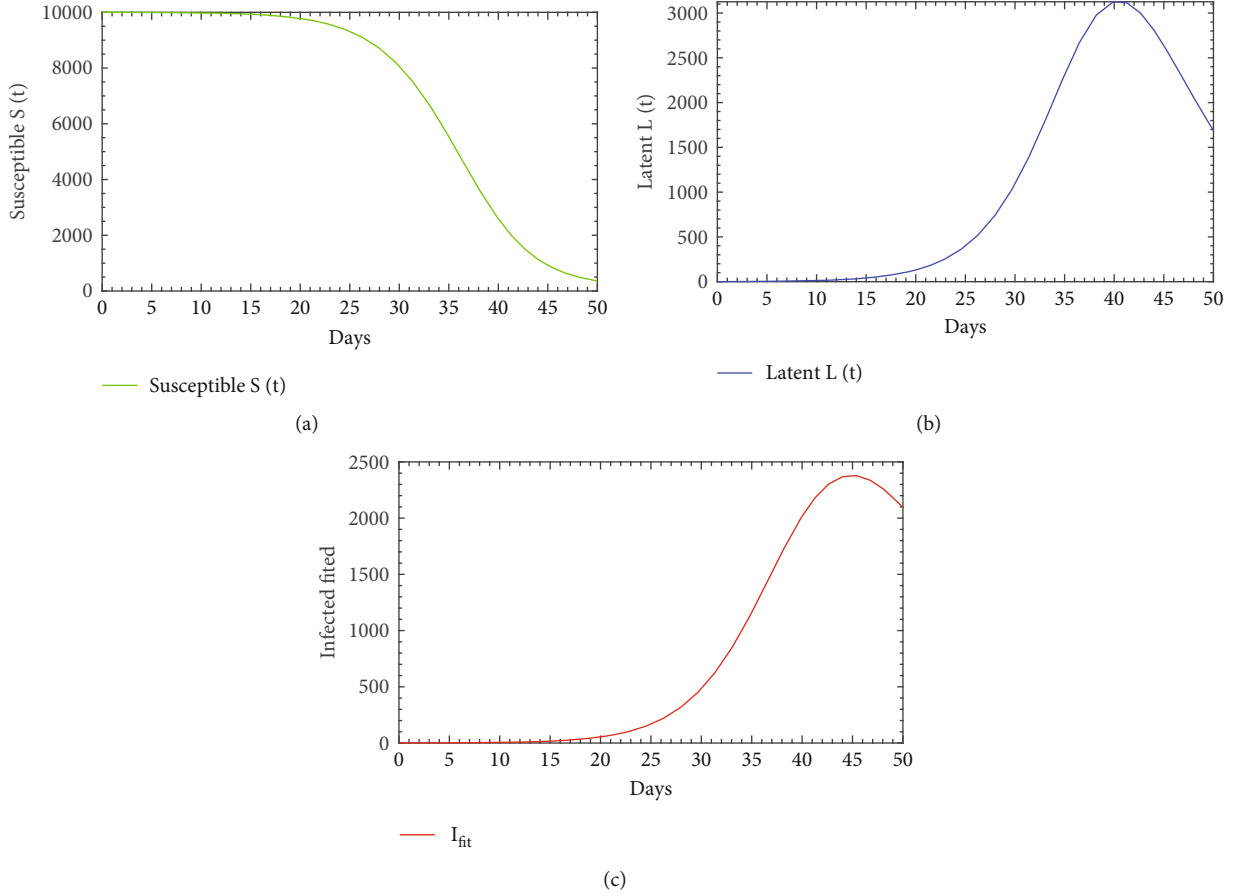
(a)

(b)

(c)

FIGURE 3: The fitted diphtheria model (1).

defined as

$$
\mathbf{g}(\mathbf{y}) = \begin{pmatrix} \lambda - \beta SI - \mu S \\ l\beta SI - (\mu + \delta)L \\ (1-l)\beta SI + \delta L - (\mu + \gamma + \alpha)I \\ \gamma I - \mu R \end{pmatrix}. \tag{6}
$$

The Jacobian matrix of $\mathbf{g}$ is obtained as

$$
\nabla \mathbf{g}(\mathbf{y}) = \begin{pmatrix} -\beta I - \mu & 0 & -\beta S & 0 \\ l\beta I & -(\mu + \delta) & l\beta S & 0 \\ (1-l)\beta I & \delta & (1-l)\beta S - (\mu + \gamma + \alpha) & 0 \\ 0 & 0 & \gamma & -\mu \end{pmatrix}. \tag{7}
$$

This Jacobian is linear in $\mathbb{R}^4$. Thus, $\nabla \mathbf{g}(\mathbf{y})$ satisfies the continuity and differentiability for an interval $I \in \mathbb{R}^4$. According to the mean value theorem,

$$
\frac{|\mathbf{g}(\mathbf{y_1}) - \mathbf{g}(\mathbf{y_2})|}{|\mathbf{y_1} - \mathbf{y_2}|} \le |\nabla \mathbf{g}(\mathbf{y}^*)|, \tag{8}
$$

where $\mathbf{y}^* \in I_1$. By assuming $|\nabla \mathbf{g}(\mathbf{y}^*)| = M$, we obtain $|\mathbf{g}(\mathbf{y_1}) - \mathbf{g}(\mathbf{y_2})| \le M|\mathbf{y_1} - \mathbf{y_2}|$ for $\mathbf{y_1}, \mathbf{y_2} \in I_1$ and thus, $\mathbf{g}(\mathbf{y})$ is bounded locally for each $\mathbf{y} \in \mathbb{R}^4$. Therefore, for all compact subset of $\mathbb{R}^4$, the derivative of $\mathbf{g}$ is continuous and bounded and thus, $\mathbf{g}$ is locally Lipschitz. Hence, according to the Picard-Lindelöf theorem, the initial value problem $y'(t) = g(y(t)), y(0) = y_0$ for $t_0 > 0$ has a unique solution $y(t)$. □

Theorem 2. *The proposed model (1) is invariant in the non-negative orthant $\mathbb{R}_+^4$.*

Proof. Let $Y = (S, L, I, R)^T$; then, model (1) will take the form

$$
\frac{dY(t)}{dt} = LY + C, \tag{9}
$$

where

$$
L = \begin{pmatrix} -(\beta I(t) + \mu) & 0 & 0 & 0 \\ l\beta I(t) & -(\mu + \delta) & 0 & 0 \\ (1-l)\beta I(t) & \delta & -(\mu + \gamma + \alpha) & 0 \\ 0 & 0 & \gamma & -\mu \end{pmatrix}, \tag{10}
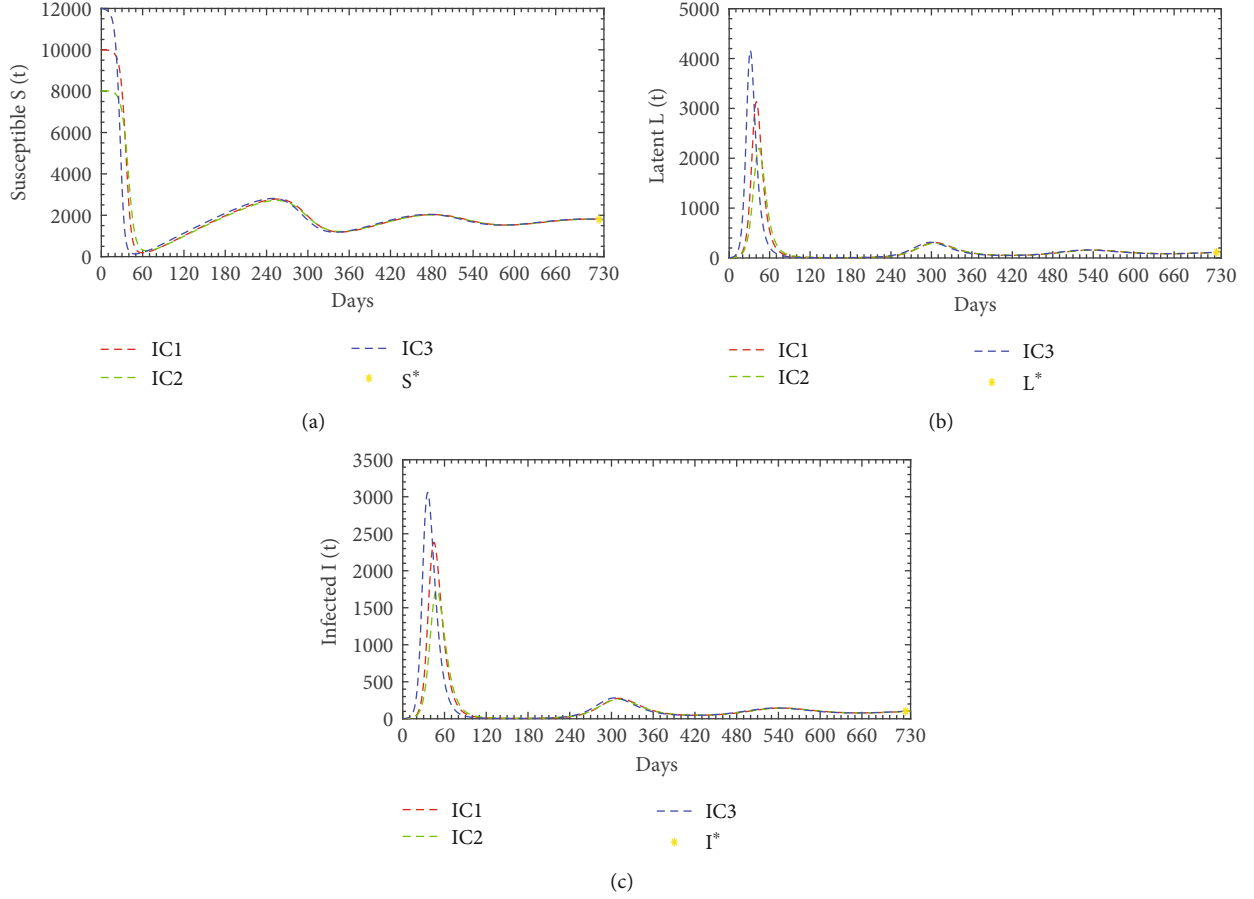$$

FIGURE 4: Population dynamics interaction between $S(t)$, $L(t)$, and $I(t)$ of diphtheria model (1) when $\mathcal{R}_0 = 5.86 > 1$ for different initial conditions.

and

$$C = \begin{pmatrix} \lambda \\ 0 \\ 0 \\ 0 \end{pmatrix}. \tag{11}$$

Here, $C \geq 0$ and in matrix L, all off-diagonal elements are greater than or equal zero. Hence, L is a Metzler matrix and the system (1) is positive invariant in $\mathbb{R}_+^4$ [32]. □

Theorem 3. *For $t > 0$, any solution (S, L, I, R) of the model (1) with condition (2) is positive.*

Proof. The R.H.S. of the model (1) is differentiable; therefore, connecting it with Cauchy problem covenants that there exists a unique maximal solution. The solution of the first equation of system (1) can be figured out alternatively as

$$\frac{dS(t)}{dt} + (\beta I(t) + \mu)S(t) = \lambda. \tag{12}$$

The solution of Equation (12) is

$$S(t) = S_0 e^{\left\{-\left(\mu t + \int_0^t \beta I(x)dx\right)\right\}} + e^{\left\{-\left(\mu t + \int_0^t \beta I(x)dx\right)\right\}} \times \int_0^t \lambda e^{\left\{\mu y + \int_0^t \beta I(u)du\right\}} dy, \tag{13}$$

for all $t > 0$. Hence, the R.H.S. of Equation (13) is greater than or equal to zero, i.e., $S(t) > 0$ for all $t > 0$. In the same way, the solution of the second, third, and fourth equations of model (1) is of the form

$$L(t) = L_0 e^{\{-(\mu+\delta)t\}} + e^{\{-(\mu+\delta)t\}} \times \int_0^t l\beta S(y)I(y) e^{\{(\mu+\delta)y\}} dy,$$

$$I(t) = I_0 e^{\left\{-\left((\mu+\gamma+\alpha)t - \int_0^t (1-l)\beta S(x)dx\right)\right\}} + e^{\left\{-\left((\mu+\gamma+\alpha)t - \int_0^t (1-l)\beta S(x)dx\right)\right\}} \times \int_0^t \delta L(y) e^{\left\{(\mu+\gamma+\alpha)y - \int_0^t (1-l)\beta S(u)du\right\}} dy,$$

$$R(t) = R_0 e^{\{-\mu t\}} + e^{\{-\mu t\}} \times \int_0^t \gamma I(y) e^{\{\mu y\}} dy, \tag{14}$$

(a)

(b)

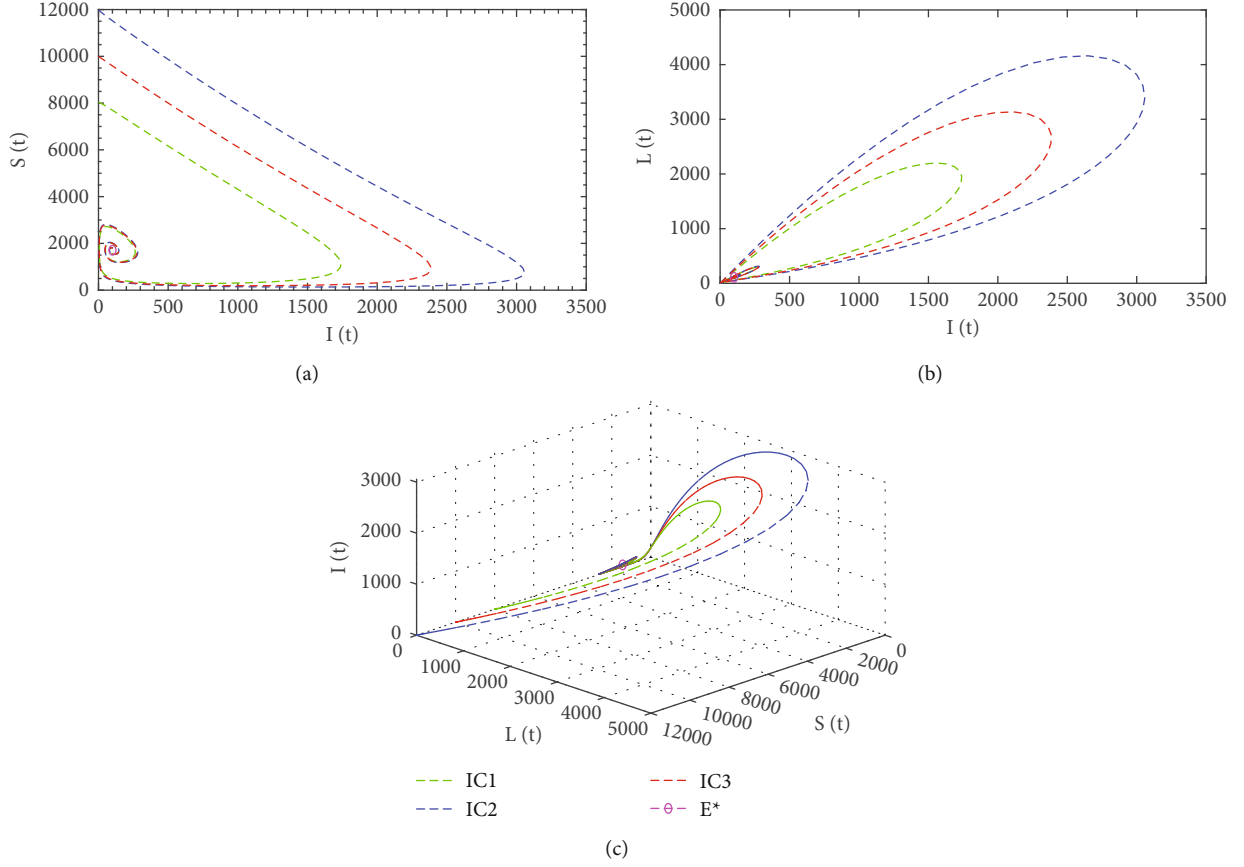--- IC1   --- IC3

--- IC2   -⊖- E*

(c)

FIGURE 5: System's phase portrait of diphtheria model (1) in 2D and 3D when $\mathscr{R}_0 = 5.86 > 1$ for different initial conditions.

respectively. Those solutions show that all $L(t), I(t)$, and $R(t)$ are greater than or equal zero $\forall t > 0$. □

Theorem 4 (boundedness). *Suppose the model (1) satisfies $S_0 > 0, L_0 > 0, I_0 > 0$, and $R_0 > 0$ and has a unique solution on $[0, t_0]$ for some $t_0 > 0$ by Theorem 1; then, the state functions $S(t), L(t), I(t)$, and $R(t)$ will be bounded and be positive $\forall t \in [0, t_0]$.*

Proof. Initially, suppose that the values of $S(t), L(t), I(t)$, and $R(t)$ are positive. From Theorem 1, for $t > 0$, there exists a solution on $[0, t]$. Now, denote the largest time by $\mathscr{T}^*$ at which all the populations are positive, or

$$\mathscr{T}^* = \sup \{t > 0 : S(s), L(s), I(s), R(s) > 0, \quad \forall s \in [0, t]\}. \tag{15}$$

Since all initial conditions are nonnegative and the solutions are continuous, hence, the solutions must be positive on an interval which is denoted as $\mathscr{T}^* > 0$. Therefore, we calculate each term on $[0, \mathscr{T}^*]$: instantly, the lower bounds on L, I, and R can be placed.

$$\frac{dL(t)}{dt} = l\beta S(t)I(t) - (\mu + \delta)L(t) \geq -(\mu + \delta)L(t), \tag{16}$$

as the reduction expressions are linear; this achieves

$$\frac{dL(t)}{L(t)} \geq -(\mu + \delta)dt, \tag{17}$$

or

$$\ln (L(t)) + \ln C \geq -(\mu + \delta)t, \tag{18}$$

or

$$L(t) \geq Ce^{-(\mu + \delta)t}. \tag{19}$$

Applying initial condition, we get

$$\begin{aligned} L(0) &\geq C, \\ \Rightarrow L(t) &\geq L(0)e^{-(\mu + \delta)t} > 0, \end{aligned} \tag{20}$$

for $t \in [0, \mathscr{T}^*]$.

Again,

$$\frac{dI(t)}{dt} = (1 - l)\beta S(t)I(t) + \delta L(t) - (\mu + \gamma + \alpha)I(t) \geq -(\mu + \gamma + \alpha)I(t), \tag{21}$$
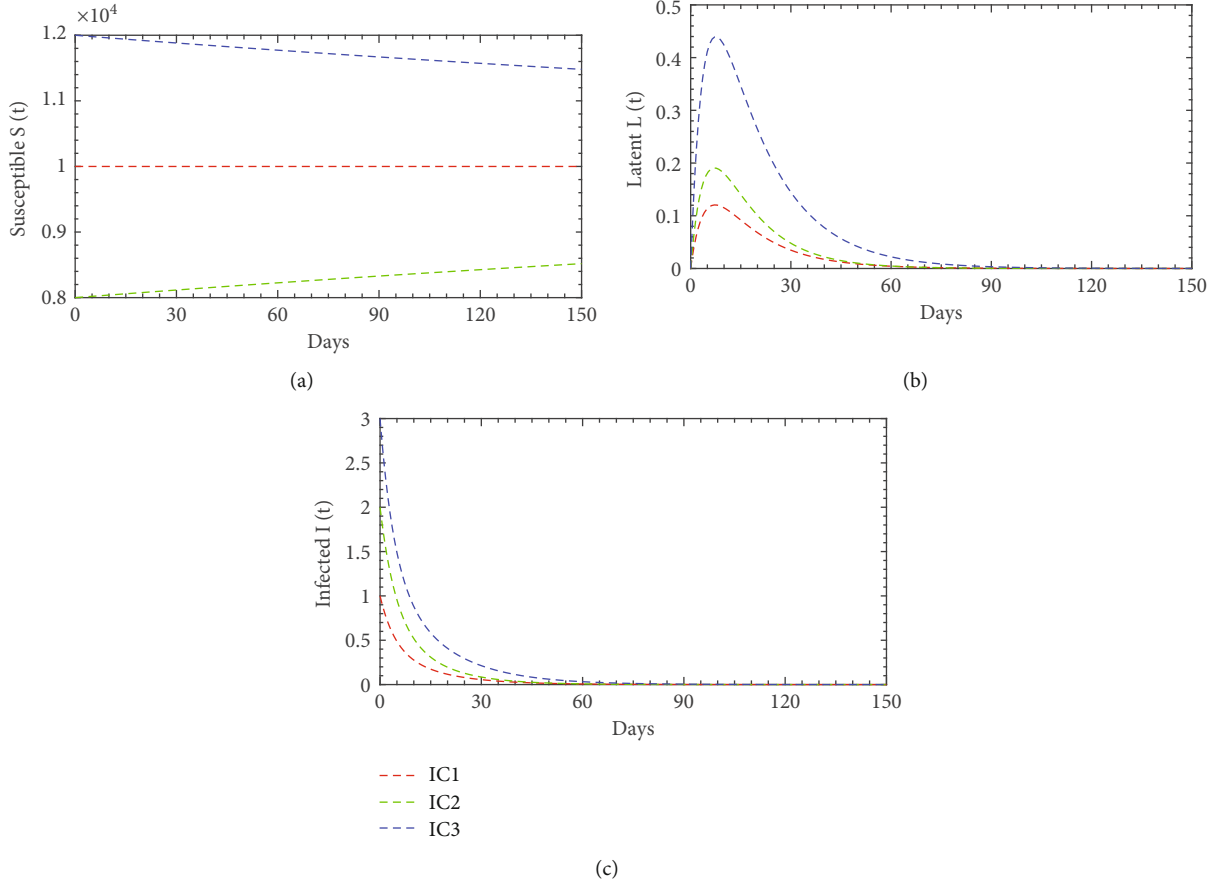
(c)

FIGURE 6: Population dynamics interaction between $S(t)$, $L(t)$, and $I(t)$ of diphtheria model (1) when $\mathcal{R}_0 = 0.302 < 1$ for different initial conditions.

as the reduction expressions are linear; this achieves

$$I(t) \geq I(0)e^{-(\mu+\gamma+\alpha)t} > 0, \tag{22}$$
$$\forall t \in [0, \mathcal{T}^*].$$

Further,

$$\frac{dR(t)}{dt} = \gamma I(t) - \mu R(t) \geq -\mu R(t), \tag{23}$$

i.e.,

$$R(t) \geq R(0)e^{-\mu t} > 0, \tag{24}$$
$$\forall t \in [0, \mathcal{T}^*].$$

Similarly, by placing the upper bound on dS/dt, we get

$$\frac{dS(t)}{dt} = \lambda - \beta S(t)I(t) - \mu S(t) \leq \lambda, \tag{25}$$

i.e.,

$$S(t) \leq S(0) + \lambda t \leq C(1 + t), \tag{26}$$

where C is an arbitrary constant which is depending on the

upper bound of $S(0)$ and λ. Now, by adding the equations for L, I, and R and placing the bounds on this sum and by the positivity of these functions, for the upper bound of $S(t)$, we get

$$\frac{d}{dt}(L + I + R) = \beta S(t)I(t) - \mu L(t) - (\mu + \alpha)I(t) - \mu R(t)$$
$$\leq \beta C(1 + t)I(t) + \mu L(t) + (\mu + \alpha)I(t) + \mu R(t)$$
$$\leq C_1(1 + t)(L + I + R), \tag{27}$$

where $C_1 \geq \max\{\beta C, \mu, (\mu + \alpha)\}$, i.e.,

$$(L + I + R)(t) \leq C_2 e^{t^2}, \tag{28}$$

where the constant $C_2 > 0$ for $t \in [0, \mathcal{T}^*]$ that only depends on $L(0), I(0), R(0)$, and C_1. For the positivity of $L(t), I(t)$, and $R(t)$ are positive, an upper bound can be placed on both L, I, and R by

$$C_2 e^{t^2} \geq (L + I + R)(t) \geq L(t),$$
$$C_2 e^{t^2} \geq (L + I + R)(t) \geq I(t), \tag{29}$$
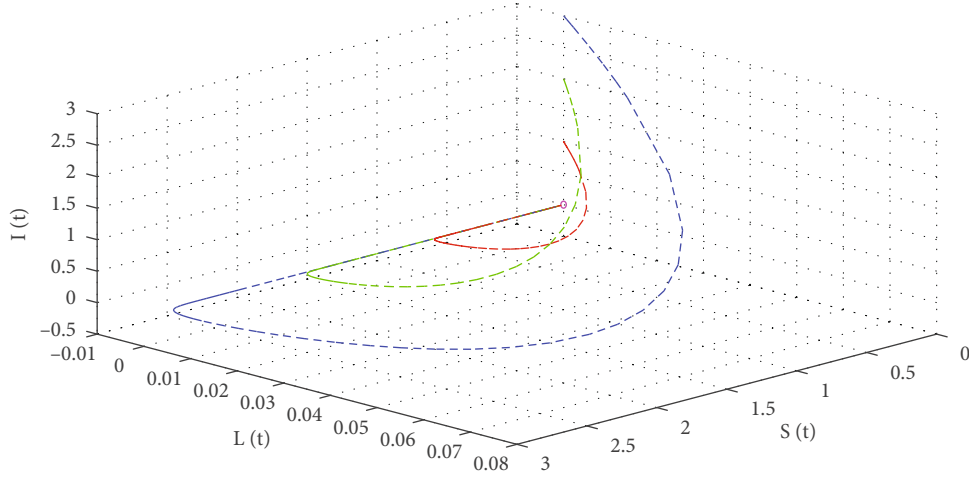$$C_2 e^{t^2} \geq (L + I + R)(t) \geq R(t).$$

FIGURE 7: System's phase of diphtheria model (1) in 3D when $\mathscr{R}_0 = 0.302 < 1$ for different initial conditions.

Now, $S(t)$ can be bounded from below using

$$\frac{dS}{dt} = \lambda - \beta SI - \mu S \geq -\beta SI - \mu S \geq -\mu S - \beta C_2 e^{t^2} S, \geq -C_3\left(1 + e^{t^2}\right)S,$$
(30)

where $C_3 \geq \max\{\beta C_2, \mu\}, \Rightarrow (dS/dt) + C_3(1 + e^{t^2})S \geq 0$, i.e.,

$$S(t) \geq S(0)e^{-C_3\int_0^t \left(1+e^{\kappa^2} d\kappa\right)} > 0.$$
(31)

Therefore, S, L, I, and R remain rigorously positive $\forall t \in [0, \mathscr{T}^*]$. Hence, there exists a $t > \mathscr{T}^*$ for the continuity, at which the state variables $S(t), L(t), I(t)$, and $R(t)$ are still positive, which contradicts with the definition of $\mathscr{T}^*$ and specifies that $S(t), L(t), I(t)$, and $R(t)$ are rigorously positive on the whole interval $[0, t]$. Moreover, all functions remain bounded with this interval; thus, the existing interval can be further extended. Actually, the bounds on S, L, I, and R obtained earlier exist on each compact time interval. For the extension of the time interval to $[0, t]\forall t > 0$ at which the solution endures and of the above discussion, the solutions continue both positive and bounded on $[0, t]$. □

4. Equilibria of the System

In this section, we trace the presence of steady states for the dynamical system of nonlinear ODEs (1), describing the Diphtheria disease dynamics. These steady states can be obtained by placing the R.H.S. of (1) to zero; we obtain

$$\lambda - \beta SI - \mu S = 0,$$
(32)

$$l\beta SI - (\mu + \delta)L = 0,$$
(33)

$$(1 - l)\beta SI + \delta L - (\mu + \gamma + \alpha)I = 0,$$
(34)

$$\gamma I - \mu R = 0.$$
(35)

Moreover, by solving the above equations, we have found two biologically meaningful equilibrium points. We

can classify these two points to be while the infection is either terminated from populations, i.e., $L = I = R = 0$, or insists in the populations $(L \neq 0, I \neq 0, R \neq 0)$ as t grows large.

We start to determine the equilibria from the nonlinear intercommunicated terms into Equations (33), (34), and (35) that give

$$I((1 - l)(\mu + \delta)\beta S + \delta l\beta S - (\mu + \delta)(\mu + \gamma + \alpha)) = 0.$$
(36)

Thus, either $I = 0$ or $S = (\mu + \delta)(\mu + \gamma + \alpha)/((1 - l)\mu + \delta)\beta$. Using $I = 0$ in Equations (33), (34), and (35), we get the disease extinction equilibrium point as

$$E^0 = (S^0, L^0, I^0, R^0) = \left(\frac{\lambda}{\mu}, 0, 0, 0\right).$$
(37)

By setting $S = (\mu + \delta)(\mu + \gamma + \alpha)/((1 - l)\mu + \delta)\beta$ into Equations (32) and (35) yields the infectious persistence equilibrium that exists at the point

$$E^* = (S, L, I, R) = \left(\frac{(\mu + \delta)(\mu + \gamma + \alpha)}{((1 - l)\mu + \delta)\beta}, \frac{l\lambda}{(\mu + \delta)}\right.$$
$$\left. - \frac{l\mu(\mu + \gamma + \alpha)}{\beta(\delta + (1 - l)\mu)}, \frac{\lambda(\delta + (1 - l)\mu)}{(\mu + \delta)(\mu + \gamma + \alpha)} - \frac{\mu}{\beta}, \frac{\gamma\lambda(\delta + (1 - l)\mu)}{\mu(\mu + \delta)(\mu + \gamma + \alpha)} - \frac{\gamma}{\beta}\right).$$
(38)

In the biological sense, E^0 is defined as a disease extinction equilibrium point in which an infection survives for a short time and then is naturally dispelled from the populations. The infection is not insisted. The other case, in which the system incline towards E^*, denoted that the populations are impotent to remove the disease spontaneously. If it closes up this remaining fact, then after a particular period, the diphtheria disease model fails its pertinency as it gets broader to keep up the populations.

5. Basic Reproductive Ratio

The basic reproductive ratio is also called basic reproductive rate or basic reproduction number and is denoted by $\mathscr{R}_0$. It

is a significant threshold value generated in epidemiology to mathematically identify the doubt of an infectious disease. This quantity represents the average number of infected persons generated by one infected person introduced into an entirely uninfected susceptible population. We use the next-generation method [33, 34] to obtain the basic reproductive ratio $\mathscr{R}_0$.

Using the next-generation matrix method on the model (1), we get

$$\mathscr{F} = \begin{pmatrix} 0 & l\beta S^0 \\ 0 & (1-l)\beta S^0 \end{pmatrix},$$
$$\mathscr{V} = \begin{pmatrix} \mu + \delta & 0 \\ -\delta & \mu + \gamma + \alpha \end{pmatrix}. \tag{39}$$

Therefore, we have,

$$\mathscr{F}\mathscr{V}^{-1} = \begin{pmatrix} \dfrac{l\delta\beta S^0}{(\mu+\gamma+\alpha)(\mu+\delta)} & \dfrac{l\beta S^0}{(\mu+\gamma+\alpha)} \\ \dfrac{(1-l)\delta\beta S^0}{(\mu+\gamma+\alpha)(\mu+\delta)} & \dfrac{(1-l)\beta S^0}{(\mu+\gamma+\alpha)(\mu+\delta)} \end{pmatrix}. \tag{40}$$

Thus, the spectral radius of the matrix $\mathscr{F}\mathscr{V}^{-1}$ and the basic reproductive ratio $\mathscr{R}_0$ are obtained [35].

$$\mathscr{R}_0 = \frac{\beta(\delta + \mu - l\mu)S^0}{(\alpha + \gamma + \mu)(\delta + \mu)}. \tag{41}$$

Putting $S^0 = \lambda/\mu$, we obtain,

$$\mathscr{R}_0 = \frac{\lambda\beta(\delta + (1-l)\mu)}{\mu(\alpha + \gamma + \mu)(\delta + \mu)}. \tag{42}$$

This expression of $\mathscr{R}_0$ represents the basic reproductive ratio for the model (1).

Remark 5. The infectious equilibrium point with the expression of basic reproduction number $\mathscr{R}_0$

$$(S^*, L^*, I^*, R^*) = \left\{ \frac{\lambda}{\mu\mathscr{R}_0}, \frac{l\lambda(\mathscr{R}_0 - 1)}{(\mu+\delta)\mathscr{R}_0}, \frac{\mu}{\beta}(\mathscr{R}_0 - 1), \frac{\gamma}{\beta}(\mathscr{R}_0 - 1) \right\}. \tag{43}$$

6. Global Stability Analysis

6.1. Global Stability at Infectious Extinction Equilibrium. For disease extinction equilibrium $E^0 = (S^0, L^0, I^0, R^0) = (\lambda/\mu, 0, 0, 0)$, we assume the following Lyapunov function:

$$U(t) = S^0 \left[\frac{S(t)}{S^0} - 1 - \ln\left(\frac{S(t)}{S^0}\right) \right] + \frac{\delta}{(1-l)\mu+\delta}L(t) + \frac{\mu+\delta}{(1-l)\mu+\delta}I(t). \tag{44}$$

By differentiation, we get

$$\frac{dU}{dt} = \left(1 - \frac{S^0}{S}\right)S' + \frac{\delta}{(1-l)\mu+\delta}L' + \frac{\mu+\delta}{(1-l)\mu+\delta}I'. \tag{45}$$

Substituting the values of S', L', and I' in the above equation, we have

$$\frac{dU}{dt} = \left(1 - \frac{S^0}{S}\right)[\lambda - \beta SI - \mu S] + \frac{\delta}{(1-l)\mu+\delta}[l\beta SI - (\mu+\delta)L]$$
$$+ \frac{\mu+\delta}{(1-l)\mu+\delta}[(1-l)\beta SI + \delta L - (\mu+\gamma+\alpha)I] = (\lambda - \mu S)\left(1 - \frac{S^0}{S}\right)$$
$$+ \beta S^0 I - \frac{(\mu+\delta)(\mu+\gamma+\alpha)}{\mu(1-l)+\delta}I. \tag{46}$$

After substituting the value of $S^0 = \lambda/\mu$, we are left with

$$\frac{dU}{dt} = -\frac{(\lambda - \mu S)^2}{\mu S} + \frac{(\mu+\delta)(\mu+\gamma+\alpha)}{\mu(1-l)+\delta}(\mathscr{R}_0 - 1). \tag{47}$$

At the disease extinction equilibrium E^0, the basic reproductive ratio $R_0 \leq 1$, and for all positive values of S, L, I, and R, it is clear that $dU/dt \leq 0$. Hence, using LaSalle's Invariance Principle [36], it is concluded that the model (1) is globally asymptotically stable.

Lemma 6. The infectious extinction equilibrium (E^0) of the model (1) is globally asymptotically stable when $\mathscr{R}_0 \leq 1$, and the disease is naturally dispelled from the populations.

6.2. Global Stability at Infectious Persistence Equilibrium. Since none of the state variables are zero at the infectious persistence equilibrium $E^* = (S^*, L^*, I^*, R^*)$, thus a Lyapunov function is assumed as

$$U(t) = \left(S - S^* - S^* \ln\left(\frac{S}{S^*}\right)\right) + B_1\left(L - L^* - L^* \ln\left(\frac{L}{L^*}\right)\right)$$
$$+ B_2\left(I - I^* - I^* \ln\left(\frac{I}{I^*}\right)\right) + B_3\left(R - R^* - R^* \ln\left(\frac{R}{R^*}\right)\right), \tag{48}$$

where B_1, B_2, and B_3 are all nonnegative constants to be obtained. This kind of Lyapunov function has been studied in [37–40].

The infectious persistence equilibrium $E^* = (S^*, L^*, I^*, R^*)$ satisfies the following equations:

$$\lambda = \beta S^* I^* + \mu S^*, \tag{49}$$

$$(\mu + \delta)L^* = l\beta S^* I^*, \tag{50}$$

$$(\mu + \gamma + \alpha) = (1-l)\beta S^* I^* + \delta L^*, \tag{51}$$

$$\mu R^* = \gamma I^*. \tag{52}$$

Now, differentiate U with respect to time t,

$$U' = \left(1 - \frac{S^*}{S}\right)S' + B_1\left(1 - \frac{L^*}{L}\right)L' + B_2\left(1 - \frac{I^*}{I}\right)I' + B_3\left(1 - \frac{R^*}{R}\right)$$
$$\cdot R' = \left(1 - \frac{S^*}{S}\right)[\beta S^* I^* + \mu S^* - \beta SI - \mu S] + B_1\left(1 - \frac{L^*}{L}\right)$$
$$\cdot l\beta SI - B_1(\mu + \delta)L + B_1(\mu + \delta)L^* + B_2\left(1 - \frac{I^*}{I}\right)[(1 - l)\beta SI + \delta L] - B_2(\mu + \gamma + \alpha)$$
$$\cdot I + B_2(\mu + \gamma + \alpha)I^* + B_3\left(1 - \frac{R^*}{R}\right)\gamma I - B_3\mu R + B_3\mu R^*,$$

$$(53)$$

which can be further simplified to

$$U' = -\mu\frac{(S - S^*)^2}{S} + \beta S^* I^*\left(1 - \frac{S^*}{S}\right) + SI[-\beta + B_1 l\beta + B_2(1 - l)\beta]$$
$$+ I[-B_2(\mu + \gamma + \alpha) + B_3\gamma + \beta S^*] + L[-B_1(\mu + \delta) + B_2\delta] + R[-B_3\mu]$$
$$- B_1 l\beta SI\frac{L^*}{L} + B_1 l\beta S^* I^* - B_2(1 - l)\beta SI^* - B_2\delta L\frac{I^*}{I}$$
$$+ B_2(1 - l)\beta S^* I^* + B_2\delta L^* - B_3\gamma I\frac{R^*}{R} + B_3\gamma I^*.$$

$$(54)$$

For the positive constants $B_1, B_2,$ and B_3, the coefficients of $SI, I, L,$ and R must be zero, that is,

$$-\beta + B_1 l\beta + B_2(1 - l)\beta = 0,\quad (55)$$

$$-B_2(\mu + \gamma + \alpha) + B_3\gamma + \beta S^* = 0,\quad (56)$$

$$-B_1(\mu + \delta) + B_2\delta = 0,\quad (57)$$

$$-B_3\mu = 0.\quad (58)$$

By solving, the above equation (55) yields

$$B_1 = \frac{\delta}{\mu + \delta}B_2,$$
$$B_2 = \frac{\mu + \delta}{(1 - l)\mu + \delta},\quad (59)$$
$$B_3 = 0.$$

For advantage, we set up new variables $x = S/S^*$, $y = L/L^*$, $z = I/I^*$, and $u = R/R^*$ to seek $S, L, I,$ and R and setting the expressions of $B_1, B_2,$ and B_3 in Equation (54), we have

$$U' = -\mu\frac{(S - S^*)^2}{S} + B_2(1 - l)\beta S^* I^*\left(2 - \frac{1}{x} - x\right) + B_1 l\beta S^* I^*\left(2 - \frac{1}{x} - \frac{xz}{y}\right)$$
$$+ B_2\delta L^*\left(1 - \frac{y}{z}\right) + B_3\gamma I^*\left(1 - \frac{z}{u}\right).$$

$$(60)$$

Multiplying by B_1 to the 2nd equation of (49) and the 3rd equation of (55) by L^* yields

$$B_1(\mu + \delta)L^* = B_1 l\beta S^* I^*,$$
$$B_1(\mu + \delta)L^* = B_2\delta L^*.\quad (61)$$

Hence, it follows that

$$-B_1 l\beta S^* I^* + B_2\delta L^* = 0.\quad (62)$$

Multiplying by $F_1(X)$ to the last equation, where $F_1(X)$ is considered as a general function that will be determined later and $X = (x, y, z, u)$, yields

$$-B_1 l\beta S^* I^* F_1(X) + B_2\delta L^* F_1(X) = 0\quad (63)$$

Multiplying the 4th equation of (49) by B_3 and the 4th equation of (55) by R^* yields

$$B_3\mu R^* = B_3\gamma I^*,$$
$$B_3\mu R^* = 0.\quad (64)$$

Hence, it follows that

$$B_3\gamma I^* = 0.\quad (65)$$

Multiplying by $F_2(X)$ to the last equation, where $F_2(X)$ is considered as a general function that will be determined later and $X = (x, y, z, u)$, yields

$$B_3\gamma I^* F_2(X) = 0.\quad (66)$$

From (54) using (63) and (66) yields

$$U' = -\mu\frac{(S - S^*)^2}{S} + B_2(1 - l)\beta S^* I^*\left(2 - \frac{1}{x} - x\right)$$
$$+ B_1 l\beta S^* I^*\left(2 - \frac{1}{x} - \frac{xz}{y} - F_1(X)\right) + B_2\delta L^*\left(1 - \frac{y}{z} + F_1(X)\right)$$
$$+ B_3\gamma I^*\left(1 - \frac{z}{u} + F_2(X)\right).$$

$$(67)$$

Now, the functions $F_1(X)$ and $F_2(X)$ are taken so that the coefficients of L^* and I^* are zero. For these cases, we get

$$F_1(X) = \frac{y}{z} - 1,\quad (68)$$

and

$$F_2(X) = \frac{z}{u} - 1.\quad (69)$$

Then, Equation (67) becomes

$$U' = -\mu\frac{(S - S^*)^2}{S} + B_2(1 - l)\beta S^* I^*\left(2 - \frac{1}{x} - x\right) + B_1 l\beta S^* I^*\left(2 - \frac{1}{x} - \frac{xz}{y} - \frac{y}{z} + 1\right)$$
$$= -\mu\frac{(S - S^*)^2}{S} + B_2(1 - l)\beta S^* I^*\left(2 - x - \frac{1}{x}\right) + B_1 l\beta S^* I^*\left(3 - \frac{1}{x} - \frac{y}{z} - \frac{xz}{y}\right).$$

$$(70)$$

By the arithmetic mean-geometric mean inequality, for equality, if and only if $S = S^*$ and $y = z = u$, the last expression must be less than or equal to zero. Thus, we have $U' \leq 0$ with equality if and only if $S = S^*$ and $L/L^* = I/I^* = R/R^*$. By LaSalle's Invariance Principle [36], for each solution, the omega-limit set remains in an invariant set that is contained in $\Omega = \{(S, L, I, R): S = S^*, L/L^* = I/I^* = R/R^*\}$. Since S must be in S^*, S' turns zero, which implies that $I = I^*$, $L = L^*$, and $R = R^*$. Thus, there is only invariant set in Ω which is singleton $\{E_1\}$. For each solution that intersects, $\mathbb{R}_{+0}^4\{L = I = R$

$= 0\}$ limits to E_1, which concludes that the disease persistence equilibrium E^* of (1) is globally asymptotically stable in $\mathbb{R}^4_{+0}\{L = I = R = 0\}$ [24].

Lemma 7. *The infectious persistence equilibrium (E^*) of the model (1) is globally asymptotically stable when $\mathcal{R}_0 > 1$, and the disease persists in the populations for a long time.*

7. Parameter Estimation

In this section, we obtain the value of the unknown parameters for the model (1). To estimate parameter values, we have assumed the initial condition of the state variables as $(S_0, L_0, I_0, R_0) = (10000, 0, 1, 0)$. There are seven parameters in our model which are to be obtained. Among these parameters, natural mortality rate μ is estimated as 0.002; the recruitment of susceptible class $\lambda = \mu S_0 = 20$; the rate which leaves $L(t)$ for $I(t)$, i.e., incubation period $\delta = 1/7$; and the fraction of $S(t)$ which moves to $L(t)$; $l = 0.95$; and disease-induced mortality rate is estimated as $\alpha = 0.0054$. These are derived from the data in the literature [30]. And the rest of the parameters are disease transmission rate β and the recovered rate γ which have to be fitted; therefore, $\theta = (\beta, \gamma)$. Consider the initial value of the parameters to be $\omega_0 = (\lambda, \mu, \alpha, l, \beta, \delta, \gamma) = (20, 0.002, 0.0054, 0.95, 0.0000065, 1/7, 0.005)$, and the initial condition of the state variables is $(S_0, L_0, I_0, R_0) = (10000, 0, 1, 0)$. Using the initial value of the parameters and the initial conditions of the state variables, the value of the unknown parameters is fitted to the model (1) with the help of the nonlinear least square (NLS) method. Table 1 contains the description and estimated or the best fitted values of the parameters. Here, we have simulated the cumulative value of the daily case data, which are illustrated in Figures 2 and 3 that also represent the population dynamic of the susceptible, latent, and infected population $S(t), L(t)$, and $I(t)$, respectively. From these figures, it is observed that the infected population (I-class) increases significantly upon the infection and arrives at the peak at the 36th day ($I(43) = 3.126 \times 10^3$); after that, it is decaying.

8. Numerical Results

To further investigate the behaviour of the model (1), we conducted various numerical investigations applying the estimations that are gained and given in Table 1. For this intention, we consider two parameter sets resembling the cases of stability of the infectious persistence equilibrium, where $\mathcal{R}_0 > 1$, and disease extinction steady state, where $\mathcal{R}_0 < 1$. The outcomes obtained for both equilibria with stability analysis are also numerically demonstrated using MATLAB R2018a.

Using the parameter values from Table 1, the basic reproductive ratio becomes $\mathcal{R}_0 = 5.86 > 1$ thereby signifying the asymptotic stability of the infected steady state. For this reason, different initial conditions of (S_0, L_0, I_0, R_0) are chosen as IC1 = $(10000, 0, 1, 0)$, IC2 = $(8000, 0, 2, 0)$, and IC3 = $(12000, 0, 3, 0)$.

Figure 4 illustrates the system dynamics of the susceptible, latent, and infected population for the three initial con-

ditions within two years, i.e., 730 days. In Figure 4(a), the susceptible population decays very sharply and reaches the nadir at 189, 283, and 134 for IC1, IC2, and IC3, respectively. As time increases, they are again increasing together and reaching a peak point of approximately 2782. Again, it is decreasing and reaches another nadir at 1525. Further, it is increasing and asymptotically stable at 1706 within two years; i.e., susceptible population would be constant. In Figure 4(b), the latent population increases sharply and reaches the first peak points 3136, 2200, and 4161 for IC1, IC2, and IC3, respectively; then, they are decreasing sharply and reach a nadir at 5 together within 3.67 months and stable about three months. As time increases, they are again increasing and reach the second peak at 305 within the next 3 months. Again, they are decaying and reach another nadir at 51 within the next 3.67 months. Further, they increase and reach the third peak point of 158 within the next 4 months. They are decaying further and reach another nadir at 85 within the next 4 months. As time increases, they are increasing further and asymptotically stable at 109 within 2 years. Moreover, in Figure 4(c), the infected population increases very sharply and reaches the first peak points at 2383, 1739, and 3058 for the same initial conditions; then, they are decaying as they are increased and reach a nadir at 5 together within 4 months and stable about three months. As time increases, they are again increasing and reaches the second peak at 280 within the next 3.33 months. Again, they are decaying and reach another nadir at 47 within the next 3.67 months. Further, they are increasing and reach the third peak at 145 within the next 4 months. They are decaying further and reach another nadir at 80 within the next 3.67 months. As time increases, they are increasing further and asymptotically stable at 100 within 2 years.

Figure 5 illustrates the system's phase portrait for different initial conditions. It represents the relative change of the susceptible $S(t)$, latent $L(t)$, and infected populations $I(t)$ to one another over time by a single trajectory. It also characterises the stability of the system. For different initial conditions, the trajectories are approaching a single point which specifies the disease persistence equilibrium point $E^* = (1706, 109, 100, 7814)$ when the basic reproduction number $\mathcal{R}_0 = 5.86 > 1$. In this case, the trajectories approach the long-term steady state, and the disease persists in the populations for $t \longrightarrow \infty$.

For disease-extinction equilibrium, we assume the value of infection transmission rate β different from Table 1 as $\beta = 0.000005$. Therefore, the basic reproductive ratio is evaluated as $\mathcal{R}_0 = 0.302 < 1$. For this case, the disease dynamics are illustrated in Figure 6 for the same initial conditions. The latent and infected populations are converged to 0 within 4 months that are illustrated in Figures 6(b) and 6(c), respectively, which indicates that the disease will be extincted from the populations by itself within 120 days. However, in Figure 6(a), in the susceptible population, only positive values remain for the different initial conditions that indicate the infection-free steady state. Moreover, Figure 7 illustrates the infection-free steady states and the interaction between the populations by three trajectories for three

different initial conditions. The trajectories are approaching a single point defined as infection-free steady-state $E^0 = (10000, 0, 0, 0)$ and remain at this point for $t \longrightarrow \infty$.

9. Conclusion

We have proposed a diphtheria epidemic model and found two steady-state equilibrium points: one is disease extinction equilibrium point E^0 (37), and another is infectious persistence equilibrium point E^* (38). We have formulated the basic reproductive number in terms of parameters. We have also shown analytically that the infectious extinction equilibrium (37) is globally asymptotically stable when the basic reproductive ratio $\mathscr{R}_0$ does not exceed unity; the infection is dispelled by itself from the populations. The infectious persistence equilibrium (38) is also globally asymptotically stable when the basic reproductive ratio $\mathscr{R}_0$ is more than unity; the disease persists in the populations at a certain level. We have fitted the daily case data from November 8, 2017, to December 27, 2017, given in [30] to our model and have evaluated the parameter's value. Both equilibria have been analyzed numerically and found a lot that matches the real scenario. We have found the first peak at 38 days for IC1 that matches with the real data, and the second and third peaks have been found at 310 days and 1.5 years, respectively, which also a lot matches with the real scenario, like the highest infection found after one month, given in [30, 41–44]. The enumerated infectious persistence equilibrium E^* is $(1706,109,100,7814)$ and infection-free steady-state E^0 is $(10000, 0, 0, 0)$. A statistical model was used to calculate the numeric value of the basic reproductive ratio $\mathscr{R}_0$ in [30] and deduced a range of estimates ranging from 4.7 to 14.8 with a median estimate of 7.2. But in this study, it has calculated $\mathscr{R}_0 = 5.86$ by involving a mathematical model, which indicates that the infection rate is very high. This study suggests applying treatments to control the diphtheria epidemic. Lastly, we hope that this study will be focused on the assumption of control strategies by constituents and policymakers.

Data Availability

The data supporting the study are accessed from the study "R. Matsuyama, A. R. Akhmetzhanov, A. Endo, H. Lee, T. Yamaguchi, S. Tsuzuki, H. Nishiura, Uncertainty and sensitivity analysis of the basic reproductive number of the diphtheria: a case study of a Rohingya refugee camp in Bangladesh, November-December 2017, PeerJ, 6 (2018) 4582. doi:10.7717/peerj.4583."

Disclosure

This work has been partially presented in my M.Sc. thesis work.

Conflicts of Interest

The authors declare that they have no conflicts of interest.

References

[1] M. Mustafa, I. Yusof, M. Jeffree, E. Illzam, S. Husain, and A. Sharifa, "Diphtheria: clinical manifestations, diagnosis, and role of immunizationin prevention," *IOSR Journal of Dental and Medical Sciences*, vol. 15, no. 8, pp. 71–76, 2016.

[2] R. Q. Zhang, H. B. Li, F. Y. Li, L. X. Han, and Y. M. Xiong, "Epidemiological characteristics of measles from 2000 to 2014: results of a measles catch-up vaccination campaign in Xianyang, China," *Journal of Infection and Public Health*, vol. 10, no. 5, pp. 624–629, 2017.

[3] L. Both, J. White, S. Mandal, and A. Efstratiou, "Access to diphtheria antitoxin for therapy and diagnostics," *Euro Surveillance*, vol. 19, no. 24, pp. 1–6, 2014.

[4] F. T. Cutts and M. Hanson, "Seroepidemiology: an underused tool for designing and monitoring vaccination programmes in low- and middle-income countries," *Tropical Medicine and International Health*, vol. 21, no. 9, pp. 1086–1098, 2016.

[5] U. Czajka, A. Wiatrzyk, E. Mosiej, K. Formińska, and A. A. Zasada, "Changes in MLST profiles and biotypes of Corynebacterium diphtheriae isolates from the diphtheria outbreak period to the period of invasive infections caused by nontoxigenic strains in Poland (1950-2016)," *BMC Infectious Diseases*, vol. 18, no. 1, pp. 1–8, 2018.

[6] M. Kizito and J. Tumwiine, "A mathematical model of Treatment and vaccination interventions of pneumococcal pneumonia infection dynamics," *Journal of Applied Mathematics*, vol. 2018, Article ID 2539465, 16 pages, 2018.

[7] S. Dittmann, "Epidemic diptheria in the newly independent states of the former USSR– situation and lessons learned," *Biologicals*, vol. 25, no. 2, pp. 179–186, 1997.

[8] Centers for Disease Control and Prevention (CDC), "Update: diphtheria epidemic–new independent states of the former Soviet Uneion, January 1995-March 1996," *MMWR. Morbidity and mortality weekly report*, vol. 45, no. 32, pp. 693–697, 1996.

[9] I. Hardy, S. Dittmann, and R. Sutter, "Current situation and control strategies for resurgence of diphtheria in newly independent states of the former Soviet Union," *The Lancet*, vol. 347, no. 9017, pp. 1739–1744, 1996.

[10] World Health Organization, *Diphtheria – Yemen disease outbreak news 22 December 2017*, 2017, December 2017, https://www.who.int/csr/don/22-december-2017-diphtheria-yemen/en.

[11] World Health Organization, *Diphtheria – Cox's Bazar in Bangladesh disease outbreak news, 13 December 2017*, 2017, December 2017, https://www.who.int/csr/don/13-december-2017-diphtheria-bangladesh/en.

[12] World Health Organization (WHO), *Weekly Situation Report #9*, World Health Organization, Bangladesh, 2018, https://reliefweb.int/sites/reliefweb.int/files/resources/sitrep09.pdf.

[13] I. F. Arifin and C. I. Prasasti, "Factors that related with diptheria cases of children in Bangkalan health centers in 2016," *Jurnal Berkala Epidemiologi*, vol. 5, no. 1, p. 26, 2017.

[14] P. Wu and H. Zhao, "Mathematical analysis of an age-structured HIV/AIDS epidemic model with HAART and spatial diffusion," *Nonlinear Analysis: Real World Applications*, vol. 60, p. 103289, 2021.

[15] M. Parsamanesh and M. Erfanian, "Stability and bifurcations in a discrete-time SIVS model with saturated incidence rate," *Chaos, Solitons and Fractals*, vol. 150, article 111178, 2021.

[16] S. Saha and G. P. Samanta, "Dynamics of an epidemic model with impact of toxins," *Physica A: Statistical Mechanics and its Applications*, vol. 527, article 121152, 2019.

[17] M. Parsamanesh, M. Erfanian, and M. Mehrshad, "Stability and bifurcations in a discrete-time epidemic model with vaccination and vital dynamics," *BMC Bioinformatics*, vol. 21, no. 1, pp. 1–15, 2020.

[18] K. A. Kabir, A. Chowdhury, and J. Tanimoto, "An evolutionary game modeling to assess the effect of border enforcement measures and socio-economic cost: export-importation epidemic dynamics," *Chaos, Solitons and Fractals*, vol. 146, article 110918, 2021.

[19] G. Samanta and S. P. Bera, "Analysis of a Chlamydia epidemic model with pulse vaccination strategy in a random environment," *Nonlinear Analysis: Modelling and Control*, vol. 23, no. 4, pp. 457–474, 2018.

[20] M. Parsamanesh and M. Erfanian, "Global dynamics of an epidemic model with standard incidence rate and vaccination strategy," *Chaos, Solitons and Fractals*, vol. 117, pp. 192–199, 2018.

[21] P. Shahrear, S. M. S. Rahman, and M. M. N. Hasan, "Prediction and mathematical analysis of the outbreak of coronavirus (COVID-19) in Bangladesh," *Results in Applied Mathematics*, vol. 10, article 100145, 2021.

[22] G. Maugeri, P. Castrogiovanni, G. Battaglia et al., "The impact of physical activity on psychological health during Covid-19 pandemic in Italy," *Heliyon*, vol. 6, no. 6, article e04315, 2020.

[23] S. Saha, G. P. Samanta, and J. J. Nieto, "Epidemic model of COVID-19 outbreak by inducing behavioural response in population," *Nonlinear Dynamics*, vol. 102, no. 1, pp. 455–487, 2020.

[24] J. Liu and T. Zhang, "Global stability for a tuberculosis model," *Mathematical and Computer Modelling*, vol. 54, pp. 836–845, 2011.

[25] D. P. Gao and N. J. Huang, "Optimal control analysis of a tuberculosis model," *Applied Mathematical Modelling*, vol. 58, pp. 47–64, 2018.

[26] C. R. Vitek and M. Wharton, "Diphtheria in the former Soviet Union: reemergence of a pandemic disease," *Emerging Infectious Diseases*, vol. 4, pp. 539–550, 1998.

[27] K. Zakikhany and A. Efstratiou, "Diphtheria in Europe: current problems and new challenges," *Future Microbiology*, vol. 7, no. 5, pp. 595–607, 2012.

[28] M. Torrea, J. L. Torrea, and D. Ortega, "A modeling of a Diphtheria epidemic in the refugees camps," *bioRxiv*, vol. 6, no. 6, p. 208835, 2017.

[29] F. Ilahi and A. Widiana, "The effectiveness of vaccine in the outbreak of diphtheria: mathematical model and simulation," *IOP Conference Series: Materials Science and Engineering*, vol. 434, 2018.

[30] R. Matsuyama, A. R. Akhmetzhanov, A. Endo et al., "Uncertainty and sensitivity analysis of the basic reproduction number of diphtheria: a case study of a Rohingya refugee camp in Bangladesh, November-December 2017," *PeerJ*, vol. 6, article e4582, 2018.

[31] Z. Islam, *Developing a mathematical model for optimal cost-effective treatment strategies applied to a diphtheria outbreak, [M.S. Thesis]*, Department of Mathematics, Bangladesh University of Engineering and Technology, Dhaka, 2020, http://lib.buet.ac.bd:8080/xmlui/bitstream/handle/123456789/5873/Full%20Thesis.pdf?isAllowed=y&sequence=1.

[32] A. Din, Y. Li, and Q. Liu, "Viral dynamics and control of hepatitis B virus (HBV) using an epidemic model," *Alexandria Engineering Journal*, vol. 59, no. 2, pp. 667–679, 2020.

[33] O. Diekmann, J. A. P. Heesterbeek, and J. A. J. Metz, "On the definition and the computation of the basic reproduction ratio R0 in models for infectious diseases in heterogeneous populations," *Journal of Mathematical Biology*, vol. 28, no. 4, pp. 365–382, 1990.

[34] J. M. Heffernan, R. J. Smith, and L. M. Wahl, "Perspectives on the basic reproductive ratio," *Journal of Royal Society Interface*, vol. 2, no. 4, pp. 281–293, 2005.

[35] P. V. D. Driessche and J. Watmough, "A simple SIS epidemic model with a backward bifurcation," *Journal of Mathematical Biology*, vol. 40, no. 6, pp. 525–540, 2000.

[36] L. Salle and P. Joseph, *The Stability of Dynamical Systems*, Society for Industrial and Applied Mathematics, 1976.

[37] Z. Ma, J. Liu, and J. Li, "Stability analysis for differential infectivity epidemic models," *Nonlinear Analysis: Real World Applications*, vol. 4, no. 5, pp. 841–856, 2003.

[38] A. Iggidr, J. Mbang, G. Sallet, and J. J. Tewa, "Multi-compartment models," *Discrete and Continuous Dynamical Systems-Series S*, vol. 2007, pp. 506–519, 2007.

[39] C. C. McCluskey, "Lyapunov functions for tuberculosis models with fast and slow progression," *Mathematical Biosciences and Engineering*, vol. 3, no. 4, pp. 603–614, 2006.

[40] H. Guo and M. Y. Li, "Global dynamics of a staged progression model for infectious diseases," *Mathematical Biosciences and Engineering*, vol. 3, pp. 513–525, 2006.

[41] K. Hsan, J. M. Misti, D. Gozal, M. D. Griffiths, and M. A. Mamun, "Diphtheria outbreak among the Rohingya refugees in Bangladesh: what strategies should be utilized for prevention and control?," *Travel Medicine and Infectious Disease*, vol. 34, article 101591, 2020.

[42] Reliefweb, "Bangladesh: diphtheria outbreak - Dec 2017 ongoing. 2019," April 2019, https://reliefweb.int/disaster/ep-2017-000177-bgd.

[43] World Health Organization, "Emergency type: Rohingya refugee crisis – WHO Bangladesh weekly situation report # 41, 2018," April 2019, http://www.searo.who.int/bangladesh/weeklysitrep41cxbban.pdf.

[44] World Health Organiation, "Emergency type: Rohingya refugee crisis – WHO Bangladesh weekly situation report # 45, 2018," April 2019, http://www.searo.who.int/bangladesh/weeklysitrep45cxbban.pdf?ua=1&ua=1.